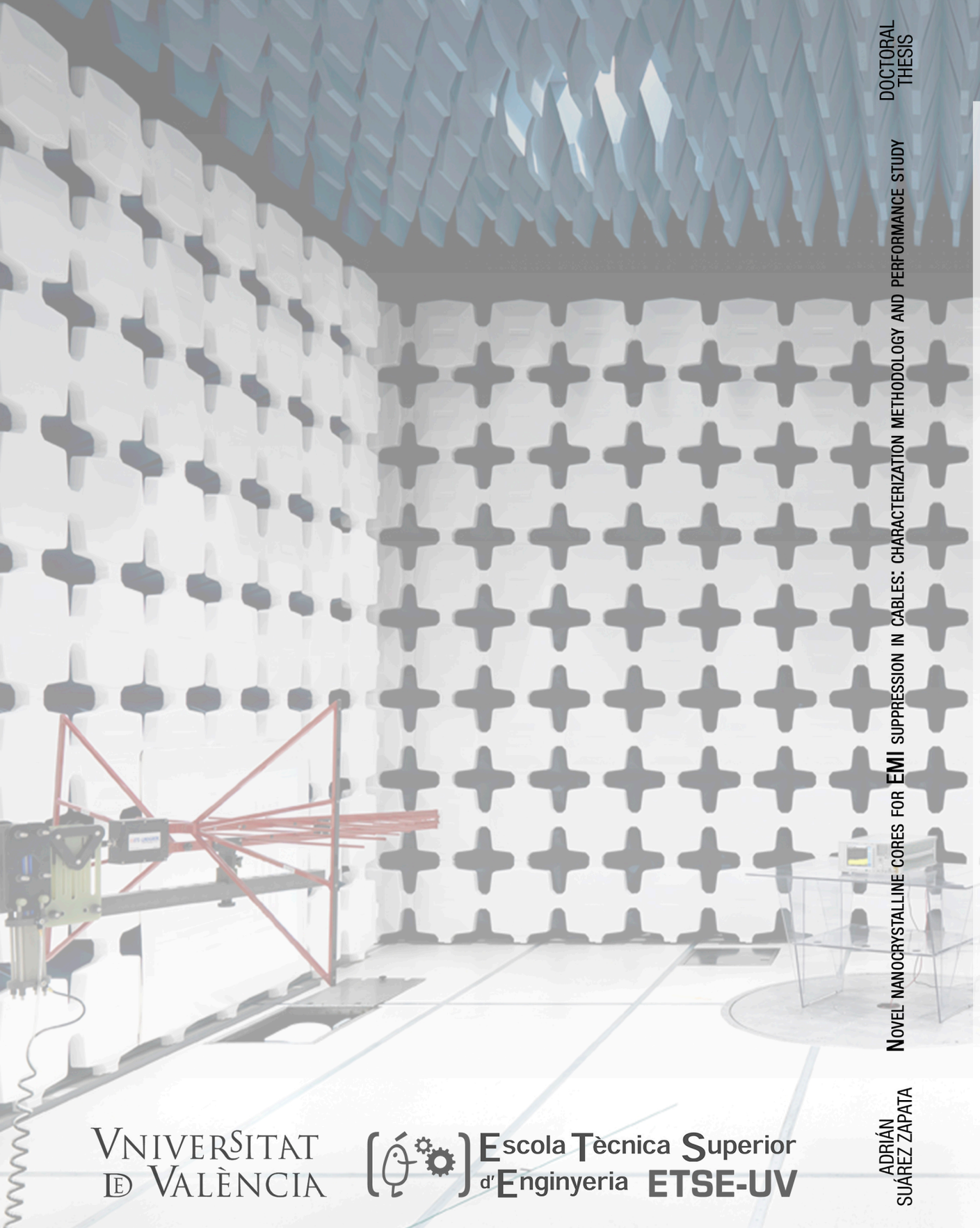

DOCTORAL THESIS

NOVEL NANOCRYSTALLINE CORES FOR EMI SUPPRESSION IN CABLES: CHARACTERIZATION METHODOLOGY AND PERFORMANCE STUDY

ADRIÁN SUÁREZ ZAPATA

DOCTORAL PROGRAMME IN ELECTRONIC ENGINEERING

DOCTORAL THESIS

NOVEL NANOCRYSTALLINE CORES FOR EMI SUPPRESSION IN CABLES: CHARACTERIZATION METHODOLOGY AND PERFORMANCE STUDY

AUTHOR:
ADRIÁN SUÁREZ ZAPATA

SUPERVISOR:
DR.ENG. JOSÉ TORRES PAÍS

MARCH 2021

VNIVERSITAT DE VALÈNCIA

Escola Tècnica Superior d'Enginyeria ETSE-UV

VNIVERSITAT DE VALÈNCIA

Escola Tècnica Superior d'Enginyeria ETSE-UV

DOCTORAL PROGRAMME IN ELECTRONIC ENGINEERING

DOCTORAL THESIS

Novel nanocrystalline cores for EMI suppression in cables: characterization methodology and performance study

Author:
Adrián Suárez Zapata

Supervisor:
Dr.Eng. José Torres País

Universitat de València (UV)
Department of Electronic Engineering

Valencia, Spain – March 2021

VNIVERSITAT DE VALÈNCIA

Escola Tècnica Superior d'Enginyeria ETSE-UV

Declaration

D. JOSÉ TORRES PAÍS, Doctor en Ingeniería Electrónica, Profesor Titular del Departamento de Ingeniería Electrónica de la Escola Tècnica Superior d'Enginyeria de la Universitat de València

HACE CONSTAR QUE:

D. ADRIÁN SUÁREZ ZAPATA, Graduado en Ingeniería Electrónica de Telecomunicación y Máster en Ingeniería Electrónica, ha realizado bajo su dirección el trabajo titulado "Novel nanocrystalline cores for EMI suppression in cables: characterization methodology and performance study", que se presenta en esta memoria para optar al grado de Doctor por la Universitat de València.

Y para que así conste a los efectos oportunos, y dando su conformidad para la presentación de este trabajo delante del Tribunal de Tesis Doctoral que corresponda, firma el presente certificado, en Valencia, a 16 de Marzo de 2021.

JOSE GABRIEL\| TORRES\| PAIS

Firmado digitalmente por JOSE GABRIEL\| TORRES\|PAIS
Fecha: 2021.03.20 11:39:24 +01'00'

Fdo. D. José Torres País

UNIVERSITAT DE VALÈNCIA
ESCOLA TÈCNICA SUPERIOR D'ENGINYERIA
Departamento de Ingeniería Electrónica

Av. De la Universidad s/n, 46100 Burjassot (Valencia)

Acta de Calificación de Tesis Doctoral

Tesis Doctoral:	NOVEL NANOCRYSTALLINE CORES FOR EMI SUPPRESSION IN CABLES: CHARACTERIZATION METHODOLOGY AND PERFORMANCE STUDY
Autor:	ADRIÁN SUÁREZ ZAPATA
Director:	Dr. JOSÉ TORRES PAÍS

El Tribunal nombrado para juzgar la Tesis Doctoral citada anteriormente, compuesto por los doctores:

Presidente: _____

Vocal: _____

Secretario: _____

Acuerda otorgarle la calificación de _____

Y para que así conste a los efectos oportunos, firmamos el presente certificado.

En Valencia, el _____ de _____ de 2021

Note to the Reader

According to the University of Valencia Doctorate Regulation[1] this PhD dissertation is presented as a compendium of at least three publications in international journals containing the results of the conducted work. Furthermore, in accordance with the aforementioned regulation and with the aim to foster the language of the University of Valencia in research and education activity, this PhD dissertation starts an extended abstract in one of the official languages of Valencian Community (Spanish). This thesis really begins at page XXIII with a short abstract in English followed by the research context, motivation, objectives, theoretical fundamentals, methodology, results and conclusions.

[1]Reglament sobre depòsit, avaluació i defensa de la tesi doctoral aprovat pel Consell de Govern de 28 de Juny de 2016. ACGUV 172/2016.
Pla d'increment de la docència en valencià (ACGUV 129/2012) aprovat i modificat pel Consell de Govern de 22 de desembre de 2016. ACGUV 308/2016.

Resumen

1. Contexto de investigación y motivación

El control de las interferencias electromagnéticas (EMI) en dispositivos electrónicos es un problema cada vez mayor al que se enfrentan los diseñadores para garantizar que los dispositivos cumplan con los requisitos de compatibilidad electromagnética (EMC) para operar simultáneamente sin inferir entre sí. Este hecho se debe a la tendencia hacia una mayor integración de componentes, la reducción del tamaño y grosor de las placas de circuito impreso (PCB) y la miniaturización de las carcasas de los dispositivos. Además, otros factores como el empleo de frecuencias de conmutación más altas en los convertidores de potencia y las velocidades de datos de comunicación en los circuitos digitales. En consecuencia, la ingeniería de EMC se realiza con el enfoque de sistema (*system approach*), teniendo en cuenta la EMC durante todo el proceso de diseño para evitar posibles problemas de EMI que podrían degradar el rendimiento del dispositivo. Por lo tanto, es vital adoptar soluciones específicas durante la etapa de diseño para cumplir con los requisitos de EMC para reducir las penalizaciones desde el punto de vista de los costes, el tiempo de comercialización y el rendimiento del producto. El proceso de prueba de EMC puede revelar que se necesita la protección de un determinado cable o incluso puede detectar una fuente EMI inesperada cuando el dispositivo diseñado está conectado a módulos externos, como una fuente de alimentación, o a otro dispositivo para comunicarse con él. Cuando los cables representan la fuente de EMI, puede traducirse en no superar los test de certificación de emisiones conducidas o radiadas, una práctica muy extendida es el empleo de un supresor de EMI, como un núcleo de cable (también conocido como ferrita de cable).

La efectividad de un núcleo de cable para reducir las EMI en cables se define por su capacidad para aumentar la densidad de flujo de una intensidad de campo específica creada alrededor de un conductor. La presencia de interferencias en un conductor genera un campo magnético no deseado a su alrededor que puede resultar en problemas de EMI. Cuando se aplica un núcleo de cable en el conductor, el campo magnético se concentra creando un flujo magnético dentro del núcleo debido a que posee una permeabilidad magnética más alta que el aire que lo rodea. De este modo, este componente es eficaz reduciendo las emisiones de EMI tanto conducidas como radiadas.

Este tipo de supresores de EMI se puede aplicar tanto a cables de comunicación, como a cables de video o multiconductores USB, para evitar interferencias que podrían propagarse a lo largo del cable y afectar a los dispositivos interconectados. Este componente también se usa ampliamente para reducir las oscilaciones de alta frecuencia en cables causadas por la conmutación en inversores y convertidores de potencia. En

este sentido, el núcleo actúa como un filtro paso-bajo, de forma que actúa únicamente ante las interferencias ubicadas en un rango de frecuencia concreto, sin afectar a la señal deseada. La selección del núcleo adecuado permite reducir el ruido de conmutación mediante el aumento de la impedancia del camino de propagación en el rango de frecuencia deseado. La aplicación de ferritas de cable es una técnica muy utilizada para reducir las EMI en cables, a pesar de los inconvenientes que la integración de un componente extra puede implicar en términos de coste y fabricación del sistema. Sin embargo, estos inconvenientes suelen compensarse con la eficacia de las ferritas de cable para filtrar las interferencias sin tener que rediseñar el circuito electrónico. Ésta es una de las principales razones por las que los diseñadores utilizan ampliamente esta solución de supresión de EMI para cumplir con los requisitos de cumplimiento de EMC.

Convencionalmente, los núcleos magnéticos más utilizados para aplicaciones de filtrado se basan en materiales cerámicos (también conocidos como materiales policristalinos o *soft ferrites*). Aunque no pertenecen al grupo de los metales, el material base de los núcleos cerámicos es el óxido de hierro Fe_2O_3 mezclado con uno o más metales de transición divalentes, como manganeso, zinc, níquel, cobalto o magnesio. Asimismo, una ventaja interesante de los materiales cerámicos es la posibilidad de fabricar componentes con muchas formas y dimensiones diferentes. Uno de los materiales cerámicos convencionales más utilizados es el MnZn, que está destinado a reducir las EMI en el rango de frecuencia que cubre desde la región de kilohercios más alta hasta la región más baja de megahercios. Otros materiales ampliamente utilizados son los basados en composiciones de NiZn, ya que representa una solución con un gran ancho de banda en términos de frecuencia de empleo.

No obstante, los materiales convencionales utilizados para fabricar núcleos de cable supresores de EMI se centran en reducir las perturbaciones en los cables en una región de frecuencia específica. En consecuencia, se tuvieron que estudiar nuevos materiales que pudieran proporcionar una supresión de EMI significativa para garantizar la compatibilidad electromagnética en aquellas regiones de frecuencia no cubiertas específicamente por las soluciones tradicionales. Los resultados mostrados por otros componentes EMC, como los choques de modo común fabricados con un nuevo material basado en composiciones nanocristalinas, han mostrado una gran efectividad en términos de pérdida de inserción (*insertion loss*) en un amplio rango de frecuencias debido a su alta permeabilidad inicial y características magnéticas.

A partir de los resultados preliminares y las características ofrecidas por el material nanocristalino, esta tesis doctoral se centra en investigar si un núcleo supresor de EMI para cables basado en material nanocristalino es capaz de proporcionar una mayor efectividad para reducir las interferencias, comparado con los materiales cerámicos convencionales. De esta manera, la hipótesis de base surgió como respuesta al tema de

discusión foco de esta investigación: ¿Podría un núcleo basado en material nanocristalino proporcionar una mayor efectividad para reducir la influencia de EMI en los cables que los materiales convencionales?

2. Objetivos

Teniendo en cuenta el contexto de la investigación y la motivación anteriormente definidos, el objetivo general de la presente tesis doctoral se define de la siguiente manera:

Estudiar, analizar y evaluar la idoneidad del material nanocristalino para fabricar supresores de EMI de núcleo de tubo para reducir las interferencias en cables como alternativa a los materiales cerámicos convencionales, tradicionalmente utilizados para producir componentes EMC.

En este sentido, se proponen los siguientes objetivos específicos (O.E.) para realizar la investigación de estos estudios doctorales que permitan dar respuesta a la hipótesis previamente planteada:

- O.E.1: Estudio y evaluación de los nuevos prototipos de núcleos de tubo basados en el novedoso material nanocristalino, para reducir los supra-armónicos en el rango de frecuencia de 2-150 kHz y los problemas de EMI que puede aparecer en la región de emisiones conducidas y radiadas (hasta 500 MHz).

- O.E.2: Determinar el rendimiento del material nanocristalino en comparación con las composiciones de ferrita de cable convencionales para reducir las EMI en cables. Analizar el rendimiento en términos de propiedades magnéticas, impedancia proporcionada y pérdida de inserción introducida en el cable, para definir las regiones de frecuencia en las que el nanocristalino es más efectivo que los núcleos cerámicos de MnZn y NiZn.

- O.E.3: Diseñar e implementar un método de configuración de medición que permita determinar el parámetro de pérdida de inserción proporcionado por un núcleo de manguito específico cuando se aplica a un cable que interconecta dos sistemas con una impedancia específica.

- O.E.4: Optimizar la selección de un núcleo supresor de EMI para cables considerando sus dimensiones. Estudiar los parámetros que relacionan la impedancia proporcionada por un núcleo con sus dimensiones para obtener la dependencia entre ellos. Esta conexión permite al diseñador determinar la atenuación de EMI necesaria para seleccionar las dimensiones optimizadas del componente considerando el volumen, peso y coste mínimos.

- O.E.5: Diseñar un modelo de simulación que permita correlacionar los resultados obtenidos del sistema de medida experimental desarrollado para obtener el rendimiento de este tipo de componentes de EMC.

- O.E.6: Determinar la efectividad de un nuevo prototipo de muestra nanocristalina basada en un núcleo de tubo partido en dos piezas. Esta muestra permite estudiar el rendimiento de una muestra nanocristalina en comparación con los componentes de MnZn y NiZn cuando se emplea como núcleo partido (*snap ferrite*).

3. Metodología

La presente tesis doctoral se basa en un compendio de publicaciones científicas las cuales han superado una revisión por pares internacionales. El cuerpo de la tesis incluye un total de tres artículos publicados en revistas indexadas en el *Journal Citation Reports* (JCR) y dos artículos enviados a congresos internacionales. Cada uno de ellos describe la investigación llevada a cabo para alcanzar cada uno de los objetivos específicos planteados en la sección anterior. En base a este formato de tesis por compendio, la metodología se desarrolla en cuatro capítulos que se abordan después de realizar una revisión de los conceptos y contenidos tratados en este estudio (Capítulo 2). En primer lugar, en el Capítulo 3 se presenta la primera publicación científica en revista y en el Capítulo 4 la segunda publicación científica en revista. Seguidamente, se incluyen las dos contribuciones a congresos (Capítulo 5) y, finalmente, se aborda la investigación publicada en el tercer artículo científico publicado en revista (Capítulo 6).

Capítulo 3 - Artículo científico I: Characterization of Different Cable Ferrite Materials to Reduce the Electromagnetic Noise in the 2–150 kHz Frequency Range

Este primer artículo científico se centra en la caracterización del nuevo material nanocristalino para reducir los problemas de EMI en el rango de frecuencia de 2–150 kHz. La estandarización con respecto a las emisiones en el rango de frecuencia de 2 a 150 kHz ha progresado en los últimos años y se clasifica en el rango de interferencias electromagnéticas conducidas como armónicos de calidad de energía (*power quality*) (2 a 9 kHz) y banda CISPR A (9 a 150 kHz). Las perturbaciones electromagnéticas ubicadas entre 2 kHz y 150 kHz se conocen como supra-armónicos. Suelen ser generados por sistemas modernos basados en convertidores de conmutación activos que normalmente se integran en aplicaciones de conversión y suministro de energía. Algunos ejemplos de este tipo de sistemas son los cargadores de baterías para vehículos eléctricos, sistemas fotovoltaicos o plantas de energía eólica. Además, estas perturbaciones también se han detectado en otros sistemas relacionados con electrodomésticos e instalaciones de

iluminación. Por lo tanto, es esencial garantizar la compatibilidad electromagnética en la banda de frecuencia de 2–150 kHz y, en consecuencia, deben proponerse nuevos materiales que puedan proporcionar una supresión significativa de EMI en este rango. Se trata de un espectral de frecuencia crítica debido a las interferencias generadas por una amplia gama de dispositivos y, en concreto, problemas de comunicación entre las nuevas tecnologías y dispositivos incorporados a la red tradicional para convertirla en una Smart Grid.

Una de las mejores ventajas de los núcleos magnéticos es su capacidad para atraer el flujo magnético y, por lo tanto, para reducir la EMI. No obstante, los materiales cerámicos convencionales, como el MnZn, generalmente se limitan a la región más alta de los kilohercios hasta la más baja de los megahercios. Otros materiales de núcleo ampliamente utilizados son los basados en composiciones de NiZn, ya que funcionan en un rango de frecuencia de banda ancha, pero generalmente no son efectivos en la región de 2–150 kHz. Los resultados obtenidos por otros componentes EMC, como los choques de modo común basados en composiciones nanocristalinas, han mostrado una efectividad significativa en términos de pérdidas de inserción (*A*) a bajas frecuencias debido a su alta permeabilidad inicial. Por tanto, a partir de estos resultados, se analiza la eficacia de otro componente EMC basado en la composición nanocristalina, concretamente en una muestra de núcleo para la supresión de EMI en cables. La razón principal por la que se estudia el rendimiento del material nanocristalino en este componente, es el elevado volumen de mercado que posee al tratarse de una solución ampliamente utilizada por los diseñadores para cumplir con los requisitos de cumplimiento de EMC.

Esta investigación se lleva a cabo desde el punto de vista del proceso de fabricación, las propiedades magnéticas y la capacidad de supresión de EMI. Este último ítem se lleva a cabo mediante dos procedimientos de análisis: un método teórico mediante la obtención de la capacidad de atenuación de EMI a partir de la impedancia, y proponiendo una nueva técnica experimental basada en la medición directa del parámetro de pérdida de inserción introducido por cada muestra analizada. Por lo tanto, es posible determinar el rendimiento de componentes nanocristalinos en comparación con las composiciones de ferrita de cable convencionales para analizar en qué medida cada uno de ellos es capaz de reducir las interferencias en este controvertido rango de frecuencias.

Los resultados presentados en esta contribución demuestran la idoneidad del prototipo de núcleo basado en una composición nanocristalina en el rango de frecuencia de 2–150 kHz en comparación con los materiales MnZn o NiZn. Existe una coincidencia significativa entre los resultados calculados y experimentales que verifica el método de caracterización experimental propuesto. Por lo tanto, tanto las mediciones teóricas como las experimentales indican que NC proporciona una pérdida de inserción más significativa

a bajas frecuencias que los materiales de MnZn y NiZn como se esperaba a partir del parámetro de permeabilidad relativa. Los resultados presentados demuestran que la nueva solución NC produce un rendimiento significativo en términos de pérdida de inserción en frecuencias superiores a 150 kHz. En consecuencia, esta primera contribución inicia una nueva línea de investigación relacionada con el novedoso estudio de rendimiento del núcleo de la manga NC para reducir la EMI a frecuencias más altas.

Capítulo 4 - Artículo científico II: Effectiveness Assessment of a Nanocrystalline Sleeve Ferrite Core Compared with Ceramic Cores for Reducing Conducted EMI

Este segundo artículo científico presenta el análisis de material nanocristalino en un rango de frecuencia extendido que cubre desde 100 kHz hasta 200 MHz. La efectividad de la supresión de EMI del componente NC se compara con la proporcionada por las soluciones MnZn y NiZn, con el objetivo de determinar las regiones de frecuencia donde cada material es efectivo. La investigación destaca la idoneidad del prototipo de NC en términos de propiedades magnéticas para reducir las EMI dentro del rango de emisiones conducidas. Este rango lo define generalmente el Comité Internacional Especial de Interferencias de Radio (CISPR), la banda de frecuencia de los estándares de prueba que abarca desde 150 kHz hasta 30 MHz (108 MHz en el caso de CISPR 25). En primer lugar, este estudio presenta una descripción de los principales parámetros que definen el comportamiento del NC y de los materiales cerámicos y, en segundo lugar, se analizan los datos obtenidos de los procedimientos experimentales para determinar directamente el parámetro de pérdida de inserción. Por lo tanto, se diseña e implementa un nuevo método de caracterización con el objetivo de obtener el parámetro de pérdida de inserción en un rango de frecuencia considerable asegurando que los efectos parásitos no modifiquen la impedancia del sistema de referencia, especialmente en la región de alta frecuencia (desde 100 MHz).

Cuando se aplica un núcleo alrededor de un conductor, el campo magnético se concentra en flujo magnético dentro del núcleo porque proporciona una permeabilidad magnética más alta que el aire. Como resultado, la corriente de ruido que fluye en el cable se reduce y, por lo tanto, se atenúa la EMI. Los supresores de EMI de núcleos de manguito se aplican ampliamente para reducir las corrientes de modo común en los cables porque, a pesar de no ser las corrientes predominantes, pueden resultar en un potencial de interferencia mucho mayor ya que sólo se requiere que fluyan unos pocos microamperios a través de un cable para no cumplir con los requisitos de emisión radiada. De esta manera, el rango de frecuencias estudiado en esta contribución abarca desde el rango de emisión conducida hasta el rango bajo de emisiones radiadas con el fin de entender cuál es el material más efectivo para reducir las EMI en función de la frecuencia.

La respuesta de la impedancia proporcionada por cada muestra ha sido obtenida matemáticamente a partir de las propiedades magnéticas y, alternativamente, mediante el parámetro de pérdida de inserción medido, con el objetivo de comparar ambos resultados con la medida experimental de la impedancia de cada una de las muestras. Este procedimiento se realiza para analizar la precisión de la medida de impedancia, considerando el procedimiento de calibración propuesto. Se verifica que las tres respuestas coinciden significativamente con el valor de la frecuencia de resonancia, ya que, a partir de este punto, la impedancia calculada a partir de los datos de permeabilidad sigue aumentando, a diferencia de las otras dos trazas.

Capítulo 5 - Artículo de contribución a congreso I: Analysis of different Sleeve Ferrite Cores Performance according to their Dimensions

En esta contribución se analiza la dependencia de la impedancia de diferentes núcleos de tubo con respecto a sus dimensiones. En primer lugar, se han comparado cinco materiales cerámicos con diferentes permeabilidades iniciales (desde 380 hasta 5000) con el nuevo núcleo de NC representando sus trazas de impedancia. Los resultados presentados muestran que NC proporciona la impedancia más alta en todo el rango de frecuencia de 1-500 MHz en comparación con los núcleos cerámicos con la misma dimensión.

La ingeniería de EMC debe abordarse con el enfoque del sistema (*system aproach*), teniendo en cuenta la EMC durante todo el proceso de diseño para evitar posibles problemas de EMI. Durante este proceso, es posible determinar que es necesario blindar un determinado cable, interfaz del sistema. Incluso esto puede decidirse en la etapa de pruebas porque aparece una fuente EMI inesperada cuando el dispositivo diseñado se alimenta a través de un sistema de alimentación externo o está conectado a otro dispositivo para comunicarse con él. La ventaja de utilizar un núcleo supresor de EMI para cables es que no implica rediseñar la electrónica y, en general, el rediseño mecánico. Ésta es una ventaja importante porque determinar en la etapa de testeo, cuál es la fuente de EMI, puede no ser sencillo. Sin embargo, esta solución implica agregar un componente extra cuyos inconvenientes resultan en incrementar el tamaño y peso del producto además del coste del componente y su instalación.

De este modo, en este manuscrito se analiza el comportamiento en términos de impedancia de algunos núcleos de manguitos según su volumen, inductancia y permeabilidad inicial. Siguiendo la ley de Snoek, el núcleo que proporciona la permeabilidad inicial más baja puede producir una permeabilidad más alta en el rango de las emisiones conducidas o radiadas. Como era de esperar, los núcleos cerámicos se han clasificado de acuerdo con la permeabilidad inicial y los materiales con

permeabilidades más bajas funcionan mejor a frecuencias más altas. En el caso del núcleo NC, proporciona el mayor valor de permeabilidad inicial, pero debido a su estructura es capaz de mantener una pendiente de caída lenta que, junto con su permeabilidad inicial extremadamente alta, muestra el mejor desempeño en todo el rango analizado (1-500 MHz).

Se han estudiado las trazas de impedancia de dos pares de núcleos con los mismos volúmenes y composición de material pero que proporcionan trazas de impedancia diferentes. Se observa una diferencia de impedancia entre núcleos con el mismo volumen y composición que demuestra que, considerar únicamente el volumen para seleccionar un componente, no es suficiente para seleccionar un núcleo, ya que un núcleo con volumen reducido puede ser capaz de ofrecer un mayor rendimiento.

Capítulo 5 - Artículo de contribución a congreso II: Determination of Core Size Dependency on the EMI Suppression in Cable Ferrites

En esta contribución se destaca la importancia de encontrar la inductancia de un núcleo de tubo *(L_m)* para determinar su efectividad. Este parámetro es proporcional a la permeabilidad relativa (μ_r) que define principalmente las propiedades magnéticas del núcleo y a las dimensiones del componente. Sin embargo, no existe una relación proporcional entre el volumen de núcleo y su rendimiento, ya que los componentes con menor volumen son capaces de proporcionar una mejor respuesta que otros con mayor volumen.

En este sentido, se realiza un análisis de muestras con diferentes tamaños con el objetivo de determinar la dependencia entre el rendimiento y la inductancia del núcleo. El objetivo principal es obtener un parámetro que relacione estas características con el fin de determinar las dimensiones optimizadas de un núcleo que pueda ofrecer la efectividad necesaria para reducir los problemas de EMI en un cierto cable. En consecuencia, se han caracterizado diferentes núcleos por su respuesta de en términos de impedancia y se han comparado entre ellos para determinar su dependencia del tamaño del núcleo.

En el caso de un núcleo de tubo, se puede considerar un toroide que tiene una sección transversal rectangular con un diámetro interior (*ID*), un diámetro exterior (*OD*) y una altura (*h*) específica. Teniendo en cuenta estos parámetros, para maximizar su impedancia se debe seleccionar la máxima relación *OD*/*ID* y altura mientras que el *ID* sea lo más ajustado posible al diámetro del cable a proteger. Sin embargo, el aumento de las dimensiones suele ser proporcional a su peso, volumen y coste. Por lo tanto, se debe lograr un equilibrio entre estas tres características y el rendimiento. De este modo, debe tenerse

en cuenta que la impedancia es proporcional al logaritmo natural de la relación del diámetro exterior al interior y directamente proporcional a la altura. Aunque *h* es directamente proporcional a la impedancia, el logaritmo natural proporciona un factor de atenuación cuando el *ID* es inferior a 2.7 veces el *OD*, por lo que es crucial no seleccionar núcleos delgados.

Por otro lado, se determina el parámetro *K* que relaciona la impedancia por unidad de inductancia del núcleo (Z_{SC}/L_0) proporcionada por tres muestras con dimensiones diferentes. El parámetro *K* permite calcular la impedancia de una nueva muestra del mismo material y geometría a partir de las nuevas dimensiones del núcleo. Esto se lleva a cabo dividiendo la impedancia medida de una determinada muestra por su inductancia del núcleo de aire (L_0). A continuación, *K* se multiplica por la inductancia del núcleo de aire del nuevo núcleo del manguito. Por lo tanto, es posible optimizar las dimensiones del componente para seleccionarlo con el mínimo volumen, peso y coste.

Capítulo 6 - Artículo científico III: Performance Study of Split Ferrite Cores designed for EMI Suppression on cables

Uno de los principales objetivos de este artículo es analizar las dependencias entre el parámetro de espaciado (*gap*) y el rendimiento en términos de impedancia proporcionada por una variación de la solución de núcleo de tubo para cables basada en un núcleo con abrazadera (*snap ferrite*). Este componente está fabricado por dos partes divididas que se juntan y son presionadas por un mecanismo de abrazadera que lo convierte en una solución rápida y fácil de instalar para reducir los problemas de EMI después del montaje en el cable. El rendimiento de tres materiales diferentes (NC, MnZn y NiZn) se analiza en términos de efectividad de los núcleos partidas. La posibilidad de partir un núcleo NC implica una técnica innovadora debido a la fragilidad de este material. Así, los resultados obtenidos de esta investigación permiten evaluar la efectividad de esta muestra frente a las cerámicas. Esta caracterización se lleva a cabo introduciendo diferentes *gaps* entre las dos partes del núcleo partido y analizando su comportamiento en términos de permeabilidad e impedancia. Los resultados obtenidos experimentalmente se corroboran con los resultados obtenidos mediante un modelo de simulación mediante el método de elementos finitos (FEM) con el objetivo de determinar el rendimiento de cada material cuando se utiliza como *snap ferrite*. Asimismo, se caracteriza la estabilidad de tres núcleos sólidos (no partidos) y núcleos partidos para determinar la influencia de las corrientes DC bias en la respuesta de impedancia proporcionada.

Existe una excelente concordancia entre los resultados simulados y los obtenidos experimentalmente en las trazas de NiZn y MnZn, mientras que hay una diferencia significativa en el caso del NC. Este hecho se correlaciona con las conclusiones obtenidas

a partir de los datos de permeabilidad efectiva de NC en el rango de frecuencia estudiado (1-500 MHz). Esto se debe a que las estructuras internas de NiZn y MnZn pueden considerarse isotrópicas, mientras que este enfoque no puede considerarse en el núcleo de NC. Cuando se parte la muestra de NC la estructura interna se modifica y no es posible estimar el rendimiento de la muestra dividida a partir de las propiedades magnéticas del núcleo sólido original.

4. Conclusiones

El material nanocristalino ha sido estudiado, analizado y evaluado en profundidad en esta tesis doctoral, demostrando ser una alternativa interesante a los materiales cerámicos convencionales, tradicionalmente utilizados para fabricar componentes de supresión de EMI. Además, esta tesis doctoral proporciona una caracterización completa de un núcleo supresor de EMI para cables a través de diferentes métodos de medida experimentales y un modelo de simulación que permite determinar su rendimiento desde el punto de vista de las propiedades magnéticas, la impedancia proporcionada y la pérdida de inserción cuando el componente se introduce en un determinado sistema.

A partir de los métodos descritos en los dos primeros artículos científicos, se concluye que:

- El núcleo de NC muestra una excelente estabilidad de la permeabilidad inicial en comparación con MnZn y NiZn. La permeabilidad inicial de NC permanece en valores superiores al 80%, hasta aproximadamente 150 °C.

- A partir de la a curva de histéresis medida, se observa que el núcleo de NC proporciona la mejor respuesta en términos de saturación magnética de los tres materiales analizados.

- Se describen y caracterizan las limitaciones del método experimental de medida de la impedancia. Es necesario considerar en el procedimiento de calibración el cable introducido en el núcleo para evitar la influencia de su impedancia en la impedancia total proporcionada por el equipo.

- Se presentan dos métodos de medida experimentales para determinar la pérdida de inserción introducida por cada núcleo evaluado. Estas técnicas generan EMI controlado sobre una carga con una impedancia estable a través de un cable caracterizado en el rango de frecuencia estudiado (2–150 kHz y 0,1–200 MHz) para determinar la pérdida de inserción.

- La pérdida de inserción proporcionada por los núcleos testados es significativamente baja en sistemas con una impedancia total cercana a 1000 Ω, incluso cuando se introduce la muestra de NC.

- Cuando las perturbaciones EMI se ubican específicamente en la región de frecuencias bajas, el MnZn representa una solución eficaz, mientras que, si se localizan a partir de 50 MHz, se puede utilizar un núcleo de NiZn. No obstante, si las interferencias EMI se distribuyen fuera de estas regiones o desde la región de baja frecuencia hasta aproximadamente 100 MHz, el núcleo de NC muestra un mejor rendimiento que los núcleos cerámicos para reducir las emisiones EMI en un rango de frecuencia de banda ancha.

Después de los resultados optimistas mostrados por el nuevo material NC y los métodos de medida experimentales implementados, los esfuerzos de investigación asociados con esta tesis doctoral se orientaron a estudiar el comportamiento de diferentes núcleos de tubo con respecto a sus dimensiones. En este sentido, primero se ha analizado el parámetro dimensional que define un núcleo, posteriormente, se determina el parámetro *K* que permite a un diseñador obtener el tamaño de un núcleo para proporcionar la impedancia necesaria para atenuar una determinada perturbación EMI. Por tanto, es posible optimizar las dimensiones del componente para seleccionarlo con el mínimo volumen, peso y coste. De los resultados presentados en las dos contribuciones a congresos, se han obtenido a las siguientes conclusiones:

- Los resultados presentados al comparar cinco materiales cerámicos con diferentes permeabilidades iniciales desde 380 hasta 5000 con el nuevo núcleo NC (μ_i = 90,000) muestran que, considerando muestras con exactamente las mismas dimensiones, NC proporciona la impedancia más alta en todo el rango de frecuencia estudiado (1-500 MHz).

- Se observa una diferencia de impedancia entre núcleos con el mismo volumen y composición que demuestra que sólo conociendo el volumen no es suficiente para seleccionar un núcleo, ya que un núcleo con bajo volumen puede proporcionar un mayor rendimiento.

- Es posible encontrar núcleos con la misma composición de material que producen la misma respuesta de impedancia pero con diferentes volúmenes. Este enfoque puede llevar a seleccionar, además del material del núcleo con el mejor rendimiento para atenuar la EMI en una frecuencia específica, el núcleo que proporciona la impedancia máxima con el volumen mínimo.

- Es interesante seleccionar la relación máxima de diámetro exterior / diámetro interno y la máxima altura al mismo tiempo que el diámetro interno es lo más ajustado posible al diámetro del cable para maximizar la impedancia de un núcleo de manguito. La impedancia es proporcional al logaritmo natural de la relación entre el diámetro exterior y el interior y directamente proporcional a la altura. Aunque h es directamente proporcional a la impedancia, el logaritmo natural proporciona un factor de atenuación cuando el *ID* es inferior a 2.7 veces el *OD*, por lo que es importante no seleccionar núcleos delgados.

- El parámetro *K* relaciona la impedancia por unidad de inductancia del núcleo, lo que permite calcular la impedancia de una nueva muestra basada en el mismo material y geometría a partir de las nuevas dimensiones del núcleo. Esta impedancia teórica se ha comparado con la obtenida experimentalmente y se obtiene una coincidencia significativa entre ambos datos.

Finalmente, las conclusiones obtenidas en las contribuciones previas fueron validadas mediante un modelo de simulación FEM. El modelo de simulación permite determinar la pérdida de inserción y la respuesta de impedancia proporcionada por un núcleo supresor de EMI para cables definido por sus propiedades magnéticas y dimensiones. Además, se estudian las dependencias entre el parámetro *gap* y el rendimiento en términos de impedancia proporcionada por los núcleos partidos basados en los tres materiales evaluados en esta tesis doctoral. De este modo, el rendimiento de estos componentes se analiza en términos de eficacia cuando los núcleos se parten. Por lo tanto, los principales hallazgos de este capítulo se resumen en las siguientes conclusiones:

Existe una excelente concordancia entre los resultados simulados y los obtenidos experimentalmente en las trazas de NiZn y MnZn, mientras que hay una diferencia significativa en el caso NC. Esto se debe a que las estructuras centrales de NiZn y MnZn pueden considerarse isotrópicas, mientras que este enfoque no puede considerarse en el núcleo NC. Cuando se divide la muestra NC, la estructura interna se modifica y no es posible estimar el rendimiento de la muestra dividida a partir de las propiedades magnéticas del núcleo sólido original.

- Se han modificado los parámetros magnéticos del modelo de simulación del material NC para obtener una respuesta más cercana a los valores obtenidos de forma experimental. Por lo tanto, el modelo se ha simulado considerando tres situaciones diferentes: sin núcleo dividido para la muestra original, núcleo partido sin introducir *gap* (situación *g0*) y núcleo partido con diferentes *gaps* (situaciones *g1*, *g2* y *g3*). Estos nuevos resultados simulados coinciden significativamente con las trazas experimentales.

- Cuando las muestras se dividen y unen sin introducir ningún *gap* (situación *g0*), la impedancia producida por la muestra de NiZn se degrada menos que las impedancias de MnZn y NC. En este caso de estudio, MnZn ofrece el mejor comportamiento en el rango de frecuencia baja y media, mientras que la muestra NC ofrece un rendimiento inferior al esperado debido a su diferente estructura interna.

- Cuando se consideran *gaps* más elevados, NiZn muestra la solución más efectiva en términos de permeabilidad e impedancia. La eficacia del núcleo de MnZn también se ha reducido, pero en menor medida que la muestra nanocristalina.

- NiZn es el material con propiedades más estables y capaz de proporcionar un mayor rendimiento y un comportamiento más predecible que aquellos con propiedades magnéticas más significativas cuando el núcleo se divide. Esta conclusión también se aplica cuando las corrientes de DC bias fluyen a través del cable a proteger.

Las conclusiones extraídas de esta investigación destacan la idoneidad y el excelente rendimiento del núcleo basado en material nanocristalino para reducir interferencias electromagnéticas en cables, considerando una amplia región de frecuencia. Esta es una de las razones por las que la empresa Würth Elektronik comenzó a comercializar una gama de núcleos supresores de EMI de material nanocristalino a finales del año pasado. Esta nueva gama de productos ha sido designada como WE-AENA Axial EMI Suppression Nanocrystalline, ofreciendo nueve núcleos toroidales y de tubo con diferentes dimensiones.

Abstract

The ideal procedure to start designing an electronic device is to consider the Electromagnetic Compatibility (EMC) from the beginning. Even so, EMC problems can appear afterward, especially when the designed system is interconnected to external devices. Thereby, Electromagnetic Interferences (EMI) could be transmitted to our device from power cables that interconnect it with an external power source or when it is connected to another system to establish a wired communication. When the cables represent the EMI source, which implies failing the conducted or radiated emissions test, a widely used technique is applying an EMI suppressor such as a sleeve core. The integration of this kind of component can involve an extra cost in terms of the production of the system. Nevertheless, this situation are usually compensated by the effectiveness of sleeve cores to filter interferences without having to redesign the electronic circuit. This is one of the main reasons designers extensively use this EMI suppression solution to meet EMC compliance requirements.

The most used EMI suppressors cores for filtering applications are based on ceramic materials (also known as polycrystalline materials or soft ferrites). One of the conventional ceramic materials most used is MnZn that is intended to reduce EMI in the frequency range from the higher Kilohertz to the very low Megahertz region. Other widely used core materials are those based on NiZn compositions since they work in a broadband frequency range. Nevertheless, conventional materials used to manufacture sleeve core EMI suppressors are focused on reducing disturbances in cables in a specific frequency region. Consequently, new materials that can provide a more significant EMI suppression had to be studied to ensure electromagnetic compatibility in those frequency regions not specifically covered by traditional solutions. The results obtained by other EMC components, such as the common-mode-chokes based on nanocrystalline compositions, have shown significant effectiveness in terms of insertion loss in a wide frequency range because of their high initial permeability. From the preliminary results and features offered by the nanocrystalline material, this Ph.D. study focuses on carrying out a thorough characterization of the performance of sleeve EMI suppressor components based on nanocrystalline material.

Thereby, the overall aim of the present doctoral thesis is studying, analyzing and evaluating the nanocrystalline material suitability to manufacture sleeve core EMI suppressor to reduce the interferences in cables as an alternative to conventional ceramic materials, traditionally used to produce EMC components. This research is carried out by designing and implementing a measurement setup method that makes it possible to determine the insertion loss parameter provided by a specific sleeve core when applied to a cable that interconnects two systems with a specific impedance. These results are

correlated with a finite element method (FEM) simulation model that makes it possible to evaluate the accuracy of the experimental data and evaluate different sleeve core samples by introducing their magnetic properties and dimensional parameters.

Finally, samples with different sizes are analyzed with the aim of determining the dependency between performance and component volume. The increase of the dimensions is usually proportional to its weight, volume and cost, thus a balance between these three features and performance should be carried out. The goal is to obtain a parameter that relates these features in order to determine the optimized dimensions of a sleeve core that can provide the effectiveness necessary to reduce a specific level of EMI in a cable.

Keywords: electromagnetic interference (EMI) suppressors, electromagnetic compatibility (EMC), nanocrystalline (NC), ceramic materials, cable filtering, finite element method (FEM) simulation, relative permeability, impedance, insertion loss.

Acknowledgements

This Thesis reflects the result of a great effort made by many people who make up and collaborate with the EMC WE - UV Chair. Thank you very much for the support and encouragement of all since you have contributed to the result presented in this work.

First, I want to thank my Ph.D. supervisor, Prof. José Torres, for his dedication, efforts, and countless pieces of advice that he has given me along the way. He allowed me to discover the world of research, transmitting to me his vocation, first as a Professor and next as a tutor for the Final Master's Thesis and this Ph.D. Thesis. José trusted me from the first moment and he has always helped me achieve the goals that I have set. It has been a long road that has sometimes been complicated, but I want to thank him that he has always tried to motivate and encourage me so that this work could go forward.

I want to make a special mention to Jorge Victoria for the trust he has placed in me, for being my mentor, for showing me some of the secrets that EMC hides, and for his work and effort to maintain, together with José, the Catedra EMC active for all these years. I also want to thank Würth Elektronik for trusting the University of Valencia to establish a Catedra and give us the opportunity to research in the field of Electromagnetic Compatibility, especially Steffen Muetsch for promoting and supporting this project.

This acknowledgment is also addressed to the DSDC Group's family (Jesús, Julio, Rai, Joaquín, Abraham y Nordin) for their continuous support and advice that has been constant in each of the different phases of the research and supporting me in my other vocation, teaching. I want to highlight Pedro's support, his technical and personal help, and those endless talks from which we have drawn so many conclusions and new ideas. Thanks also to the Shielding and Thermal team of Würth Elektronik, especially Antonio and Víctor, for all the hours in the lab and all the good times we have had. I also want to mention in this section the members and friends of the IEEE Student Branch of the ETSE-UV, especially Dani, Sebas, Isma, and Rafa, with whom I have shared so many experiences and fun times.

Finally, I want to thank all my family and friends for their support for taking an interest in the evolution of the Thesis. Especially to my parents and my sister for always being by my side, listening to me, advising me, and encouraging me in difficult times. Of course, a thousand thanks to my wife, Isa, because she has done a doctorate in patience and understanding. She has always motivated me to keep going, finish this long road, and have helped me to disconnect in times of stress with her happiness and fun.

Agradecimientos

Esta Tesis refleja el resultado de un gran esfuerzo realizado por un gran número de persona que componen y colaboran con la Cátedra EMC WE – UV. Muchas gracias por el apoyo y ánimo de todos, ya que habéis contribuido al resultado que se presenta en esta memoria.

En primer lugar, quiero agradecer a mi tutor de Tesis, el Prof. José Torres, toda su dedicación, esfuerzo e innumerables consejos que ha ido dándome a lo largo de todo el camino. Él me dio la oportunidad de entrar en el mundo de la investigación, contagiándome su vocación, primero como Profesor y, seguidamente, como tutor del Trabajo Fin de Máster y de la presente Tesis. José confió desde el primer momento en mí y me ha ayudado siempre a conseguir los objetivos que me he propuesto. Ha sido un largo camino que en ocasiones se ha complicado, pero quiero agradecerle que siempre haya tratado de motivarme y animarme para que este trabajo pudiera salir adelante.

Quiero hacer una mención especial a Jorge Victoria por la confianza que ha depositado en mí, por ser mi mentor y por mostrarme algunos de los secretos que esconde la EMC y por su trabajo y esfuerzo por mantener, junto con José, el marco de la Cátedra EMC activo durante todos estos años. También quiero agradecer a Würth Elektronik que haya confiado en la Universitat de València para establecer una Cátedra y darnos la oportunidad de investigar en el campo de la Compatibilidad Electromagnética, especialmente, a Steffen Muetsch por impulsar este proyecto.

Este agradecimiento también va dirigido a la familia del Grupo DSDC (Jesús, Julio, Rai, Joaquín, Abraham y Nordin), por su respaldo continuo y consejos que han sido constantes en cada una de las diferentes fases de la investigación y apoyarme en mi otra vocación, la docencia. Quiero destacar el respaldo de Pedro, su apoyo en lo técnico y lo personal y por esas infinitas charlas de las que tantas conclusiones y nuevas ideas hemos extraído. Dar las gracias también al equipo de Shielding y Thermal de Würth Elektronik, especialmente a Antonio y Víctor, por todas las horas de laboratorio y todos los buenos momentos que hemos pasado. También quiero hacer mención en este apartado a los miembros y amigos de la Rama IEEE de Estudiantes de la ETSE-UV, especialmente a Dani, Sebas, Isma y Rafa, con los que he compartido tantas experiencias y ratos divertidos.

Por último, quiero agradecer a toda mi familia y amigos el apoyo por interesarse por la evolución de la Tesis. Especialmente, a mis padres y a mi hermana por estar siempre a mi lado, escuchándome, aconsejándome y animándome en los momentos difíciles. Y, por supuesto, dar mil gracias a mi mujer, Isa, porque ella ha realizado un doctorado en paciencia y comprensión, siempre me ha motivado para seguir adelante, a terminar este largo camino y me ha ayudado a desconectar en los momentos de agobio con su optimismo y alegría.

Table of contents

List of figures

Chapter 1. INTRODUCTION

This introductory chapter sets out the context and unresolved challenges of the research topic covered in this doctoral thesis. Thereby, the initial hypothesis and the expected achievements in the objectives of the thesis are presented.

1.1 Research context and motivation

The control of electromagnetic interferences (EMI) in electronic devices is an increasing issue faced by designers in order to ensure that devices comply with electromagnetic compatibility (EMC) requirements to operate simultaneously without inferring with each other. This fact is due to the trends towards higher component integration, printed circuit board (PCB) size and thickness reduction, and the miniaturization of the device housings. Besides, other factors such as higher switching frequencies in power converters and communication data rates in digital circuits could lead to producing EMI problems. Consequently, EMC engineering should be handled with the system approach, considering EMC throughout the design process to prevent possible EMI problems that could degrade device performance. Therefore, adopting specific solutions as early as possible in the design stage to meet the EMC requirements is of primary importance to reduce penalties from the standpoint of costs, time-to-market, and performance. The EMC testing process can reveal that the protection of a certain cable is needed or may even detect an unexpected EMI source when the designed device is connected to external modules such as a power supply or to another device to communicate with it. When the cables represent the EMI source, which implies failing the conducted or radiated emissions test, a widely used technique is applying an EMI suppressor such as a sleeve core.

The sleeve core effectiveness to reduce EMI in cables is defined by its capability to increase the flux density of a specific field strength created around a conductor. The presence of noise current in a conductor generates an undesired magnetic field around it that can result in EMI problems. When a sleeve core is applied in the conductor, the magnetic field is concentrated into magnetic flux inside the core because it provides a higher magnetic permeability than air. Thereby, the sleeve core is effective in reducing both conducted and radiated EMI emissions.

This component represents a solution when the cables turn into an EMI source. It can be applied to peripheral and communication cables such as multiconductor USB or video cables to prevent interferences that could be propagated along the wire affecting the interconnected devices. This component is also widely used to reduce high-frequency oscillations caused by the increasingly fast switching in power inverters and converters with cables attached without scarifying the switching speed and increasing the power loss. Therefore, selecting the proper sleeve core makes it possible to reduce the switching noise by increasing the propagation path impedance in the desired frequency range. The application of sleeve cores is a widely used technique to reduce EMI in cables, despite the drawbacks that the integration of an extra component can involve in terms of cost and production of the system. Nevertheless, these drawbacks are usually compensated by the effectiveness of cable ferrites to filter interferences without having to redesign the electronic circuit. This is one of the main reasons designers extensively use this EMI suppression solution to meet EMC compliance requirements.

Conventionally, the most used ferrite cores for filtering applications are based on ceramic materials (also known as polycrystalline materials or soft ferrites). Although they do not belong to the metals group, the starting material of ceramics is iron oxide Fe_2O_3 mixed with one or more divalent transition metals, such as manganese, zinc, nickel, cobalt, or magnesium. Moreover, an interesting advantage of ceramic materials is the possibility of manufacturing components with many different shapes and dimensions. One of the conventional ceramic materials most used is MnZn that is intended to reduce EMI in the frequency range from the higher Kilohertz to the very low Megahertz region. Other widely used core materials are those based on NiZn compositions since they work in a broadband frequency range.

Nevertheless, conventional materials used to manufacture sleeve core EMI suppressors are focused on reducing disturbances in cables in a specific frequency region. Consequently, new materials that can provide significant EMI suppression had to be studied to ensure electromagnetic compatibility in those frequency regions not specifically covered by traditional solutions. The results obtained by other EMC components, such as the common-mode-chokes based on nanocrystalline compositions, have shown significant effectiveness in terms of insertion loss in a wide frequency range because of their high initial permeability.

From the preliminary results and features offered by the nanocrystalline material, this Ph.D. study focuses on investigating if sleeve EMI suppressor components based on nanocrystalline material is capable of providing greater performance in reducing interferences, compared to conventional ceramic materials. Thereby, unresolved questions emerged the hypothesis that triggered the focus of this research: Could a sleeve

core component based on nanocrystalline material provide greater effectiveness to reduce the influence of EMI on cables than conventional materials?

1.2 Research objectives

Considering the research context and motivation above defined, the overall aim of the present doctoral thesis is defined as follows:

To study, analyze and evaluate the nanocrystalline material suitability to manufacture sleeve core EMI suppressor to reduce the interferences in cables as an alternative to conventional ceramic materials, traditionally used to produce EMC components.

The following specific objectives (S.O.) are proposed and investigated throughout this doctoral study to achieve the general goal:

- S.O.1: Study and evaluation of the new sleeve core prototypes based on the novel nanocrystalline material to reduce supraharmonics in the 2–150 kHz frequency range and EMI problems into the conducted and radiated region (up to 500 MHz).

- S.O.2: Determine the performance of nanocrystalline compared to conventional cable ferrite compositions to reduce the EMI in cables. Analyze the performance in terms of the magnetic properties, impedance provided and insertion loss introduced in order to define the frequency regions where nanocrystalline is more effective than MnZn and NiZn ceramic cores.

- S.O.3: Design and implement a measurement setup method that makes it possible to determine the insertion loss parameter provided by a specific sleeve core when applied to a cable that interconnects two systems with a specific impedance.

- S.O.4: Optimize the selection of a sleeve core EMI suppressor by considering its dimensions. Study the parameters that relate the impedance provided by a sleeve core with its dimensions to obtain the dependency between them. This connection allows a designer to determine the EMI attenuation needed to select the optimized dimensions of the component with the minimum volume, weight, and cost.

- S.O.5: Design a simulation model that makes it possible to correlate the results obtained from the experimental measurement setup developed to obtain a sleeve core EMI suppressor's performance.

- S.O.6: Determine the effectiveness of a new prototype nanocrystalline sample based on a split core. This sample makes it possible to study a nanocrystalline

sample's performance compared to MnZn and NiZn components when employed as a snap-on core.

1.3 Thesis structure

This doctoral thesis is organized into seven chapters covering the evolution of the implemented research work. The main body comprises a collection of three peer-reviewed scientific articles and two peer-reviewed scientific conference articles that address the research objectives listed in Section 1.2.

Chapter 1 introduces the overall context, motivation, and objectives of this research topic, together with a description of its structure.

Chapter 2 provides a summary of the theoretical background and literature review for providing the basis on which this Ph.D. study has been developed. These fundamentals firstly cover a brief overview of the problems derived from Electromagnetic Interference Phenomena and the description of sleeve core EMI suppressors as a solution to reduce these problems. Subsequently, the characterization of these components from the standpoint of the magnetic properties, impedance, and insertion loss. The methods described are intended to characterize, specifically, the novel nanocrystalline when used to manufacture sleeve core EMI suppressors by comparing it with conventional ceramic materials.

Chapter 3 focuses on the study of the characterization methodologies for sleeve core EMI suppressors from the standpoint of the magnetic properties. As a preliminary assessment, the characterization methods described in the literature have been carried out to experimentally determine the magnetic properties such as relative permeability, Curie temperature, and B-H loop. The performance of the novel prototype of nanocrystalline sleeve core is compared to conventional ceramic materials. The characterization of the three different sleeve core solutions to reduce in terms of impedance and insertion loss performance is carried out in the 2–150 kHz frequency range. This is a critical frequency spectral due to interferences generated by a wide range of devices and, specifically, communication problems in the new technologies and devices incorporated into the traditional grid to convert it into a Smart Grid.

Chapter 4 presents a description of the main parameters that define nanocrystalline and ceramic materials' behavior. A new characterization setup is implemented with the aim of obtaining the insertion loss parameter in a considerable frequency range ensuring that the parasitic effects do not modify the reference system impedance, especially in the high-frequency region (from 100 MHz). These results make it possible to determine the impedance provided and compare it with the results obtained from directly measured impedance and the impedance determined from the magnetic properties of each material.

Thereby, the frequency range studied covers from conducted emission range to the low range of radiated emissions in order to understand which is the most effective material to reduce them depending on the frequency.

Chapter 5 covers the study of different sleeve cores based on the same material composition with the aim of determining the core size dependency in terms of the EMI suppression. The results presented show the relation between core inductance, dimensions and impedance as well as how to determine the optimum core size. Consequently, different sleeve cores have been characterized by their impedance response and compared between them in order to determine their core size dependency.

Chapter 6 corresponds to the characterization of a variation of this cable filtering solution based on openable core clamp or snap ferrites. This component is manufactured by two split parts pressed together by a snap-on mechanism that turns this into an easy to install quick solution for reducing post-cable assembly EMI problems. The results obtained experimentally are corroborated with the results obtained by a finite element method (FEM) simulation model that corroborates the accuracy of the experimental measurement setup results.

Chapter 7 summarizes the general and specific conclusions drawn from this doctoral thesis. In addition, this chapter identifies possible lines for future research in order to continue the research work presented in this thesis.

1.4 Thesis framework

The present doctoral thesis summarizes its author's research efforts, during the period 2014-2021, as a member of the Digital Systems and Communications Design (DSDC) Group in the Electronic Engineering Department of the University of Valencia (Universitat de València).

Specifically, this doctoral study has been carried out within the Catedra EMC WE-UV framework, representing a collaboration agreement between the University of Valencia and the company Würth Elektronik eiSos. The Catedra EMC is a wide and long-term academic collaboration, which reaches one or more areas of knowledge and extends its activities to all the areas of the university activity:

- Teaching and dissemination of science, technology, and culture.
- Training and attraction of talent.
- Research and Innovation.

Thereby, this Ph.D. study is covered by the Research and Innovation area of the Catedra. It has been supported by the company's expertise and university experts, as well as their installations, materials, and laboratory resources. In this context, the author has

carried out an appropriate amount of state-of-the-art developments, including magnetic materials analysis, instrumentation and calibration, mechanical designs, design and development of sleeve cores characterization setups, laboratory and field experiments, advanced data analysis, and finite element method based numerical simulations.

Throughout these research experiences, the author has presented and discussed the research work's status and prepared working plans to carry out some of the experiments derived in the publications appended to this thesis.

Chapter 2. BACKGROUND

This chapter introduces the theoretical background and literature review for providing the basis on which this Ph.D. study has been developed. These fundamentals firstly cover a brief overview of the problems derived from Electromagnetic Interference Phenomena and the description of sleeve core EMI suppressors as a solution to reduce these problems. Subsequently, the characterization of these components from the standpoint of the magnetic properties, impedance, and insertion loss. The methods described are intended to characterize the novel Nanocrystalline when used to manufacture sleeve core EMI suppressors by comparing it with conventional ceramic materials. The results obtained with the presented methods will allow obtaining sufficient information to answer all the unknowns regarding the nanocrystalline material's performance as an EMI suppressor.

2.1 Brief overview

2.1.1 Electromagnetic interference phenomena

Electromagnetic interference can be defined as electromagnetic signals that unintentionally disturb an electrical or electronic system's normal operation. These perturbances can affect the electrical or magnetic magnitudes (voltage, current or electromagnetic field) of its circuits, even if they do not reach their effects be appreciated externally.

The problem of interferences is an issue that design engineers continually face [1]. Electromagnetic interferences can cause different kinds of problems in digital and analog systems, leading to malfunctions, system reboots, or even permanent damage to the system if the system is not properly designed or protected [2]. The security of an electronic system where there are devices that produce electromagnetic disturbances and elements or small-signal circuits, sensitive to such disturbances, depends on the compatibility of the signal levels used. Thereby, it is convenient to comply with specific design and installation rules that make it possible to make the disturbance levels generated by the interferences source elements compatible with the signal levels used by the possible victim elements or elements sensitive to such interferences [3].

Some standards establish the maximum limits of interferences to ensure that the equipment is compatible and does not interfere. Thus, electromagnetic compatibility is the ability of a system to operate satisfactorily in its electromagnetic environment without introducing disturbances above the normalized limits in that environment and withstanding those produced by other equipment. Electromagnetic compatibility is regulated by standards that require compliance with the limits of electromagnetic interferences in electronic systems by studying all the phenomena of generation, propagation, and susceptibility to electromagnetic interferences. In order to comply with these regulations applied to electronic equipment, it is necessary to carry out measurements to certify that this equipment complies with regulations.

When analyzing an EMI problem, the following elements should be identified (see Figure 2.1): the source of interferences, the propagation path, and receivers affected by the interferences. Based on this concept, when a designer faces an EMI problem, he/she must analyze the system, identify these three elements, and deal with interferences applying these strategies: eliminate EMI sources, increase the EMI immunity of the victim element and/or decrease the energy transmitted through the propagation path.

Figure 2.1. Main elements in electromagnetic interference phenomena.

2.1.2 Propagation and coupling of electromagnetic interference

EMI can spread through different means or paths, as shown in Figure 2.2, so they can be grouped into:

- Conducted interference: when the propagation path is an electrical conductor that joins the sources with the affected receiver such as power cables, signal cables, metal chassis...
- Radiated interferences: they can be classified as far- or near-field depending on the propagation's wavelength and the distance between the source and victim elements. Radiated far-field interferences are identified when carried out through electromagnetic fields, fulfilling the following condition: propagation distance > wavelength / 2π. Radiated near-field interferences are called coupling and can be identified as inductive coupling or capacitive coupling between neighboring conductors, depending on whether the interference is propagated by a magnetic or electric field, respectively.

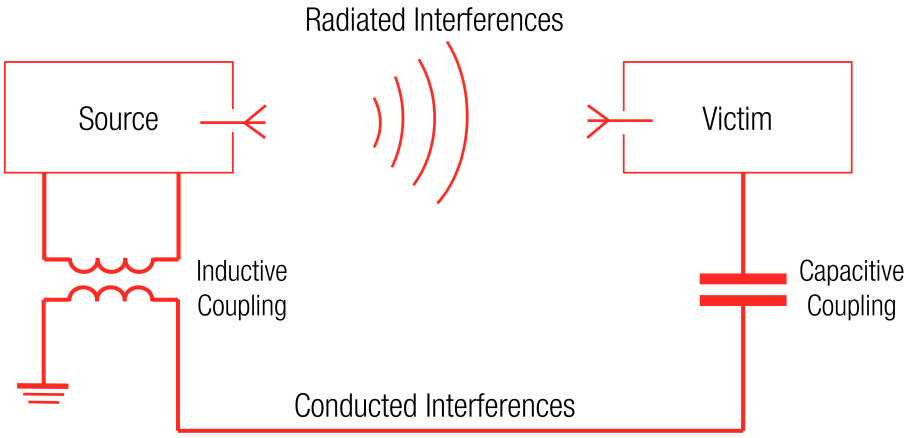

Figure 2.2. Kind of propagation and coupling of electromagnetic interference.

The most appropriate strategy is to consider electromagnetic compatibility during the system design stage since, if EMC is ignored until the problem arises during the first functional tests or product certification, the solutions usually result in a higher cost [4]. The possibility of applying specific techniques for the elimination of interferences is reduced as a system is developed. At the same time, the cost of EMI reduction increases [5]. However, it is not always possible to predict EMI problems during the design stage because it is complicated to emulate the real environment in which the system will work. Another possibility is that the designed system complies with the standards, but the problems appear when interconnected with other equipment or facilities. When this situation occurs, the right approach is to suppress EMI at its source whenever possible, rather than increasing immunity through victim circuit protections. This technique works best since a single EMI source can find multiple paths of spread and affect different victims. If it is not possible to act directly on the source, it is recommended to focus on the EMI propagation path or, finally, on the affected receiver.

Detection and correct characterization of the EMI is an essential factor in designing a suitable solution. Thus, it is essential to perform EMI measurements using different instrumentation, measuring probes and antennas to detect the electromagnetic fields that can provide information to the designer from undesired signals. From these measurements, it will be possible to detect the magnitude of the disturbances and in which frequency range the problems are located to select the most optimal solution.

2.1.3 Applications of EMI suppressor sleeve cores

The Magnetic Field (*H*) is associated with electrodynamic phenomena and appears whenever there are electric currents. The *H* field can produce effects capable of seriously

disturbing the operation of an electronic circuit. Whenever current flows in a circuit, this current creates a magnetic field in that circuit, which will vary as the current varies. Consequently, in any circuit that carries an alternating current, variations of magnetic flux occur. According to Lenz's law, an electromotive force will be induced by the field variation. Therefore, if the current is constant, there will be no induced electromotive force.

Considering that the flux density (*B*) is proportional to the product of the permeability of the medium and the incident *H* field, *B* is the result of the action of *H* in a magnetic circuit, and its intensity will be higher or lower depending on the permeability of the matter (μ_r). For the shielding of conductors against EMI, the most common is to use ferromagnetic materials since they present a permeability much higher than that of vacuum (μ_0).

When introducing the sample, the external field deforms considerably, being, at each point, the resultant of the initial magnetic field and the field created by the orientation of the magnetic domains. As shown in **Figure 2.3**, the material concentrates the field lines and regions outside and close to the material, reducing the emitted field.

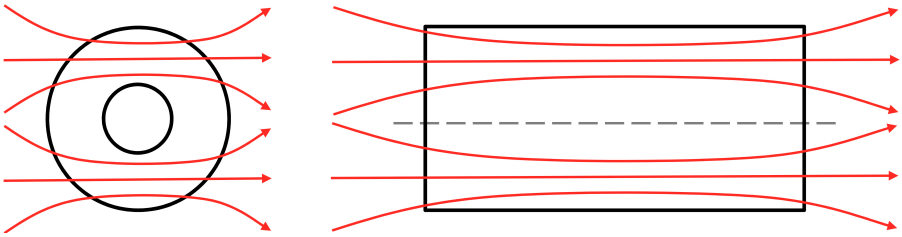

Figure 2.3. Management of H field through introducing a sleeve core.

As explained above, unexpected EMI sources in cables can appear in our system when connected to another device. One of the most used techniques for reducing interferences in cables is applying an EMI suppressor such as sleeve cores to them. This EMI suppressor provides selective attenuation of undesired interference components that the designer may wish to suppress and it does not affect the intended signal. Thereby, this component is widely used to filter EMI in power cables to reduce high-frequency oscillations generated by switching transients or parasitic resonances within a circuit, and EMI in peripheral cables of electronic devices such as multiconductor USB or video cables.

From the standpoint of the magnetic properties, a sleeve core is defined by the relative permeability since it is the main parameter that describes the performance of a specific magnetic material to concentrate the magnetic flux in the core. This parameter is

generally expressed through its complex form represented by the real component (μ') that quantifies the real or inductive part and the imaginary or resistive component (μ'') that is related to the material ability to absorb the electromagnetic interferences [6,7].

Currents that flow in cables (with two or more conductors) can be divided into differential mode (DM) and common mode (CM) depending on the directions of propagation. Although DM currents are usually significantly higher than CM currents, one of the most common EMI radiated problems is originated by CM currents flowing through the cables of the system [8]. CM currents have a much greater interfering potential, despite not having a high value. This fact is due to only a few microamps are required to flow through a cable to fail radiated emission requirements [5,9]. The use of sleeve cores is an efficient solution to filter the CM currents in cables because, if a pair of adjacent conductors is considered, when the core is placed over both signal and ground wires, the CM noise is reduced. As shown in Figure 2.4, the CM currents in both wires flow in the same direction, so the two magnetic fluxes in the sleeve core are added together, and the filtering action occurs in the sleeve core. The intended (DM) current is not affected by the presence of the sleeve core because the DM current travels in opposite directions and is transmitted through the signal and returns. Thus, the current of the two conductors is opposing, meaning they cancel out and the sleeve core has no effect [10]. In the case of wanting to filter the DM currents, it would be necessary to use a sleeve core in each of the conductors of the cable.

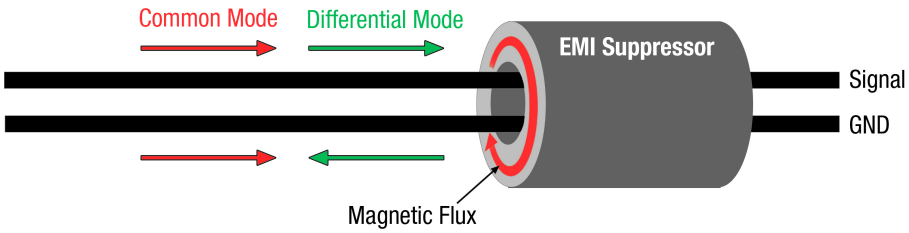

Figure 2.4. Diagram of CM and DM currents passing through a sleeve core with two adjacent conductors (signal and return paths).

An external power supply (Figure 2.5) can be considered a specific example of the application of sleeve cores to reduce EMI in terms of both radiated and conducted emissions. Within the conducted emission range (150 kHz – 30 MHz), the conductors of the system are generally too short to be considered an EMI antenna source since the impedance of possible parasitic inductors is low, and the impedance of parasitic capacitors is typically high. Nevertheless, in the radiated emissions range (from 30 MHz), the parasitic associated with conductors and power line EMI filters can be significant if conductors are long enough to be considered an unintended antenna [11].

External power supplies typically incorporate discrete inductors, capacitors in the AC input circuitry to implement common mode, and differential mode filters before the input bridge and the switching stage. This filtering stage's main objective is to attenuate the interferences that can be conducted out from the power supply to the AC input power lines. Accordingly, the internal PCB is designed to hold these filtering components in order to pass regulatory safety and EMC testing. When these techniques are considered, a power supply design may meet conducted and radiated emission requirements when tested in isolation. Nevertheless, when the power supply is added to a complete system, the system may fail emissions testing due to the interferences emitted from the system load to the designed power supply through the DC output cable back. One of the most common solutions to solve this EMI problem is integrating a sleeve core that reduces the undesired interferences without affecting the DC intended signal.

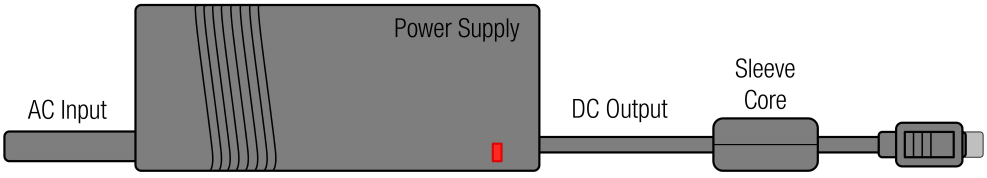

Figure 2.5. Diagram of an external power supply elements.

The advantage of using this EMI solution is that it does not involve redesign the electronics and, generally, the mechanical redesign. This is an essential advantage because determining in the testing stage, which is the EMI source, may not be straightforward. However, using a sleeve core involves adding an extra component whose drawbacks result in increasing the product's size and weight besides the cost of the filtering component and its installation. Therefore, this is an effective solution to attenuate EMI emissions in cables when it is not possible to solve the problem through a system redesign, but it is essential to strike a balance between performance and other factors such as weight, dimensions, and cost [12].

2.2 Properties of the cores' materials

Sleeve cores are manufactured with magnetic material that allows them to control interferences in a certain frequency range with a specific ratio. The values of these two parameters mainly depend on the EMI suppressor intrinsic composition and internal structure. Conventionally, the most used ferrite cores for filtering applications are based on ceramic materials (also known as polycrystalline materials or soft ferrites). Although they do not belong to the metals group, the starting material of ceramics is iron oxide Fe_2O_3 mixed with one or more divalent transition metals, such as manganese, zinc, nickel, cobalt, or magnesium [13]. The most common combinations are manganese and zinc (MnZn) or nickel and zinc (NiZn) due to their heat resistance, stability over a wide

temperature range, hardness, and high resistance to pressure [14]. It is possible to obtain samples that provide initial permeabilities of the order of 1000–20,000 and provide a low resistivity (0.1–100 Ω·m) based on MnZn material. For this material, the range of frequency for EMI suppression applications covers from hundreds of kilohertz to some megahertz. Regarding NiZn material, this provides initial permeabilities of the order of 100–2000 so that it is intended for a higher frequency operation than MnZn, covering from tens of megahertz up to several hundreds of megahertz. In terms of resistivity, NiZn material reaches high values (about 104–106 Ω·m) [14–16]. Moreover, an interesting advantage of ceramic materials is the possibility of manufacturing components with many different shapes and dimensions [14,17].

The manufacturing procedure can be divide into the steps presented in Figure 2.6. First, the base materials are weighted into the desired proportions and wet mixed in ball mills to obtain a uniform distribution and particle size. Next, the water is removed in a filter press, and the ferrite is loosely pressed into blocks and dried. It is then pre-fired (calcined) at about 1000°C to form the ferrite. The pre-sintered material is then milled to obtain a specific particle size. Subsequently, the dry powder is mixed with an organic binder and lubricants before being shaped by a pressing technique to obtain the final form. Finally, the resultant green core is subjected to a heating and cooling cycle, reaching temperatures higher than 1150°C, promoting any unreacted oxides to be formed into ferrite. The manufacturing procedure and the material mix are essential to define a ceramic core's magnetic properties [13,15,16,18].

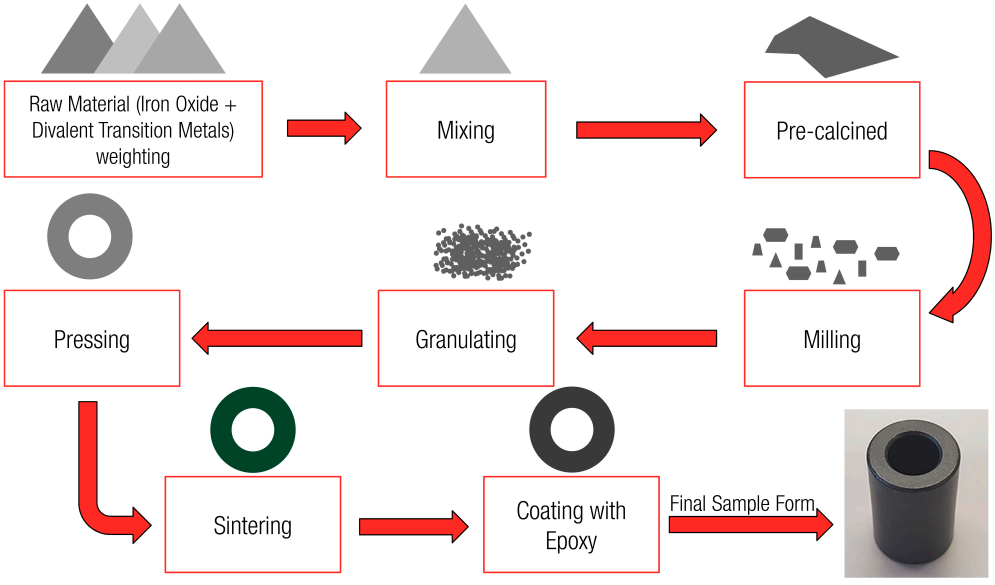

Figure 2.6. Diagram of the manufacturing procedure of ceramic cores.

Besides the EMI suppressors based on ceramic materials, it is possible to use an innovative material based on a nanocrystalline (NC) structure. NC sleeve core represents an innovative and increasingly used solution for EMI suppression in cables which has demonstrated excellent magnetic properties to reduce interferences from the low-frequency region to the mid-frequency range. The NC material structure presents the advantage of designing smaller components (can reduce its volume by 50–80%) with more significant magnetic properties for EMI suppression compared to ceramic materials [19–24]. These properties are achieved through a complex manufacturing procedure.

NC cores' manufacturing procedure (Figure 2.7) is quite different from the used for ceramic production since it is formed by a continuous laminar structure that is wound to form the final core. The tape-wound structure is based on an amorphous ribbon of only 7-25 micrometers in thickness. It is generated by melting the base material by heating it at 1300°C and depositing it on a high-speed cooling wheel (100 km/h) that reduces the temperature of the material to 20°C at the rate of 106 K/s. After that, the rolled material is exposed to an annealing process, usually under a transversal and longitudinal magnetic field. This treatment affects the magnetic properties resulting in ultrafine crystals with a size of the order of 7–20 nm. Finally, an epoxy coating or an additional protective case is needed to protect the sample, due to the brittle nature of the tape. Depending on the parameters selected during the manufacturing procedure, NC samples can provide initial permeability values in the range of 15,000 to 150,000. Electrical resistivity is relatively high even if it is considered a metallic material, generally over 10-6 Ω·m [15,18,23]. The last stage of this procedure corresponds to applying a protective coating or a plastic housing that protects the obtained cores due to the brittle nature of the tape.

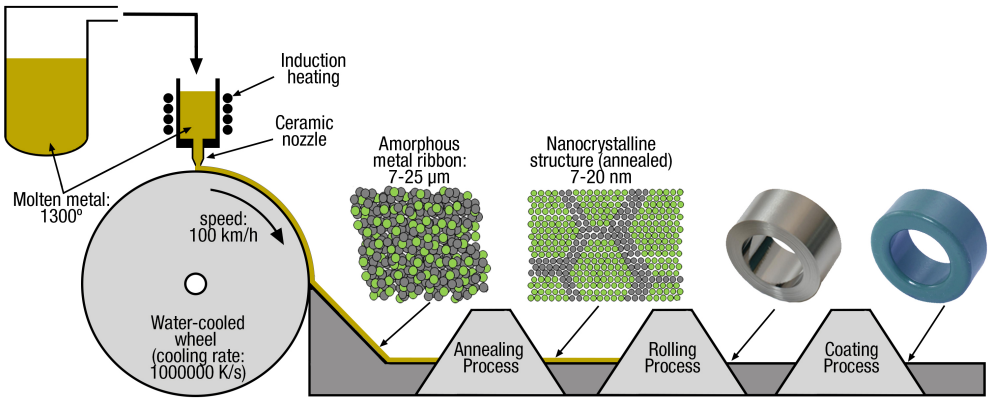

Figure 2.7. Diagram of the manufacturing procedure of nanocrystalline cores.

Figure 2.8 shows three micrographs of the three specific materials analyzed in this study that has been obtained through scanning electron microscopy (SEM). In these

photographs, it is possible to observe the difference between the ceramic materials, where the grain size is in the order of tens of micrometers and NC material, where the grain size is in the order of nanometers.

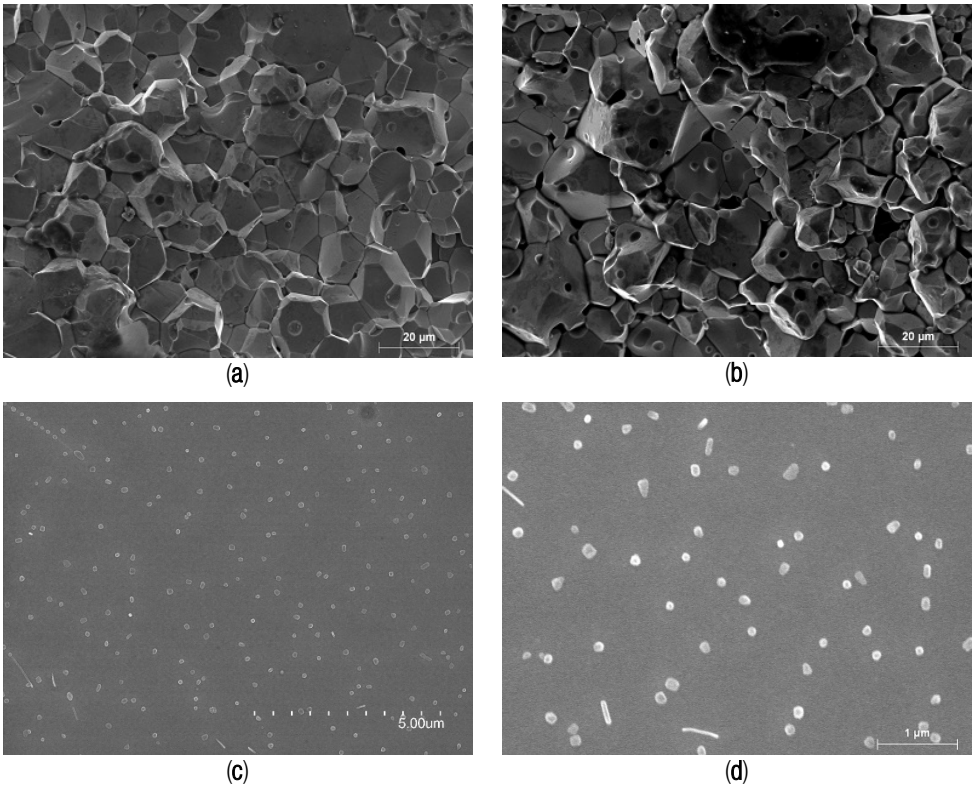

Figure 2.8. SEM photographs of ceramics and nanocrystalline core materials: (a) MnZn material composition; (b) NiZn material composition; (c) NC material composition; (d) NC material composition zoom in.

2.3 Magnetic properties

One of the most important parameters that define the ability of a material to absorb electromagnetic interferences is the relative permeability (μ_r) [25]. The permeability relates the magnetic flux density of a certain magnetic field in a defined medium, so that when a sleeve core is placed around a cable, the magnetic flux is concentrated in it. This ability to concentrate the magnetic flux is described by the material's internal properties and it is represented through the permeability complex parameter. By dividing the relative permeability into its complex it is possible to obtain more information about the material analyzed. The real component (μ') quantifies the real or inductive part and the imaginary

or resistive component (μ'') is related to the material ability to absorb the electromagnetic interferences [6,7,26]. The complex relative permeability is expressed by Equation (1):

$$\mu_r(f) = \mu'(f) - j\mu''(f) \quad (1)$$

The information generally provided by manufacturers focuses on the initial permeability (μ_i) or the impedance value at some frequency points. From this data, it might seem that, selecting the component with the highest initial permeability, makes it possible to concentrate the maximum flux value in the core. Nevertheless, a sleeve core with a significant initial permeability might provide a low relative permeability (μ_r) value at higher frequencies reducing its effectiveness to attenuate EMI disturbances. According to IEC 60401-3 standard, μ_i describes the relative permeability of a material at low values of magnetic flux density (B) and it is defined using closed magnetic circuits for $f \leq 10$ kHz, $B < 0.25$ mT, $T = 25$ °C. This configuration makes it possible to characterize sleeve cores without risk of saturation and, therefore, it is easier to compare different compositions. This parameter could suggest that the maximum concentration of flux in the core is achieved by selecting the core material that provides the highest μ_i possible. Nevertheless, a core that provides a high μ_i at 10 kHz that relative permeability might be significantly reduced at frequencies in the frequency range of the regulatory limit where it should have an effect. An approximation of Snoek's Law can be used as a governing rule of EMI suppression in order to explain the relation between magnetic saturation (B_s), initial permeability (μ_i), and resonance frequency (f_m) [27]:

$$f_m = B_S/\mu_i \quad (2)$$

Note that the value of B_s can be considered constant bellow the resonance frequency under the conditions described in IEC 60401-3. Equation (2) shows that the higher the operation frequency, the lower the permeability, and vice versa. Thus, if the material provides high initial permeability, the frequency falls off will be low and vice versa. For this reason, MnZn cores are typically focused on the high kHz, or at most, the very low MHz region since this material yields an initial permeability value between 1000–20,000 [28, 29]. Regarding NiZn materials, they usually provide an initial permeability that varies between 100–2000, so they are able to more effectively filter electromagnetic noise within a high-frequency range [30,31]. Otherwise, the NC material shows a much higher initial permeability than ceramic materials because its internal structure and manufacturing process improve its magnetic properties.

Figure 2.9 represents the relative permeability traces of NC, MnZn and NiZn cable core compositions split into real and imaginary components. Frequency resonance is an important value in this graph as it is the point where real and imaginary parts crosses and, thus, the material changes its dominant behavior. The values represented in this graph have been measured with specific and calibrated equipment by following two

setups depending on the frequency range selected. From 1 MHz to 100 MHz, the complex relative permeability has been obtained with an E4991A Material Analyzer equipment (Keysight) together with its 16454A Magnetic Material Test Fixture. The 16454A makes it possible to carry out accurate permeability measurements of round-shaped magnetic materials due to the construction of this fixture, creating one turn around the core without magnetic flux leakage. Thereby, it is possible to obtain complex permeability direct readouts of complex permeability. This equipment does not allow measuring permeability from 1 kHz to 1 MHz, so a second method is employed in which relative permeability of magnetic material is obtained from the self-inductance of a round-core that has a closed loop. This second setup provides the value of effective permeability derived from the inductance measurement results and it is described in detail in Subsection 2.4.

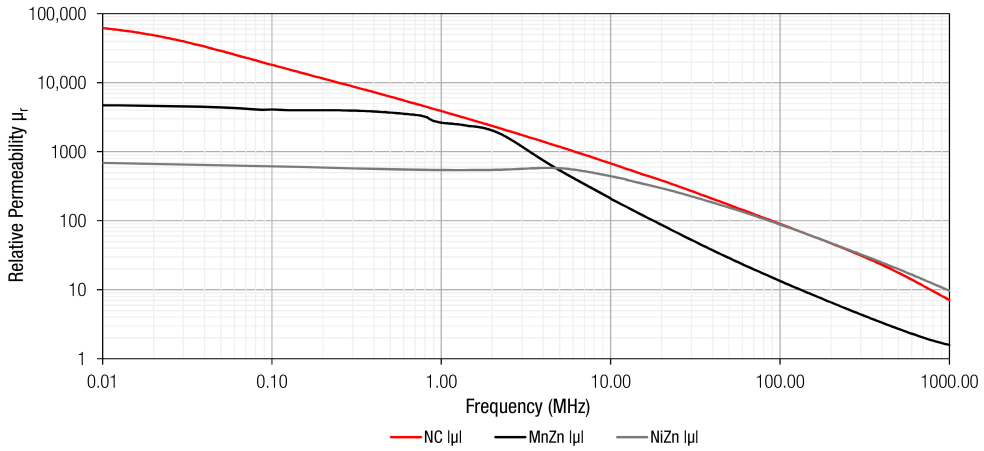

Figure 2.9. Diagram of the manufacturing procedure of nanocrystalline cores.

More information about the sleeve cores analyzed can be obtained by splitting into real and imaginary components the complex relative permeability of the three materials. These traces allow one to determine the magnetic resonance frequency of each material, as shown in Figure 2.10. This corresponds to the frequency value at which the real part of the relative permeability begins to fall and the imaginary part reaches the maximum peak [32]. Generally, the inductance component is steady below the f_m and decreases significantly from this frequency value [22]. The NC minigraph shows the lower frequency value at which the f_m takes place; however, the absorption loss represented by the imaginary part shows the weakest slope, if it is compared with MnZn and NiZn imaginary traces. From this information, together with the fact that NC provides a higher initial permeability, results in this sleeve core solution could yield a greater attenuation ratio in a broader frequency range than ceramic cores. There is also a capacitance component that represents the dielectric effects of the magnetic material. This appears in the

bandwidth above the f_m, where the inductive component of the permeability becomes negative [25,33]. As can be observed in **Figure 2.10**, this stray capacitance due to the magnetic material is noted beyond 1.8 MHz and 85.1 MHz and 282.7 MHz in the case of MnZn, NC, and NiZn cores, respectively.

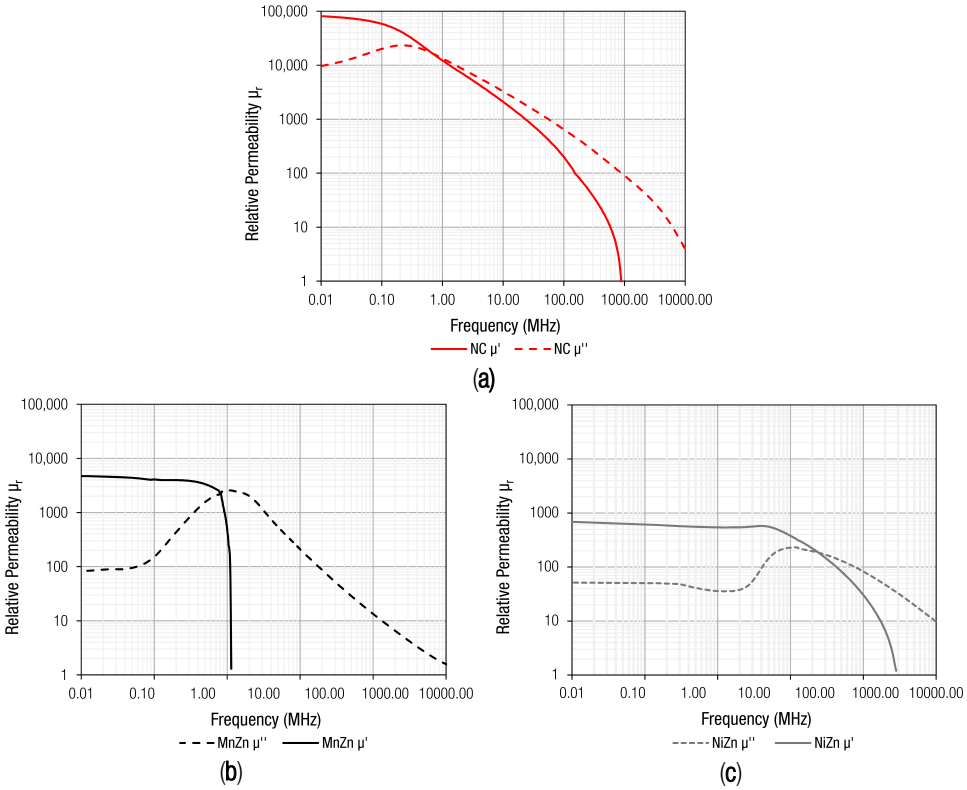

Figure 2.10. Complex relative permeability split into real and imaginary components: (a) NC sleeve core; (b) MnZn sleeve core; (c) NiZn sleeve core.

The characterization of each of the three studied materials (MnZn, NiZn, and NC) has been performed by selecting sleeve core samples with similar dimensions. Specifically, the MnZn sample selected shows an initial permeability of about 5000, whereas the NiZn sample selected of about 620. For the first and second articles published a NC sample with an initial permeability of about 90,000 is selected, whereas the sample used in the third contribution of about 30,000. Note that the NC sample studied in the third article published is 2.3 mm shorter, so that the ceramic samples have also been cut to have more similar dimensions. The dimensional parameters of the samples used in the first and second contributions are shown in **Table 1**. The dimensional parameters of the samples used in the third contribution are shown in **Table 2**.

Table 1. Lists of sleeve core samples used in the first and second research articles.

Magnetic Material	Outer Diameter (OD) (mm)	Inner Diameter (ID) (mm)	Height (h) (mm)	Thickness (mm)
NC90K	18.9	12.9	27.7	6.0
MnZn	18.6	10.2	28.5	8.4
NiZn	18.6	10.2	28.5	8.4

Table 2. Lists of sleeve core samples used in the third research article.

Magnetic Material	Outer Diameter (OD) (mm)	Inner Diameter (ID) (mm)	Height (h) (mm)	Thickness (mm)
NC30K	18.9	12.9	27.7	7.5
MnZn	18.6	10.2	28.5	8.4
NiZn	18.6	10.2	28.5	8.4

Another essential parameter to find out the performance of a certain magnetic material is the Curie temperature, as it indicates at which temperature it loses its ferromagnetism [34]. **Figure 2.11** shows the change of initial permeability over a temperature range from −60°C to 180°C. This characterization has been performed with the equipment E4980A Precision LCR Meter (Keysight) that provides the initial permeability through measuring the real part of complex permeability parameter [35] and carrying out temperature sweep. Thereby, in order to evaluate the component, it has been introduced into the CST-Temperature Test Chamber series T-40. From these graphs, we can observe the great stability of the initial permeability of NC EMI suppressor compared to MnZn and NiZn. NC initial permeability (90,000) remains at values higher than 80%, up to about 150 °C.

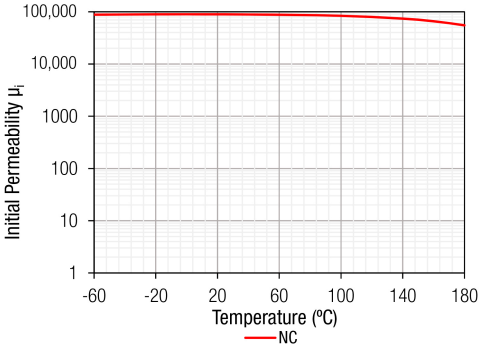

(a)

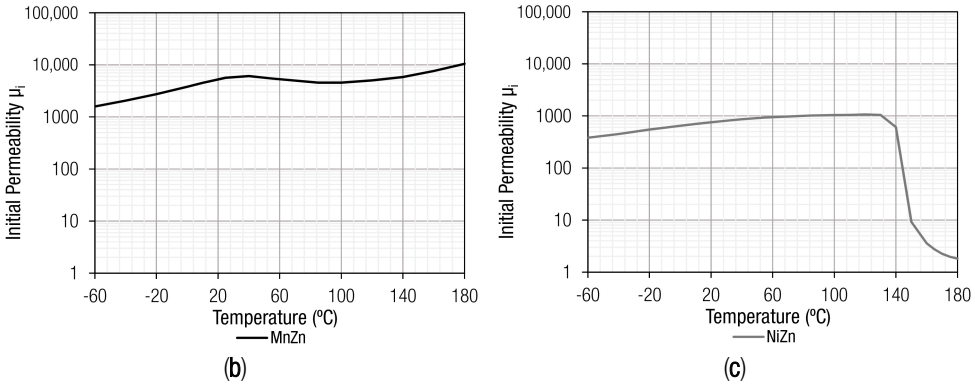

Figure 2.11. Initial permeability versus temperature for three different cable cores: (a) MnZn; (b) NiZn; (c) NC.

A great deal of information can be learned about the magnetic properties of a material by studying its hysteresis loop. A hysteresis or B-H loop shows the relationship between the induced magnetic flux density (B) and the magnetizing force (H). The loop is generated by measuring the magnetic flux of a ferromagnetic material while the magnetizing force is changed. As is shown in Figure 5, the hysteresis loop of three cable cores is measured with the equipment BsT-Pro B-H-Analyzer. From this graph, it is possible to observe that NC provides the higher magnetic saturation (B_S), which is at the point where the flux density tends to level off. B_S is defined as the maximum flux density attainable in a material at a given temperature and above this B_S value, it is not possible to further increase B by further increasing H. At B_S, almost all of the magnetic domains are aligned and an additional increase in the magnetizing force will produce very little increase in magnetic flux. When is reduced to zero, it does not return to zero, as it can be seen that some magnetic flux remains in the materials even though the magnetizing force is zero. This is referred to as remnant flux density (B_R), the point on the graph that indicates the remanence or level of residual magnetism in the materials when $H = 0$. NC EMI suppressor shows the highest value of B_R. At this point, a part of the magnetic domain remains aligned, whereas the other part has lost its alignment. As the magnetizing force is increased from zero in the opposite direction, the flux density decreases to zero. This is called the point of coercivity of the material (H_C) and represents the magnetizing force required to remove the residual magnetism from the material. At this point, the reversed magnetizing force has flipped enough of the domains so that the net flux within the material is zero. The maximum value of coercivity is provided by the NiZn sleeve core so that this composition material needs to be subjected to a larger magnetizing force to reduce its flux density to zero.

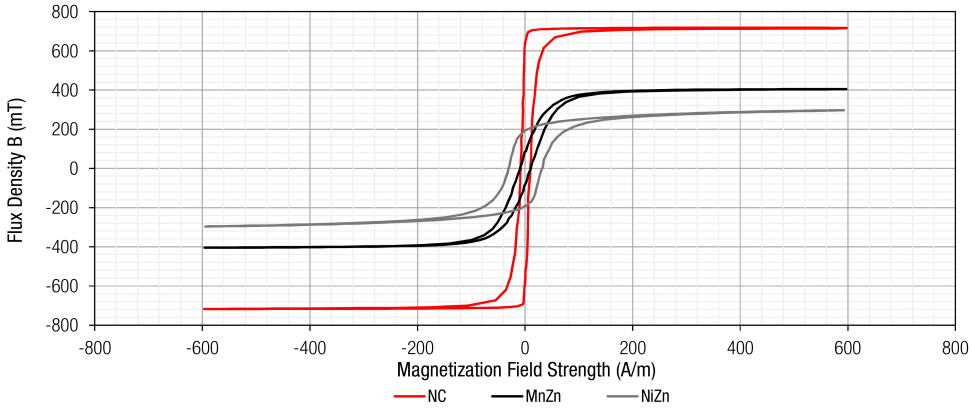

Figure 2.12. Hysteresis curve measured for NC, MnZn and NiZn sleeve cores.

2.4 Impedance

Although the permeability parameter is used to describe the behavior of the core material, the performance of a certain sleeve core takes into account, besides the material features, other variables such as the self-inductance defined by the dimensions and the shape. Thereby, sleeve cores are usually defined and classified by specifying the magnitude of the impedance (Z_{SC}), which is obtained from the equivalent component parameters such as resistance (R) and inductance (L) [27,35]. The magnitude of the impedance is given by Equation 3:

$$|Z_{SC}| = \sqrt{R^2 + (X_L)^2} \tag{3}$$

where R corresponds to the equivalent resistance and X_L is the impedance of the inductive part of the sleeve core. The vector relationship between impedance and permeability components is shown in Figure 2.13.

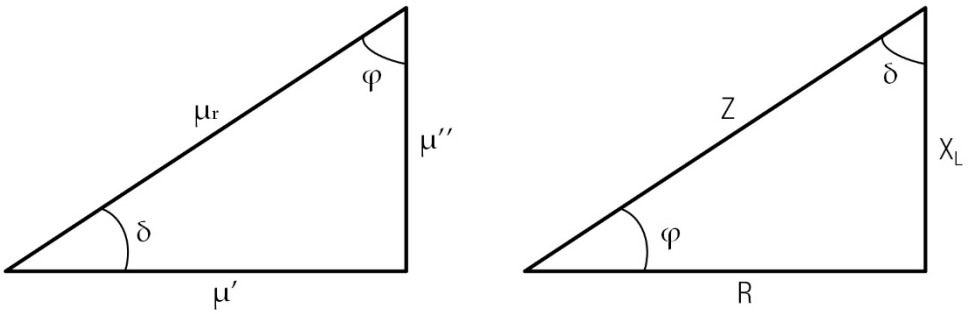

*Figure 2.13. Vector relationship between μ_r, μ'', and μ'' (**left**); vector relationship between Z, R and X_L ($2\pi fL$) (**right**).*

There is a proportional relation between the attenuation ratio or insertion loss provided by a certain sleeve core and the impedance of the system where it is set. Thus, it is essential to select an EMI suppressor that provides an impedance value that is higher than the system impedance at the frequency to be filtered. This is due to the fact they are more effective when used on cables connected to circuits with low impedance [5].

A sleeve core can be represented by a simplified equivalent circuit consisting of an inductance, a resistance, and a capacitance, as shown in **Figure 2.14**. This circuit represents a sleeve core within the frequency range analyzed in this contribution without taking into consideration the system where it could be placed since the surrounding elements may introduce additional parasitic effects. The behavior of the sleeve core at a low-frequency range is usually mostly inductive, blocking interference currents due to its inductive reactance (X_L). The impedance becomes more resistive (R) as the frequency is increased, absorbing and dissipating disturbances as heat. Hence, L and R are the predominant components below the ferromagnetic resonance frequency (f_m); however, from this frequency value, the stray capacitance of the ferromagnetic material becomes predominant, defining the fall slope of the impedance. Regarding C, it represents a parasitic capacitance because of the winding effect [22]. When a sleeve core is set around a cable, it is equivalent to one turn or one winding coil. An interesting feature of sleeve cores is the possibility of winding the wire around them multiple times, considering each pass of the cable through the sleeve core as one turn. This technique results in an increase of the EMI suppressor impedance proportionally to the number of turns squared. Nevertheless, increasing the number of turns (N), it is possible to increase to obtain a higher inductance L value, but at the same time, the stray capacitance C increases, shifting the point of maximum impedance to a lower frequency value [25,36]. Therefore, there is a balance between the number of turns and winding capacitance, because a higher number of turns implies a worse performance at high frequencies. This last fact could generate a self-resonance (*SRF*) at a certain frequency. Above the value of the *SRF*, the impedance becomes predominantly capacitive and the effectiveness of the sleeve core to filter EMI is degraded [37,38]. Therefore, *SFR* could superpose the ferromagnetic resonance due to the intrinsic material parameters described above. This is one of the main reasons why more than two or three turns are not usually used in EMI suppressors intended for cables.

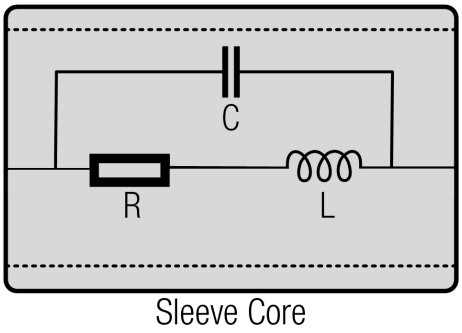

Figure 2.14. Simplified sleeve core equivalent circuit.

The translation of the complex relative permeability components to the inductive and resistive parts is related by the inductance of the core considering its magnetic properties (L_m), geometry and its size and frequency (ω). This relation is expressed by Equation 4.

$$Z_{SC} = \omega L_m \tag{4}$$

The core inductance is a useful parameter to evaluate the effectiveness of a set of sleeve cores depending on their dimensions. This can be obtained from the Ampere's Law defining the core as a toroid which consists of *N* turns and has a rectangular cross-section with inner radius (*IR*), outer radius (*OR*), and height (*h*):

$$\oint \vec{B} d\vec{s} = \oint B ds = B \oint ds = B(2\pi r) = \mu_0 \mu_r NI \tag{5}$$

where μ_0 represents the permeability of free space and *I* the current around the core. Subsequently, the magnitude of the magnetic field inside the sleeve core that is defined by a torus is given by

$$B = \frac{\mu_0 \mu_r NI}{2\pi r}. \tag{6}$$

The magnetic flux through one turn of the sleeve core may be obtained by integrating over the rectangular cross-section (a rectangle whose sides are defined by *r*), which is the subtraction of the *OR* and *IR*, and *h*, defining the differential area element with $dIR = h\, dr$:

$$\Phi_B = \iint \vec{B} d\overrightarrow{IR} = \int_{IR}^{OR} \left(\frac{\mu_0 \mu_r NI}{2\pi r}\right) h\, dr \tag{7}$$

$$L_0 = \frac{N\Phi_B}{I} = \frac{\mu_0 N^2 h}{2\pi} ln\left(\frac{OR}{IR}\right). \tag{8}$$

Consequently, the inductance of the core considering its material composition (L_m) is given by Equation 9, and inserting this parameter in Equation 4, it is possible to relate the core inductance with the impedance provided by this, as shown in Equation 10.

$$L_m = \mu_r L_0 = \frac{\mu_0 \mu_r N^2 h}{2\pi} ln\left(\frac{OR}{IR}\right) \tag{9}$$

$$Z_{SC} = \omega \frac{\mu_0 \mu_r N^2 h}{2\pi} ln\left(\frac{OR}{IR}\right) \tag{10}$$

This relation between relative permeability and impedance can be used to link the complex components of the relative permeability to the resistive and inductive parts of the magnitude of the impedance provided by a certain sample core. Thereby, it is possible to determine the R and X_L parameters of a sleeve core with specific dimensions by knowing the complex relative permeability parameters through the quasi-static model [25]. Generally, this model can evaluate cores up to the *SFR* since, beyond this frequency value, the static magnetic flux distribution can fluctuate. This deviation could be because the core dimensions, saturation, core losses, and frequency-dependent magnetic effects that are significant above the *SFR* are not considered [22]. Equations (11) and (12) show the link between the material permeability and dimensions of the sleeve core with the impedance:

$$L = \frac{\mu_0 \mu' N^2 S}{\ell} \tag{11}$$

$$R = \frac{\mu_0 \mu'' N^2 \omega S}{\ell} \tag{12}$$

where μ_0 is the permeability of the air, μ' is the inductance permeability component, μ'' is the loss permeability component of the sleeve core, ℓ is the effective magnetic path length of a toroidal core (m), N is the number of turns of a cable to carry out the measurement, S corresponds to the toroidal core cross-sectional area (m^2) and ω is the angular frequency.

The experimental magnitude of the impedance of each sample is obtained by using a Vector Network Analyzer or an Impedance Analyzer equipment connected to the Terminal Adapter 16201A (Keysight). The sleeve core is connected by means of the Spring Clip Fixture 16092A (Keysight) that is connected to the 16200B test fixture [39]. After it is properly calibrated, this measurement setup is able to characterize samples up to 500 MHz since this is the upper-frequency limit at which the 16200B test fixture can operate. Thereby, this setup is based on the measurement of the sample's impedance by means of introducing along the core a wire with a defined length and cross-section, which is connected to the equipment. The wire selected should be as short as possible, but long enough to achieve the desired turns (N) around the sleeve core. The influence of the wire

in the total impedance measured can only be neglected if its length is short compared to the wavelength and this limit is usually a least 1/10 of the wavelength (λ). At the same time, this length increase causes the *SRF* to shift to a lower region, considering not only the impedance of the core but also the impedance introduced by the cable [36,40]. Subsequently, considering these conditions, a calibration procedure has been performed with the aim of reducing the influence of the AWG cable. After calibrating the system setup, the fixtures are internally compensated by impedance standard calibration in order to take into account the electrical length path and the impedance variations caused by parasitic elements and it is possible to determine the impedance provided by the core.

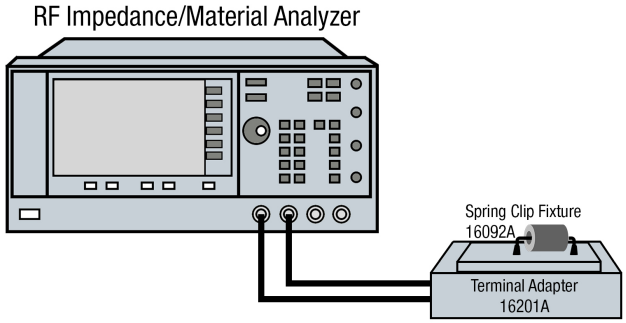

Figure 2.15. Setup for measuring impedance of sleeve core samples.

The influence of DC bias current in the cable where the sleeve core is attached can be characterized by adding to the last measurement setup the 16200B External DC Bias adapter. This fixture allows supplying a bias current through the sleeve core up to 5 A by using a 7 mm port and an external DC current source, as shown in Figure 2.16 [41].

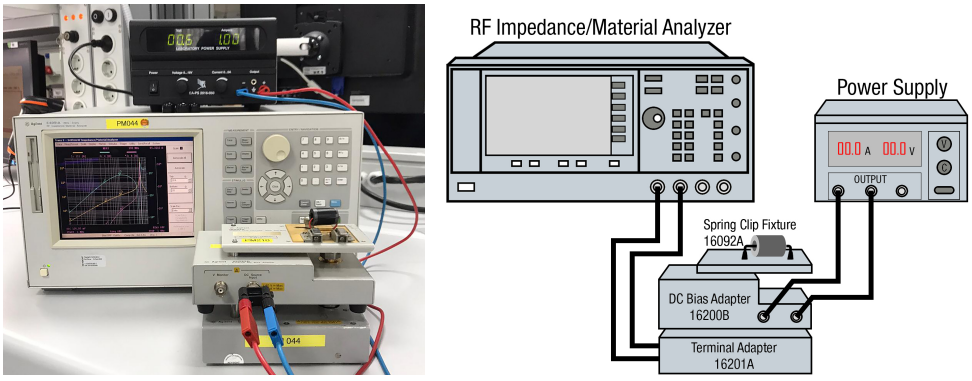

Figure 2.16. Impedance measurement setup with the DC bias test fixture connected: (a) Photography of the measurement setup; and, (b) Diagram blocks of the measurement setup.

2.5 Insertion loss

There is a proportional relation between the attenuation ratio or insertion loss (*A*) provided by a certain sleeve core and the impedance of the system where it is set. Thereby, it is essential to select a sleeve core that provides an impedance value higher than the system impedance at the frequency where the interferences are located. The insertion loss that a sleeve core is able to yield is strongly dependent on the impedance of the system in which it is placed, besides its impedance response depending on the frequency. Therefore, these EMI suppressors are more effective when used on cables connected to circuits with low impedance [5]. Sometimes it is difficult to determine the impedance of the system with EMI problems accurately; however, depending on the signals that flow through the cable, it is possible to estimate this value [35]:

- Ground surfaces usually present impedances from 1 to 2 Ω.
- Supply voltage lines have impedances from 10 to 20 Ω.
- Video, clock, and data lines from 50 Ω to 90 Ω.
- Long data lines from 90 Ω to 150 Ω and higher.

The datasheets of sleeve core components generally only specify the impedance at several frequency points or the graph of the magnitude of the impedance in the frequency range where it is more effective. In contrast to this fact, another kind of EMC component datasheets, such as common-mode-chokes, show the attenuation ratio or insertion loss in terms of decibels (*dB*) that are able to provide. The theoretical insertion loss of a specific sleeve core can be determined from its impedance response by considering the equivalent circuit approach shown in Figure 2.17. In this schematic, it is identified the impedance Z_A of a system A that is connected through a cable with a system B with an equivalent impedance Z_B. Thereby, the sleeve core is attached to the cable that interconnects both systems and introduces an impedance Z_{SC} with the aim of increase the impedance of the cable and, therefore, introducing an insertion loss in those frequencies where the interferences are located.

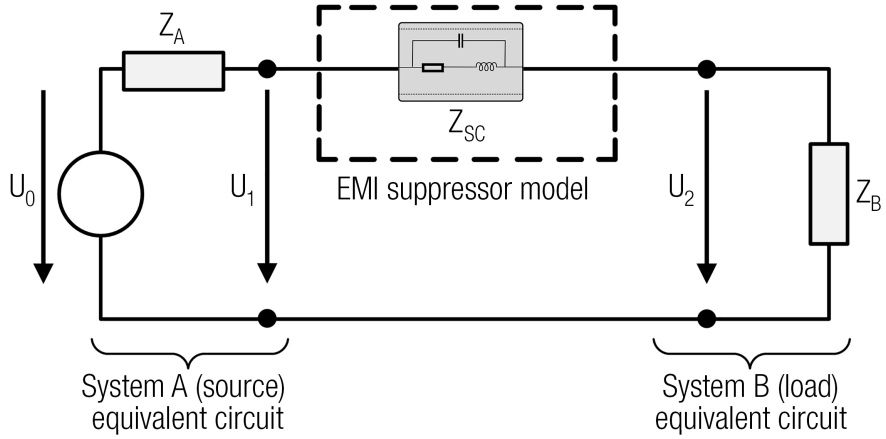

Figure 2.17. *Diagram of source and load equivalents circuits used to determine the insertion loss parameter of a sleeve core when it is introduced into the cable that connects the two systems (A and B).*

According to this diagram, when the system impedance is known, the insertion loss in terms of decibels can be calculated through Equation (13) from the impedance of the sleeve core (Z_{SC}):

$$A(dB) = 20\,log\left(\frac{Z_A+Z_{SC}+Z_B}{Z_A+Z_B}\right). \quad (13)$$

This theoretical insertion loss can be used as a reference value to be compared with the experimental insertion loss measured by emulating the equivalent circuit diagram shown in Figure 2.17. In order to carry out the performance of the sleeve core, it is considered that the source and load impedance are known, and the parameter of study is the impedance of the sleeve core. Therefore, two experimental measurement setups based on generating controlled EMI conducted emissions into a load with a stable impedance over two frequency ranges. The first experimental setup is focused on characterizing EMI suppressors in the low-frequency region (from 2 kHz to 150 kHz). System A is represented by a low-frequency signal generator NSG-4060/1 (TESEQ) with 50 Ω of output impedance. Thereby, this fixed impedance is considered as Z_A. The probe connected to this generator separates the signal and the ground terminals, making it possible to attach the sleeve core under test only in the signal path. The main objective of this part of the setup is focused on characterizing the performance of the sleeve core by simulating the electromagnetic interferences that can appear in a real system. Different resistance loads are connected to the two terminals of the probe in order to evaluate the sleeve cores performance with different values of load impedance, a PCB (Printed Circuit Board) which holds several values of impedance, has been designed. This circuit is intended for switching among four different values of Z_B (5 Ω, 50 Ω, 100 Ω, and 1000 Ω). Since the performance of the samples under test relies on the load impedance. This

part of the setup allows us to study each material composition's behavior in systems with different load values. The signal that flows through the signal terminal is acquired with a low-frequency current probe that is connected to a Spectrum Analyzer. This equipment is employed for measuring the amplitude of the signal generated as a reference and the signal when the sleeve core under test is placed around the signal terminal connected to the generator as shown in Figure 2.18.

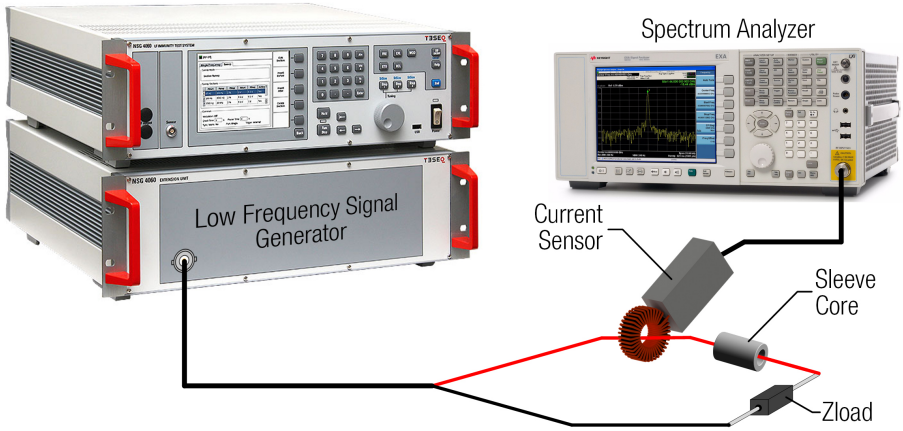

Figure 2.18. Experimental measurement setup diagram to characterize sleeve core samples under test in the 2–150 kHz frequency range.

The second setup is based on the same fundamentals as the first one, but it covers a higher frequency range by emulating the diagram shown in Figure 2.17. This setup takes as a reference the IEC 61000-4-6 standard (Testing and measurement techniques—immunity to conducted disturbances, induced by radio-frequency fields) and it consists of a continuous wave simulator (CWS) for testing conducted RF immunity within a frequency range from 100 kHz to 230 MHz that emulates the electromagnetic conducted interferences. This equipment is the CWS500N1 Continuous Wave Simulator (EM Test) and it provides a 50 Ω output impedance that represents the Z_A in the insertion losses equivalent circuit diagram. A coaxial cable connects the CWS500N1 to the CAL 801 (Ametek CTS), which is employed to ensure a 100 Ω load in the whole analyzed frequency range. Together with the output impedance of the CWS500N1, this impedance represents a $Z_A = 150$ Ω in the equivalent circuit diagram. The other side of this diagram is formed by another CAL 801 that provides a 100 Ω load that is connected to a spectrum analyzer with an input impedance of 50 Ω. Accordingly, the sum of these two impedances provides the impedance of $Z_B = 150$ Ω. Both sides of the equivalent circuit emulated (A and B) are connected by means of an AWG26 cable of 150 mm, maintaining a distance of 35 mm from the ground metal layer that interconnects all the parts. This cable simulates a reference line that can be characterized and employed to introduce the sleeve cores under

test into the setup to analyze how the emulated interferences are attenuated. Therefore, a previous calibration measurement is first carried out to ensure the stability and linearity of the system, generating a sinus frequency sweep with an amplitude of 140 dBµV. Once the reference signal is obtained, the sleeve core is introduced into the reference line of the insertion loss setup and the sinus frequency sweep is repeated. With these two measurements, it is possible to subtract them in order to obtain the attenuation rate or insertion loss performance of each of the sleeve cores and compare them in terms of decibels instead of impedance. Figure 2.19 shows the measurement setup described implemented inside an anechoic chamber.

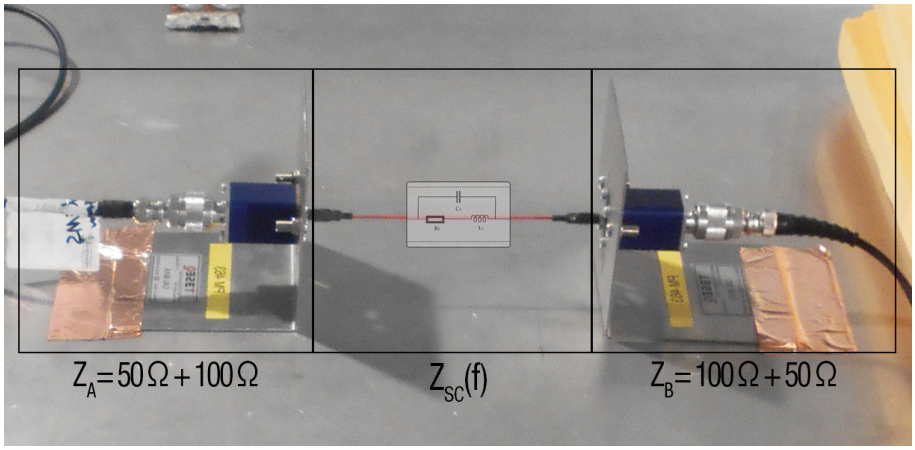

Figure 2.19. Experimental measurement setup diagram to characterize sleeve core samples under test in the 100 kHz – 230 MHz frequency range.

2.6 Simulation model

A Finite Element Method (FEM) simulation model has been designed through an electromagnetic analysis simulator (HFSS, Ansys Electronics Desktop) to correlate the results obtained with the data provided by the experimental measurement setup. This simulation model makes it possible to evaluate sleeve cores based on the three different materials analyzed in this research. Other parameters such as the dimensions or the system source and load (Z_A and Z_B) can be modified in order to study the response of the sleeve core in terms of insertion loss and impedance. The proposed simulation model is shown in Figure 2.20. It is formed by a copper conductor that crosses a cylindrical core defined by the material properties of the three analyzed components (NC, MnZn and NiZn). The conductor is connected to two ports (source and load) referenced to a perfect electrical plane located at a certain distance under it. This simulation setup represents a transmission line based on a parallel line (or single-wire) considering a single wire over a ground plane that allows designing a system with a characteristic impedance of $Z_0 = 150$

Ω. This parameter is fixed by selecting the distance from the plane to the center of the conductor $H = 15$ mm, the diameter of the conductor $d = 4.9$ mm, and considering that it is surrounded by air [42–44]. Setting the ports' impedance to 150 Ω, makes it possible to extract the sleeve core's impedance under test without the characterization system influences the results obtained. The model has been designed with $Z_0 = Z_A = Z_B = 150$ Ω value is a reference value adopted in different EMC standards to characterize and calibrate devices such as Common Mode Absorption Devices (CMAD) intended for measuring EMI disturbances in cables [45]. These fixtures are characterized using the through-reflect-line (TRL) calibration method based on measuring the S-parameters of CMADs, as described in CISPR 16-1-4 [45]. Therefore, this simulation model provides a reference system that can extract the impedance introduced in the conductor by the EMI suppressor component.

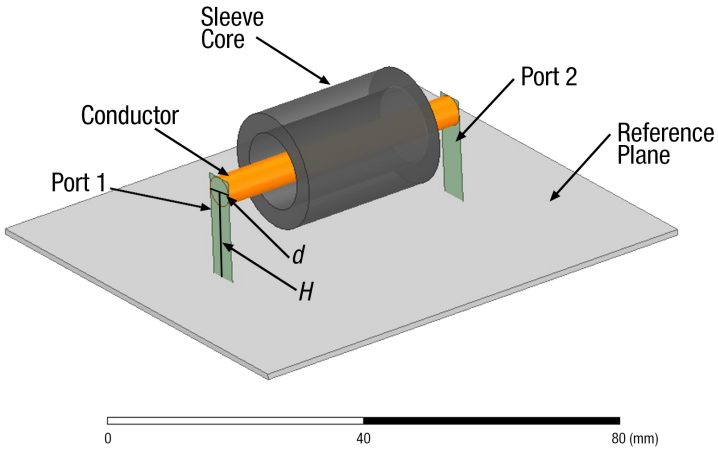

Figure 2.20. Simulation model to evaluate the sleeve cores performance.

Furthermore, the simulation model makes it possible to split into two parts the sleeve core under test to study the performance of a variation of this kind of component known as openable core clamp or snap ferrite. This component is manufactured by two split parts pressed together by a snap-on mechanism which turns this into an easy to install quick solution for reducing post-cable assembly EMI problems. The main advantage of snap cores compared to solid sleeve cores is the possibility to add them to the final design without manufacturing a specific cable that includes this component before assembling its connectors. Thereby, the relationship between the impedance provided by the sample and the air gap introduced can be specifically examined. The procedure performed to emulate the performance of this component when they are split into two openable parts is based on a parametric gap sweep that makes it possible to observed the response of each material when it is split. This technique makes it possible to determine the sleeve

core's impedance when it is split into two parts and a specific gap is introduced as shown in Figure 2.21.

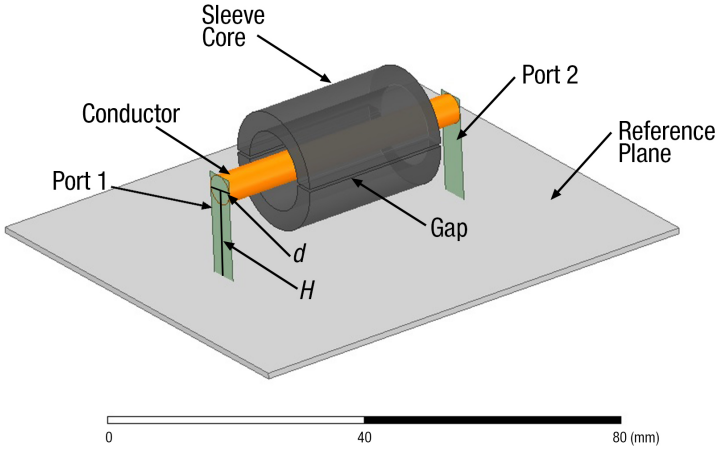

Figure 2.21. Simulation model to evaluate the performance of openable clamp cores with a specific gap introduced.

When an air gap is included in a closed magnetic circuit, the circuit's total permeability is called the effective relative permeability (μ_e) and this is lower than the permeability of the original solid core without the presence of the air gap. In terms of EMI suppression, reducing the relative permeability in a sleeve core is generally related to decreasing its ability to attenuate interferences. However, the presence of an air gap is sometimes desired to increase the DC bias capability of the core or to reduce the permeability to achieve a more predictable and stable response with the aim of shifting the resonance frequency (f_m) to higher values to reduce the effects of dimensional effects [46,47].

When the two parts of the split-core are joined, a certain air gap remains between them that results in a magnetic reluctance (R_m) increase, since the gap represents an opposition to the magnetic flux (Φ) normal flow [16,48]. As shown in Figure 2.22, this effect is analogous to adding a series resistor in an electronic circuit to reduce the magnitude of the current. In Figure 2.22, R_c represents the reluctance of the core, R_g the reluctance of the gap, Φ the magnetic flux that flows through the magnetic path length of the core (l_c), ℓ_g the length of the air gap, i the current that flows through the conductor, and N is the number of turns.

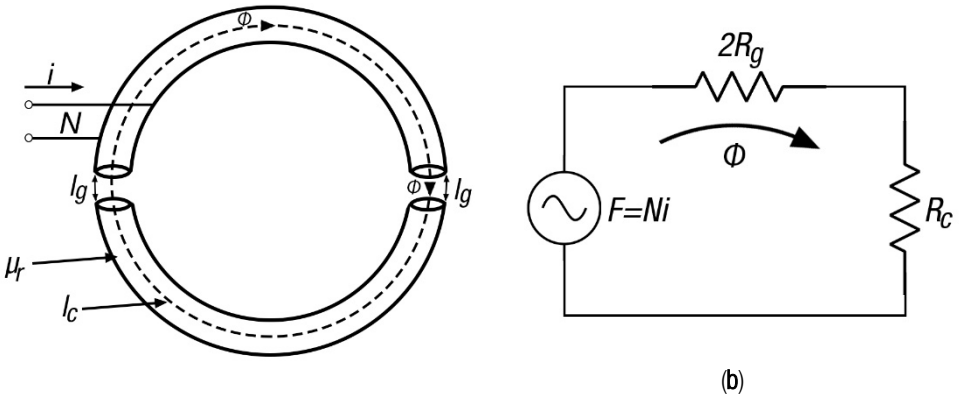

Figure 2.22. Split-core with air gaps: (a) Magnetic flux distribution diagram; and, (b) The magnetic circuit of a split-core with two air gaps.

The general expression to obtain the magnetic reluctance is given by [16]:

$$R_m = \frac{\ell}{\mu_r \mu_0 A} \ [H^{-1}] \tag{14}$$

where ℓ corresponds to the magnetic path length and S to the cross-sectional area. The ℓ and S parameters are obtained from the dimensional features of the sample, considering a toroid with a rectangular cross-section:

$$\ell = \pi \left(\frac{OD}{2} + \frac{ID}{2}\right) [m] \tag{15}$$

$$S = h \left(\frac{OD}{2} - \frac{ID}{2}\right) \ [m] \tag{16}$$

where h core's height, and the OD and ID are the outer and inner diameter, respectively. The overall reluctance of the split-core considering the air gap can be calculated from Equation (14) as the sum of the reluctance core (R_c) and reluctance air gap (R_g) [13,49]:

$$R_m = R_c + 2R_g = \frac{\ell_c - \ell_g}{\mu_r \mu_0 A} + \frac{2\ell_g}{\mu_0 A} \ [H^{-1}] \tag{17}$$

thereby, the air gap factor (F_g) is

$$F_g = \frac{R_m}{R_c} = \frac{R_c + 2R_g}{R_c} = 1 + \frac{2R_g}{R_c} = 1 + \frac{\mu_r 2\ell_g}{\ell_c} \tag{18}$$

and the effective relative permeability of a core with an air gap is [13,16,50]:

$$\mu_e = \frac{\mu_r}{1 + \frac{\mu_r 2\ell_g}{\ell_c}} = \frac{\mu_r}{F_g}. \tag{19}$$

Equation (19) represents the most common and simplified model to approximate the effective permeability caused by an air gap since it underestimates the value of μ_e because it does not consider the effect of the fringing flux across the air gap [51]. In the case of toroid cores, to estimate the influence of the air gap introduced when the core is split into two parts, it is usually considered ℓ_g twice the spacer thickness [16,51].

Chapter 3. Study of the NC magnetic properties and its EMI suppression performance in the 2–150 kHz.

This chapter focuses on the study of characterization methodologies for sleeve core EMI suppressors. As a preliminary assessment, the characterization methods described in the literature have been carried out to experimentally determine the magnetic properties such as relative permeability, Curie temperature, and B-H loop. Subsequently, the appended research article include a detailed description of the reviewed and proposed experimental procedure to acquire the insertion loss performance of each of the three magnetic materials analyzed. These studies have made it possible to compare the performance provided by the novel NC sleeve core solution with the conventional ceramic materials based on MnZn and NiZn compositions.

3.1 Scientific article I

Title: Characterization of Different Cable Ferrite Materials to Reduce the Electromagnetic Noise in the 2–150 kHz Frequency Range.

Authors: Adrian Suarez, Jorge Victoria, Antonio Alcarria, Jose Torres, Pedro A. Martinez, Julio Martos, Jesus Soret, Raimundo Garcia-Olcina, and Steffen Muetsch.

Published in: Materials (MDPI), vol. 11, no. 2, p. 174 (2018).
DOI: 10.3390/ma11020174

Impact factor: 2.972 (2018).

Quartile (category: "Materials Science, Multidisciplinary"): Q2 (2018)

Citations: 9 (accessed on March 2021).

Description: Materials (ISSN 1996-1944; CODEN: MATEG9) is a peer-reviewed, open access journal of materials science and engineering published semimonthly online by MDPI. The Portuguese Materials Society (SPM), Spanish Materials Society (SOCIEMAT)

and Manufacturing Engineering Society (MES) are affiliated with Materials. Its 5 year impact factor is 3.532, a JIF percentile of 65.358 with a rank of 102/293 in 2018. The impact factor, quartile, 5 year impact factor, JIF percentile, and rank information have been obtained from Journal Citation Reports (JCR) database according to the publication year. The citations have been consulted in the Scopus database.

Summary:

This first scientific article is focused on the characterization of the novel nanocrystalline material to reduce EMI problems in the 2–150 kHz frequency range. Standardization regarding emissions in the 2–150 kHz frequency range has been progressing in recent years and it is classified into the conducted electromagnetic interferences range as power quality harmonics (2–9 kHz) and CISPR A band (9–150 kHz). Electromagnetic disturbances located from 2 kHz to 150 kHz are known as supraharmonics. They are generated by modern systems based on active switching converters that are generally integrated into power conversion and supply applications such as battery electric vehicle chargers, photovoltaic systems, or wind power plants. Furthermore, these disturbances have also been detected in other systems related to household appliances and lighting installations. Thereby, it is essential to ensure electromagnetic compatibility in the 2–150 kHz frequency band and, consequently, new materials that can provide significant EMI suppression have to be proposed. This is a critical frequency spectral due to interferences generated by a wide range of devices and, specifically, communication problems in the new technologies and devices incorporated into the traditional grid to convert it into a Smart Grid.

One of the best advantages of magnetic cores is their ability to attract magnetic flux and, therefore, to reduce EMI. Nevertheless, the conventional ceramic materials such as MnZn are generally limited to the higher Kilohertz and very low Megahertz region. Other widely used core materials are those based on NiZn compositions since they work in a broadband frequency range, but they are generally not effective in the 2–150 kHz region. The results obtained by other EMC components, such as the common-mode-chokes based on nanocrystalline compositions, have shown significant effectiveness in terms of insertion loss at low frequencies because of their high initial permeability. Therefore, from these results, it is analyzed the effectiveness of another EMC component based on the nanocrystalline composition, such as sleeve cores. Designers extensively use this EMI suppression solution to meet EMC compliance requirements.

This research is carried out from the point of view of the manufacturing process, magnetic properties and EMI suppression ability. This last item is carried out through two analysis procedures: a theoretical method by determining the attenuation ratio from the

impedance parameter and proposing a new experimental technique based on directly measuring the insertion loss parameter introduced by each sample under test. Thus, it is possible to determine the performance of nanocrystalline compared to conventional cable ferrite compositions to reduce the interferences in this controversial frequency range.

The results presented in this contribution demonstrate the suitability of the novel sleeve core based on nanocrystalline composition in the 2–150 kHz frequency range compared with MnZn or NiZn materials. There is a significant match between calculated and experimental results that verifies the experimental characterization method proposed. Thereby, both theoretical and experimental measurements indicate that NC provides more significant insertion loss at low frequencies than MnZn and NiZn materials as expected from the relative permeability parameter.

The system impedance parameter has been modified to study the performance of the sleeve cores under test by introducing different load impedances and the results show that the attenuation ratio is too low in systems with a total impedance close to 1000 Ω, even when the NC sample is introduced. The analysis has been carried out with one and two turns around the sleeve cores to consider each material's performance when the number of turns is increased. These last results show that the difference between measured and calculated insertion loss is reduced when the winding is increased. This could occur because the inductance and resistance parts of the magnitude impedance are shift to lower frequencies. Thus, it can generate a change in the trend of the insertion loss measured trace. The last graph of this contribution shows an approach of the performance that the samples under test are able to provide up to 1 MHz. The results presented demonstrate that the novel NC solution yields a significant performance in terms of insertion loss in frequencies higher than 150 kHz. Consequently, this first contribution starts a new research line related to the novel NC sleeve core performance study to reduce EMI at higher frequencies.

materials

MDPI

Article

Characterization of Different Cable Ferrite Materials to Reduce the Electromagnetic Noise in the 2–150 kHz Frequency Range

Adrian Suarez [1,*], Jorge Victoria [1,2], Antonio Alcarria [1,2], Jose Torres [1], Pedro A. Martinez [1], Julio Martos [1], Jesus Soret [1], Raimundo Garcia-Olcina [1] and Steffen Muetsch [2]

[1] Department of Electronic Engineering, University of Valencia, Burjassot 46100, Spain; jorge.victoria@we-online.de (J.V.); antonio.alcarria@we-online.de (A.A.); jose.torres@uv.es (J.T.); pedro.a.martinez@uv.es (P.A.M.); julio.martos@uv.es (J.M.); jesus.soret@uv.es (J.S.); raimundo.garcia@uv.es (R.G.-O.)

[2] Würth Elektronik eiSos GmbH & Co. KG, Waldenburg 74638, Germany; steffen.muetsch@we-online.de

* Correspondence: adrian.suarez@uv.es; Tel.: +34-963-544-146

Received: 13 December 2017; Accepted: 18 January 2018; Published: 23 January 2018

Abstract: The gap of standardization for conducted and field coupled electromagnetic interferences (EMI) in the 2–150 kHz frequency range can lead to Electromagnetic Compatibility (EMC) problems. This is caused by power systems such as Pulse Width Modulation (PWM) controlled rectifiers, photovoltaic inverters or charging battery units in electric vehicles. This is a very important frequency spectral due to interferences generated in a wide range of devices and, specifically, communication problems in the new technologies and devices incorporated to the traditional grid to convert it into a Smart Grid. Consequently, it is necessary to provide new solutions to attenuate this kind of interference, which involves finding new materials that are able to filter the electromagnetic noise. This contribution is focused on characterizing the performance of a novel material based on nanocrystalline and comparing it to most common material compositions such as MnZn and NiZn. This research is carried out from the point of view of the manufacturing process, magnetic properties and EMI suppression ability. This last item is carried out through two analysis procedures: a theoretical method by determining the attenuation ratio by measuring impedance parameter and proposing a new empirical technique based on measuring directly the insertion loss parameter. Therefore, the main aim of this characterization process is to determine the performance of nanocrystalline compared to traditional cable ferrite compositions to reduce the interferences in this controversial frequency range. From the results obtained, it is possible to deduce that nanocrystalline cable ferrite provides the best performance to filter the electromagnetic noise in the 2–150 kHz frequency range.

Keywords: cable ferrite; electromagnetic interferences; low frequency emissions; nanocrystalline; relative permeability; insertion loss

1. Introduction

Standardization regarding disturbances in the 2–150 kHz frequency range has been progressing in recent years and can be classified into the conducted electromagnetic interferences (EMI) range as power quality harmonics (2–9 kHz) and CISPR A band (9–150 kHz) [1,2]. Nevertheless, there is still a gap in the standardized limits that can result in interferences between devices at the 2–150 kHz band. Electromagnetic disturbances located from 2 kHz to 150 kHz are known as supraharmonics and they are generated by most mains related to power conversion applications, like battery electrical vehicles chargers [3] or photovoltaic systems [4]. Furthermore, these disturbances have also been detected in

other kinds of systems related to household appliances such as washing machines [5] and lighting installations [6].

One of the reasons for this problem is the lack of knowledge and controllability of the low voltage harmonic grid impedances and the high sensitivity of devices to generate electromagnetic disturbances. These interferences can be caused by internal circuit topology or the presence of certain neighbor devices connected to the same grid [7]. An important problem caused by this kind of electromagnetic noise is related to the systems and devices included in the electrical network to convert it into a Smart Grid [8]. This is a significant area because one of the main consequences of a Smart Grid is a strong increase in use of electronics to include the intelligence in the power system. This means that the correct function of electronic equipment needs to be taken into account for implementing a smart power grid, which integrates intelligently, the actions of all users in order to promote renewable energy sources and efficiently use of electricity.

Specifically, most of the smart meters used to determine the power consumption are typically equipped with communication interfaces to transmit the readings to the network operator or Power Company through Power Line Communication (PLC) protocol (9 to 95 kHz). By lacking proper legislation, the frequency band 2–150 kHz has been used as the 'garbage' band during the last years [9], generating as a result, interferences in the PLC communication. Therefore, it has to be guaranteed that the unintentional emissions or interferences are lower than the intentional emission by the PLC in order to ensure its proper functionality in the 2–150 kHz frequency band.

Thereby, it is essential to ensure the electromagnetic compatibility (EMC) in the 2–150 kHz frequency band in terms of radiated and conducted disturbances. Consequently, new solutions in terms of EMI filtering have to be proposed with the aim of reducing the electromagnetic noise, which can cause disturbances in this spectral band. An interesting component that is widely used by designers to meet EMC compliance requirements is ferrite.

Ferrite is a generic term for a class of nonconductive ceramics that are based on materials such as oxides of iron, cobalt, nickel, zinc or magnesium. Ferrite manufacturers have even designed their own compositions, this implies that there is a large variety of ferrite combinations.

Ferrites provide an inexpensive way of coupling high-frequency resistance into a circuit without introducing power loss at dc or affecting any low-frequency signals present. Traditionally, ferrites have been most effective in providing attenuation of unwanted signals above 1 MHz because these components can provide the suppression of high-frequency oscillations, common-and differential-mode filtering, and the reduction of conducted and radiated emissions [10,11]. The material used to make a ferrite determines the frequency range of applicability. They are available in many different configurations, such as thru-hole beads on leads, surface-mount beads, sleeve cable cores, flat cable cores, snap on cores, toroids, etc. This contribution is focused on analyzing the performance of cable cores, also known as cable ferrites, because these components slip over a conductor lead and, hence provide a solution against EMI without the need of electronic circuit redesign.

One of the best advantages of ferrite cores is their ability to attract magnetic flux and, therefore, to suppress electromagnetic noise without grounding. In this way, when a cable is passed through a ferrite core, the magnetic field generated by the cable is concentrated inside the core and it is converted to heat and dissipated by the magnetic loss of the ferrite. Cable ferrite EMI suppressors are applied widely in electronics and telecommunications since they are able to suppress interference over a wide frequency range. They are generally focused on filtering interferences in the Megahertz band and the most common compositions are MnZn and NiZn variety [12,13]. The use of MnZn cable ferrites is usually limited to the higher Kilohertz and very low Megahertz region, whereas ferrite cores made of NiZn material work in a broadband frequency range which can cover several hundreds of Megahertz and even frequencies about 1 GHz.

The target of this research is to determine the performance of a novel cable ferrite component based on nanocrystalline (NC) material with the aim of studying its suitability for solving or reducing EMC problems in the frequency range of 2–150 kHz. Some researchers have looked into the use of NC

compositions [14] to make other EMC components, such as the common-mode-choke (CMC) in order to filter low frequency electromagnetic interferences. This is because NC cores allow the volume of the component can be reduced by 50–80% [15] and provide higher permeability and insertion losses (A) at low frequencies [16]. Thereby, a prototype of NC core is characterized and compared with MnZn and NiZn traditional ceramic cores in order to determine the effectiveness of each material in that controversial frequency range. This is firstly performed by measuring and analyzing typical core parameters provided by datasheet product such as relative permeability and impedance response. Subsequently, an experimental characterization procedure is described and carried out with the aim of determine the insertion loss parameter of each cable ferrite. This parameter is usually estimated by means of the cable ferrite impedance [11]; however, this contribution proposes an experimental method, which simulates supraharmonics generated to determine the attenuation ration that NC, MnZn and NiZn cable ferrites can provide at CISPR A band. Therefore, a comparison between the insertion loss parameter calculated theoretically from the cable ferrite impedance and the attenuation measured with the experimental setup is performed.

2. Materials and Methods

2.1. Cable Ferrites Characterization

Cable cores belong to ferromagnetic materials and it can be divided into three groups: ceramics, metals and composite materials. MnZn and NiZn cable ferrites characterized in this research are included into ceramic materials, whereas the NC core is classified as metal. The cable ferrites that have been characterized in this contribution have been selected because they have similar dimensions and, at the same time, they are composed with different materials. Thereby, it is possible to evaluate their performance to solve electromagnetic noise problems found below 150 kHz. These parameters are shown in Table 1.

Table 1. Lists of cable ferrites used in this contribution.

Ferrite Part Number	Magnetic Material	External Diameter (mm)	Internal Diameter (mm)	Height (mm)
M-4304-02	NC	18.9	12.9	27.7
74277255	MnZn	18.6	10.2	28.5
74270055	NiZn	18.6	10.2	28.5

Ceramics are also known as polycrystalline materials and, although they do not belong to metals, they can contain metal oxide such as manganese oxide or zinc oxide. The main characteristics of ceramics are their strong adhesion forces, heat resistant, hardness, brittleness and high resistance to pressure. The manufacturing process is performed by mixing the oxides, calcining the material obtained, breaking the calcined mixture, transform it into granular, pass these grains through a pressing process, synthetized the material and, finally, cover it with an epoxy resin to reduce its conductivity. One of the main advantages of ceramics manufacturing process is the possibility of creating cores with many different shapes.

NC is a magnetic material which is being increasingly used in other types of applications where low frequency electromagnetic noise can become a problem, such as energy storage, current sensors or electronic filters [17]. The main advantage of NC material is because of the material's intrinsic properties it can be used to design more reduced components with better magnetic properties for low frequency applications. NC cable ferrite, as opposed to MnZn and NiZn, is not a solid core since it is formed by a rolled up about 20 μm metal film. Figure 1 shows the cross section of the NC core in which it is possible to observe the metal film and the coated material used to press and protect it. The external coated layer is very important due to the metal film being very brittle, thus, any breaking could generate discontinuities in the material and deteriorate its performance. Consequently, one limitation

of this material is its ability to manufacture different core shapes because the metal film cannot be cut and it is not possible to manufacture air gap or snap cores.

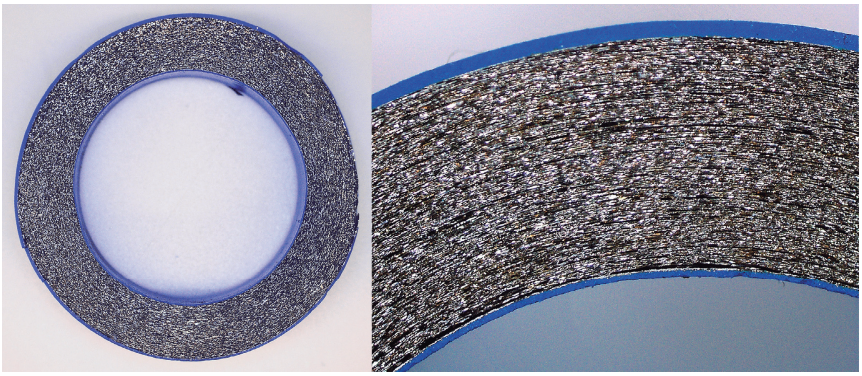

Figure 1. Cross section of nanocrystalline (NC) cable ferrite internal layers.

The NC production process is much more complex than the ceramic because, firstly, it consists of heating the material at 1300 °C in order to melt it. This material composition is mainly based on Fe, which has been added Nb, Mo and Cu amorphous metals, as well as metalloids Si and B in order to form the glass and stabilize the amorphous structure [18,19]. Once the material is converted into liquid melt, this is poured on a cooling wheel which is spinning around at 100 km/h with the aim of reducing the material temperature at a cooling rate of 10^6 K·s^{-1} [16]. This high cooling rate is necessary to generate the amorphous structure and define the thickness of the film about 20 μm. Subsequently, the film is rolled up to form the cylindrical core and it is subjected to an annealing process in which this is heated between about 500 °C and 600 °C to achieve the nanocrystalline state. During this step, the material is submitted to magnetic fields in order to improve its magnetic properties. This crystallization process of Fe-(Si,B) glasses with the addition of small amounts of amorphous metals lead to the creation of ultrafine grain sizes of typically 10–15 nm [20]. Figure 2 shows three micrographs of the samples obtained using scanning electron microscopy (SEM, Hitachi, Tokyo, Japan). In these photographs, it is possible to observe the difference between the ceramic materials where the grain size is in the order of tens of micrometers and NC material where the grain size is in the order of nanometers.

One of the most important parameters that describes the material's capacity to absorb electromagnetic noise is the permeability (μ), which is defined by micro-structural factors such as, the distribution of grain size, domain wall, spin rotation, the amount of pore and the homogeneity of chemical composition inside grain [21]. The permeability parameter relates the magnetic flux density to the magnetic field in a defined medium, thus, when a ferromagnetic material such a cable ferrite is placed in a magnetic field, the magnetic flux is concentrated in it. Thereby, the parameter that determines the factor, by which the induction (B) is modified when a material is introduced, is the relative permeability (μ_r) [22]. The losses of the magnetic flux can be quantified by separating it into its complex form so that the real component is related to the reflection or inductive part and the imaginary component provides the losses or absorption part [23,24]. The real part is represented by μ' which defines the magnetic flux that the material is able to reflect and the imaginary part corresponds to μ'' which describes the core material effectiveness to absorb the magnetic noise.

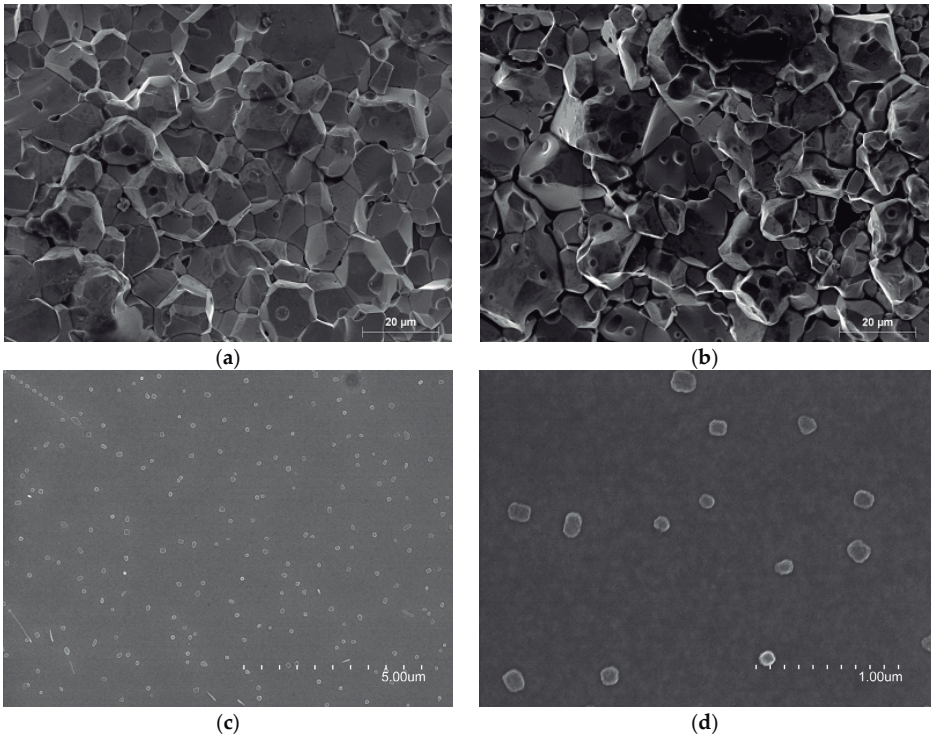

(**a**) (**b**)

(**c**) (**d**)

Figure 2. SEM photographs of ceramics and nanocrystalline core materials: (**a**) MnZn material composition; (**b**) NiZn material composition; (**c**) NC material composition; (**d**) NC material composition zoom in.

The behavior of these parameters depends on the material internal composition and it is usually represented versus the frequency. One way of knowing the performance of the three different cable ferrites materials mentioned above, is through examining the permeability parameter. Ceramic materials are defined by a high saturation and a permeability between 100 and 15,000 depending on its internal characteristics [25]. In the case of the MnZn cable ferrite, it represents a very important soft magnetic material because of its high initial magnetic permeability, saturation magnetization, electrical resistivity and low power losses [26]. Likewise, its practical range of frequencies is the medium frequency range that is going from some tens of kHz to a few MHz [27]. With regard to NiZn ferrites, they are one of the most versatile soft magnetic materials, especially suitable for high-frequency applications due to their high magnetic permeability from tens of MHz to hundreds of MHz and its larger cut-off frequency compared to another composition like MnZn [21]. In terms of composition, both ceramic materials are mostly based on iron oxide (Fe_2O_3) with a proportion of about 70%. In this way, NiZn cable ferrite contains a higher amount of Zn to improve the cut-off frequency with the aim of attenuate electromagnetic noise at higher frequencies [28,29]. Furthermore, Cu is introduced in the NiZn composition in order to reduce the firing temperature to ease the manufacturing process as well as improve electromagnetic properties at high frequencies [30]. On the other hand, NC presents a much higher initial permeability than ceramic materials because it has been annealed and subjected to a magnetization process. This improvement of magnetic properties produces a very significant increase in the permeability, reaching values about 100,000 [16].

Figure 3 represents the relative permeability traces of NC, MnZn and NiZn cable ferrite compositions split into real and imaginary components. Frequency resonance is an important value in this graph as it is the point where real and imaginary parts crosses and, thus, the material changes its dominant behavior. The values represented in this graph have been measured with specific and calibrated equipment by following two setups depending on the frequency range selected. From 1 MHz to 100 MHz, the complex relative permeability has been obtained with a E4991A Material Analyzer equipment (Keysight, Santa Rosa, CA, USA) together with its 16454A Magnetic Material Text Fixture. The 16454A makes it possible to carry out accurate permeability measurements of round-shaped magnetic materials due to the construction of this fixture creating one turn around the core without magnetic flux leakage. Thereby, it is possible to obtain complex permeability direct readouts of complex permeability. This equipment does not allow us to measure permeability from 1 kHz to 1 MHz, so a second method is employed in which relative permeability of magnetic material is obtained from the self-inductance of a round-core that has a closed loop. This second setup provides the value of effective permeability derived from the inductance measurement results by using Equations (1) and (2). This procedure is carried out with a E5061B Vector Network Analyzer (Keysight, Santa Rosa, CA, USA) together with a Terminal Adapter 16201A (Keysight, Santa Rosa, CA, USA) and the Spring Clip Fixture 16092A (Keysight, Santa Rosa, CA, USA) by rolling three turns in the cable ferrite component in order to evaluate the inductance with respect to the ends of the wire [31].

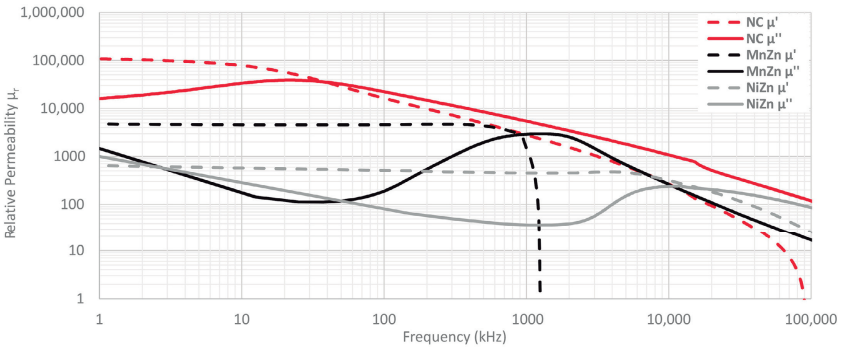

Figure 3. Complex Relative Permeability of NC, MnZn and NiZn cable ferrites compositions.

The relative permeability parameter and impedance of a certain cable ferrite are conditioned by, on the one hand, the imaginary component is related to the loss or resistive component and, on the other hand, the real component corresponds to the inductance component. The mathematical expressions which demonstrate this are given by:

$$\mu' = \frac{\ell L}{\mu_0 N^2 A} \quad (1)$$

$$\mu'' = \frac{\ell R}{\mu_0 N^2 \omega A} \quad (2)$$

where ℓ corresponds to average magnetic path length of toroidal core [m], μ_0 is the permeability of the air, N is the number of turns given with a cable to carry out the measure, A is the cross-sectional area of the toroidal core [m^2], ω is the angular frequency, R is the resistive or loss component and L is the inductance component of the cable ferrite.

One of the most used parameters for comparing different EMI core materials is the initial permeability (μ_i). This parameter describes the relative permeability of a material at low values of B (below 0.1 T). Low flux has the advantage that every cable ferrite can be measured without risk

of saturation and, therefore, it is easier to compare different compositions. According to IEC 60401-3, μ_i is defined using closed magnetic circuits for f $\leq$ 10 kHz, B < 0.25 mT, T = 25 °C. Another important parameter to find out the performance of a certain magnetic material is the Curie temperature as it indicates at which temperature it loses its ferromagnetism [16]. Figure 4 shows the change of initial permeability over a temperature range from −60 °C to 180 °C. This characterization has been performed with the equipment E4980A Precision LCR Meter (Keysight, Santa Rosa, CA, USA) that provides the initial permeability through measuring the real part of complex permeability parameter [11] and carrying out temperature sweep. Thereby, in order to evaluate the component, it has been introduced into the CST-Temperature Test Chamber series T-40. From these graphs, we can observe the great stability of the initial permeability of NC cable ferrite compared to MnZn and NiZn. NC initial permeability remains at values higher than 80%, up to about 150 °C.

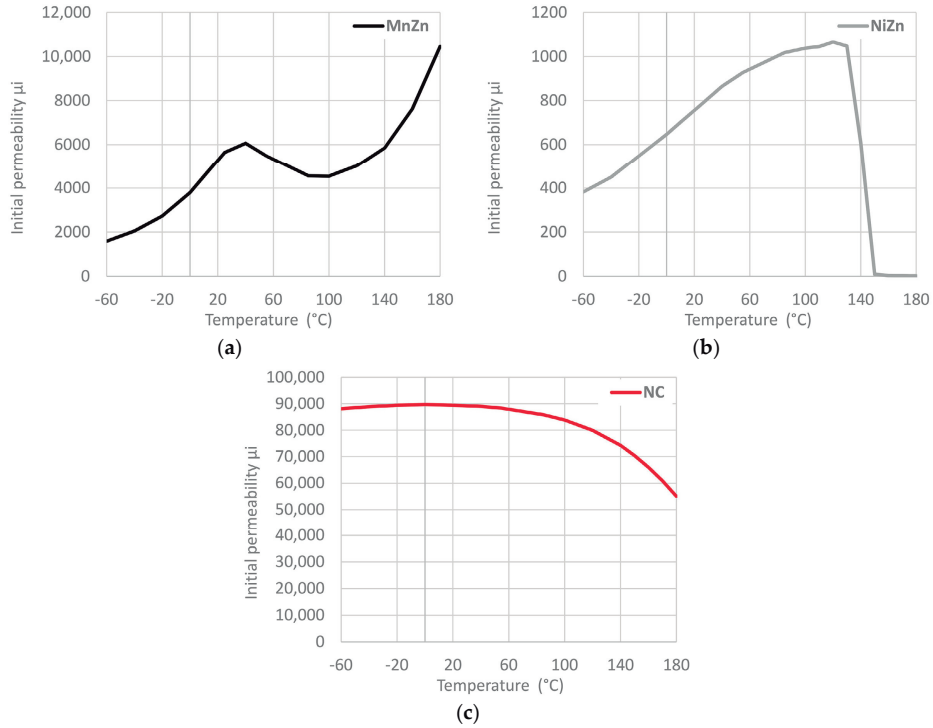

Figure 4. Initial permeability versus temperature for three different cable ferrites: (**a**) MnZn; (**b**) NiZn; (**c**) NC.

A great deal of information can be learned about the magnetic properties of a material by studying its hysteresis loop. A hysteresis or B-H loop shows the relationship between the induced magnetic flux density (B) and the magnetizing force (H). The loop is generated by measuring the magnetic flux of a ferromagnetic material while the magnetizing force is changed. As is shown in Figure 5 the hysteresis loop of three cable ferrites is measured with the equipment BsT-Pro B-H-Analyzer. From this graph, it is possible to observe that NC provides the higher magnetic saturation (B_S), that is in the point where the flux density tends to level off. B_S is defined as the maximum flux density attainable in a material at a given temperature and above this value B_S, it is not possible to further increase B by further increasing H. At B_S, almost all of the magnetic domains are aligned and an additional increase in the magnetizing force will produce very little increase in magnetic flux. When is reduced to zero, it does

not return to zero as it can be seen that some magnetic flux remains in the materials even though the magnetizing force is zero. This is referred to as remnant flux density (B_R), the point on the graph that indicates the remanence or level of residual magnetism in the materials when H = 0. NC cable ferrite shows the higher value of B_R. At this point, a part of the magnetic domain remains aligned, whereas the other part has lost its alignment. As the magnetizing force is increased from zero in the opposite direction, the flux density decreases to zero. This is called the point of coercivity of the material (H_C) and represents the magnetizing force required to remove the residual magnetism from the material. At this point, the reversed magnetizing force has flipped enough of the domains so that the net flux within the material is zero. The maximum value of coercivity is provided by the NiZn cable ferrite so that this composition material needs to be subjected to a larger magnetizing force to reduce its flux density to zero.

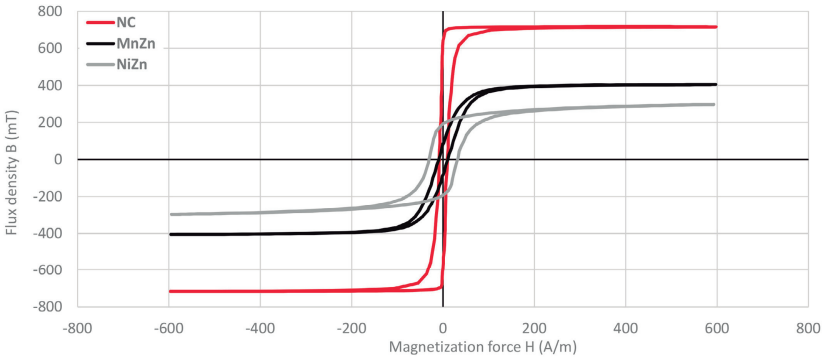

Figure 5. Hysteresis curve measured for NC, MnZn and NiZn cable ferrites.

Most important parameters of the three cable ferrites are summarized in the Table 2 in order to numerically compare the values observed in the above graphs.

Table 2. Magnetic properties of cable ferrites.

Ferrite PN	Material	Initial Perm [1]	Curie Temp [2]	Sat. Flux Density [3]	Sat. Field Density [4]	Coercivity [5]	Resonance Frequency
M-4304-02	NC	89,400	150 °C	717.8 mT	222.4 A/m	8.5 A/m	33 kHz
74277255	MnZn	5638	>180 °C	404.8 mT	477.4 A/m	9.2 A/m	875 kHz
74270055	NiZn	783	135 °C	296.7 mT	567.9 A/m	30.9 A/m	16.5 MHz

Test conditions: [1] 10 kHz, <0.5 mT, 25 °C; [2] 10 kHz, <0.5 mT; [3,4,5] 10 kHz, 600 A/m, 25 °C.

Although the permeability is one of the most important parameters which defines the performance of a cable ferrite, other means of characterizing this component are through specifying the magnitude of the impedance versus frequency. The magnitude of the impedance is given by:

$$|Z_F| = \sqrt{R^2 + (X_L)^2} \quad (3)$$

where R is the equivalent resistance of the cable ferrite and X_L is the impedance of the inductive part. The datasheets of this kind of component generally provide the trace of the ferrite impedance in the frequency range where it is effective or only specify the impedance at several frequency points. The recommended frequency range for various ferrite materials when used in noise suppression applications is shown in Figure 6. As it can be observed, traditional ferrite components such as MnZn

and NiZn are available for use over the frequency range of 150 kHz to 1 GHz, whereas NC is intended for covering the low frequency range.

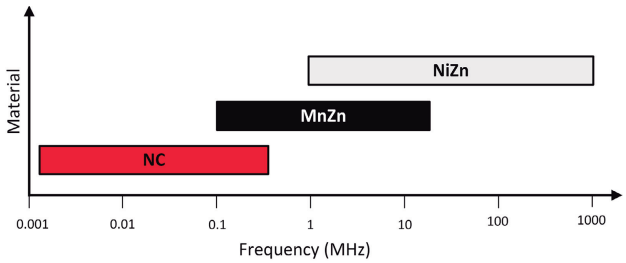

Figure 6. Material composition versus frequency range covered.

The most common ferrite geometry used in noise-suppression applications is the cylindrical core. A cable ferrite placed around a cable can be effective in reducing both conducted and radiated electromagnetic emission. Thereby, the greater the length of the cylinder, the higher the impedance, so an increase of the core length is equivalent to using several ferrites together. The attenuation or insertion loss provided by a certain cable ferrite depends on the impedance of the system in which this is placed; thus, the cable ferrite should have an impedance higher than the system impedance at the frequency of interest. Hence, they are used most effectively in low-impedance circuits [10].

An interesting characteristic of cable ferrites is the possibility of turning the cable to be filtered around them multiple times. With this technique, the ferrite impedance can be increased proportional to the number of turns squared. However, there is a balance between number of rolls and interwinding capacitance because of the higher the number of turns, the worse the performance at high frequencies. Therefore, the behavior of a cable ferrite can be improved in the 2–150 kHz frequency range, although it should not be overlooked. It is not common to use more than two or three turns. In this research, the characterization is performed by winding one and two turns in the cable ferrites.

2.2. Theoretical Insertion Loss Calculation Method

One of the most common methods used to characterize a cable ferrite is based on measuring its impedance. The impedance of a cable ferrite can be separated into two components. When this EMC component is used to suppress electromagnetic noise, the loss resistance (R), which represents the losses, needs to be taken into account. Figure 7 illustrates the contribution of loss resistance as well as inductance (X_L) to the magnitude of the impedance of the NC cable ferrite analyzed in this research. The parameters plotted on this graph have been measured through carrying out the inductance measurement method, but in this case, only one turn is rolled in the component [31]. Thereby, it can be observed in Figure 7 how the inductance is stable in a certain frequency range and show strong frequency range dependence above around 10 kHz. Above 30 MHz the inductance falls sharply, down to zero at around 80 MHz. The loss component (R) grows continuously with frequency and reaches the same value as the X_L component at the ferromagnetic resonance frequency. The resistance value rises until MHz range and dominates over the magnitude impedance (Z_F). Therefore, in this cable ferrite, the absorption part is dominant and the ability to reduce the electromagnetic noise is greater because of the ferromagnetic resonance frequency. This behavior can also be observed in Figure 3 where complex permeability of three materials is represented.

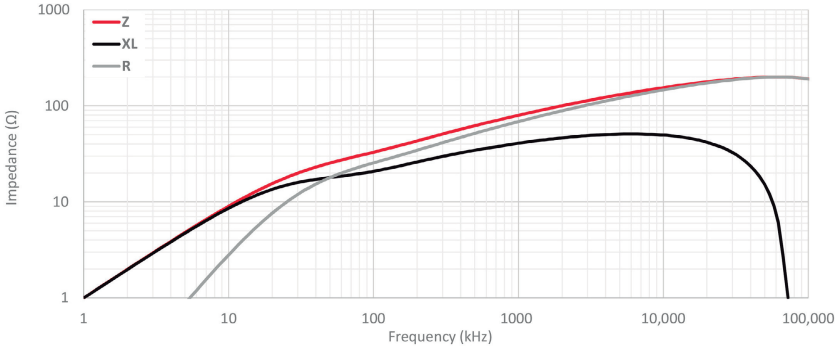

Figure 7. Magnitude of the impedance measured of NC cable ferrite and its components R and X_L.

The attenuation that this kind of component is able to provide in a certain conductor is not usually specified in datasheets in contrast to other EMC products such as common-mode-chokes. This is because the insertion attenuation or insertion loss that a cable ferrite is able to provide mainly depends on the impedance of the system in which it is placed. Subsequently, the source impedance (Z_A) and the load impedance (Z_B) of the system with electromagnetic interference problems as well as the impedance which the ferrite core introduces in that system (Z_F) are related in order to obtain an approach of the insertion loss parameter [11]. According to this, taking into account the system impedance and the ferrite impedance in a specific frequency value, the insertion loss in terms of decibels can be theoretically calculated by using this equation:

$$A(dB) = 20 \log \frac{Z_A + Z_F + Z_B}{Z_A + Z_B} \quad (4)$$

The block diagram used to obtain this equation and to analyze the effect of placing a cable ferrite into a certain system is shown in Figure 8.

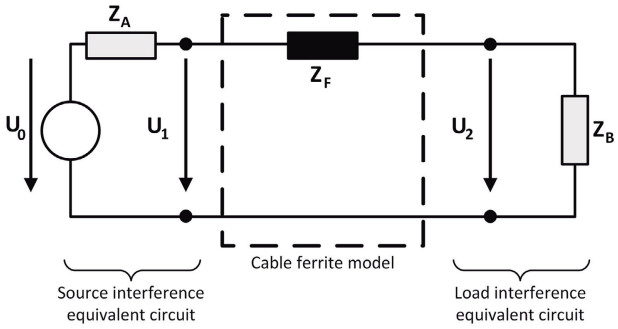

Figure 8. Diagram of source and load equivalents circuits used to determine the insertion loss parameter of a cable ferrite when it is introduced into a system.

2.3. Insertion Loss Experimental Measurement Setup

The setup used to determine the insertion loss of several cable ferrites is focused on simulating the block diagram shown in Figure 8, where the source and load impedance are known and the parameter to study is the impedance of the ferrite core. Thereby, the setup designed to simulate that diagram is shown in Figure 9 and it consists of:

- A low frequency immunity test system based on the NSG-4060/1 Low Frequency Signal Generator (TESEQ, Luterbach, Switzerland) with 50 Ω of output impedance is employed to generate the reference signal that crosses the cable ferrite. Thus, this 50 Ω output resistance represents the Z_A in the insertions loss block diagram. This sine wave generator and integrated power amplifier consists of a signal generator able to provide signals for the frequency range of 15 Hz to 150 kHz. The probe connected to this generator separates the signal and the ground terminals to place the cable ferrite only in the signal path. The main objective of this part of the setup is focused on characterizing the performance of cable ferrites in this range of frequencies through simulating the electromagnetic noise which can appear in a real system.
- The N9010A Spectrum Analyzer (Keysight, Santa Rosa, CA, USA) is used both for measuring the amplitude of the signal generated as a reference and the signal when the cable ferrite is placed around the cable. This equipment makes it possible to analyze the attenuation provided by each kind of cable ferrite in the range of 2–150 kHz. The measurement is carried out with a low frequency current probe which measures the signal before and after placing the cable ferrite.
- Different resistance loads are employed to evaluate the performance and robustness of ferrites. In order to analyze the characteristics of cable ferrites with different values of load impedance, a PCB (Printed Circuit Board) which holds several values of impedance has been designed. This circuit is intended for switching among four different values of Z_B 5 Ω, 50 Ω, 100 Ω and 1000 Ω. Since the performance of cable ferrites relies on the load impedance, this part of the setup allows us to study the behavior of each material composition in systems with different load values.

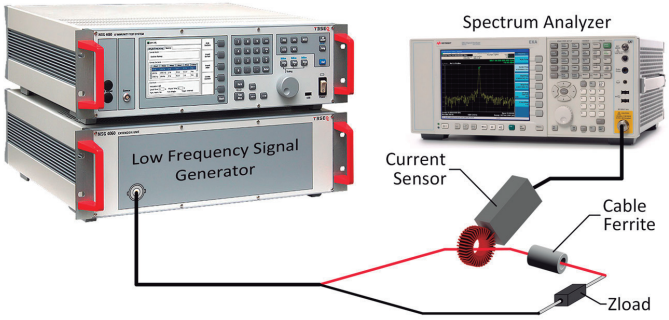

Figure 9. Measurement setup diagram to characterize cable ferrites in the 2–150 kHz frequency range.

Therefore, the test is carried out by attaching the current probe in the signal terminal of the signal generator probe and measuring the noise emitted with the Spectrum Analyzer. This is tuned to measure the interference signal generated by the Low Frequency Signal Generator in the 2–150 kHz band. This measurement process is repeated twice: only measuring the signal terminal, and measuring with the cable ferrite placed around the signal terminal.

Subsequently, both stored signals will be compared and the attenuation rate or insertion loss parameter of a certain cable ferrite can be determined by subtracting the reference signal with the signal measured after attaching the EMC component. Both measurements are acquired with the max-hold option enabled in the Spectrum Analyzer in order to compare them.

3. Results and Discussion

The results presented in this part, correspond to the analysis of the acquired data through the theoretical and experimental methods described above. Firstly, the insertion loss parameter of the three cable ferrites under test has been calculated accordingly with the described theoretical method.

Subsequently, the insertion loss parameter measured by following the experimental setup explained are plotted in order to compare both methods and characterize the three cable ferrites at low frequency range. Considering this, it is possible to evaluate the performance of nanocrystalline cable ferrite to provide a solution to filter the electromagnetic noise in the 2–150 kHz spectrum range and compare it with another material analyzed.

3.1. Theoretical Insertion Loss Results

As it has been described in Section 2.2, theoretical insertion loss parameter is calculated from the magnitude of the impedance. Figure 10 shows that the impedance of NC cable ferrite is higher than MnZn and NiZn components until 700 kHz. From this frequency, MnZn cable ferrite provides a greater performance, although its initial magnitude impedance is lower, the angle of slope of its trace is higher than NC. With regard to NiZn cable ferrite trace, it can be observed how its impedance is much lower if this is compared with NC and MnZn materials because it is destined to a higher frequency range.

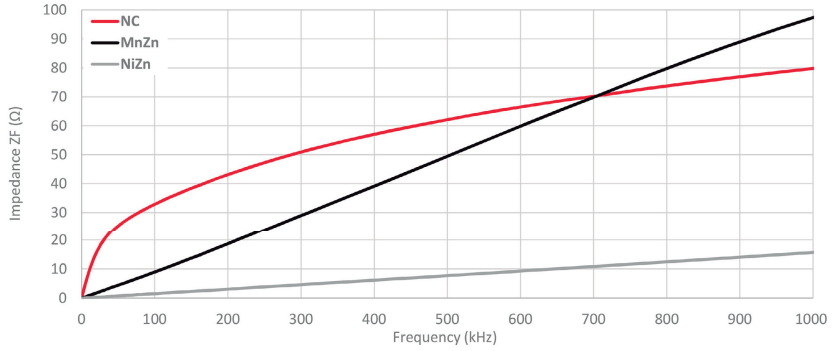

Figure 10. Impedance comparison of the three cable ferrites measured with 1 turn.

This measurement has been repeated, but in this case, by using two turns as shown in Figure 11. This change generates higher values of magnitude impedance in the three traces and a shift in the cross point of NC and MnZn traces. Thereby, if the 100 kHz point is taken as a reference, three traces have been increased about four times (the number of turns squared). Specifically, in the case of NC from 33.2 Ω to 132.7 Ω, MnZn 9.2 Ω to 36.6 Ω and NiZn cable ferrite from 1.6 Ω to 5.0 Ω. As regards the cross point between NC and MnZn traces, it has been moved from 705 kHz to 680 kHz when two turns are wound in the cable ferrites.

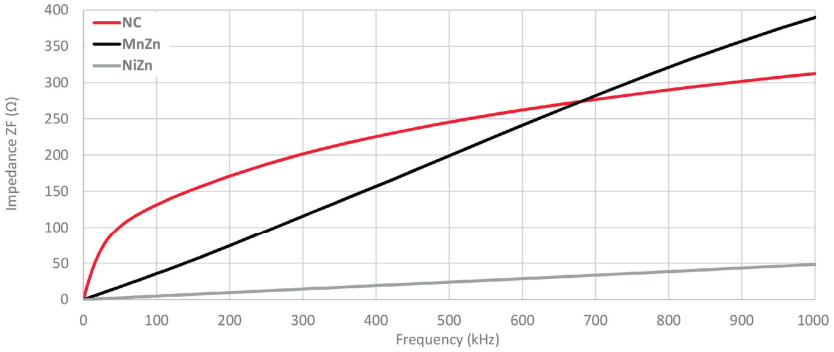

Figure 11. Impedance comparison of the three cable ferrites measured with 2 turns.

A zoom in on 2–150 kHz frequency range is performed as shown in Figure 12 in order to analyze in detail the impedance provided for each cable ferrite when one and two turns are wound. This graph demonstrates the huge difference among the impedance provided by NC cable ferrite and the others. If 100 kHz is taken as a reference, NC provides 24.0 Ω more than MnZn and 31.6 Ω than NiZn cable ferrites with one turn. Considering two turns, NC impedance is 96.1 Ω higher than MnZn and 127.7 Ω. It can be also observed that NC with one turn is even higher than MnZn with two turns until 88 kHz.

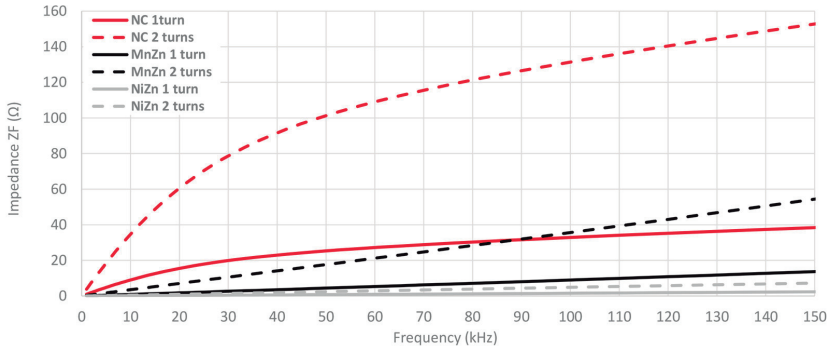

Figure 12. Impedance comparison of the three cable ferrites measured with 1 and 2 turns in the low frequency range.

Once the magnitude impedance has been analyzed, the insertion loss parameter is calculated through Equation (4) from Z_F measured of each cable ferrite, Z_A = 50 Ω and Z_B = 5 Ω. Figure 13 shows the calculated or theoretical insertion loss parameter of the three cable ferrites with one and two turns of cable are wound. As illustrated in Figure 13, NC is again the composition that provides the best performance to attenuate the electromagnetic noise until 150 kHz. Moreover, all insertion loss traces are proportional to the magnitude impedance represented above. Taking 100 kHz as a reference point, NC attenuates 2.8 dB more than MnZn and 3.8 dB than NiZn cable ferrites with one turn. In the case of two turns, NC attenuation is 6.3 dB higher than MnZn and 9.9 dB than NiZn cable ferrites.

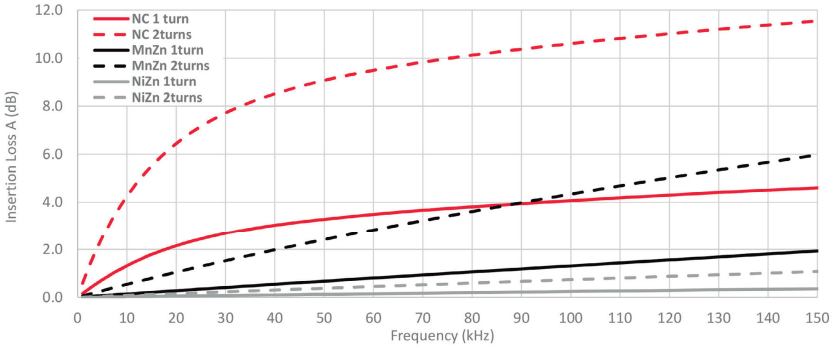

Figure 13. Theoretical insertion loss comparison depending on the material composition calculated with a 5 Ω load and winding 1 and 2 turns.

Another factor to consider is the performance of cable ferrites in systems with different impedance and, thus, it could be interesting to study the insertion loss parameter by including several values of Z_A and/or Z_B in Equation (4). Consequently, Figure 14 shows a comparison among the insertion

loss parameter calculated from Z_F measured of each cable ferrite with one turn, setting Z_A = 50 Ω and Z_B = 5 Ω or Z_B = 50 Ω. This chart illustrates how, the higher the system output impedance in which the cable ferrite is included, the lower the insertion loss that is able to provide the cable ferrite. At the 100 kHz frequency point, there is a difference of 1.6 dB between the NC traces with 5 Ω and 50 Ω, 0.5 dB in the case of MnZn traces and 0.2 dB for NiZn traces.

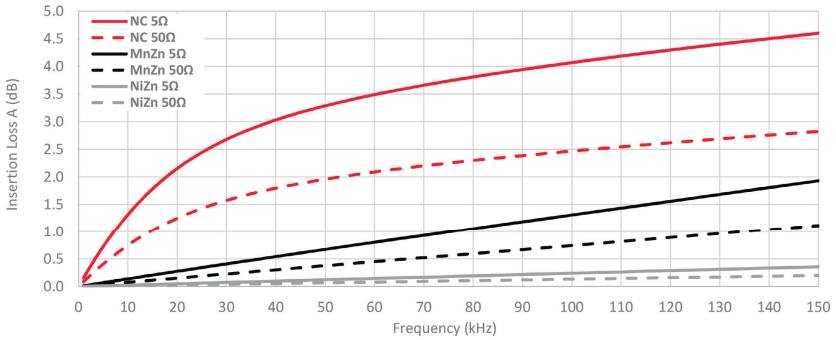

Figure 14. Theoretical insertion loss comparison depending on the material composition calculated with 5 Ω and 50 Ω loads by winding 1 turn.

This connection between the system impedance and the ability of cable ferrites to attenuate the interferences is displayed in Figure 15, where the insertion loss is calculated by setting Z_A = 50 Ω and Z_B is switched among the next values: 5 Ω, 50 Ω, 100 Ω and 1000 Ω. The material selected to analyze this connection is the NC because it provides the best performance in this frequency range. Thereby, this graph shows that the theoretical insertion loss is much reduced when the impedance of the system is close to 1 kΩ. However, if the system has an input impedance of 50 Ω and an output impedance less than 100 Ω the NC cable ferrite with one turn can provide useful behavior.

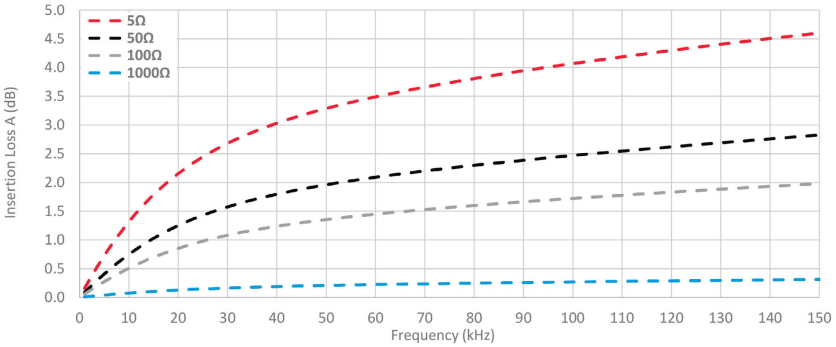

Figure 15. Theoretical insertion loss comparison depending on load calculated with 5 Ω, 50 Ω, 100 Ω and 1000 Ω loads by winding 1 turn in the NC cable ferrite.

3.2. Experimental Insertion Loss Results

The experimental insertion loss is measured by following the procedure explained in Section 2.3. Figure 16 shows an example of the measurement method used to determine the insertion loss parameter with one turn (a) and two turns (b). Experimental insertion loss is determined by subtracting to the trace 1 (yellow), which represents the reference before placing any cable ferrite in the system, one of

the other three traces. Trace 2 (blue) represents the signal measured after placing the NC cable ferrite, trace 3 (purple) corresponds to MnZn and trace 4 (blue) is acquired when the NiZn cable ferrite is placed. Therefore, the insertion loss of NC cable ferrite at 100 kHz is given by subtracting markers 1 and 2 represented in the table below the spectrum in (a) in the case of one turn and (b) in the case of two turns. As a result of this step, the insertion loss obtained for the NC cable ferrite is 3.486 dB with one turn and 9.993 dB when the cable ferrite is wound with two turns. Consequently, by extrapolating this method to the whole frequency range of 2–150 kHz it is possible to obtain the performance of each material in terms of attenuation ratio.

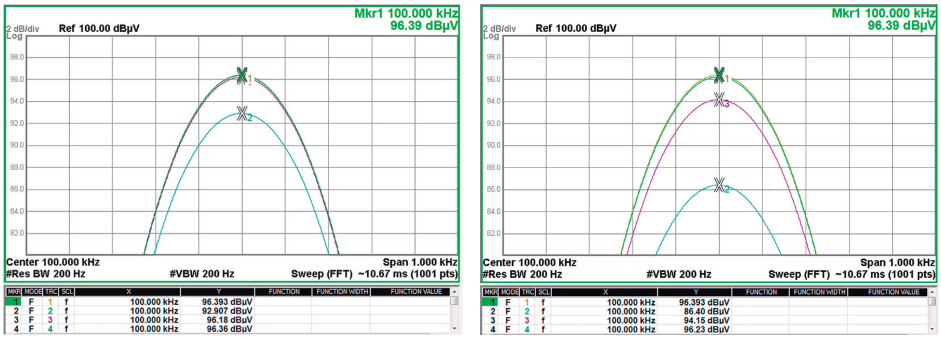

(**a**) (**b**)

Figure 16. Experimental attenuation measured with a spectrum analyzer for each cable ferrite material with a 5 Ω (Reference: trace 1 yellow, NC: trace 2 blue, MnZn: trace 3 purple, NiZn: trace 4 green): (**a**) Signal measured after placing each cable ferrite with one turn; (**b**) Signal measured after placing each cable ferrite with two turns.

A comparison between the theoretical insertion loss and the insertion loss measured with the three material cable ferrites with one turn wound is shown in Figure 17. The measured value of NC cable ferrite is 1.2 dB lower than the theoretical NC trace at 20 kHz, although, at 100 kHz this difference is reduced up to 0.6 dB. Nevertheless, in the case of MnZn and NiZn, the higher the frequency, the higher the difference between theoretical and experimental insertion loss. Hence, the NC traces trend is very similar but the theoretical and experimental traces of MnZn and NiZn do not follow the same trend.

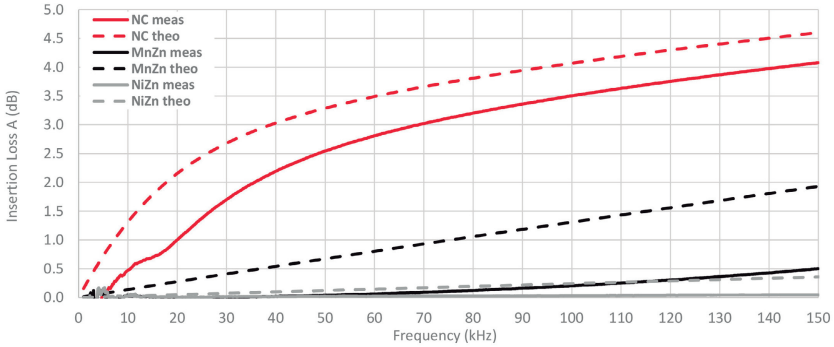

Figure 17. Experimental insertion loss comparison depending on the material composition calculated with a 5 Ω load by winding 1 turn.

Figure 18 shows the same comparison as the last graph but in this case, the number of turns wound with the cable in the cable ferrite is two. It can be observed how the difference between theoretical and measured traces is lower with two turns. At 20 kHz, the NC insertion loss measured is 1.8 dB lower than theoretical value and this difference is reduced up to in 0.6 dB at 100 kHz. Thus, the relative error has been reduced taking into account that the attenuation ratio has been almost tripled (from 3.5 dB to 10.1 dB at 100 kHz in the case of measured insertion loss traces). With regard to MnZn, the trend of measured insertion loss trace has been modified and the difference with the theoretical trace has been reduced. This effect can also be observed in the NiZn traces, although to a lesser extent than NC and MnZn.

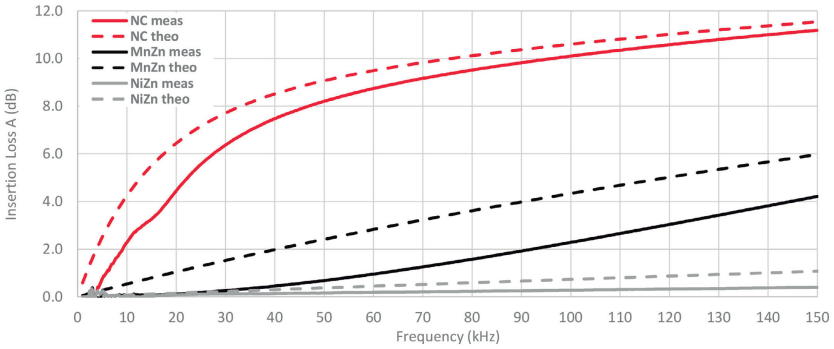

Figure 18. Experimental insertion loss comparison depending on the material composition calculated with a 5 Ω load by winding 1 turn.

Another point to take into account is the connection between the impedance of the system where the cable ferrite is placed and the insertion loss that it is able to provide. In order to evaluate this, the insertion loss of the NC cable ferrite is measured by setting Z_A = 50 Ω and modifying Z_B among the next values: 5 Ω, 50 Ω, 100 Ω and 1000 Ω. Figure 19 shows this comparison combined with the theoretical insertion loss traces showed in the Figure 15. According to the graph, traces that represent measured insertion loss are lower than theoretical traces, although the trend of both is very similar. Just as for the theoretical NC trace, the experimental insertion loss measured shown in this graph is insignificant when the system impedance is close to 1000 Ω.

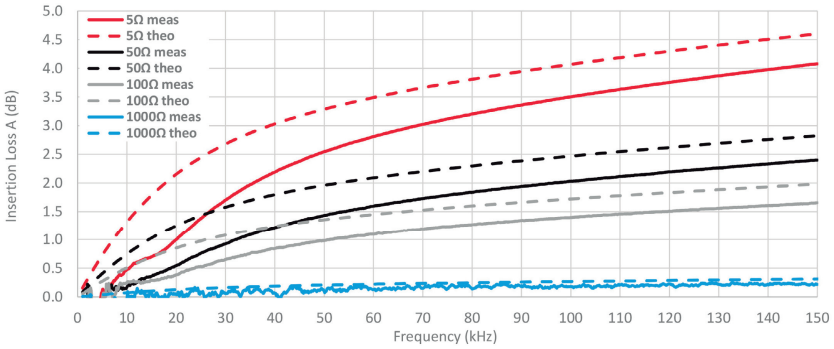

Figure 19. Comparison between experimental and theoretical insertion loss of NC cable ferrite depending on the load by winding 1 turn.

Figure 20 shows the same comparison as Figure 19, but in this case, two turns are wound in the NC cable ferrite. Therefore, the difference between measured and theoretical insertion loss is reduced regardless of the system impedance. Moreover, it can be observed that the higher the frequency, the lower the difference between theoretical and experimental insertion loss.

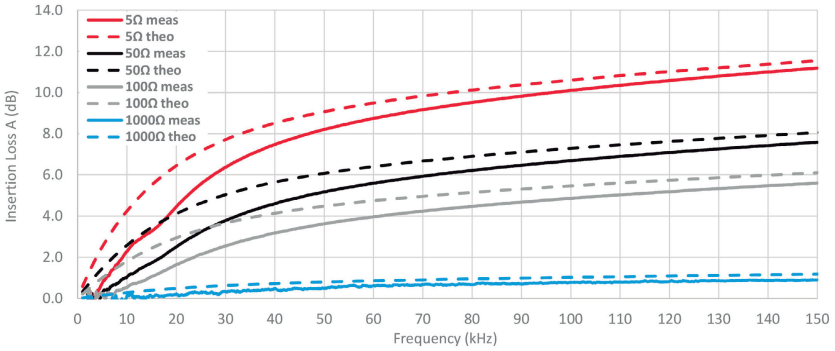

Figure 20. Comparison between experimental and theoretical insertion loss of NC cable ferrite depending on the load by winding 2 turns.

Considering that the difference between theoretical and experimental insertion loss traces is lower at high frequencies, the insertion loss has been measured with a general purpose signal generator with the aim of obtaining a qualitative trend up to 1 MHz. This measurement has been carried out for the three cable ferrites with one turn and compared to the calculated insertion loss in Figure 21. Therefore, it is possible to observe that the difference between NC traces is lower at high frequency and MnZn traces match at 700 kHz. Nevertheless, the difference between NiZn traces is higher at 1 MHz.

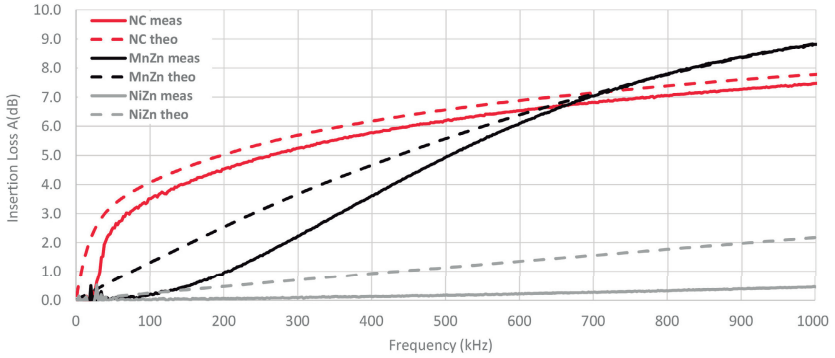

Figure 21. Comparison between experimental and theoretical insertion loss of different cable ferrites depending on the material composition by winding 1 turn at higher frequencies.

4. Conclusions

A characterization of a novel nanocrystalline cable ferrite and a comparison with traditional materials has been performed from the point of view of magnetic properties, manufacturing process and EMI suppression ability.

The results presented in this contribution demonstrate the suitability of cable ferrites based on nanocrystalline composition in the 2–150 kHz frequency range in comparison with others based on

MnZn or NiZn. This has been verified theoretically through calculating the insertion loss from the measured impedance of each cable ferrite material and taking into account the system impedance where the component is placed. A way of determining the attenuation ratio or insertion loss through an experimental setup has been proposed and these measurements have been matched with the theoretical insertion loss in order to check the accuracy of this technique. Thereby, the measurements performed both theoretical and experimental, indicate that NC provides greater losses at low frequencies than MnZn and NiZn as shown the relative permeability graph.

The system impedance parameter has been modified to study the performance of cable ferrites with several output impedances and the results show that the attenuation ratio is too low in systems with an impedance close to 1000 Ω. Likewise, the analysis has been done with one and two turns around the cable ferrites in order to take into account the performance of each material when the number of turns is increased. These last measurements show that the difference between measured and calculated insertion loss is reduced when the winding is increased. This could take place because the inductance and resistance parts of the magnitude impedance are shifted to lower frequencies. Thus, it can generate a change in the trend of the insertion loss measured trace. This difference between theoretical and experimental data can be also analyzed from the point of view of permeability because, as shown Figure 21, theoretical and experimental values are nearer from the frequency resonance point in which losses are higher. In the case of NC, this takes place at 45 kHz and from this point, it is possible to observe a reduction in the difference between theoretical and experimental traces. With regard to MnZn, there is a nearness between theoretical and experimental traces as the frequency increases and, both traces match from the frequency resonance point up to higher frequencies. The same effect could be observed at 10 MHz where the absorption part starts being more dominant in the case of NiZn cable ferrite. Consequently, a new line of research can be carried out from the results of this contribution, because this setup can be adapted to determine the insertion loss with the aim of evaluating cable ferrites at higher frequencies. This method could make it possible to study the accuracy of the insertion loss mathematical expression in order to know if R (μ'') and X_L (μ') should be considered with a different weight in this theoretical approximation.

Acknowledgments: This work was supported by the Catedra Würth-EMC, a research collaboration agreement between the University of Valencia and Würth Elektronik eiSos GmbH & Co. KG.

Author Contributions: J. Victoria and J. Torres conceived and designed the experimental measurement setup; A. Alcarria, P.A. Martinez, J. Soret and J. Martos performed the experiments; A. Suarez, R. Garcia-Olcina and P.A. Martinez analyzed the data; A. Suarez, R. Garcia-Olcina, J. Soret, J. Martos, J. Torres and J. Victoria wrote and reviewed the paper.

Conflicts of Interest: The authors declare no conflict of interest. The founding sponsors had no role in the design of the study; in the collection, analyses, or interpretation of data; in the writing of the manuscript, and in the decision to publish the results.

References

1. Bollen, M.; Olofsson, M.; Larsson, A.; Rönnberg, S.; Lundmark, M. Standards for supraharmonics (2 to 150 kHz). *IEEE Electromagn. Compat. Mag.* **2014**, *3*, 114–119.
2. Luszcz, J. High Frequency Harmonics Emission in Smart Grids. In *Power Quality Issues*; Zobaa, A., Ed.; InTech: Rijeka, Croatia, 2013; pp. 277–280.
3. Schöttke, S.; Meyer, J.; Schegner, P.; Bachmann, S. Emission in the frequency range of 2 kHz to 150 kHz caused by electrical vehicle charging. In Proceedings of the International Symposium on Electromagnetic Compatibility, Gothenburg, Sweden, 1–4 September 2014; pp. 620–625.
4. Rönnberg, S.; Bollen, M.; Larsson, A. Emission from small scale PV-installations on the low voltage grid. In Proceedings of the International Conference on Renewable Energies and Power Quality, Córdoba, Spain, 8–10 April 2014; pp. 617–621.
5. Bartak, G.F.; Abart, A. EMI of emissions in the frequency range 2 kHz–150 kHz. In Proceedings of the 22nd International Conference and Exhibition on Electricity Distribution, Stockholm, Sweden, 10–13 June 2013.

6. Gil-de-Castro, A.; Rönnberg, S.K.; Bollen, M.H.; Moreno-Muñoz, A. Study on harmonic emission of domestic equipment combined with different types of lighting. *Int. J. Electr. Power Energy Syst.* **2014**, *55*, 116–127.
7. Subhani, S.; Cuk, V.; Coben, J.F.G. A Literature Survey on Power Quality Disturbances in the Frequency Range of 2–150 kHz. In Proceedings of the International Conference on Renewable Energies and Power Quality, Málaga, Spain, 8–10 April 2017; pp. 405–410.
8. Smolenski, R. Conducted Electromagnetic Interference (EMI) in Smart Grids. In *Power Systems*; Springer Science & Business Media: London, UK, 2012.
9. Coenen, M.; van Roermund, A. Conducted mains test method in 2–150 kHz band. In Proceedings of the International Symposium on Electromagnetic Compatibility, Gothenburg, Sweden, 1–4 September 2014; pp. 601–604.
10. Ott, H.W. *Electromagnetic Compatibility Engineering*; John Wiley & Sons: Hoboken, NJ, USA, 2009; pp. 225–234.
11. Brander, T.; Gerfer, A.; Rall, B.; Zenkner, H. *Trilogy of Magnetics: Design Guide for EMI Filter Design, SMP & RF Circuits*, 4th ed.; Swiridoff Verlag: Künzelsau, Germany, 2010.
12. Lukovic, M.D.; Nikolic, M.V.; Blaz, N.V.; Zivanov, L.D.; Aleksic, O.S.; Lukic, L.S. Mn-Zn ferrite round cable EMI suppressor with deep grooves and a secondary short circuit for different frequency ranges. *IEEE Electromagn. Compat. Mag.* **2013**, *49*, 1172–1177.
13. Tsutaoka, T. Frequency dispersion of complex permeability in Mn-Zn and Ni-Zn spinel ferrites and their composite materials. *J. Appl. Phys.* **2003**, *93*, 2789–2796.
14. Herzer, G.; Vazquez, M.; Knobel, M.; Zhukov, A.; Reininger, T.; Davies, H.A.; Sanchez Ll, J.S. Round table discussion: Present and future applications of nanocrystalline magnetic materials. *J. Magn. Magn. Mater.* **2005**, *294*, 252–266.
15. Thierry, W.; Thierry, S.; Benoît, V.; Dominique, G. Strong volume reduction of common mode choke for RFI filters with the help of nanocrystalline cores design and experiments. *J. Magn. Magn. Mater.* **2006**, *304*, 847–849.
16. Herzer, G. Modern soft magnets: Amorphous and nanocrystalline materials. *Acta Mater.* **2013**, *61*, 718–734.
17. Liu, Y.; Han, Y.; Liu, S.; Lin, F. Pulse Magnetic Properties Measurement and Characterization of Fe-Based Nanocrystalline Cores for High-Voltage Pulse Magnetics Applications. *IEEE Trans. Power Electron.* **2015**, *30*, 6883–6896.
18. Davies, H.; Gibbs, M. *Handbook of Magnetism and Advanced Materials*; Kronmüller, K., Parkin, S., Eds.; John Wiley & Sons: London, UK, 2007; Volume 4.
19. Boll, R.; Hilzinger, HR.; Warlimont, H. *The Magnetic, Chemical and Structural Properties of Glassy Metallic Alloys*; Hasegawa, R., Ed.; CRC Press: Boca Raton, FL, USA, 1983.
20. Yoshizawa, Y.; Oguma, S.; Yamauchi, K. New Fe-based soft magnetic alloys composed of ultrafine grain structure. *J. Appl. Phys.* **1988**, *64*, 6044–6046.
21. Kawano, K.; Hachiya, M.; Iijima, Y.; Sato, N.; Mizuno, Y. The grain size effect on the magnetic properties in NiZn ferrite and the quality factor of the inductor. *J. Magn. Magn. Mater.* **2009**, *321*, 2488–2493.
22. Goldman, A. *Modern Ferrite Technology*, 2nd ed.; Springer Science & Business Media: Pittsburgh, PA, USA, 2006.
23. Suarez, A.; Victoria, J.; Alcarria, A.; Torres, J. Characterization of electromagnetic noise suppression sheet for aerospace applications. In Proceedings of the ESA Workshop on Aerospace EMC, Valencia, Spain, 23–25 May 2016; pp. 1–6.
24. Sharma, A.; Rahman, N.; Obol, M.; Afsar, M. Precise characterization and design of composite absorbers for wideband microwave applications. In Proceedings of the European Microwave Conference, Paris, France, 28–30 September 2010; pp. 160–163.
25. Jiles, D. *Introduction to Magnetism and Magnetic Materials*, 3rd ed.; CRC Press: Boca Raton, FL, USA, 2016.
26. Hu, P.; Yang, H.B.; Pan, D.A.; Wang, H.; Tian, J.J.; Zhang, S.; Wang, X.; Volinsky, A.A. Heat treatment effects on microstructure and magnetic properties of Mn-Zn ferrite powders. *J. Magn. Magn. Mater.* **2010**, *322*, 173–177.
27. Beatrice, C.; Bottauscio, O.; Chiampi, M.; Fiorillo, F.; Manzin, A. Magnetic loss analysis in Mn-Zn ferrite cores. *J. Magn. Magn. Mater.* **2006**, *304*, e743–e745.
28. Sun, G.L.; Li, J.B.; Sun, J.J.; Yang, X.Z. The influences of Zn^{2+} and some rare-earth ions on the magnetic properties of nickel-zinc ferrites. *J. Magn. Magn. Mater.* **2004**, *281*, 173–177.
29. Costa, A.C.F.M.; Tortella, E.; Morelli, M.R.; Kiminami, R.H.G.A. Synthesis, microstructure and magnetic properties of Ni-Zn ferrites. *J. Magn. Magn. Mater.* **2003**, *256*, 174–182.

30. Stergiou, C.A.; Zaspalis, V. Analysis of the complex permeability of NiCuZn ferrites up to 1 GHz with regard to Cu content and sintering temperature. *Ceram. Int.* **2014**, *40*, 357–366.
31. Keysight E5061B-3L3/3L4/3L5 LF-RF Network Analyzer with Option 005 Impedance Analysis Function. Available online: http://literature.cdn.keysight.com/litweb/pdf/5990-7033EN.pdf (accessed on 22 November 2017).

Chapter 4. CHARACTERIZATION METHOD PROPOSAL TO DETERMINE THE NANOCRYSTALLINE EMI SUPPRESSOR PROPERTIES.

This chapter presents a new characterization setup is implemented with the aim of obtaining the insertion loss parameter in a considerable frequency range ensuring that the parasitic effects do not modify the reference system impedance, especially in the high-frequency region (from 100 MHz). These results make it possible to determine the impedance provided and compare it with the results obtained from directly measured impedance and the impedance determined from the magnetic properties of each material. Thereby, the frequency range studied covers from conducted emission range to the low range of radiated emissions in order to understand which is the most effective material to reduce them depending on the frequency.

4.1 Scientific article II

Authors: Effectiveness Assessment of a Nanocrystalline Sleeve Ferrite Core Compared with Ceramic Cores for Reducing Conducted EMI.

Authors: Adrian Suarez, Jorge Victoria, Jose Torres, Pedro A. Martinez, Antonio Alcarria, Julio Martos, Raimundo Garcia-Olcina, Jesus Soret, Steffen Muetsch and Alexander Gerfer.

Published in: Electronics (MDPI), vol. 8, no. 7, p. 800 (2019).
DOI: 10.3390/electronics8070800

Impact factor: 2.412 (2019).

Quartile (category: "Engineering, Electrical & Electronics"): Q2 (2019)

Citations: 7 (accessed on March 2021).

Description: Electronics (ISSN 2079-9292; CODEN: ELECGJ) is an international peer-reviewed open access journal on the science of electronics and its applications published

semimonthly online by MDPI. Its JIF percentile is 53.195 with a rank of 125/266 in 2019. The impact factor, quartile, JIF percentile, and rank information have been obtained from Journal Citation Reports (JCR) database according to the publication year. The citations have been consulted in the Scopus database.

Summary:

This second scientific article introduces the novel nanocrystalline material analysis in an extended frequency range that covers from 100 kHz to 200 MHz. The NC EMI suppression effectiveness is compared to the provided by MnZn and NiZn solutions with the aim of determining the frequency regions where each material is effective. The research highlights the suitability of an NC novel component in terms of its magnetic properties to reduce EMI within the conducted emissions range. This range is generally defined by the International Special Committee on Radio Interference (CISPR) test standards frequency band covering from 150 kHz up to 30 MHz (108 MHz in the case of CISPR 25). First, this study presents a description of the main parameters that define NC and ceramic materials' behavior and, secondly, by analyzing the data obtained from experimental procedures, it is possible to determine the insertion loss parameter directly. Hence, a new characterization setup is implemented with the aim of obtaining the insertion loss parameter in a considerable frequency range ensuring that the parasitic effects do not modify the reference system impedance, especially in the high-frequency region (from 100 MHz).

When a sleeve core is applied in a conductor, the magnetic field is concentrated into magnetic flux inside the core because it provides a higher magnetic permeability than air. As a result, the flowing noise current in the cable is reduced and, thus, the EMI is attenuated. Sleeve cores EMI suppressors are widely applied to reduce common-mode currents in cables because despite not being the predominant currents, they can result in a much greater interfering potential. Only a few microamps flowing through a cable are required to fail radiated emission requirements. Thereby, the frequency range studied in this contribution covers from conducted emission range to the low range of radiated emissions in order to understand which is the most effective material to reduce them depending on the frequency.

This contribution covers the following items:

- An extensive characterization of the relative magnetic permeability is carried out with the aim of analyzing its components (μ_r, μ', μ'') and relate them with the impedance components (Z_{SC}, X_L, R) provided by the sleeve core.

- The limitations of the measurement impedance setup are described and characterized. Consequently, it is necessary to consider the wire introduced into the sleeve core in the calibration procedure in order to avoid the influence of its impedance in the total impedance provided by the equipment. It has been demonstrated that the influence of the cable in the total impedance can introduce parasitic effects, especially from 200 MHz when a 150 mm cable is employed.

- The phase angle (φ), which is defined by the angle whose sine is X_L/R has been studied to determine the behavior of the three sleeve cores under test. When it corresponds to 90°, the core works as a pure inductor, whereas for 0°, it works as a pure resistor. If the phase reaches negative values, the sleeve core reduces its EMI suppression ability due to the fact that it is starting to show a capacitive and an undesired behavior in terms of filtering effectiveness.

- An experimental measurement set up to determine the insertion loss introduce by each sleeve core under test is presented. This technique is based on generating controlled EMI into a load with a stable impedance through a characterized cable over the frequency range studied (from 100 kHz up to 200 MHz) to determine the insertion loss.

- The impedance response has been obtained mathematically from the magnetic properties and the measured insertion loss parameter with the aim of comparing it with the experimental impedance response measurement of each of the sleeve core samples. This procedure is performed to analyze the accuracy of the impedance measurement considering the calibration procedure proposed. It is verified that the three responses significantly match up to the resonance frequency value, since from this point, the impedance calculated from the permeability data continues increasing, unlike the other two traces.

Consequently, the novel NC sleeve core prototype's performance has been compared with the effectiveness provided by ceramic cores. It has been analyzed the performance of each EMI suppression solution from the standpoint of the magnetic properties, impedance, and insertion loss. Considering all the data presented in this contribution, it is concluded that NC represents an EMI filtering solution to reduce the interferences in the low- and medium-frequency regions (up to 50 MHz). If the EMI disturbance is specifically located in the low-region MnZn represents an effective solution, whereas if the EMI problems are located from 50 MHz, a NiZn core may be used since it provides a similar performance to NC. Nonetheless, if the EMI interferences are distributed outside of these regions or from the low-frequency region up to about 100 MHz, the NC sleeve

core shows a better performance than ceramics to reduce EMI emissions in a wideband frequency range.

electronics

MDPI

Article

Effectiveness Assessment of a Nanocrystalline Sleeve Ferrite Core Compared with Ceramic Cores for Reducing Conducted EMI

Adrian Suarez [1,*], Jorge Victoria [1,2], Jose Torres [1], Pedro A. Martinez [1], Antonio Alcarria [2], Julio Martos [1], Raimundo Garcia-Olcina [1], Jesus Soret [1], Steffen Muetsch [2] and Alexander Gerfer [2]

[1] Department of Electronic Engineering, University of Valencia, 46100 Burjassot, Spain
[2] Würth Elektronik eiSos GmbH & Co. KG, 74638 Waldenburg, Germany
* Correspondence: adrian.suarez@uv.es; Tel.: +34-963-544-146

Received: 21 June 2019; Accepted: 15 July 2019; Published: date

Abstract: The interconnection of different electronic devices or systems through cables is becoming more difficult due to the hard restrictions related to electromagnetic compatibility (EMC) in order to comply with requirements. Therefore, the use of EMC components is a good solution to manage the problems associated with the filtering of electromagnetic interference (EMI) in cables and to pass the compliance test. In this sense, sleeve ferrite cores become a very interesting solution since they can be set around a wire and, hence, they provide an effective solution against EMI without having to redesign the electronic circuit. This contribution is focused on the characterization of the performance of a sleeve ferrite core based on a novel nanocrystalline (NC) novel material for EMI suppression and comparing it to the most conventional ceramic ferrite cores such as MnZn and NiZn. The research highlights the suitability of an NC novel component in terms of its magnetic properties to reduce EMI within the conducted emissions range. This range is generally defined by the International Special Committee on Radio Interference (CISPR) test standards frequency band that covers from 150 kHz up to 30 MHz (108 MHz in the case of CISPR 25). First, this study presents a description of the main parameters that define the behavior of NC and ceramic cores and, secondly, by analyzing the data obtained from experimental procedures, it is possible to directly determine the insertion loss parameter. Hence, this characterization procedure is used to obtain the performance of NC material compared to the conventional sleeve ferrite core compositions employed to filter the interferences in this problematic frequency range. As can be deduced from the results obtained, an NC sleeve ferrite core provides the best performance in terms of EMI filtering within a significant frequency range between 100 kHz and 100 MHz.

Keywords: nanocrystalline (NC); sleeve ferrite core; cable ferrite; cable filtering; electromagnetic interference (EMI) suppression; conducted emissions; relative permeability; impedance; insertion loss

1. Introduction

The fast development of electrical and electronic products has become an increasingly serious electromagnetic interference (EMI) problem faced by engineers and scientists [1]. This situation intensifies the presence of interference generated by electromagnetic fields; therefore, it is becoming increasingly difficult to ensure all devices operate simultaneously in the context of electromagnetic compatibility (EMC) without inferring with each other [2].

EMI can be one of the main causes that generates the degradation (performance-wise) of an electronic system; this usually occurs at frequencies that are higher than the signals traveling the

circuit. The most common sources of these interferences include natural ones (such as atmospheric electrical phenomena), power lines, auto ignition or radio frequency (RF) interference.

In terms of the kind of disturbance that is transmitted, EMI is divided into two categories: conducted and radiated emissions; regarding the way the electromagnetic field is propagated. In the case of radiated EMI, it is caused by induction whereas conducted EMI is generated by physical contact of conductors. Thus, in the low frequency range EMI is generally emitted via conduction and, in the high frequency region via radiation. Likewise, conducted EMI can be classified into two kind of currents in terms of different directions of leading: differential mode (DM) and common mode (CM) [3]. In the correct working of a circuit, a differential current is designed to flow in order to obtain a clear signal. When opposing currents are created and flow in the same direction as the intended current, the differential intended currents are canceled. In CM, currents flow in both conductors in the same direction and are not suppressed as they are non-intentional (EMI) currents [4,5].

This contribution is focused on the filtering of conducted EMI in which the upper limit is specified by CISPR-based test standards (CISPR 11, 14-1 and 32) up to 30 MHz, except for CISPR 25, where the applicable upper frequency extends to 108 MHz [6]. In particular, the most common EMI sources that interfere in the conducted range are switch-mode power converters [7]. Both embedded DC–DC converters are intended for a large number of commonly used electronic devices [8] and high–low voltage DC–DC converters employed to charge Electric Vehicle batteries [9] contribute to the generation of EMI in this frequency band. In order to avoid, or at least reduce EMI, suppressors should work as low-pass filters, suppressing signals with frequencies higher than the intended signal frequency value [1]. Nowadays, most electronic products are connected to the main power network or are designed to be interconnected with others through cables. These cable interconnections are becoming more difficult due to the hard restrictions related to the accomplishment of EMC compliance. Thereby, the use of EMC components is a good solution to manage the problems linked to the EMI filtering in cables and pass the compliance test. In this sense, sleeve ferrite cores (also known as cable ferrites) are a very interesting solution since they can be set around a wire and provide an effective solution against EMI without having to redesign the electronic circuit. These components are widely used in EMI filtering applications because they are usually applied to be set on power cables or peripheral cables of electronic devices in order to prevent electromagnetic disturbance that could be propagated along the wire, as shown in Figure 1 [10,11]. This filtering method enables limiting of the conducted emissions [12,13] and can be applied in electronics and telecommunications elements [2,7,14]. Therefore, when a disturbance current is flowing in the peripheral and/or power wires connected to the device, the manufacturer usually decides to attach a sleeve ferrite core to encircle these cables. This is due to the fact that the sleeve ferrite core introduces a certain insertion loss (A) by which the disturbance current flowing through it is reduced and, therefore, EMI is attenuated [15]. Furthermore, these cores are ideally suited for reducing the EMI interferences because they are very effective against CM currents [4,10].

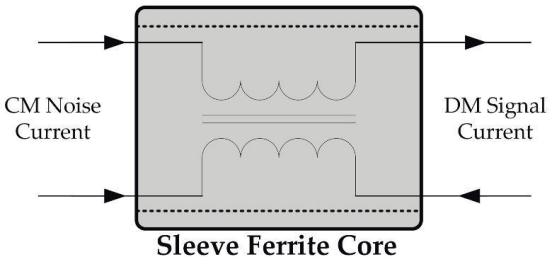

Figure 1. Diagram of common mode (CM) and differential mode (DM) currents passing through a ferrite core.

The mechanism used by a sleeve ferrite core to filter electromagnetic noise is the increase of the cable impedance in those frequencies that can hold disturbances. When a ferrite core encircles a

conductor lead it should pass the intended signal frequency and should block the EMI frequency components. Thereby, a sleeve ferrite core is able to manage the line impedance through its magnetic properties, providing a low impedance to the intended signal and increasing the conductor impedance for suppressing interferences within a specific frequency spectrum. The material and production technique used to make a ferrite core defines its magnetic properties and determines the frequency range of suitability. Conventionally, ferrite core materials for EMI suppression are based on MnZn and NiZn and their combinations [16–18]. The use of MnZn sleeve ferrite cores is generally centered on the range that covers from some hundreds of KHz to some MHz, in contrast to ferrite cores made of NiZn material that works in a broadband frequency range that can cover from tens of MHz up to several hundreds of MHz [4]. The results presented in [19] highlighted the great suitability of NC cable ferrite to filter electromagnetic interference in a low-frequency region. Furthermore, data obtained from its magnetic properties indicate that this EMC solution could also provide good performance in terms of EMI suppression at higher frequencies. In this sense, some researchers have investigated the use of NC structure compositions to make EMC components because this kind of core can reduce its volume by 50–80% and can yield greater magnetic properties and insertion losses compared to other sleeve ferrite cores [20–23].

Consequently, a prototype of the novel NC structure is characterized in relation to MnZn and NiZn conventional ceramic cores with the aim of determining the effectiveness of this novel material compared to the current solutions in the conducted frequency range. This is firstly presented in Section 2 by defining the magnetic properties of each material through measuring the relative permeability parameter. Subsequently, Section 2 also describes the performance of NC sleeve ferrite core compared with the ceramic cores from the point of view of the magnitude of the impedance and its complex components since this is the parameter most used by manufacturers to describe the performance of a sleeve ferrite core. In Section 3, the experimental setup designed to simulate a system with conducted emissions problems is described. This measurement procedure is used to determine the attenuation ratio that NC, MnZn and NiZn sleeve ferrite cores are able to offer in the frequency region between 100 kHz to 200 MHz. In Section 4, the data obtained from magnetic properties of the three different cores and the impedance measured are compared with the data obtained from the experimental measurement setup. This step is carried out in order to verify that the data obtained by the three different procedures match and, thus, it is ensured that they are properly acquired, since some investigations conclude that the measurement of the impedance parameter is not accurate from a certain frequency value [24–26]. It is essential to obtain an actual and verified impedance value because this parameter is employed as a reference to determine the accuracy of the experimental measurement setup employed to obtain the EMI suppression ability in terms of decibel for each sleeve ferrite core. Furthermore, Section 4 compares the results based on the insertion loss parameter of an NC core and ceramic ones, as well as extrapolating the results considering systems with different impedances to show the dependence of the filtering performance with the impedance of the system where the sleeve ferrite core is introduced [27]. Finally, important conclusions regarding the frequency ranges where NC is more suitable than ceramic sleeve ferrite cores are summarized in Section 5, in order to establish the extent to which NC suppresses those conducted EMI problems that current ceramic sleeve ferrite cores are unable to solve.

2. Sleeve Ferrite Core Characterization

Sleeve ferrite cores are manufactured from a magnetic material that allows them to control RF noise in cables and reduce it at a certain frequency range. This range mainly depends on their intrinsic composition and internal structure. Ferrite cores belong to the ferromagnetic materials field and can be categorized into three groups: ceramics, composite materials and metals. Conventionally, the most used sleeve ferrite cores are based on ceramic materials such as MnZn and NiZn, whereas the NC core characterized in this research is included in metals. Ceramics are also known as polycrystalline materials because they can contain metal oxides, such as manganese or zinc oxide. The features that have made ceramics the most popular filtering solution are their strong adhesion forces, heat-resistance, hardness and high resistance to pressure. One of the main advantages of the ceramics is

the possibility of manufacturing filtering components with many different shapes. In contrast to ceramics, currently, the manufacture of NC cores with different shapes is complicated due to the fact it is not a simple solid core. NC cores are formed by metal film layers that are rolled up to reach the desired size. This shape cannot be cut safely without undermining its EMI suppression ability because when the core is cut, small shortcuts are caused between the layers, lowering the magnetic properties of the core. Therefore, it is difficult to create snap ferrite cores that can be clamped on a cable because they are not a solid core. Nevertheless, the structure of the novel NC material presents the advantage of designing smaller components with greater magnetic properties for low-frequency applications due to its intrinsic properties which are obtained by means of its complex manufacturing procedure [19]. This process consists of melting the material by heating it at 1300 °C. Next, the liquid is deposited on a wheel in order to cool it through spinning around at 100 km/h with the aim of reducing its temperature at a cooling rate of 106 K/s. Thereby, the amorphous structure is generated and the thickness of the film is defined. Thereafter, the film is rolled up to form the sleeve core and it is exposed to an annealing process where it is warmed up to 600 °C to achieve the nanocrystalline structure. Finally, strong magnetic fields are applied to the material in order to get greater magnetic properties. Hence, from comparing its magnetic properties to those provided by ceramic cores, it is possible to consider that NC can not only provide a high attenuation ratio in the ultra-low frequency range (9 kHz to 150 kHz) but also, it could be more effective than ceramic cores throughout an upper frequency range.

When an electrical conductor carrying a certain current is inserted through a sleeve ferrite core, it produces a magnetic field. Sleeve ferrite cores are designed to absorb the magnetic field, inducing currents, into its internal structure. These currents, known as eddy currents [28], are dissipated by the core as heat and they mainly define the loss ability of the component. Eddy currents can fluctuate depending on the strength of the field, frequency and material grain size [29].

The evaluation of the novel NC sleeve ferrite core is carried out by analyzing the performance regarding two kinds of ceramic cores, with the aim of analyzing the frequency range where NC is more effective at suppressing conducted EMI. One of the cores selected is based on MnZn, a material widely used to reduce EMI in the low-frequency region and the other selected core is made of NiZn that is generally employed to filter EMI from some tens of Megahertz. Thus, it is important that the analyzed sleeve ferrite cores have a similar volume. One of the most significant parameters of a sleeve ferrite core is the height or length of the core since the electromagnetic absorption ratio varies only the log of the division between the external and the internal diameter, but is directly related with the length [4]. Accordingly, the ceramic MnZn and NiZn sleeve ferrite cores characterized in this contribution have been selected as they have dimensions similar to the manufactured novel NC core prototype. These parameters are shown in Table 1.

Table 1. Lists of sleeve ferrite cores used in this research.

Ferrite Part Number	Magnetic Material	External Diameter (OD) (mm)	Internal Diameter (ID) (mm)	Length (mm)
M-4304-02	NC	18.9	12.9	27.7
74277255	MnZn	18.6	10.2	28.5
74270055	NiZn	18.6	10.2	28.5

2.1. Magnetic Properties

One of the most important parameters that defines the ability of a material to absorb electromagnetic interferences is the relative permeability (μ_r) [13]. The permeability relates the magnetic flux density of a certain magnetic field in a defined medium, so that when a sleeve ferrite core is placed around a certain cable, the magnetic flux is concentrated in it. This ability to concentrate the magnetic flux is described by the material's internal properties and it is represented through the permeability complex parameter. The losses of the magnetic flux can be determined by dividing it into its complex form; in this way, the real component (μ') quantifies the real or inductive part and

the imaginary or resistive component (μ'') is related to the material ability to absorb the electromagnetic interferences [30,31]. Thereby, the complex relative permeability is expressed by:

$$\mu_r(f) = \mu'(f) - j\mu''(f) \quad (1)$$

One governing rule of EMI suppression that relates the permeability to the frequency in powder ferrite cores is Snoek's Law [4] given by (2):

$$f_m = B_S/\mu_i \quad (2)$$

where f_m corresponds to the ferromagnetic resonance frequency, B_S is the magnetic saturation and μ_i the initial permeability. This last parameter is measured at low frequency (usually at 10 kHz with a temperature of 25 °C) and it is used for manufacturers to organize the filtering ability of cable ferrites. Equation (2) shows that the higher the frequency of operation, the lower the permeability, and vice versa. Thus, if the material provides high initial permeability, the frequency fall off will be low and vice versa. For this reason, MnZn ferrite cores are normally focused on the high kHz or at most, the very low MHz region since this material yields an initial permeability value between 3000–10,000 [32,33]. With regard to NiZn materials, they usually provide an initial permeability that varies between 500–1200, so they are able to more effectively filter electromagnetic noise within a high-frequency range [34,35]. Otherwise, the NC material shows a much higher initial permeability than ceramics due to its internal structure and manufacturing process that improve its magnetic properties. This results in an important increase in the initial permeability, reaching values of nearly 100,000 [22].

The magnitude of the relative permeability of the NC material is represented together with MnZn and NiZn permeability traces in Figure 2 to study the frequency region covered by each material [10]. This graph shows that from the point of view of the magnetic properties, the NC core, despite being the material with higher initial permeability provides higher permeability than the ceramic materials throughout almost the entire frequency range studied. MnZn is able to provide a permeability around 3000 up to the 2 MHz point, providing a similar value to NC at this frequency point. In the high-frequency region, NC demonstrates a better performance than NiZn although it is possible to observe how the slope of NC is greater and, thus, NiZn may be more effective. In this way, the NC core, despite being the material with a higher initial permeability, provides higher permeability than the ceramic materials throughout the frequency range studied.

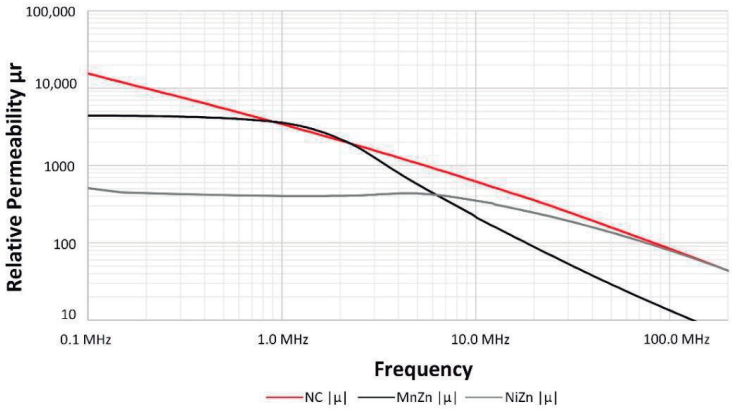

Figure 2. Relative Permeability of nanocrystalline (NC) compared with MnZn and NiZn sleeve ferrite cores compositions.

More information about the sleeve ferrite cores analyzed can be obtained by splitting into real and imaginary components the complex relative permeability of the three materials. These traces allow one to determine the magnetic resonance frequency (f_m) of each material, as shown in Figure 3. This

corresponds to the frequency value at which the real part of the relative permeability begins to fall and the imaginary part reaches the maximum peak [36]. Generally, the inductance component is steady below the f_m and decreases significantly from this frequency value [24]. The NC minigraph shows the lower frequency value at which the f_m takes place; however, the absorption loss represented by the imaginary part shows the weakest slope, if it is compared with MnZn and NiZn imaginary traces. From this information, together with the fact that NC provides a higher initial permeability, results in this sleeve ferrite solution could yield a greater attenuation ratio in a wider frequency range than ceramic cores. The equipment used to carry out these relative permeability measurements is based on the E4991A Material Analyzer (Keysight, Santa Rosa, CA, USA) that is interconnected with the 16454A Magnetic Material Text Fixture. This fixture measures accurately the permeability parameter of round-shaped magnetic materials because its features emulate one turn winding the core without magnetic flux leakage. Consequently, direct readouts of the complex permeability are obtained.

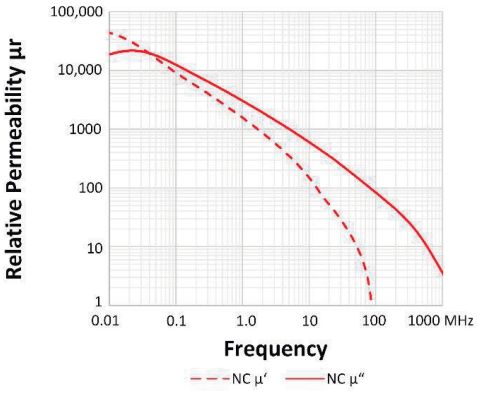

(**a**)

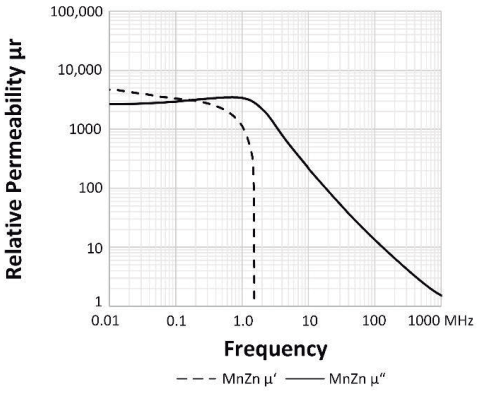

(**b**)

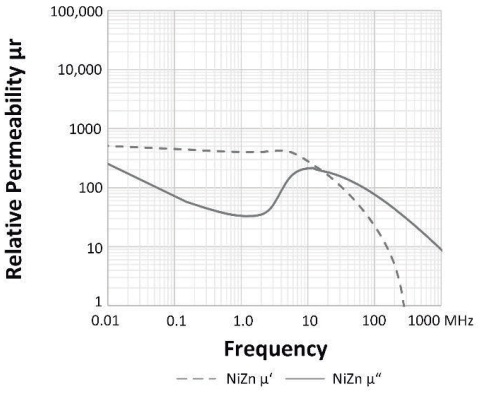

(**c**)

Figure 3. Complex relative permeability split into real and imaginary components: (**a**) NC sleeve ferrite core; (**b**) MnZn sleeve ferrite core; (**c**) NiZn sleeve ferrite core.

There is also a capacitance component that represents the dielectric effects of the ferrite magnetic material. This appears in the bandwidth above the f_m, where the inductive component of the permeability becomes negative [13,37]. As can be observed in Figure 3, this stray capacitance due to the magnetic material is noted beyond 1.8 MHz and 85.1 MHz and 282.7 MHz in case of MnZn, NC and NiZn cores, respectively.

2.2. Impedance and Phase Description

Although the permeability parameter is used to describe the behavior of the core material, the performance of a certain sleeve ferrite core takes into account, besides the material features, other variables such as the self-inductance defined by the dimensions and the shape. Thereby, sleeve ferrite cores are usually defined and classified through specifying the magnitude of the impedance (Z_F), which is obtained from the equivalent component parameters such resistance (R) and inductance (L) [4,27]. The magnitude of the impedance is given by:

$$|Z_F| = \sqrt{R^2 + (X_L)^2} \quad (3)$$

where R corresponds to the equivalent resistance and X_L is the impedance of the inductive part of the sleeve ferrite core. The vector relationship between impedance and permeability components is shown in Figure 4.

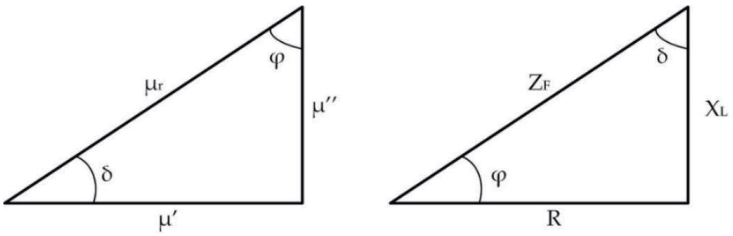

Figure 4. Vector relationship between μ_r, μ'', and μ'' (**left**); vector relationship between Z_F, R and X_L ($2\pi fL$) (**right**).

There is a proportional relation between the attenuation ratio or insertion loss provided by a certain sleeve ferrite core and the impedance of the system where it is set. Thus, it is essential to select a sleeve ferrite core that provides an impedance value that is higher than the system impedance at the frequency to be filtered. This is due to the fact they are more effective when they are used on

cables connected to circuits with low impedance [5]. Sometimes it is difficult to accurately determine the impedance of the system with EMI problems; however, depending on the kind of lead, it is possible to estimate this value: for instance, ground leads usually present between 1 and 2 Ω, supply voltage lines have impedances from 10 to 20 Ω and video, clock and data lines from 90 Ω to 150 Ω [27].

A sleeve ferrite core can be represented by a simplified equivalent circuit consisting of an inductance, a resistance and a capacitance, as shown in Figure 5. This circuit represents a sleeve ferrite core within the frequency range analyzed in this contribution without taking into consideration the system where it could be placed, since the surrounding elements may introduce additional parasitic effects. The behavior of the sleeve ferrite core at a low-frequency range is usually mostly inductive, blocking CM currents due to its inductive reactance (L_F). The impedance becomes more resistive (R_F) as the frequency is increased, absorbing and dissipating CM currents as heat. Hence, L_F and R_F are the predominant components below the ferromagnetic resonance frequency; however, from this frequency value, the stray capacitance of the ferromagnetic material becomes predominant, defining the fall slope of the impedance. Regarding C_F, it represents a parasitic capacitance because of the winding effect [24]. When a sleeve ferrite is set around a cable, it is equivalent to one turn or one winding coil. An interesting feature of sleeve ferrite cores is the possibility of winding the wire around them multiple times, considering each pass of the cable through the sleeve core as one turn. This technique results in an increase of the ferrite impedance proportionally to the number of turns squared. Nevertheless, increasing the number of turns also increases the winding capacitance C_F, shifting the point of maximum impedance to a lower frequency value [25]. Therefore, there is a balance between the number of turns and winding capacitance, because a higher number of turns implies a worse performance at high frequencies. Nevertheless, increasing the number of turns N, it is possible to increase to obtain a higher inductance L_F value, but at the same time, the stray capacitance C_F increases [13]. This last fact could generate a self-resonance (SRF) at a certain frequency. Above the value of the SRF, the impedance becomes predominantly capacitive and the effectiveness of the sleeve ferrite core to filter EMI is degraded [38,39]. Therefore, SFR due to C_F could superpose the ferromagnetic resonance due to the intrinsic material parameters described above. This is one of the main reasons why more than two or three turns are not usually used. In this contribution, the characterization is carried out by winding one and two turns in the sleeve ferrite cores.

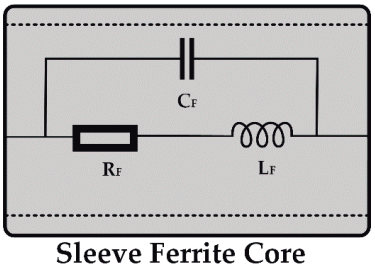

Figure 5. Simplified sleeve ferrite core equivalent circuit.

The measurement setup currently in use by manufacturers for characterizing a sleeve ferrite core is based on the measurement of its impedance by means of introducing along the core a wire with a defined length and cross-section, which is connected to an Impedance Analyzer. The wire selected should be as short as possible, but long enough to achieve one and two turns around the sleeve ferrite core. With this conventional method, the influence of the wire in the total impedance measured can only be neglected if its length is short compared to the wavelength and this limit is usually a least 1/10 of the wavelength (λ). Some investigations have evaluated this measurement method and agree that it is not sufficiently accurate for very high frequency characterizations, because if an AWG26 (American Wire Gauge) cable is used, the minimum length required to wind two turns around the NC sleeve ferrite core is 150 mm. As a result, the maximum frequency that can be measured is 200 MHz (following the restriction of $\lambda/10$). If this procedure is used to characterize sleeve ferrite cores

from 200 MHz, the wire represents a series inductance whose value becomes higher as the wire length increases. At the same time, this length increase causes the SRF to shift to a lower region, considering not only the impedance of the core but also the impedance introduced by the cable [25,26]. In the case of winding only one turn around the sleeve ferrite core, it is possible to use an AWG26 cable with a length of 70 mm with the aim of reducing the influence of the cable in the total impedance measurement. Figure 6 shows the impedance of both AWG cables used to determine the impedance of the sleeve ferrite cores. From these traces, the magnitude of the impedance provided by the two cables employed to measuring the impedance of the sleeve ferrite cores can be observed. It is important to take this fact into account, especially in those sleeve cores whose impedance can be similar to the impedance provided by the cable.

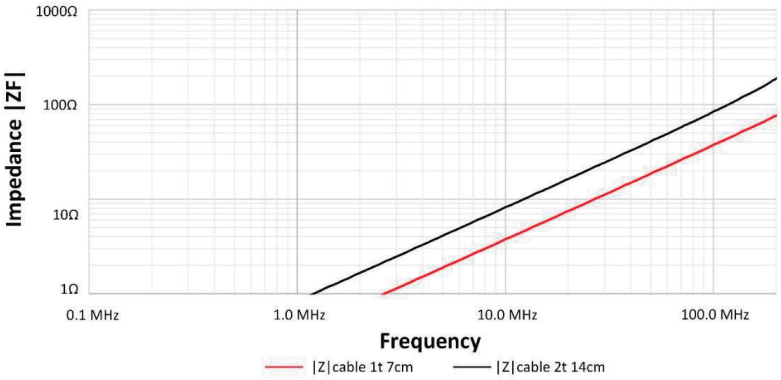

Figure 6. Magnitude of the impedance of the AWG26 (American Wire Gauge) wires used to measure the impedance of the sleeve ferrite cores.

Subsequently, considering these conditions, a calibration procedure has been performed with the aim of reducing the influence of the AWG cable, especially in the frequencies closer to the (λ/10) limit, when the 150 mm cable is employed. Taking this fact into consideration, it is possible to determine the direct impedance measurement through the E5061B Vector Network Analyzer (Keysight, Santa Rosa, CA, USA) connected to the Terminal Adapter 16201A (Keysight, Santa Rosa, CA, USA) and the Spring Clip Fixture 16092A (Keysight, Santa Rosa, CA, USA) [40]. These fixtures are internally compensated by impedance standard calibration in order to take into account the electrical length path and the impedance variations caused by parasitic elements. The measurements of R and X_L obtained from the three sleeve ferrite cores with this setup are shown in Figure 7. Figure 7a shows the magnitude of the impedance measurement in which the most effective range of EMI suppression in the NC sleeve ferrite core compared to the ceramic cores analyzed can be observed. This minigraph shows that MnZn provides the higher impedance from 0.88 MHz to 2.73 MHz and NiZn offers a more effective behavior from 91.61 MHz, whereas in the rest of the frequencies, NC sleeve ferrite yields the best performance. If this data is compared to the permeability traces, it is possible to observe a correlation between both characterization methods, since MnZn provides a greater response than NC within a similar frequency region, which is shown in the permeability graph. With regard to the comparison between the NC and NiZn sleeve ferrite core, NC shows a higher impedance value of up to 91.61 MHz. At this frequency value, the inductance component of the analyzed NC sleeve ferrite core reaches negative values that match the SRF point. Consequently, the capacitive component of the core generates a degradation in the impedance performance, reducing it sharply with respect to NiZn sleeve ferrite core. In Figure 7b–d, the resistive (R) and inductance (X_L) components can be observed in order to know the contribution of each of them related to the total impedance. As described above, the studied sleeve ferrites show higher values of X_L within the low-frequency region; however, these become less important as the frequency increases

if compared to the R component. The resonance frequency of MnZn and NC cores is located at 2.02 MHz whereas the resonance frequency of NiZn is located above 200 MHz.

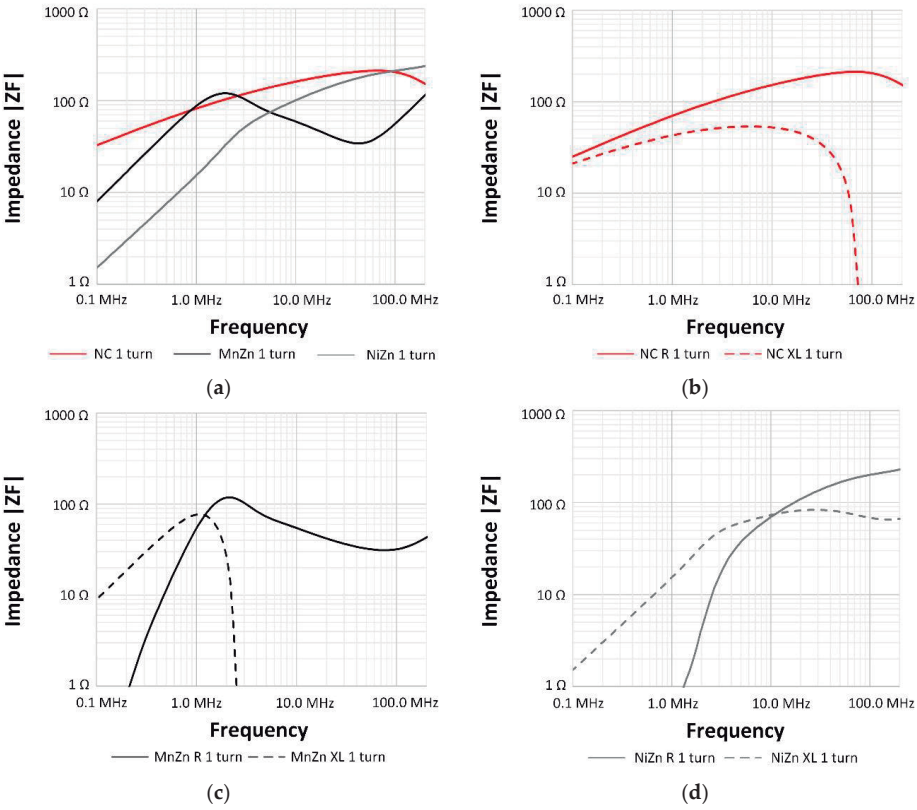

Figure 7. Impedance measurements of the NC, MnZn and NiZn sleeve ferrites winding around them 1 turn: (**a**) Magnitude impedance of three cable ferrites; (**b**) NC R and X_L impedance components; (**c**) MnZn R and X_L impedance components; and, (**d**) NiZn R and X_L impedance components.

The impedance traces obtained by winding two turns into the sleeve ferrite cores are shown in Figure 8. The increase of the number of turns generates higher values of the impedance magnitude in the three traces and causes a shift in the cross points of different sleeve ferrite traces. Therefore, NC provides the best performance up to 0.76 MHz, as well as in the frequency region from 2.75 MHz to 68.10 MHz. If the 10 MHz frequency point is taken as a reference, the values of the three traces have been increased about four times (the number of turns squared). Specifically, in the case of NC from 159.9 Ω to 651.2 Ω, MnZn 55.3 Ω to 227.0 Ω and NiZn cable ferrite from 100.9 Ω to 415.9 Ω.

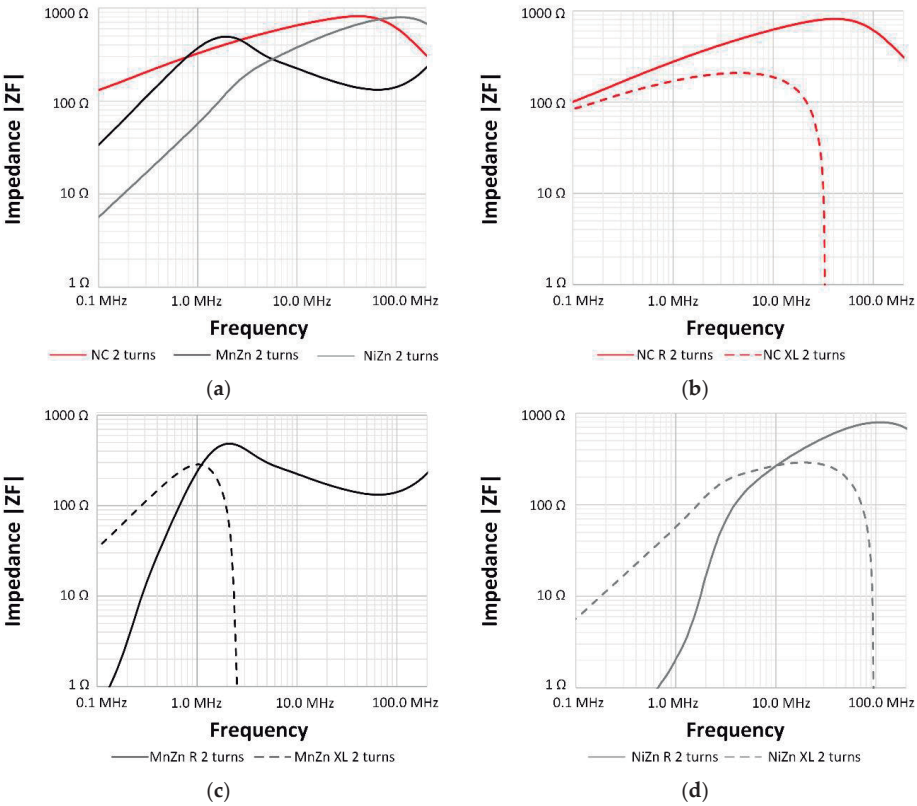

Figure 8. Impedance measurements of the NC, MnZn and NiZn sleeve ferrites after winding around them by two turns: (**a**) Magnitude impedance of three cable ferrites; (**b**) NC R and X_L impedance components; (**c**) MnZn R and X_L impedance components; (**d**) NiZn R and X_L impedance components.

From this data, the phase angle, which is defined by the angle whose sine is X_L/R (ϕ) can be represented. In this way, it is possible to determine the behavior of a certain sleeve ferrite core by means of studying its phase: when it corresponds to 90°, the ferrite core works as a pure inductor, whereas for 0°, it works as a pure resistor. If the phase reaches negative values, the sleeve ferrite core reduces its EMI suppression ability due to the fact that it is starting to show a capacitive and undesired behavior. Figure 9a shows the course of the phase angle of NC sleeve ferrite cores that can be used as a frequency response indication and it can be compared with the ceramic sleeve ferrite cores. Note that in the NC case, the phase angle goes from 68° to 0° in the frequency range 0.01–72.50 MHz for one turn and 0.01–33.13 MHz for two turns. NC becomes more resistive than the other sleeve ferrites at lower frequencies and the transition between inductive and resistive behavior is less abrupt, since the phase of MnZn goes from 90° to 0° in the frequency range 0.01–2.52 MHz, matching for one and two turns and, in the case of NiZn, it crosses 0° at 94.55 MHz for two turns and beyond this frequency point, for one turn. Thus, it is possible to observe the broadband effectiveness than can provide the NC sleeve ferrite core in relation to ceramic ones.

These graphs also allow one to determine from which frequency value the phase angle of each sleeve ferrite becomes negative and, therefore, the component shows a capacitive behavior. As it has been described, in the case of MnZn, this frequency value corresponds to the f_m, whereas for NC and NiZn, it is possible to observe that the phase angle trace crosses 0° at a lower frequency value, which demonstrates their complex relative permeability traces. This effect is caused by the shift of the SFR due to two factors: (a) the stray capacitance added to the sleeve ferrite response when the cable is winding it and (b) due to the self-resonance produced by the sleeve ferrite core dimensions (with

smaller cores of the same material, the SFR appears at a higher frequency value). Therefore, the impedance magnitude is increased by winding a higher number of turns around the sleeve ferrite core but, at the same time, the effective frequency range is reduced.

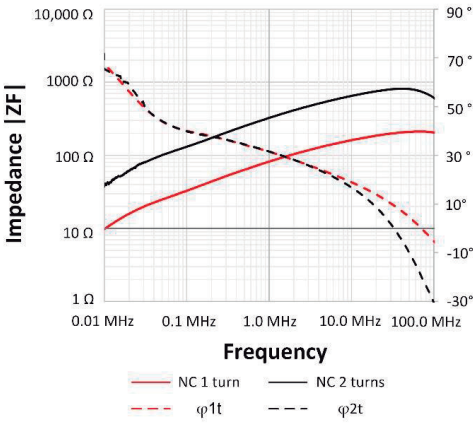

(**a**)

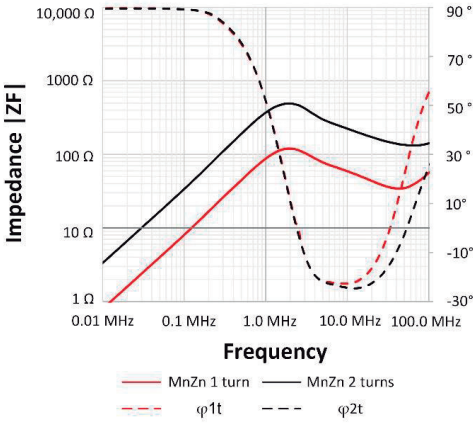

(**b**)

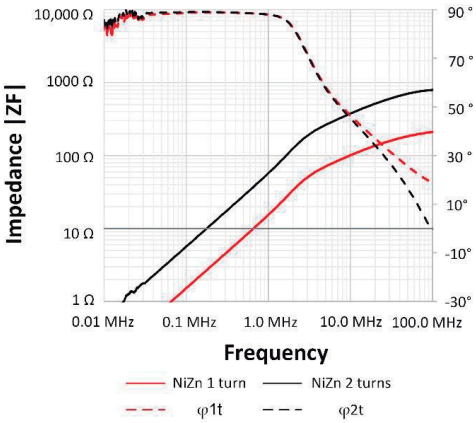

(**c**)

Figure 9. Comparison of the magnitude impedance and angle phase of X_L/R of the NC sleeve ferrite core compared to MnZn and NiZn by winding around them one and two turns: (**a**) NC sleeve ferrite core; (**b**) MnZn sleeve ferrite core; (**c**) NiZn sleeve ferrite core.

In order to validate the impedance used to characterize the novel NC and ceramic sleeve ferrite cores, in Section 4, this data is compared with the impedance calculated from the relative permeability through the quasi-static model from the real and imaginary permeability components and the dimension of the sleeve ferrite core [13]. Generally, this model can be used for evaluating cores up to the SFR, since beyond this frequency value, the static magnetic flux distribution can fluctuate. This deviation could be because the core dimensions, saturation, core losses, and frequency-dependent magnetic effects that are significant above the SFR are not being taken into account [24]. Equations (4) and (5) show the link between the material permeability and dimensions of the sleeve ferrite core with the impedance (inductance and resistance components):

$$L = \frac{\mu_0 \mu' N^2 A}{\ell} \tag{4}$$

$$R = \frac{\mu_0 \mu'' N^2 \omega A}{\ell} \tag{5}$$

where μ_0 is the permeability of the air, μ' is the inductance permeability component, μ'' is the loss permeability component of the sleeve ferrite, ℓ is the effective magnetic path length of a toroidal core (m), N is the number of turns of a cable to carry out the measurement, A corresponds to the toroidal core cross-sectional area (m^2) and ω is the angular frequency.

3. Insertion Loss

The datasheets of sleeve ferrite core components generally only specify the impedance at several frequency points or the graph of the magnitude of the impedance in the frequency range where it is more effective. In contrast to this fact, other kind of EMC component datasheets, such as common-mode-chokes, show the attenuation ratio or insertion loss in terms of decibels (dB) that are able to provide. This is because the insertion loss that a sleeve ferrite core is able to yield is strongly dependent on the impedance of the system in which it is placed besides its own impedance response. Subsequently, the equivalent circuit approach to determine the insertion loss parameter of a certain sleeve ferrite core, has to consider the source impedance (Z_A) and the load impedance (Z_B) of the system with electromagnetic interference problems, as well as the impedance introduced by the ferrite core in that system (Z_F) [27]. The equivalent circuit diagram employed to determine this impedances relation and analyze the effect of introducing a sleeve ferrite core into a certain system is shown in Figure 10.

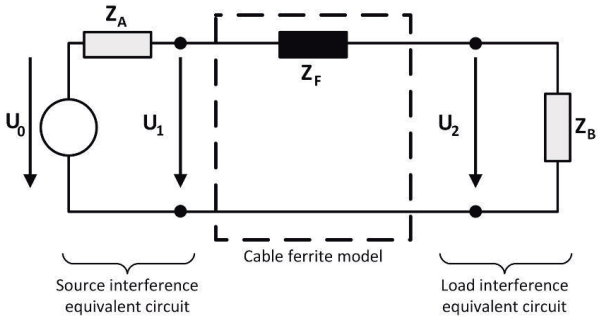

Figure 10. Diagram of source and load equivalents circuits used to determine the insertion loss parameter of a sleeve ferrite core when it is introduced into a system.

According to this diagram, when the system impedance is known, the insertion loss (A) in terms of decibels can be calculated through the Equation (6) from the impedance of the sleeve ferrites (Z_F) shows in Section 3:

$$A(dB) = 20 \log\left(\frac{Z_A + Z_F + Z_B}{Z_A + Z_B}\right) \quad (6)$$

It can be observed that for a given source and load impedances, increasing the impedance of the cable ferrite will increase the insertion loss. This theoretical insertion loss is used as a reference value to evaluate the experimental insertion loss measured through emulating the equivalent circuit diagram shown in Figure 10. In order to carry out the performance of the sleeve ferrite core, it is considered that the source and load impedance are known and the parameter of study is the impedance of the sleeve ferrite core. Therefore, an experimental measurement setup based on generating controlled EMI conducted emissions into a load with a stable impedance over the frequency range studied (from 150 kHz up to 200 MHz) to determine the insertion loss of the NC sleeve ferrite core and compare it with the insertion loss of ceramic cores. This setup takes as a reference the IEC 61000-4-6 standard (Testing and measurement techniques—immunity to conducted disturbances, induced by radio-frequency fields) and it consists of a continuous wave simulator (CWS) for testing conducted RF immunity within a frequency range from 100 kHz to 230 MHz that emulates the electromagnetic conducted interferences. This equipment is the CWS500N1 Continuous Wave Simulator (EM Test, Reinach, Switzerland) and it provides a 50 Ω output impedance that represents the Z_A in the insertion losses equivalent circuit diagram. A coaxial cable connects the CWS500N1 to the CAL 801 (Ametek CTS, Reinach, Switzerland), which is employed to ensure a 100 Ω load in the whole analyzed frequency range. This impedance, together with the output impedance of the CWS500N1, represents a Z_A = 150 Ω in the equivalent circuit diagram. The other side of this diagram is formed by another CAL 801 that provides a 100 Ω load that is connected to a spectrum analyzer N9010A (Keysight, Santa Rosa, CA, USA) with an input impedance of 50 Ω. Accordingly, the sum of these two impedances provides the impedance of Z_B = 150 Ω. Both sides of the equivalent circuit emulated (A and B) are connected by means of an AWG26 cable of 150 mm, maintaining a distance of 35 mm from the ground metal layer that interconnects all the parts. This cable simulates a reference line that can be characterized and employed to introduce the NC and the ceramic sleeve ferrite cores into the setup to analyze how the emulated interferences are attenuated. Therefore, a previous calibration measurement is first carried out in order to ensure the stability and linearity of the system, generating a sinus frequency sweep with an amplitude of 140 dBμV. Once the reference signal is obtained, the sleeve ferrite core is introduced into the reference line of the insertion loss setup and the sinus frequency sweep is repeated. With these two measurements, it is possible to subtract them in order to obtain the attenuation rate or insertion loss performance of each of the sleeve ferrite cores and compare them in terms of decibels instead of impedance. Figure 11 shows the measurement setup described implemented inside an anechoic chamber.

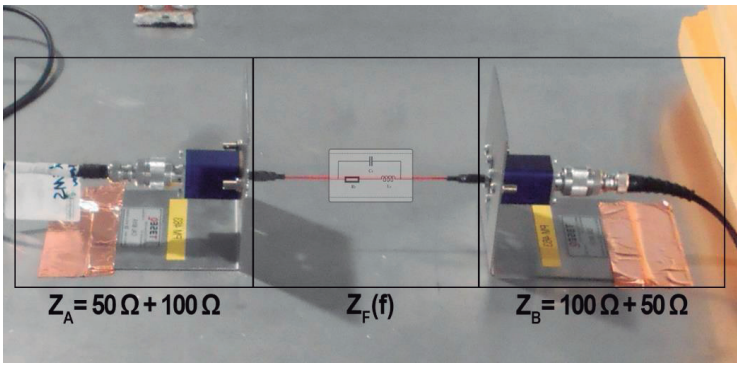

Figure 11. Experimental measurement setup for characterizing NC and ceramic sleeve ferrite cores in terms of decibels.

4. Results and Discussion

This section is focused on analyzing the insertion loss measured with the experimental setup described above and comparing the performance of the novel NC sleeve ferrite core with those of MnZn and NiZn cores in terms of the attenuation ratio. As it has been explained, the characterization of sleeve ferrite cores in the high-frequency region presents some difficulties that can result in a reduction in the measurement accuracy beyond some tens of Megahertz. This is generally due to internal factors such as the influence of the measurement setup (length of the cable used as a reference line or the stability of the source and load impedances depending on the frequency) and external factors (isolation of external interferences). For this reason, firstly, a comparison between the data obtained mathematically from the magnetic properties and the impedance response measurement of the sleeve ferrite core is contrasted. This is carried out with the aim of verifying if the response obtained from the insertion loss setup matches the behavior obtained from the permeability and impedance analysis. Therefore, Figure 12 shows the impedance of the novel NC sleeve ferrite cores together with the ceramic cores determined from three different methods: (a) determined from the complex relative permeability components, (b) directly measured and (c) computed from the insertion loss measurement setup and extracting the Z_F parameter through Equation (6). As can be observed in the case of the novel NC sleeve ferrite core, the traces both in the characterization with one and two turns wound from low frequencies up to the resonance point. From this point, at which the SFR occurs, the trace calculated from the relative permeability continues increasing, unlike the other two traces. This is due to the features of the sleeve ferrite selected, since the impedance values obtained from the permeability equations are only validated up to the resonance point. With regard to the ceramic cores, in the case of MnZn, the traces match up to the frequency of about 70 MHz, where the red traces (direct measurement of the impedance) shows a resonance that can be generated by the impedance of the cable used for the characterization. This effect is only shown in this sleeve ferrite core because, in the high-frequency region, its impedance is similar to the cable impedance and the influence of this can be observed. The NiZn sleeve ferrite core shows a more significant difference than NC in the low-frequency range where it does not have a good performance, but it represents the best fit between the three traces in the high-frequency region because this core has the SFR point beyond 200 MHz considering one turn wound and about 100 MHz considering two turns.

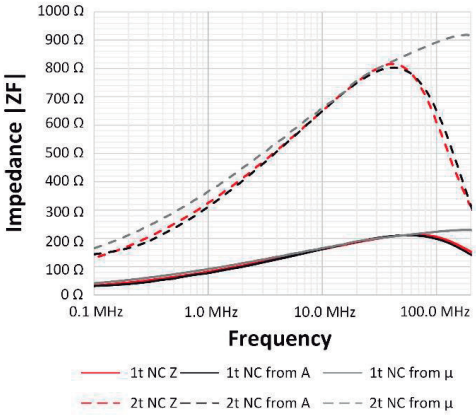

(**a**)

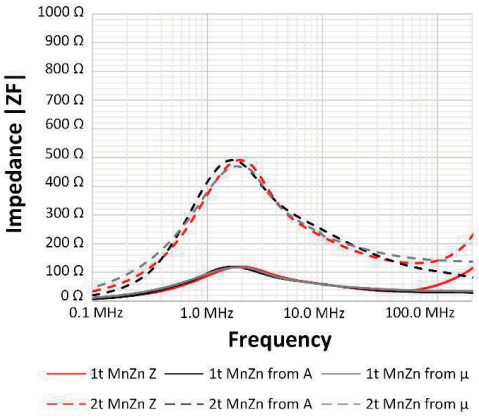

(**b**)

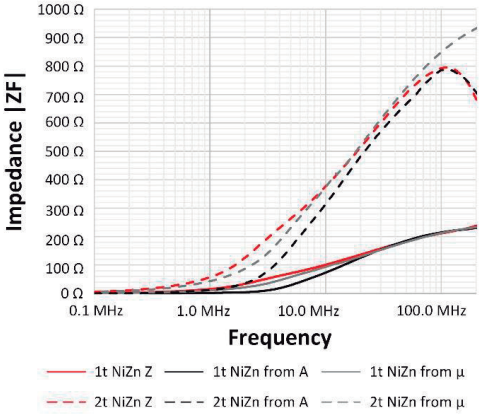

(**c**)

Figure 12. Comparison of the impedance obtained from three different procedures considering one and two turns wound around the sleeve ferrite core: measuring it directly, mathematically from the relative permeability and extracted from the experimental insertion loss. (**a**) NC sleeve ferrite core; (**b**) MnZn sleeve ferrite core; and, (**c**) NiZn sleeve ferrite core.

Thus, it can be deduced that the measurements obtained with the insertion loss setup can be considered since this method is able to provide accurate measurements with lower influence on the cable used as reference line than the impedance measurement method. Furthermore, with this setup, it is possible to determine the ability of the NC sleeve ferrite core in relation to the widely used MnZn and NiZn cores to suppress electromagnetic noise in cables in the frequency region from 100 KHz to 200 MHz. Therefore, the performance of the three sleeve ferrites characterized in Section 2 can be studied with the aim of determining their ability to filter conducted EMI in terms of decibels instead of the impedance. The theoretical insertion loss parameter is calculated as it has been described in Section 3, this is from the magnitude of the impedance (Z_F) of each sleeve ferrite and also, considering the source and load impedances of the system where it is placed. The impedances selected to represent the source and load are defined by the IEC 61000-4-6 standard, taking $Z_A = Z_B = 150\ \Omega$. The sum of these parameters represents a total impedance of 300 Ω; therefore, the sleeve ferrite core must provide a huge value of impedance to obtain an insertion loss higher than three dB. The three sleeve ferrite cores analyzed in this contribution are able to provide values closer to 200 Ω in the case of NC and NiZn and 100 Ω in the case of MnZn (winding one turn). Thus, the results shown in Figures 13 and 14 could be taken as a reference in those systems that present a high load and source impedance.

Subsequently, Figure 13 shows the insertion loss parameter measured by means of the experimental setup described, winding one turn around each sleeve ferrite core. As is shown in the impedance data, the novel NC sleeve ferrite core is able to provide a better performance than ceramic cores in most of the analyzed frequency range. It is only surpassed by the MnZn core in the frequency range at which it provides the peak attenuation ratio (0.72–2.62 MHz). The NC core also yields a greater response than NiZn in the low- and medium-frequency region analyzed since it is able to provide a higher attenuation ratio than NiZn up to 78.65 MHz. From this frequency value, the insertion loss provided by the NiZn sleeve ferrite core keeps increasing to reach a value close to 5 dB at 200 MHz, whereas NC begins to lose effectiveness.

The same comparison is shown in Figure 14, but in this case, the sleeve ferrites are wound with two turns. By winding by two turns, it possible that the NC and NiZn cores are able to provide attenuation rates higher than 10 dB. The predominance of each sleeve ferrite core for the analysis of two turns winding is very similar to the obtained for one turn, since MnZn yields a slightly better response than NC around its resonance frequency, whereas NC improves the MnZn performance below 0.59 MHz and beyond 2.62 MHz. If the novel NC sleeve ferrite core is compared to the NiZn core, the first is able to provide significantly greater performance up to 44.40 MHz. At this frequency value, the resonance is produced in the NC sleeve ferrite core, providing the higher value of attenuation (11.31 dB) and starting to reduce its effectiveness. NC and NiZn traces cross at 76.28 MHz, indicating that beyond this frequency point, NiZn is able to more effectively filter the interferences in the high-frequency region of the whole characterized conducted range. It is important to note that by winding for two turns for the sleeve ferrites, they have improved in a similar way their performance, providing a maximum insertion loss between 2.24-times and 2.90-times greater. Nevertheless, it is possible to observe the drawbacks of this technique in the traces of the NC sleeve ferrite core, since the maximum peaks of attenuation have shifted to about 12.30 MHz. This shift is not shown in the MnZn trace because the resonance observed for this material is due to the ferromagnetic resonance defined by the magnetic features, not for the SFR.

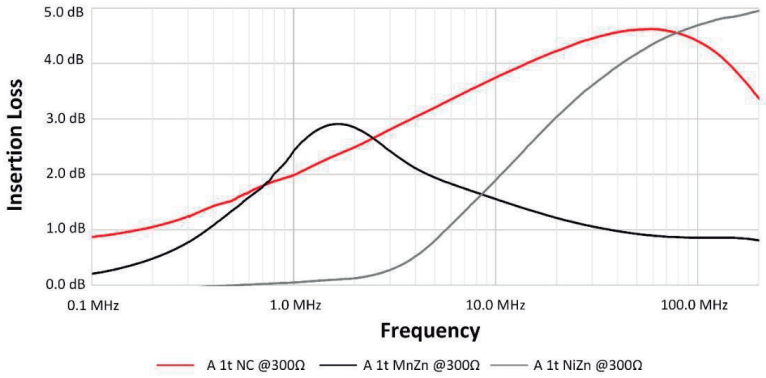

Figure 13. Comparison of the experimental insertion loss determined for NC, MnZn and NiZn sleeve ferrite cores by winding one turn.

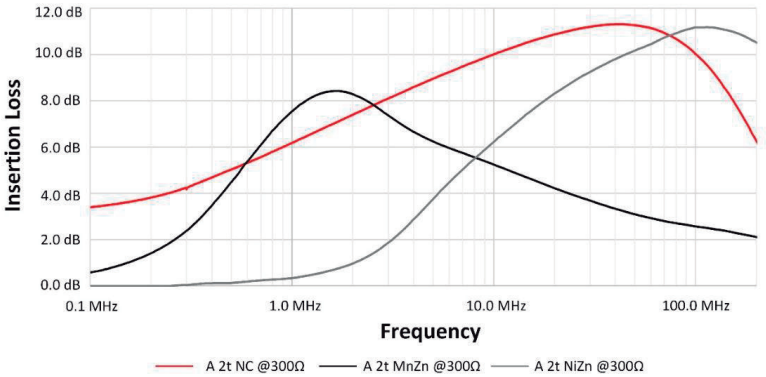

Figure 14. Comparison of the experimental insertion loss determined for NC, MnZn and NiZn sleeve ferrite cores by winding two turns.

As has been described, the insertion loss provided by a certain sleeve ferrite core is not only dependent on its intrinsic properties but also on the impedance of the line where it is placed. Therefore, it is possible to obtain the insertion loss of the analyzed sleeve ferrite cores through determining their impedance from the insertion loss data measured with the setup described in Section 3. This is carried out by extracting the Z_F parameter from Equation (6), by knowing the insertion loss (that has been measured and represented in Figures 13 and 14) and Z_A and Z_B (the sum of both represents 300 Ω). This Z_F can be evaluated together with other impedance values of the system impedance ($Z_A + Z_B$) by using Equation (6). Figure 15 shows the performance of the NC sleeve ferrite core compared with the ceramic cores, considering a system impedance of 10 Ω (continuous traces) and 100 Ω (discontinuous traces). This computed insertion loss has been obtained considering the impedance of the three different sleeve ferrite cores after winding only one turn. Note that, the efficiency of the sleeve ferrite cores has doubled in the system with 100 Ω and multiplied by six, reaching the 26.61 dB as a maximum value in the case of NC, when a system with an impedance of 10 Ω is considered.

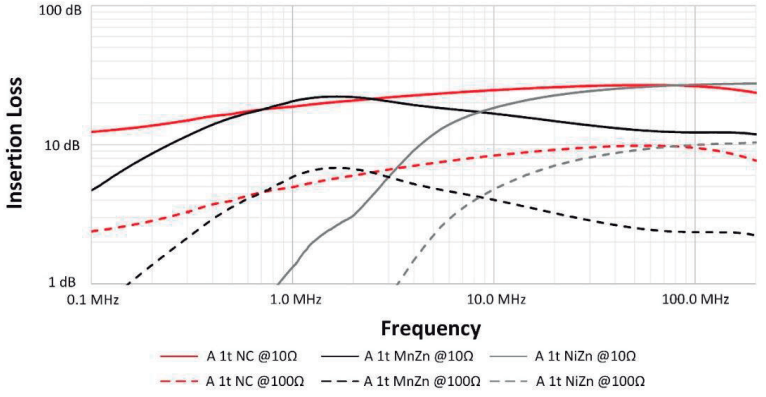

Figure 15. Extrapolation of the measured insertion loss for systems with an impedance of 100 Ω and 10 Ω, considering one turn for NC, MnZn and NiZn sleeve ferrite cores.

5. Conclusions

Considering the results presented, the suitability of the novel NC sleeve ferrite core prototype in comparison with MnZn and NiZn ceramic cores is validated since it is able to provide a broadband

EMI filtering solution in the frequency region studied. Whereas MnZn provides higher attenuation only in the frequencies near to its resonance peak (about 1.8 MHz with a bandwidth of 2.0 MHz), NC yields a great insertion loss throughout the frequency band from 100 KHz to 100 MHz. Regarding the high-frequency region (from 50 MHz), the NiZn sleeve ferrite core provides similar results to the NC solution, achieving a better performance between 78.65 MHz and 76.28 MHz for winding by one and two turns, respectively. In terms of attenuation, the performance of three sleeve ferrites was evaluated through a measurement setup that considers a system with 150 Ω of source and load impedance. The results obtained were compared with those obtained from the measurement of the relative permeability and by directly measuring the impedance and showed good agreement. Thus, the insertion loss measurement setup provides results that can be considered in order to analyze the performance of the NC sleeve ferrite core compared with the ceramic cores.

Therefore, considering all the data presented in this contribution, it is possible to conclude that the novel NC sleeve ferrite core prototype represents an EMI filtering solution to reduce the conducted interferences in the low- and medium-frequency regions (up to 50 MHz). If the EMI disturbance is located specifically in the region covered by MnZn or from 50 MHz, a ceramic core that provides similar performance to that of the NC one may be used. Nonetheless, if the EMI interferences are distributed outside of these regions or from the low-frequency region up to about 100 MHz, the NC sleeve ferrite core shows a better performance than ceramics to reduce EMI emissions in a wideband frequency range.

Author Contributions: Conceptualization, A.S., J.V. and J.T.; Formal analysis, A.S., P.A.M., R.G.-O. and J.S.; Investigation, A.S., J.V., P.A.M., A.A. and J.M.; Methodology, P.A.M., A.A. and J.M.; Project administration, J.T., S.M. and A.G.; Supervision, J.V. and J.T.; Writing—original draft, A.S., J.V. and J.T.; Writing—review & editing, J.V., J.T., P.A.M., A.A., J.M., R.G.-O., J.S., S.M. and A.G.

Funding: The APC was funded by Universitat de València.

Acknowledgments: This work was supported by the Catedra Würth-EMC, a research collaboration agreement between the University of Valencia and Würth Elektronik eiSos GmbH & Co. KG.

Conflicts of Interest: The authors declare no conflict of interest. The founding sponsors had no role in the design of the study; in the collection, analyses, or interpretation of data; in the writing of the manuscript, and in the decision to publish the results.

References

1. Valenzuela, R. Novel Applications of Ferrites. *Phys. Res. Int.* **2012**, *2012*, 1–9. doi:10.1155/2012/591839.
2. Li, H.; Li, Z.; Zhang, B.; Tang, W.K.; Halang, W.A. Suppressing electromagnetic interference in direct current converters. *IEEE Circuits Syst. Mag.* **2009**, *9*, 10–28. doi:10.1109/MCAS.2009.934705.
3. Underwood, S.J. DC-DC converters suppress EMI: Minimizing EMI at its Source. *Power Electron. Technol.* **2002**, *28*, 14–21.
4. Goldman, A. *Modern Ferrite Technology*, 2nd ed.; Springer Science & Business Media: Pittsburgh, PA, USA, 2006.
5. Ott, H.W. *Electromagnetic Compatibility Engineering*; John Wiley & Sons: Hoboken, NJ, USA, 2009.
6. Hegarty, T. An Overview of Conducted EMI Specifications for Power Supplies. Available online: http://www.ti.com/lit/wp/slyy136/slyy136.pdf (accessed on 31 May 2019).
7. Mainali, K.; Oruganti, R. Conducted EMI Mitigation Techniques for Switch-Mode Power Converters: A Survey. *IEEE Trans. Power Electron.* **2010**, *25*, 2344–2356. doi:10.1109/TPEL.2010.2047734.
8. Zhu, H.; Liu, D.; Zhang, X.; Qu, F. Reliability of Boost PFC Converters with Improved EMI Filters. *Electronics* **2018**, *7*, 413. doi:10.3390/electronics7120413.
9. Zhai, L.; Zhang, T.; Cao, Y.; Yang, S.; Kavuma, S.; Feng, H. Conducted EMI Prediction and Mitigation Strategy Based on Transfer Function for a High-Low Voltage DC-DC Converter in Electric Vehicle. *Energies* **2018**, *11*, 1028. doi:10.3390/en11051028.
10. Urabe, J.; Fujii, K.; Dowaki, Y.; Jito, Y.; Matsumoto, Y.; Sugiura, A. A Method for Measuring the Characteristics of an EMI Suppression Ferrite Core. *IEEE Trans. Electromagn. Compat.* **2006**, *48*, 774–780. doi:10.1109/TEMC.2006.884507.

11. Hartmann, M.; Ertl, H.; Kolar, J.W. EMI Filter Design for a 1 MHz, 10 kW Three-Phase/Level PWM Rectifier. *IEEE Trans. Power Electron.* **2011**, *26*, 1192–1204. doi:10.1109/TPEL.2010.2070520.
12. Lukovic, M.D.; Nikolic, M.V.; Blaz, N.V.; Zivanov, L.D.; Aleksic, O.S.; Lukic, L.S. Mn-Zn Ferrite Round Cable EMI Suppressor with Deep Grooves and a Secondary Short Circuit for Different Frequency Ranges. *IEEE Trans. Magn.* **2013**, *49*, 1172–1177. doi:10.1109/TMAG.2012.2219064.
13. Cuellar, C.; Tan, W.; Margueron, X.; Benabou, A.; Idir, N. Measurement method of the complex magnetic permeability of ferrites in high frequency. In Proceedings of the Instrumentation and Measurement Technology Conference (I2MTC), Graz, Austria, 13–16 May 2012; pp. 63–68.
14. University of York. Link PCP—EMC Aspects of Mobile Telecommunications Systems, Appendix G—Coupling of EMI to Cables: Theory and Models (Final Report). Available online: https://pdfs.semanticscholar.org/cd27/bdd7dab556ce1d0c8e1da41cf9a5605f3d4f.pdf (accessed on 30 November 2018).
15. Urabe, J.; Fujii, K.; Harun, A.M.B.; Matsumoto, Y.; Sugiura, A. A study of EMI suppression characteristics of ferrite cores. In Proceedings of the 17th International Zurich Symposium on Electromagnetic Compatibility (EMC), Zurich, Switzerland, 27 February–3 March 2006; pp. 622–625.
16. Damnjanovi, M.; Stojanovi, G.; Živanov, L.; Desnica, V. Comparison of different structures of ferrite EMI suppressors. *Microelectron. Int.* **2006**, *23*, 42–48. doi:10.1108/13565360610680758.
17. Stojanović, G.; Lečić, N.; Damnjanović, M.; Živanov, L. Electrical and temperature characterization of NiZn ferrites. *Int. J. Appl. Electromagn. Mech.* **2011**, *35*, 165–176. doi:10.3233/JAE-2011-1329.
18. Saotome, H.; Sakaki, Y. Complex permeability of polycrystalline Mn-Zn and Ni-Zn ferrites. *Electr. Eng. Jpn.* **1998**, *123*, 1–7. doi: 10.1002/(SICI)1520-6416(19980430)123:2<1::AID-EEJ1>3.0.CO;2-9.
19. Suarez, A.; Victoria, J.; Alcarria, A.; Torres, J.; Martinez, P.A.; Martos, J.; Soret, J.; Garcia-Olcina, R.; Muetsch, S. Characterization of Different Cable Ferrite Materials to Reduce the Electromagnetic Noise in the 2–150 kHz Frequency Range. *Materials* **2018**, *11*, 174. doi:10.3390/ma11020174.
20. Herzer, G.; Vazquez, M.; Knobel, M.; Zhukov, A.; Reininger, T.; Davies, H.A.; Sanchez Ll, J.S. Round table discussion: Present and future applications of nanocrystalline magnetic materials. *J. Magn. Magn. Mater.* **2005**, *294*, 252–266. doi:10.1016/j.jmmm.2005.03.042.
21. Thierry, W.; Thierry, S.; Benoît, V.; Dominique, G. Strong volume reduction of common mode choke for RFI filters with the help of nanocrystalline cores design and experiments. *J. Magn. Magn. Mater.* **2006**, *304*, 847–849. doi:10.1016/j.jmmm.2006.03.014.
22. Herzer, G. Modern soft magnets: Amorphous and nanocrystalline materials. *Acta Mater.* **2013**, *61*, 718–734.
23. Liu, Y.; Han, Y.; Liu, S.; Lin, F. Pulse Magnetic Properties Measurement and Characterization of Fe-Based Nanocrystalline Cores for High-Voltage Pulse Magnetics Applications. *IEEE Trans. Power Electron.* **2015**, *30*, 6883–6896. doi:10.1109/TPEL.2014.2386916.
24. Naishadham, K. Closed-Form Design Formulas for the Equivalent Circuit Characterization of Ferrite Inductors. *IEEE Trans. Electromagn. Compat.* **2011**, *53*, 923–932. doi:10.1109/TEMC.2011.2116795.
25. Weinschrott, A.; Weinschrott, A. New measurement method for high frequency cable mounted ferrites. In Proceedings of the 2005 International Symposium on Electromagnetic Compatibility, Chicago, IL, USA, 8–12 August 2005; pp. 312–314.
26. Schulze, S.; Al-Hamid, M.; Leone, M. Detailed study of different cable ferrite characterization methods using simulation and measurement. In Proceedings of the 2017 International Symposium on Electromagnetic Compatibility-EMC Europe, Angers, France, 4–7 September 2017; pp. 1–5.
27. Brander, T.; Gerfer, A.; Rall, B.; Zenkner, H. *Trilogy of Magnetics: Design Guide for EMI Filter Design, SMP & RF Circuits*, 4th ed.; Swiridoff Verlag: Künzelsau, Germany, 2010.
28. Saito, T.; Takemoto, S.; Iriyama, T. Resistivity and core size dependencies of eddy current loss for Fe-Si compressed cores. *IEEE Trans. Magn.* **2005**, *41*, 3301–3303. doi:10.1109/TMAG.2005.854905.
29. Moongilan, D. Termination effects on attenuation properties of ferrites installed around cable conductors. In Proceedings of the 2013 International Symposium on Electromagnetic Compatibility, Denver, CO, USA, 5–9 August 2013; pp. 107–112.
30. Suarez, A.; Victoria, J.; Alcarria, A.; Torres, J. Characterization of electromagnetic noise suppression sheet for aerospace applications. In Proceedings of the ESA Workshop on Aerospace EMC, Valencia, Spain, 23–25 May 2016; pp. 1–6.

31. Victoria, J.; Suarez, A.; Torres, J.; Martinez, P.A.; Alcarria, A.; Martos, J.; Garcia-Olcina, R.; Soret, J.; Muetsch, S.; Gerfer, A. Transmission Attenuation Power Ratio Analysis of Flexible Electromagnetic Absorber Sheets Combined with a Metal Layer. *Materials* **2018**, *11*, 1612. doi:10.3390/ma11091612.
32. Hu, P.; Yang, H.B.; Pan, D.A.; Wang, H.; Tian, J.J.; Zhang, S.; Wang, X.; Volinsky, A.A. Heat treatment effects on microstructure and magnetic properties of Mn-Zn ferrite powders. *J. Magn. Magn. Mater.* **2010**, *322*, 173–177. doi:10.1016/j.jmmm.2009.09.002.
33. Beatrice, C.; Bottauscio, O.; Chiampi, M.; Fiorillo, F.; Manzin, A. Magnetic loss analysis in Mn-Zn ferrite cores. *J. Magn. Magn. Mater.* **2006**, *304*, e743–e745. doi:10.1016/j.jmmm.2006.02.209.
34. Sun, G.L.; Li, J.B.; Sun, J.J.; Yang, X.Z. The influences of Zn^{2+} and some rare-earth ions on the magnetic properties of nickel-zinc ferrites. *J. Magn. Magn. Mater.* **2004**, *281*, 173–177,doi:10.1016/j.jmmm.2004.04.099.
35. Costa, A.C.F.M.; Tortella, E.; Morelli, M.R.; Kiminami, R.H.G.A. Synthesis, microstructure and magnetic properties of Ni-Zn ferrites. *J. Magn. Magn. Mater.* **2003**, *256*, 174–182. doi:10.1016/S0304-8853(02)00449-3.
36. Snelling, E.C. *Soft Ferrites, Properties and Applications*, 2nd ed.; Butterworth: Boston, MA, USA, 1988.
37. Reeve, W.D.; Hagen, T. Applying and Measuring Ferrite Beads: Part I Ferrite Bead Properties and Test Fixtures. Available online: http://www.reeve.com/Documents/Articles%20Papers/Ferrite%20Beads/Reeve-Hagen_FerriteBeads_P1.pdf (accessed on 30 November 2018).
38. Paul, C.R. *Introduction to Electromagnetic Compatibility*, 2nd ed.; Wiley Interscience: Hoboken, NJ, USA, 2006.
39. Ott, H.W. *Noise Reduction Techniques in Electronic Systems*; John Wiley & Sons: Hoboken, NJ, USA, 1988.
40. Keysight E5061B-3L3/3L4/3L5 LF-RF Network Analyzer with Option 005 Impedance Analysis Function. Available online: http://literature.cdn.keysight.com/litweb/pdf/5990-7033EN.pdf (accessed on 30 November 2018).

Chapter 5. Analysis of the sleeve core dimensions dependency on the EMI suppression performance.

This chapter focuses on characterizing the performance of different sleeve cores based on the same material composition with the aim of determining the core size dependency in terms of the EMI suppression. The results presented show the relation between core inductance, dimensions and impedance as well as how to determine the optimum core size.

5.1 Scientific conference article I

Title: Analysis of different Sleeve Ferrite Cores Performance according to their Dimensions.

Authors: Adrian Suarez, Jorge Victoria, Pedro A. Martinez, Antonio Alcarria, Jose Torres, and Ismael Molina.

Published in: 2019 International Symposium on Electromagnetic Compatibility - EMC EUROPE, IEEE. Barcelona, Spain.
DOI: 10.1109/EMCEurope.2019.8872078

Description: The International Symposium on Electromagnetic Compatibility - EMC EUROPE is an international conference with a high scientific level supported by IEEE and the EMC Society. It is an annual conference that promotes EMC research, innovation and international cooperation. The submitted contributions are subjected to the peer review process to assess the quality of the manuscript before it is published in IEEE Xplore database, one of the most comprehensive interdisciplinary engineering databases in the world.

Summary:

This scientific conference article analyzes the impedance dependence of different sleeve cores with respect to their dimensions has been carried out. Firstly, five ceramic materials with different initial permeabilities from 380 up to 5000 have been compared with the novel NC core by representing their impedance traces. The results presented show that NC provides the highest impedance throughout the frequency range of 1-500 MHz compared with ceramic cores with the same dimension.

The EMC engineering should be dealt with the system approach, considering EMC throughout the design process to prevent possible EMI problems. During this process, it is possible to determine that it is needed to shield a certain cable, system interface or, even, this may be decided in the testing stage because an unexpected EMI source appears when the designed device is supplied via an external power system, or it is connected to another device to communicate to it. This situation could lead to the cables that interconnect the systems could represent the EMI source that supposes failing the conducted emissions test or the radiated emission test because the cable acts as an antenna at a certain frequency. The advantage of using an EMI suppressor sleeve core is that it does not involve redesign the electronics and, generally, the mechanical redesign. This is an important advantage because determining at the testing stage, which is the EMI source, may not be straightforward. However, this solution involves adding an extra component whose drawbacks result in increasing the size and weight of the product besides the cost of the filtering component and its installation.

The results presented in this manuscript correspond to the analysis of the acquired data by comparing sleeve cores with different compositions (NC, MnZn, and NiZn) and dimensions. Thereby, the performance in terms of impedance of some sleeve cores according to their volume, inductance and initial permeability are analyzed. Following Snoek's Law, the core that provides the lower initial permeability may yield a higher permeability in the range of the conducted or radiated emissions. As expected, the ceramic cores have been classified according to the initial permeability, and the materials with lower permeabilities work better at higher frequencies. In the case of NC core, it provides the higher initial permeability value, but due to its structure it is able to maintain a slow fall slope that together with its extremely high initial permeability, yields the best performance throughout the analyzed range (1–500 MHz).

The impedance traces of two pairs of cores with the same volumes and material composition but provide different impedance traces have been studied. It is observed an impedance difference between sleeve cores with the same volume and composition that demonstrates that only the volume information is not enough to select a core, since a core with low volume is able to provide a greater performance. This is due to, even though

each pair has the same volume, in this case, the inductance of the core is higher in those with larger height. Following this idea, it is possible to find cores with the same material composition that provide the same impedance response but having different volumes. This approach can lead to select, besides the core material with the best performance to attenuate EMI in a certain frequency, the sleeve core that provides the maximum impedance with the minimum volume. In this sense, it has to be taken into account that the inner diameter of the core is the most restrictive parameter due to it has to be selected according to the cable to be protected.

Analysis of different Sleeve Ferrite Cores Performance according to their Dimensions

Adrian Suarez
Department of Electronic Engineering
University of Valencia
Valencia, Spain
adrian.suarez@uv.es

Jorge Victoria
Würth Elektronik eiSos GmbH & Co. KG
Waldenburg, Germany
jorge.victoria@we-online.de

Pedro A. Martinez
Department of Electronic Engineering
University of Valencia
Valencia, Spain
pedro.a.martinez@uv.es

Antonio Alcarria
Würth Elektronik eiSos GmbH & Co. KG
Waldenburg, Germany
antonio.alcarria@we-online.de

Jose Torres
Department of Electronic Engineering
University of Valencia
Valencia, Spain
jose.torres@uv.es

Ismael Molina
Würth Elektronik eiSos GmbH & Co. KG
Waldenburg, Germany
ismael.molinaalba@we-online.de

***Abstract*— Sleeve ferrite core is an EMI suppressor widely used to reduce the conductive and radiated electromagnetic noise in cables. The interconnection of different electronic systems through cables is becoming more difficult due to the hard restrictions related to EMC compliance requirements. Thereby, the research of new solutions able to provide a great attenuation ratio in a wide frequency band is a challenge. This contribution focuses on analyzing and comparing the performance of a novel sleeve ferrite solution based on a nanocrystalline (NC) structure with several materials with different compositions. This component is able to provide a high initial permeability value at the same time that maintains it up to some tens of megahertz. In terms of dimensions, NC suppressors can provide the same effectiveness than other materials with more reduced dimensions. The analysis of the impedance dependence of a sleeve ferrite core with its dimensions has been carried out. Five ceramic materials with different initial permeabilities from 380 up to 5000 has been compared with the NC core through representing their impedance traces. The results presented shows that NC provides the higher impedance throughout the frequency range of 1-500 MHz when it is compared with ceramic cores with the same dimensions.**

Keywords—Electromagnetic interference (EMI) suppressors, sleeve ferrite cores, nanocrystalline (NC)

I. Introduction

The fast development and wide deployment of electrical and electronic equipment has intensified significantly the presence of electromagnetic interference (EMI) pollution. This trend leads to increase the interference induced by electric and magnetic fields, being increasingly more difficult to ensure all devices operate simultaneously in the context of electromagnetic compatibility (EMC) without interfering each other [1]. The interconnection of different electronic systems through cables is becoming more difficult due to the hard restrictions related to EMC compliance requirements. The use of EMC components that allow reducing the degradation in performance of an electronic device caused by electromagnetic disturbances is a good solution to pass compliance test. Nevertheless, these solutions usually focus on EMI filtering or shielding and, besides raising the price of electronics, they can also increase the volume and weight of the system [2].

One of the EMI suppressor widely used to reduce the conductive and radiated noise is the sleeve ferrite core, since it can work as low-pass filter blocking signals with frequencies higher than a certain frequency value [3]. This component is used in power cables due to it is especially effective when used to damp out high-frequency oscillations generated by switching transients or parasitic resonances within a circuit. Sleeve ferrites are also installed around peripheral cables of electronic devices such as video cables or universal serial bus (USB) cables in order to prevent electromagnetic disturbance from propagating along the cable [4]. Thereby, the attachment of a sleeve ferrite to encircle cables with EMI introduces a certain insertion loss (A) by which the disturbance current flowing through them is reduced and thus EMI is attenuated. This component is very effective against common mode (CM) currents since a ferrite placed around the cable is able to reduce the magnetic field through increasing the cable impedance to these currents that flows in the same direction in each conductor of the cable. This effect provides a means of discriminating between unwanted CM interference and desired differential mode (DM) signals, which should be unaffected, when these belong to a similar frequency range [5]. The attenuation ratio provided by a sleeve ferrite depends on the source and the load impedances of the circuit where it is introduced. Accordingly, the ferrite is used most effectively in systems with impedances that are no larger than the ferrite impedance since it must add an impedance higher than the sum of the source and load impedance at the frequency of interest with the aim of blocking noise currents by adding a significant impedance to the path [6].

The material and manufacturing technique used to make a sleeve ferrite defines its magnetic properties and determines the frequency range of applicability. Traditionally ferrite core materials for EMI suppression are based on MnZn and NiZn through their different compositions [7]. The information generally provided by manufacturers focuses on the initial permeability (μ_i) or the impedance value at some frequency points. From this data it could be seem that selecting the ferrite with the highest initial permeability it is possible to concentrate the maximum flux value in the core. Nevertheless, a sleeve ferrite with a significant initial permeability might provide a low relative permeability (μ_r) value at higher

978-1-7281-0594-9/19/$31.00 © 2019 IEEE

frequencies reducing its effectiveness to attenuate EMI disturbances.

A comparison of several materials with different compositions are analyzed in this contribution with the aim of comparing them with a novel sleeve ferrite solution based on a nanocrystalline (NC) structure. This component is able to provide a high initial permeability value at the same time that maintains it up to some tens of megahertz [8]. In terms of dimensions, NC EMI suppressors can provide the same effectiveness than other materials with a volume 50–80% higher [10], [11]. Consequently, a NC sleeve ferrite core is characterized and compared with different ceramic material compositions in order to determine its effectiveness in the EMI frequency region. Firstly, in the section II, the three different analyzed materials are classified from their magnetic properties defined by the relative permeability parameter (μ_r). Section III explains the relation between the inductance of the core and the effectiveness to filter EM interferences. Subsequently, in section IV the performance of different ferrite materials is evaluated from the point of view of the impedance response, depending on their dimensions. Finally, the main conclusions are summarized in section V.

II. Magnetic Properties

Ferrite cores belong to the ferromagnetic materials field and, specifically, MnZn and NiZn are included in the ceramic materials subgroup whereas NC core is classified within the metals subgroup. The main characteristics of ceramics are their heat-resistance, hardness, brittleness, high resistance to pressure and the possibility of creating cores with many different shapes. This last characteristic is the main drawback of the novel NC core due to it is formed by 20 µm metal film layers that are rolled up to form the cylindrical core with the desired size. Fig. 1 shows the metal films that conforms the structure of the NC core analyzed in this contribution. Thereby, the NC core cannot be split into two or more parts without undermining its EMI suppression ability due to if films are separated the relative permeability is reduced. Nevertheless, at the same time, this kind of structure is main advantage of NC core structure since it makes it possible to design more reduced and lighter components with greater magnetic properties due to its intrinsic properties obtained by means of a complex crystallization procedure [8].

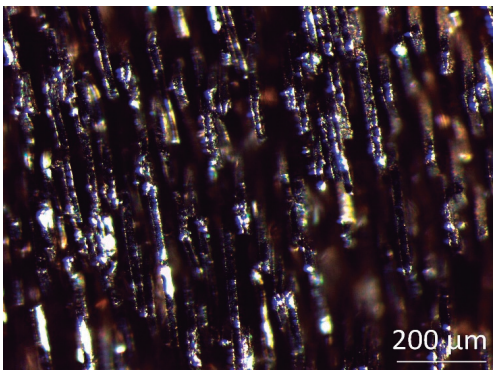

Fig. 1. Internal metal layers of the nanocrystalline core structure.

Besides the internal structure of NC core, another factor that defines its effectiveness is the production process. This is much more complex than the ceramic. The first step of the process consists of melting the material by heating it at 1300 °C. Next, the liquid is poured on a cooling wheel which is spinning around at 100 km/h with the aim of reducing its temperature at a cooling rate of 106 $K \cdot s^{-1}$, generating the amorphous structure and defining the thickness of the film about 20 µm. Subsequently, the film is rolled up to form the cylindrical core and it is subjected to an annealing process in which this is heated up to 600 °C to achieve the nanocrystalline state. Finally, strong magnetic fields are applied to the material in order to improve its magnetic properties [8].

For both ceramics and NC ferrites the chemical composition, internal structure and the manufacturing process defines the range in which frequency range the sleeve ferrite is able to provide the best attenuation. The main parameter that defines the ability of a certain material to concentrate the flux in the core is the relative permeability. The effectiveness to attenuate EM interferences of a certain material can be quantified by separating μ_r into its complex form so that the real component is related to the stored energy or inductive part (µ´) and the imaginary component that provides the losses or resistive part (µ´´). From this parameter it is possible obtain the initial permeability value of a certain core. According to IEC 60401-3 standard, μ_i describes the relative permeability of a material at low values of magnetic flux density (B) and it is defined using closed magnetic circuits for $f \leq 10$ kHz, $B <$ 0.25 mT, $T = 25$ °C. This configuration makes it possible to characterize sleeve ferrites without risk of saturation and, therefore, it is easier to compare different compositions. Fig. 2 shows the behavior of three different materials in terms of their complex relative permeability: NC ($\mu_i = 90.000$), MnZn ($\mu_i = 5.000$) and NiZn ($\mu_i = 620$).

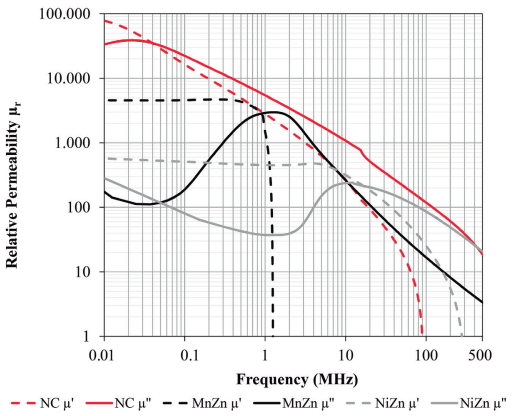

Fig. 2. Complex relative permeability of NC ($\mu_i = 90.000$), MnZn ($\mu_i = 5.000$) and NiZn ($\mu_i = 620$) core compositions.

This parameter could suggest that the maximum concentration of flux in the core is achieved by selecting the ferrite core material that provides the highest μ_i possible. Nevertheless, a core that provides a high μ_i at 10 kHz that relative permeability might be significantly reduced at frequencies in the frequency range of the regulatory limit where it should have an effect. An approximation of the Snoek's Law can be used as a governing rule of EMI suppression in order to explain the relation between magnetic saturation (B_s), initial permeability (μ_i) and resonance frequency (f_m):

$$f_m = B_S/\mu_i \quad (1)$$

Note that the value of B_s can be considered constant bellow the resonance frequency under the conditions described in IEC 60401-3.

Ferrites are generally based on MnZn and NiZn, however, this compositions can be modified by changing the mix of the materials used to fabricate the ferrite material. This makes it possible to find sleeve ferrite cores of a same material with different value of μ_i. MnZn ferrites tend to have higher μ_i than NiZn, but following the Snoek's Law, their permeabilities decreases more abruptly than NiZn as frequency increases. Table I shows the main features of the magnetic core materials analyzed in this contribution. As it can be observed, MnZn core provides a great value of initial permeability if it is compared with NiZn materials, whereas in the case of NC core the initial permeability is extremely higher due to its internal structure.

TABLE I. COMPARATIVE BETWEEN CORE MATERIALS

Identification	Material Type	Initial Permeability (μ_i)
IP90K	NC	90000
IP5K	MnZn	5000
IP1K5	NiZn	1500
IP800	NiZn	800
IP620	NiZn	620
IP380	NiZn	380

The relative permeability is a complex parameter that can be represented through both real and imaginary parts that can be related to the inductive and resistive components of the impedance inserted into the line passed through the sleeve ferrite. Although permeability parameter is used to describe the behavior of the core material, the performance of a certain sleeve ferrite core is determined by means of other variables such as the dimensions and shape, besides the material features. Thereby, sleeve ferrites are usually defined through specifying the magnitude of the impedance (Z_F), which is obtained from the inductive reactance (X_L) and resistance (R) equivalent component parameters. The ratio of these components depends on the frequency since the resistive part dominates at the higher frequencies and the energy is absorbed by the core.

III. SLEEVE FERRITE CHARACTERIZATION: DIMENSIONS DEPENDENCY

The core inductance (L_F) is a useful parameter to evaluate the effectiveness of a set sleeve ferrite cores depending on their dimensions. This can be obtained from the Ampere's Law defining the sleeve ferrite as a toroid which consists of N turns and a rectangular cross section with inner radius (IR), outer radius (OR) and height (h). The magnetic flux (Φ_B) through one turn of the sleeve ferrite may be obtained by integrating over the rectangular cross section (a rectangle whose sides are defined by r (the subtraction of the OR and IR) and h, defining the differential area element with $dIR = hdr$. Thereby, the total flux is determined by $N\Phi_B$ and, thus, L_F is given by [9]:

$$L_F = \frac{N\Phi_B}{I} = \frac{\mu_0\mu_r N^2 h}{2\pi} ln\left(\frac{OR}{IR}\right) \quad (2)$$

Equation 2 shows that the core inductance depends on the magnetic material relative permeability, the geometrical factors and the number of turns that can be increased by winding the cable more than one turn around the sleeve ferrite. An important revelation given by this equation is the importance of specific dimensions, since the impedance for a given core material is proportional to the natural logarithm of the ratio of outside to inside radius and directly proportional to the height. Sometimes this equation can be found expressed by the outside and inside diameters (OD and ID, respectively) of the sleeve ferrite instead of OR and IR due to the gauge of a cable is generally defined by the diameter. This means that an increase of the height core should be more predominant in impedance determination. This parameter is proportional to the relative permeability parameter, thus, it can be used to compare cores as long as it was carried out bellow the resonance frequency [6].

IV. RESULTS AND DISCUSSION

The results presented in this part, correspond to the analysis of the acquired data by comparing sleeve ferrite cores with different compositions and dimensions. Thereby, the ability of different sleeve ferrite cores to reduce EMI in cables is analyzed by comparing the novel NC core structure with ceramic cores. Firstly, the impedance versus frequency traces for the six materials gathered in Table I is studied. Subsequently, the performance in terms of impedance of some sleeve ferrite cores according to their volume, inductance and initial permeability are analyzed. The sleeve ferrites characterized in this section are summarized in Table II.

TABLE II. SLEEVE FERRITE CORES CHARACTERIZED

Identification	Material Type	μ_i	OD (mm)	ID (mm)	h (mm)
C1	NiZn	620	17.5	10.7	25.0
C2	NiZn	620	16.0	9.0	28.0
C3	NiZn	620	16.0	9.0	17.0
C4	NiZn	620	14.1	6.3	18.0
C5	NiZn	1500	12.0	3.6	25.0
C6	NiZn	1500	12.0	6.1	45.0
C7	NiZn	620	14.1	6.3	18
C8	NiZn	620	12.0	5.6	20.0
C9	NiZn	620	26.0	15.5	28.5
C10	NC	90000	18.9	12.9	27.7
C11	MnZn	5000	18.6	10.2	28.5
C12	NiZn	1500	28.0	18.0	28.5
C13	NiZn	800	17.5	9.5	28.5
C14	NiZn	620	20.5	11.5	29.0
C15	NiZn	380	14.2	6.35	28.5

Fig. 3 shows a comparison between some traditional ferrite materials based on MnZn and NiZn compared to the novel NC core structure through their impedance response. With the aim of extracting the dimension variable, the six impedance traces have been measured through using the same core sizes (ODxIDxh: 16x8x8 mm). These traces allow observing that in case of ceramics, it could seem more attractive to select a core with a high initial permeability value than one with a lower value. Nevertheless, following the Snoek's Law, the core that provides the lower initial permeability may yield a higher permeability in the range of the conducted or radiated emissions. As expected, the ceramic cores are classified according to the initial permeability at low

frequencies and the materials with lower permeabilities work better at higher frequencies. Thereby, the IP380 shows the lowest impedance value at low frequency range, but its raise slope is higher than the rest at higher frequencies. On the contrary, the MnZn material (IP5K) provides a great impedance response at some megahertz having its maximum value at 2 MHz and decreasing abruptly from this point. In the case of NC core, it provides the higher initial permeability value, but due to its structure it is able to maintain a slow fall slope that together with it has an initial permeability much higher than MnZn and NiZn materials, it yields the best performance throughout the analyzed range.

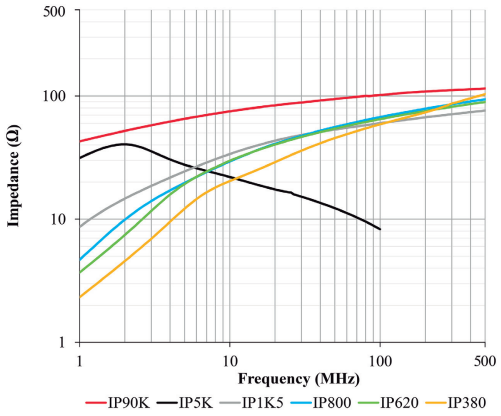

Fig. 3. Impedance versus frequency traces for different material composition depending on the initial permeability. Comparison between MnZn and NiZn materials with the novel NC structure.

As it has been explained bellow, the impedance provided by a sleeve ferrite is not always dependent on the volume of the core. This fact is shown in Fig. 4 by means of the impedance traces of two pairs of cores that have the same volumes and material composition but provide different impedance traces. The set of cores represented by the red traces have a volume of 3.8 cm3 and the black traces 2.3 cm3. This impedance difference between sleeve ferrites with the same volume and composition demonstrates that only the volume information is not enough to select a core, since a core with low volume is able to provide a greater performance. This is due to, even though each pair has the same volume, in this case the inductance of the core is higher in those with larger height. In this sense, C2 yields up to around 90 Ω more than C1 at 200 MHz and C4 provides around 50 Ω more than C3 from 50 MHz to 100 MHz.

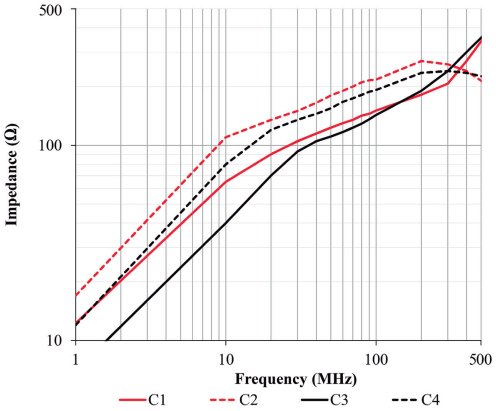

Fig. 4. Impedance versus frequency traces for two pairs of sleeve ferrites (each pair has the same volume). The red traces represent the impedance of cores with a volume of 3.8 cm3 and black traces a pair of cores with a volume of 2.3 cm3.

Following this idea, it is possible to find ferrite cores with the same material composition that provide the same impedance response but having different volumes. This approach can lead to select, besides the core material with the best performance to attenuate EMI in a certain frequency, that sleeve ferrite which provides the maximum impedance with the minimum volume. This selection criteria can be taken in applications where the EMI disturbance is not high enough to cause saturation of the core. In this sense, it has to be taken into account that the inner diameter of the core is the most restrictive parameter due to it has to be selected according to the cable to be shielded. Fig. 5 shows three groups of sleeve ferrite cores with similar impedance traces. Each of them is based on the same material composition and have the same core inductance. The set of cores represented by the red traces have a L_F of 9.1 uH and the black traces of 1.8 ± 0.1 uH. The first pair of cores formed by C5 and C6 have the same core inductance although the height of C6 is 20 mm larger than C5 because this is balanced by the higher diameters distance of C5. However, this different dimensions lead to the volume of the C6 corresponds to 1.5 times higher than C5. Under similar conditions, three cores with different height and diameters ratio compose the second group represented by the grey traces. The relation between them is given by VolumeC9 = 8.3xVolumeC7 = 4.3xVolumeC8. In this case, the difference between volumes and dimensions is quite significant and, thus, the right selection of the sleeve ferrite core may be turned into the use of a smaller component. This impedance difference between sleeve ferrites with the same volume and composition, demonstrates that only the volume information is not enough to select a core, since a core with low volume could be able to provide a greater performance. This is due to, even though each pair has the same volume, in this case the inductance of the core is higher in those with larger height. In this sense, SL2 yields up to around 90 Ω more than SL1 at 200 MHz and SL4 around 50 Ω more than SL3 from 50 MHz to 100 MHz.

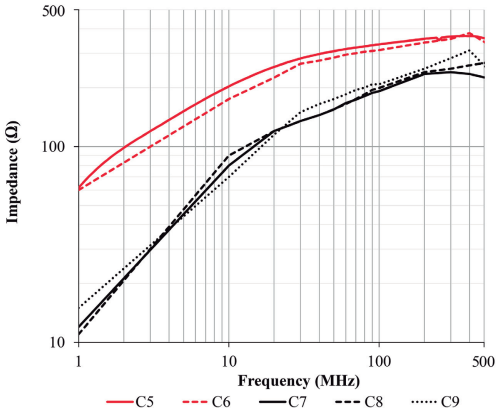

Fig. 5. Impedance versus frequency traces for two groups of sleeve ferrites (each group has a very similar inductance). The red traces represent the impedance of two cores with an inductance of 9.1 uH and black traces an inductance of 1.8 ± 0.1 uH.

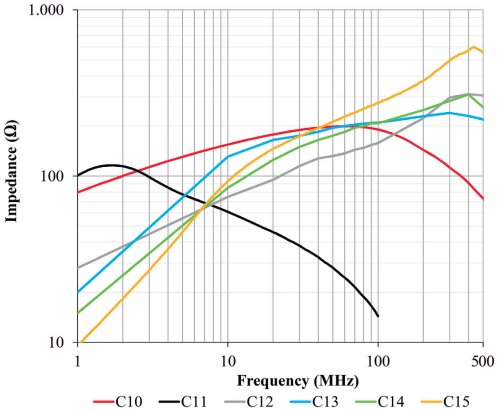

Fig. 6. Impedance provided by a NC core with a volume of 4.2 cm^3 and cercamic cores with larger volume. Comparison between MnZn and NiZn materials with the novel NC structure.

Once it has been analyzed the relation between volume, core inductance and impedance, a comparison between ceramic materials with the NC core is carried out. Because of its magnetic properties, this component is able to provide a great impedance response from low frequencies up to some ten of megahertz as shown in Fig. 6. In this graph, the impedance of a NC sleeve ferrite (C10) with a volume of 4.2 cm3 is represented and compare with MnZn and NiZn cores based on the different compositions. The selection of ceramic cores has been performed through looking for those with enough dimensions that makes it possible to yield a higher value of impedance within the frequency range studied in this research. Thereby, the MnZn (C11) core is able to provide a greater value of impedance than NC from 1 MHz up to 2.7 MHz and it has a volume of 5.4 cm3. The NiZn core with the highest initial permeability value is the C12 (10.3 cm3) and its impedance leads the NC trace from 120 MHz. The traces of C13 and C14 improve the impedance of the NC core at 60 MHz and 80 MHz, respectively. C13 has a higher permeability than C14 and yields more impedance at low frequencies, however, it begins to degrade before. The dimensions and the core inductance of these last two cores are very similar and the difference between them is practically defined by their relative permeability. The volume of C13 core is 4.83 cm3 and C14 corresponds to 6.56 cm3. Finally, C15 represents the core with the lowest initial permeability and, for this reason, it has been necessary to select a large sleeve ferrite (11.3 cm3) to be compared with the impedance provided by the NC sleeve ferrite. The trace of C15 crosses with the NC ones at 40 MHz, representing the NiZn sleeve ferrite composition with the best performance if they are compared with NC. This sleeve ferrite, besides being the NiZn core that improve NC impedance before, offers a significant value of impedance at hundreds of megahertz, reaching a maximum value of 599 Ω at 433 MHz.

V. Conclusions

The analysis of the impedance dependence of different sleeve ferrite cores with respect to their dimensions has been carried out. Firstly, five ceramic materials with different initial permeabilities from 380 up to 5000 has been compared with the novel NC core through representing their impedance traces. The results presented shows that NC provides the higher impedance throughout the frequency range of 1-500 MHz when it is compared with ceramic cores with the same dimension.

Thereby, some cores have been evaluated in order to quantify the influence of dimensions over the impedance and it has been determined that the core inductance parameter offers more accurate information than the volume value. This is due to the choice of a sleeve ferrite core with higher volume than other does not ensure that it provide a higher impedance. However, the core inductance takes into account the value of the core dimensions and it is proportional to the impedance. From the results reported, it is possible to conclude that the height of the core is usually more predominant than the fatter of this. Subsequently, some sleeve ferrite cores based on the different ceramic materials has been selected with the aim of they are able to provide a comparable impedance response. This makes it possible to determine what dimensions are needed by each material to be comparable with the NC impedance trace at least in some part of the frequency range where the NC core is effective. The results show that all the ferrites that can provide an impedance response comparable with the NC impedance have dimensions larger than this and they only can improve the NC behavior in some part of the frequency range. These ranges are provided in particular by the MnZn sleeve that shows a better response from 1-2.7 MHz and the best core based on NiZn that is able to improve the NC impedance value from 40 MHz.

All things considered, if the EMI disturbance is located specifically in the low frequency region or from 40 MHz it could be used a ceramic core despite of it has a larger dimensions than NC solution. Nevertheless, if the EMI problems are distributed from the low frequency region up to around 100 MHz the best performance is provided by the NC sleeve ferrite core due to, with optimized and reduced dimensions, it represents a wideband EMI filtering solution.

REFERENCES

[1] R. Valenzuela, "Novel applications of ferrites," *Phys. Res. Int*., vol. 2012, pp.1–9, 2012.

[2] X. C. Tong, "Advanced Materials and Design for Electromagnetic Interference Shielding," in *Electromagnetic Interference Shielding Fundamentals and Design Guide*. Boca Raton, FL, USA: CRC, 2009, ch.1, pp. 11–20.

[3] N. V. Blaž, M. D. Luković, M. V. Nikolic, O. S. Aleksić and L. D. Živanov, "Heterotube Mn-Zn Ferrite Bundle EMI Suppressor With Different Magnetic Coupling Configurations," in *IEEE Transactions on Magnetics*, vol. 50, no. 8, pp. 1-7, Aug. 2014, doi: 10.1109/TMAG.2014.2310436.

[4] H. W. Ott, *Electromagnetic Compatibility Engineering*. New York, NY, USA: Wiley, 2011, pp. 225–233.

[5] T. Williams. *EMC for Product Designers*. Burlington, MA, USA: Elsevier Science & Technology, 2006, pp. 361–364.

[6] C. Paul, *Introduction to Electromagnetic Compatibility*. Hoboken, NJ, USA: Wiley, 2006, pp. 299–419.

[7] A. Goldman, *Modern Ferrite Technology*. Pittsburgh, PA, USA: Springer, 2006.

[8] A. Suarez, et al. "Characterization of Different Cable Ferrite Materials to Reduce the Electromagnetic Noise in the 2–150 kHz Frequency Range," *Materials*, vol. 11, no. 2, pp. 1–20, 2018.

[9] F. E. Terman, Radio Engineers Handbook. New York, NY, USA: McGraw-Hill, 1945.

[10] W. Thierry, S. Thierry, V. Benot, and G. Dominique, "Strong volume reduction of common mode choke for RFI filters with the help of nanocrystalline cores design and experiments," *J. Magnetism Magnetic Mater.*, vol. 304, no. 2, pp. e847–e849, 2006.

[11] G. Herzer, "Modern soft magnets: Amorphous and nanocrystalline materials," *Acta Materialia*, vol. 61, no. 3, pp. 718–734, 2013.

5.2 Scientific conference article II

Title: Determination of Core Size Dependency on the EMI Suppression in Cable Ferrites.

Authors: Adrian Suarez, Jorge Victoria, Jose Torres, Pedro A. Martinez, Víctor Martínez, Ismael Molina, Steffen Muetsch, Raimundo Garcia-Olcina, Jesus Soret, and Julio Martos.

Published in: 2020 International Symposium on Electromagnetic Compatibility - EMC EUROPE, IEEE. Rome, Italy.
DOI: 10.1109/EMCEUROPE48519.2020.9245745

Description: The International Symposium on Electromagnetic Compatibility - EMC EUROPE is an international conference with a high scientific level supported by IEEE and the EMC Society. It is an annual conference that promotes EMC research, innovation and international cooperation. The submitted contributions are subjected to the peer review process to assess the quality of the manuscript before it is published in IEEE Xplore database, one of the most comprehensive interdisciplinary engineering databases in the world.

Summary:

The second conference scientific contribution highlights the importance of finding the inductance of a sleeve core (L_m) to determine its effectiveness. This parameter is proportional to the complex permeability parameter (μ_r) that mainly defines the core's magnetic properties and its dimensions. Nevertheless, as it has been verified in the conference scientific article I, it does not exist a proportional relation between the volume of a sleeve core and its performance, since components with lower volume are able to provide greater response than others with higher volume.

An analysis of samples with different sizes is carried out in this contribution with the aim of determining the dependency between performance and core inductance. The main objective is to obtain a parameter that relates these features in order to determine the optimized dimensions of a sleeve core that can provide the effectiveness necessary to reduce EMI problems in cables. Consequently, different sleeve cores have been characterized by their impedance response and compared between them in order to determine their core size dependency.

The translation of the complex relative permeability components to the impedance provided is related to the sleeve core's inductance considering its magnetic properties (L_m), geometry and size, and frequency (ω). From L_m parameter, it is considered how the dimensions and geometry of a certain core contribute to determining its ability to

attenuate EMI in cables. Particularly, in the case of a sleeve core, it can be considered a toroid that has a rectangular cross-section with a specific inner diameter (*ID*), outer diameter (*OD*), and height (*h*). Considering these parameters, to maximize its impedance it is interesting to select the maximum *OD*/*ID* ratio and height while the *ID* is as tight as possible to the cable diameter. Nevertheless, the increase of the dimensions is usually proportional to its weight, volume and cost. Hence, a balance between these three features and performance should be carried out. Thereby, it should be taken into account that the impedance is proportional to the natural logarithm of the ratio of the outer to the inner diameter and directly proportional to the height. Note that, even though *h* is directly proportional to the impedance, the natural logarithm provides an attenuation factor when the *ID* is lower than 2.7 times the *OD*, so that it is crucial not selecting thin cores since, for instance, *OD*/*ID* ratios of 2.0 or 1.5 reduce the performance of the sleeve core about 30% and 60%, respectively.

Subsequently, the *K* parameter that relates the impedance per unit of core inductance (Z_{SC} / L_0) provided by three samples with quite different dimensions is determined. The *K* parameter makes it possible to calculate the impedance of a new sample based on the same material and geometry from the new core dimensions. It is carried out by dividing the impedance measured of a certain sample by its air core inductance (L_0). Next, the *K* obtained is multiplied by the air core inductance of the new sleeve core. This principle is validated by calculating the impedance of a second core from the *K* parameter (obtained by a first core) and the second core L_0 parameter. This theoretical impedance of the second core is compared with the experimentally obtained and a significant match between both data is obtained.

All things considered, the *K* parameter allows a designer to determine the size of a sleeve core to provide the necessary impedance to attenuate a specific EMI disturbance. Hence, it is possible to optimize the component's dimensions to select it with the minimum volume, weight, and cost.

Determination of Core Size Dependency on the EMI Suppression in Cable Ferrites

A. Suarez[1], J. Victoria[2], J. Torres[1], P. A. Martinez[1], V. Martinez[2], I. Molina[2], S. Muetsch[2], R. Garcia-Olcina[1], J. Soret[1] and J. Martos[1]
[1]*Department of Electronic Engineering, University of Valencia,* Valencia, Spain
adrian.suarez@uv.es
[2]*Product Management, Würth Elektronik eiSos GmbH & Co. KG,* Waldenburg, Germany
jorge.victoria@we-online.de

***Abstract*—Electromagnetic Compatibility (EMC) engineering should be approached via the systems approach, considering EMC throughout the design to anticipate possible electromagnetic interferences (EMI) problems. Nevertheless, an EMI source may appear when the designed device is supplied via an external power system or it is connected to another device to communicate to it. In these both cases, the cables or interfaces that interconnect the systems could represent the EMI source. Thereby, one of the most common techniques for reducing EMI in cables is the application of an EMI suppressor such as sleeve ferrite cores to them. The advantage of this solution is that it does not involve redesign the electronics and, generally, the mechanical redesign. This is an interesting point since the analysis at this time to find which of the possible interference path combinations are contributing to the problem may not be simple. However, this solution involves the addition of an extra component whose drawbacks result in increasing the size and weight of the product besides the cost of the filtering component and its installation. This contribution focuses on characterizing the performance of different cable ferrites based on the same material composition with the aim of determining the core size dependency in terms of the EMI suppression. The results presented show the relation between core inductance, dimensions and impedance as well as how to determine the optimum core size.**

Keywords—Electromagnetic interference (EMI) suppressors, sleeve ferrite cores, cable ferrites, core size dependency

I. Introduction

The fast development of electrical and electronic devices has become an increasingly serious electromagnetic interference (EMI) problem faced by engineers and scientists in order to design systems that comply with electromagnetic compatibility (EMC) requirements [1]. This is the reason why EMC engineering should be dealt with the system approach, considering EMC throughout the design process to prevent possible EMI problems [2]. During this process, it is possible to determine that it is needed to shield a certain cable or interface of the system or, even, this may be decided in the testing stage because an unexpected EMI source appears when the designed device is supplied via an external power system or it is connected to another device to communicate to it. This situation could lead to the cables that interconnect the systems could represent the EMI source that supposes failing the conducted emissions test or the radiated emission test because of the cable acts as an antenna at a certain frequency. Thus, one of the most used technique for reducing interferences in cables is the application of an EMI suppressor such as sleeve ferrite cores to them since, when it is properly used, it can be effective in reducing conducted and/or radiated emissions from cables, as well as well as suppressing high-frequency pickup in this [2]. The advantage of this solution is that it does not involve redesign the electronics and, generally, the mechanical redesign [3]. This is an important advantage because determining at the testing stage which is the EMI source, may not be simple. However, this solution involves the addition of an extra component whose drawbacks result in increasing the size and weight of the product besides the cost of the filtering component and its installation [4].

The sleeve ferrite component (also known as cable ferrites) is generally used as an EMI suppressor that works as a low-pass filter, providing selective attenuation of high-frequency components that the designer may wish to suppress from the EMC point of view and it has no effect on the intended lower-frequency functional signal [5], [6]. Thereby, this component is widely used in order to filter EMI in power cables to reduce high-frequency oscillations generated by switching transients or parasitic resonances within a circuit. It is also used in peripheral cables of electronic devices such as multiconductor USB or video cables to prevent interferences that could be propagated along the wire affecting the devices interconnected [2], [6]. The effectiveness of a sleeve ferrite to reduce EMI in cables is defined by its capability to increase the flux density of a certain field strength created around a conductor. The current flowing through the conductor produces magnetic flux in the circumferential direction that passes through the sleeve ferrite material, producing an internal inductance. Therefore, the placement of the magnetic material around the conductor leads to increase its inductance. The inductance of the core (L_F) is proportional to the complex permeability parameter (μ_r) that mainly defines the magnetic properties of a sleeve ferrite and its dimensions [3], [6]. Nevertheless, it has been verified that it does not exist a proportional relation between the volume of a sleeve ferrite core and its performance, since components with lower volume are able to provide greater response than other with higher volume [7], [8].

An analysis of several Ni-Zn sleeve ferrite cores with an initial permeability (μ_i) of 620 with different sizes is carried out in this contribution with the aim of determining the dependency between performance and ferrite core inductance. The main objective is the determination of a parameter that relates these features in order to obtain the optimized dimensions of a sleeve ferrite core that is able to provide the effectiveness necessary to reduce EMI problems in cables. Consequently, different Ni-Zn sleeve ferrite cores have been characterized by means of their impedance response and compared between them in order to determine their core size dependency. Firstly, in the section II, the analyzed material is described from their magnetic properties defined by the relative permeability parameter (μ_r). Section III explains the mechanism of filtering used by sleeve ferrite cores, includes the data of the analyzed sleeve ferrite cores and describes the relation between core inductance and size dependency. Subsequently, in section IV the performance of different sleeve ferrite cores is evaluated from the point of view of the

978-1-7281-5579-1/20/$31.00 ©2020 IEEE

impedance response. Finally, the main conclusions are summarized in section V.

II. Magnetic Properties

Ni-Zn ferrite cores belong to ferromagnetic materials and, specifically, are included in the ceramic materials. Ceramics are also known as polycrystalline materials and, although they do not belong to metals, they can contain metal oxide such as ferrite, nickel and zinc. The main characteristics of ceramics are their strong adhesion forces, heat resistant, hardness, brittleness and high resistance to pressure. The manufacturing process is performed by mixing the oxides, calcining the material obtained, breaking the calcined mixture, transform it into granular, pass these grains through a pressing process that sinters the material and, finally, covering it with an epoxy resin to reduce its conductivity. One of the main advantages of ceramics manufacturing process is the possibility of creating cores with many different shapes. On the other hand, one of ceramic core drawbacks is their weight due to this is higher if it is compared with other solutions such as those based on nanocrystalline structure [9], [10].

Ni-Zn ferrites are one of the most versatile soft magnetic materials, especially focused on filtering EMI disturbances in a broadband frequency range which can cover from some Megahertz to several hundreds of Megahertz [11]. From the standpoint of the composition, this ceramic material is mainly based on iron oxide (Fe_2O_3) with a proportion of about 70%. The proportion of Ni and Zn material is balanced depending on the frequency range where the cable ferrite is more effective, since a higher amount of Zn improves the cut-off frequency with the aim of attenuate electromagnetic noise at higher frequencies [12]. Moreover, Cu material is introduced in the Ni-Zn composition to reduce the firing temperature to ease the manufacturing process as well as improve electromagnetic properties at high frequencies [13].

The relative permeability (μ_r) is the main parameter that describes performance of a certain material to concentrate the magnetic flux in the core. In order to analyze the behavior of the material it is interesting to separate it into its complex form: the real component (μ_r') quantifies the inductive part and the imaginary or resistive component (μ_r'') is related to the material ability to absorb the electromagnetic interferences [O]. Fig. 1 shows the behavior of both real and imaginary components and the magnitude of the real permeability for the Ni-Zn ($\mu_i = 620$) material. These traces allow one to determine the magnetic resonance frequency (f_m) at which the real part of the relative permeability begins to fall and the imaginary part reaches the maximum peak. The inductance component is steady below the f_m and decreases significantly from this frequency value [14]. A capacitance stray component that represents the dielectric effects of the ferrite magnetic material appears in the bandwidth above the f_m, where the inductive component of the permeability becomes negative. As can be observed in Fig. 1, this stray capacitance due to the magnetic material should be noted beyond 282.7 MHz.

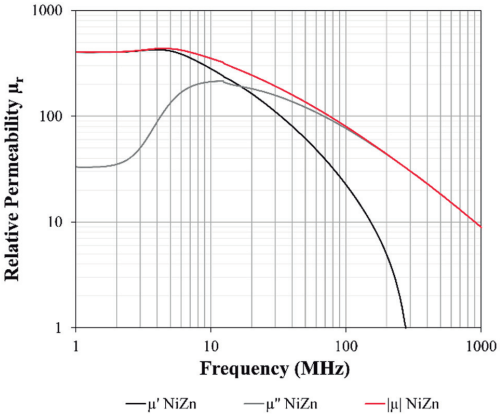

Fig. 1. Complex relative permeability of Ni-Zn ($\mu_i = 620$) core composition.

The Ni-Zn material characterized in this contribution shows a μ_i about 620, so that its EMI suppression ability is more effective from several tens of Megahertz. As shows the relative permeability response, this material has a soft falling slope that makes it suitable for filtering interferences in the low part of the radiated emissions spectrum.

III. EMI Suppression Mechanism: Impedance Management

One of the most common EMI radiated problems is originated by common-mode currents from the cables of a system. These currents, despite not having a high value compared to those produced by intended signals (differential mode currents), they have a much greater interfering potential since only a few microamps of common-mode current is required flowing through a cable is need to fail radiated emission requirements. Sleeve ferrite cores are very effective to filter the currents in common-mode flowing through cables that generates this kind of EMI problem. This is why all conductors included into the cable have unintended current flowing in the same direction that produces a net magnetic field around the cable. Thereby, when a ferrite is applied to the cable, the resulting magnetic field is affected and the impedance of the cable will be increased to these common-mode currents. The main advantage of this solution is that the ferrite has no effect on the intended differential-mode signal due to the direct and return currents produced by a pair of adjacent conductors generate two magnetic fields equals and opposites, and, thus the resultant is null. Consequently, the only currents attenuated by the sleeve ferrite placed around the cable will be those in common-mode. This kind of harmful current is generally caused by poor connection of the cable with the system ground or due to the distance between the signal conductors and the return paths when dealing with multiconductor cables. This ability to attenuate only the undesirable common-mode disturbances is a fundamental aspect when the intended and unintended are located near in the frequency spectrum [2], [3].

As described in section II, the ability of a certain sleeve ferrite core to attenuate a stray magnetic field is defined by its complex relative permeability. The real and imaginary parts of this can be expressed through the inductive (L_F) and resistive (R_F) components that represents the magnitude of the

impedance introduced into the cable (Z_F) as is shown in Fig. 2.

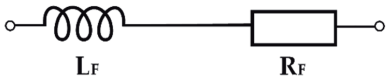

Fig. 2. Equivalent circuit for series representation of a sleeve ferrite core.

The translation of the complex relative permeability components to the inductive and resistive parts is related by the inductance of the ferrite core considering its magnetic properties (L_F), geometry and its size and the frequency (ω). This relation is expressed as

$$Z_F = \omega\, L_F. \tag{1}$$

The core inductance is an interesting parameter to determine the performance of a cable ferrite. From this parameter, it is possible to consider how the dimensions and geometry of a certain core contribute to determine its ability to attenuate EMI in cables. Particularly, in the case of a sleeve ferrite core can be considered a toroid that has a rectangular cross section with a certain inner diameter (*ID*), outer diameter (*OD*) and height (*h*). According to Ampere's Law, the magnetic induction (*B*) inside the torus is given by

$$B = \frac{\mu_0 NI}{2\pi r} \tag{2}$$

where *N* is the number of turns, *I* is the current flowing through it and *r* is the distance from the middle of the toroid to the center of the cross section. The magnetic flux (Φ_B) through one turn of the air toroid without considering its material is determined by integrating over the rectangular cross section, obtaining the relation that follows [15]:

$$L_0 = \frac{N\Phi_B}{I} = \frac{\mu_0 N^2 h}{2\pi} ln\left(\frac{OD}{ID}\right). \tag{3}$$

The inductance of the core considering its material composition (L_F) is given by

$$L_F = \mu_r L_0 = \frac{\mu_0 \mu_r N^2 h}{2\pi} ln\left(\frac{OD}{ID}\right). \tag{4}$$

Thereby, by dividing the impedance measured of a certain cable ferrite by its air core inductance (L_0), the *K* parameter is determined. The *K* parameter makes it possible to calculate the impedance of a new ferrite based on the same material and geometry from the dimensions of the new core. This can be carried out through multiplying *K* by the air core inductance of the new cable ferrite:

$$K = \frac{Z_F}{L_0}. \tag{5}$$

Considering the parameters that define the cable ferrite dimensions, to maximize the Z_F provided the cable ferrite it is interesting to select the maximum *OD*/*ID* ratio and height at the same time that the *ID* is as tight as possible to the cable diameter. Nevertheless, the increase of the dimensions is usually proportional to the weight, volume and cost of it. Hence, a balance between these three features and performance should be carried out. Thereby, it should be taken into account that the impedance is proportional to the natural logarithm of the ratio of the outer to inner diameter and directly proportional to the height. Note that, even though *h* is directly proportional to the impedance, the natural logarithm provides an attenuation factor when the *ID* is lower than 2.7 times the *OD*, so that it is important not selecting thin ferrites since, for instance, *OD*/*ID* ratios of 2.0 or 1.5 reduce the performance of the cable ferrite about 30% and 60%, respectively.

The attenuation provided by a cable ferrite depends on the impedance that presents the source system (Z_A) and the load system (Z_B) where it is placed. Thus, the cable ferrite is more effective when Z_A and Z_B have a low impedance interface, since cable ferrite should provide an impedance greater than the sum of the source and load impedance at the frequency with EMI disturbance. This is due to the cable ferrite should suppress undesired currents by introducing a significant impedance (greater than the sum of Z_A and Z_B) to the path. According to the simplified circuit diagram, the attenuation or insertion loss (A) provided by a cable ferrite is given by

$$A(dB) = 20\, log\left(\frac{Z_A+Z_F+Z_B}{Z_A+Z_B}\right). \tag{6}$$

This expression shows how a cable ferrite can provide a significant attenuation in low-impedance interfaces such as power lines. For example, if Z_A and Z_B are 5 Ω and the cable ferrite provides 100 Ω at a certain frequency, the insertion loss provided is 20.8 dB. However, often it is difficult to known the value of the equivalent impedance of a system, so that, it is generally to consider a value of 150 Ω. In this case, the sum of both system impedances is 300 Ω, thus the effectiveness of the cable ferrite if its impedance is 100 Ω. If the attenuation is calculated for this case through (6), an insertion loss equal to 2.5 dB is obtained.

The cable ferrites analyzed in section IV have been grouped by its L_0 value, considering the initial permeability value. Thereby, it has been taken as a reference core (CR) five sleeve ferrite with the same *OD*/*ID* ratio and with five different *h* values: 10.0, 20.0, 30.0, 40.0 and 50.0 mm (CR_10, CR_20, CR_30, CR_40 and CR_50, respectively). Their performances in terms of magnitude impedance has been measured and are shown in Fig. 3. From this graph it is possible to verify how the *h* is clearly connected to Z_F, since the larger the value of the length, the higher the value of the impedance. These traces show that the maximum value of the impedance of all CR samples is located close to 130 MHz, and from this frequency value, the performance is slowly reduced.

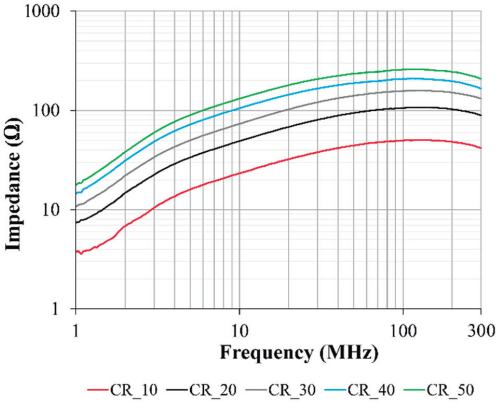

Fig. 3. Comparison between reference cable ferrites mantaining the same *OD*/*ID* ratio and varing their height.

Therefore, Table I summarizes the main features of the CR.

TABLE I. REFERENCE CABLE FERRITES CHARACTERIZED

ID	h (mm)	OD (mm)	ID (mm)	OD/ID (mm)	Volume (cm^3)	L_0 (nH)
CR_50	50.0	19.0	11.5	1.65	8.98	5.02
CR_40	40.0	19.0	11.5	1.65	7.19	4.02
CR_30	30.0	19.0	11.5	1.65	5.39	3.01
CR_20	20.0	19.0	11.5	1.65	3.59	2.01
CR_10	10.0	19.0	11.5	1.65	1.80	1.00

Subsequently, cable ferrites characterized in section IV are summarized in Table II, detailing their main features.

TABLE II. CABLE FERRITES CHARACTERIZED

ID	h (mm)	OD (mm)	ID (mm)	OD/ID (mm)	Volume (cm^3)	L_0 (nH)
C1	50.0	15.9	7.9	2.00	7.40	6.93
C2	45.0	12.0	6.1	1.97	3.77	6.09
C3	28.5	14.0	6.3	2.22	3.50	4.55
C4	28.5	15.5	7.3	2.12	4.18	4.29
C5	28.5	16.0	8.0	2.00	4.30	3.95
C6	28.5	26.0	13.0	2.00	11.35	3.95
C7	15.0	12.0	3.6	3.33	1.54	3.61
C8	28.5	17.5	9.5	1.84	4.83	3.48
C9	25.0	14.2	7.2	1.97	2.94	3.40
C10	25.0	14.0	7.2	1.94	2.83	3.32
C11	28.0	16.0	9.0	1.78	3.85	3.22
C12	28.5	14.0	8.2	1.71	2.88	3.05
C13	28.5	26.0	15.5	1.68	9.75	2.95
C14	18.0	14.1	6.3	2.24	2.25	2.90
C15	18.3	14.0	7.2	1.94	2.07	2.43

IV. RESULTS AND DISCUSSION

The results presented in section, correspond to the analysis of the measured data by comparing sleeve ferrite cores with the same compositions and different dimensions. From the study of the acquired data, the mathematical relation *K* between impedance and air core inductance is evaluated. The main objective is, therefore, verifying that relation to determine the impedance response of a certain core from the *K* relation and its dimensions. Thereby, it will be possible to evaluate different sleeve ferrite core sizes with the aim of determining a balance between performance and core dimensions, weight and cost.

Firstly, the behavior of the sleeve ferrite cores summarized in Table II is studied through classifying them in terms of their L_0. This is carried out with the three largest reference cores defined in Table I (CR_50, CR_40 and CR_30). Fig. 4 shows a comparison between the materials based on the same composition of Ni-Zn that has been produced with different dimensions. In this case, the sleeve cores that provides a similar inductance than CR_50 are C1, C2, C3, C4 and C5. The main features of these cores has been included in Table III. As it can be observed from the graph and Table III, there is a proportional relation between the core inductance and the impedance since those cores with higher L_0 than CR_50 provides traces of impedance higher than this. In terms of inductance, C1 yields 1.91 nH and C2 1.07 nH more than CR_50, resulting in C1 provides 89.7 Ω and C2 49.4 Ω than CR_50 at 100 MHz, respectively. These results evidence that it is not always true that the sleeve ferrite core with higher dimensions is able to provide more attenuation, since CR_50 is 1.21 and 2.38 times larger than C1 and C2, respectively. This difference is caused by the amount of material concentrated per unit of length represented by the *OD/ID* ratio, since CR_50 provides 0.10 nH/mm in terms of height or length of the core, whereas C1 and C2 offer 0.14 nH/mm. From the standpoint of the impedance this leads to CR_50 provides 5.16 Ω/mm, whereas the impedance per unit of height of C1 and C2 is 6.96 Ω/mm and 6.83 Ω/mm. On the other hand, the cores C3, C4 and C5 in spite of having an *OD/ID* ratio larger than CR_50 their inductance and impedance is lower due to they are shorter than this. Despite all that, CR_50 is the only of this set of six sleeve ferrite cores that can be installed on a cable with a dimeter higher than 8.0 mm.

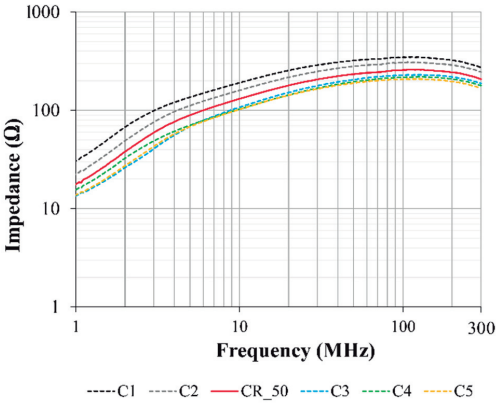

Fig. 4. Comparison between CR_50 reference cable ferrite and other cores with similar inductance by means of their impedance response.

TABLE III. PARAMETERS OF THE CABLE FERRITES SIMILAR TO CR_50

ID	h (mm)	OD/ID (mm)	Vol. (cm^3)	L_0 (nH)	Z_F @100 MHz (Ω)	L_0/h (nH/mm)	Z_F/h (Ω/mm)
C1	50.0	2.00	7.40	6.93	347.9	0.14	6.96
C2	45.0	1.97	3.77	6.09	307.5	0.14	6.83
CR_50	30.0	19.0	5.39	5.02	258.2	0.10	5.16
C3	28.5	2.22	3.50	4.55	228.0	0.16	8.00
C4	28.5	2.12	4.18	4.29	217.4	0.15	7.63
C5	28.5	2.00	4.30	3.95	207.8	0.14	7.29

The sleeve ferrite cores with similar inductance than CR_40 have been grouped in Fig. 5 and Table IV. The sleeve ferrites cores compared in this graph have an inductance closer to the reference core than in Fig. 4. As it can be observed in the graph, this leads to obtain similar impedance traces. CR_40 has almost the same response than C5 and C6 samples due to their inductance is practically the same in spite of CR_40 is significantly larger than the others are. The reason of this similarity in the impedance is due to C5 and C6 have an *OD/ID* ratio higher than CR_40, compensating that difference in the height. This can be also analyzed from the L_0/h and Z_F/h parameters since C5 and C6 show higher values than CR_40. Hence, a designer could select between one of cable ferrites included in Table IV if an EMI suppression at 100 MHz that requires an impedance value about 200 Ω.

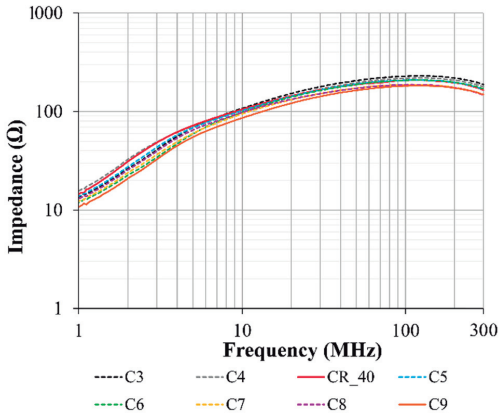

Fig. 5. Comparison between CR_40 reference cable ferrite and other cores with similar inductance by means of their impedance response.

TABLE IV. PARAMETERS OF THE CABLE FERRITES SIMILAR TO CR_40

ID	h (mm)	OD/ID (mm)	Vol. (cm^3)	L_0 (nH)	Z_F @100 MHz (Ω)	L_0/h (nH/ mm)	Z_F/h (Ω/mm)
C3	28.5	2.22	3.50	4.55	228.0	0.16	8.00
C4	28.5	2.12	4.18	4.29	217.4	0.15	7.63
CR_40	40.0	1.65	7.19	4.02	208.0	0.10	5.20
C5	28.5	2.00	4.30	3.95	207.8	0.14	7.29
C6	28.5	2.00	11.35	3.95	207.4	0.14	7.28
C7	15.0	3.33	1.54	3.61	186.9	0.24	12.46
C8	28.5	1.84	4.83	3.48	187.0	0.12	6.56
C9	25.0	1.97	2.94	3.40	181.9	0.14	7.28

Fig. 6 and Table V show the response and the main characterization parameters of those cable ferrites that have a similar inductance value than CR_30. From these set of cores, it is interesting to focus on the parameters that describe the performance of CR_30, C12 and C13 since that have a very similar *OD/ID* ratio and height, but different *OD* and *ID*.

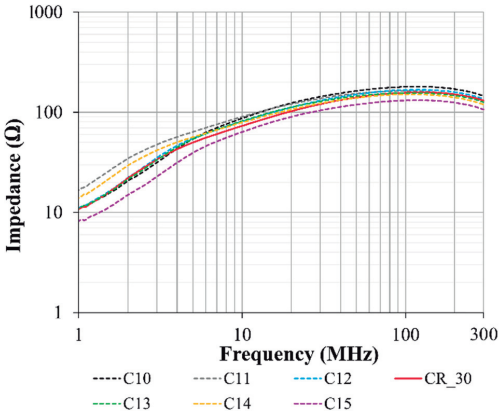

Fig. 6. Comparison between CR_30 reference cable ferrite and other cores with similar inductance by means of their impedance response.

TABLE V. PARAMETERS OF THE CABLE FERRITES SIMILAR TO CR_30

ID	h (mm)	OD/ID (mm)	Vol. (cm^3)	L_0 (nH)	Z_F @100 MHz (Ω)	L_0/h (nH/ mm)	Z_F/h (Ω/mm)
C10	25.0	1.97	2.94	3.32	181.9	0.14	7.28
C11	25.0	1.94	2.83	3.22	179.8	0.13	7.19
C12	28.5	1.71	2.88	3.05	167.1	0.11	5.86
CR_30	30.0	1.65	5.39	3.01	156.9	0.10	523
C13	28.5	1.68	9.75	2.95	156.7	0.10	5.50
C14	18.0	2.24	2.25	2.90	150.8	0.16	8.38
C15	18.3	1.94	2.07	2.43	131.4	0.13	7.18

Thereby, depending on the diameter of the cable that it want be filtered against interferences, it could be possible to select between these three solutions since them provides the same performance.

Subsequently, the *K* parameter that provides information about the impedance per unit of core inductance (Z_F/ L_0) is determined from of three cable ferrites with quite different sizes is shown in Fig. 7. The cable ferrites selected to obtain this parameter are CR_50, C7 and C3. The selection of these different cores in terms of their dimensions makes it possible to evaluate the tolerance of the *K* parameter depending on the features of the original cores. It is important to study this tolerance in order to determine the behavior of a new cable ferrite from the impedance of other original sleeve core of the same material and the dimensions of this new sample. It can be observed that the three traces have a quite similar response, having a difference between them of 28.17 Ω/nH (C7-C3) and 6.44 Ω/nH (C7-CR_50) at 25 MHz. This difference is even lower in the high-frequency region, since it is reduced up to 16.65 Ω/nH (C7-C3) and 3.40 Ω/nH (C7-CR_50) at 100 MHz.

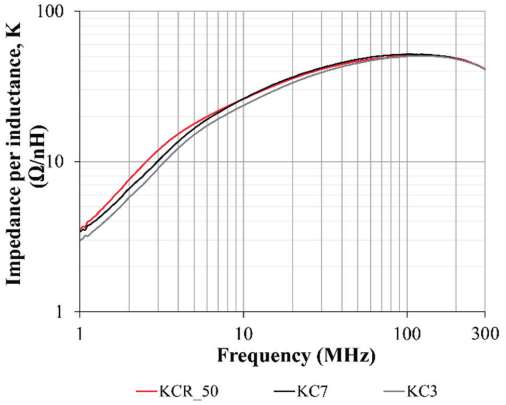

Fig. 7. Impedance per unit of core inductance (Z_F/ L_0) or *K* calculated from three different sleeve ferrite cores: CR_50, C7 and C3.

Therefore, the impedance of CR_20 and CR_10 is calculated by multiplying their inductance by the *K* parameter obtained from CR_50, C7 and C3 cores. Thereby, three theoretical impedance traces are obtained for each of CR_20 and CR_10. Fig. 8 shows a comparison between the measured CR_20 and CR_10 impedance with the calculated from *K* parameter. The results obtained show a significant match between both pair of traces and, thus, it is possible to determine the response of a certain cable ferrite from its dimensions and the impedance of another core based on the same material without having to measure it.

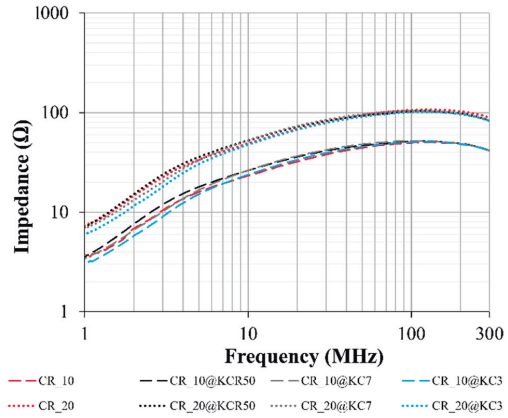

Fig. 8. Comparison between the impedance measured and calculated of the CR_10 and CR_20 cores. The dotted lines correspond to the measured impedance of the CR_10 core (red) and the impedances calculated through *K* parameter obtained from CR_50, C7 and C3. The dashed lines correspons to the measured impedance of the CR_20 core (red) and the impedances calculated through *K* parameter obtained from CR_50, C7 and C3.

V. Conclusions

The analysis of cable ferrites based on the same Ni-Zn composition with different dimensions have been analyzed with the aim of determining the core size dependency in terms of the EMI suppression. Firstly, three cores with the same *OD*/*ID* ratio has been compared to cores with different dimensions that have similar core inductance. Thereby, fifteen cable ferrites has been classified into three different groups and compared to each of three reference cores (CR_50, CR_40 and CR_30 that present a similar inductance. From these three graphs it is concluded that there is a direct relation between the inductance of the core and impedance response. Likewise, the results obtained evidence that it is not always true that the cable ferrite with higher dimensions is able to provide more attenuation. This can be caused when the impedance inductance provided by the amount of material concentrated per unit of length represented by the *OD*/*ID* ratio is more significant than the height.

Subsequently, the *K* parameter that relates the impedance per unit of core inductance (Z_F/ L_0) provided by three cable ferrites with quite different dimensions is obtained. The results obtained show that it is possible to obtain a similar data although the sizes of the core are different. Thereby, it is determined the relation between core inductance, dimensions and impedance as well as the possibility of determining the optimum core size to obtain a certain impedance response. This has been verified by calculating the impedance response of a certain cable ferrite from introducing its dimensions and the *K* parameter of other core based on the same material without having to measure it.

All things considered, the *K* parameter allows a designer to determine the size of a sleeve ferrite core to provide the necessary impedance to attenuate a certain EMI disturbance. Hence, it is possible to optimize the dimensions of the core to select it with the minimum volume, weight and cost.

References

[1] R. Valenzuela, "Novel applications of ferrites, " *Phys. Res. Int.*, vol. 2012, pp.1–9, 2012.

[2] H. W. Ott, *Electromagnetic Compatibility Engineering*. New York, NY, USA: Wiley, 2011, pp. 5–233.

[3] T. Williams, *EMC for Product Designers*. Burlington, MA, USA: Elsevier Science & Technology, 2006, pp. 361–364.

[4] X. C. Tong, "Advanced Materials and Design for Electromagnetic Interference Shielding, " in *Electromagnetic Interference Shielding Fundamentals and Design Guide*. Boca Raton, FL, USA: CRC, 2009, ch.1, pp. 11–20.

[5] N. V. Blaž, M. D. Luković, M. V. Nikolic, O. S. Aleksić and L. D. Živanov, "Heterotube Mn-Zn Ferrite Bundle EMI Suppressor With Different Magnetic Coupling Configurations," in *IEEE Transactions on Magnetics*, vol. 50, no. 8, pp. 1-7, Aug. 2014, doi: 10.1109/TMAG.2014.2310436.

[6] C. Paul, *Introduction to Electromagnetic Compatibility*. Hoboken, NJ, USA: Wiley, 2006, pp. 299–419.

[7] A. Suarez, J. Victoria, P. A. Martinez, A. Alcarria, J. Torres and I. Molina, "Analysis of different Sleeve Ferrite Cores Performance according to their Dimensions," *2019 International Symposium on Electromagnetic Compatibility - EMC EUROPE*, Barcelona, Spain, 2019, pp. 88-93. doi: 10.1109/EMCEurope.2019.8872078

[8] A. Goldman, *Modern Ferrite Technology*. Pittsburgh, PA, USA: Springer, 2006.

[9] A. Suarez, et al. "Characterization of Different Cable Ferrite Materials to Reduce the Electromagnetic Noise in the 2–150 kHz Frequency Range," *Materials*, vol. 11, no. 2, pp. 1–20, 2018.

[10] W. Thierry, S. Thierry, V. Benot, and G. Dominique, "Strong volume reduction of common mode choke for RFI filters with the help of nanocrystalline cores design and experiments," *J. Magnetism Magnetic Mater.*, vol. 304, no. 2, pp. e847–e849, 2006.

[11] K. Kawano, M. Hachiya, Y. Iijima, N. Sato and Y. Mizuno, "The grain size effect on the magnetic properties in NiZn ferrite and the quality factor of the inductor," J. *Magn. Magn. Mater.*, vol. 321, no. 16, pp. 2488–2493, 2009.

[12] A. C. F. M. Costa, E. Tortella, M. Morelli and R. Kiminami, "Synthesis microstructure and magnetic properties of Ni–Zn ferrites," *J. Magn. Magn. Mater.*, vol. 256, no. 1, pp. 174–182, 2003.

[13] C. A. Stergiou and V. Zaspalis, "Analysis of the complex permeability of NiCuZn ferrites up to 1 GHz with regard to Cu content and sintering temperature," *Ceram. Int.*, vol. 40, no. 1, pp. 357–366, 2014.

[14] A. Suarez, et al. "Effectiveness Assessment of a Nanocrystalline Sleeve Ferrite Core Compared with Ceramic Cores for Reducing Conducted EMI," *Electronics*, vol. 8, no. 7, pp. 800–821, 2019.

[15] F. E. Terman, *Radio Engineers Handbook*. New York, NY, USA: McGraw-Hill, 1945.

Chapter 6. FEM SIMULATION MODEL DESIGN TO EVALUATE THE PERFORMANCE OF SOLID AND SPLIT SLEEVE CORES.

This chapter aims to characterize a variation of this cable filtering solution based on openable core clamp or snap ferrites. This component is manufactured by two split parts pressed together by a snap-on mechanism which turns this into an easy to install quick solution for reducing post-cable assembly EMI problems. The results obtained experimentally are corroborated with the results obtained by a finite element method (FEM) simulation model that corroborates the accuracy of the results obtained by the experimental measurement setup.

6.1 Scientific article III

Title: Performance Study of Split Ferrite Cores designed for EMI Suppression on cables.

Authors: Adrian Suarez, Jorge Victoria, Jose Torres, Pedro A. Martinez, Antonio Alcarria, Joaquin Perez, Raimundo Garcia-Olcina, Jesus Soret, Steffen Muetsch, and Alexander Gerfer.

Published in: Electronics (MDPI), vol. 9, no. 12, p. 1992 (2020).
DOI: 10.3390/electronics9121992

Impact factor: 2.412 (2019).

Quartile (category: "Engineering, Electrical & Electronics"): Q2 (2019)

Citations: 1 (accessed on March 2021).

Description: Electronics (ISSN 2079-9292; CODEN: ELECGJ) is an international peer-reviewed open access journal on the science of electronics and its applications published semimonthly online by MDPI. Its JIF percentile is 53.195 with a rank of 125/266 in 2019. The impact factor, quartile, JIF percentile, and rank information have been obtained from

Journal Citation Reports (JCR) database according to the publication year. The citations have been consulted in the Scopus database.

Summary:

One of the main objectives of this contribution is to analyze the dependencies between the gap parameter and the performance in terms of impedance provided by a variation of the sleeve core solution based on an openable core clamp or snap ferrite. This component is manufactured by two split parts pressed together by a snap-on mechanism which turns this into an easy to install quick solution for reducing post-cable assembly EMI problems. The performance of three different materials (NC, MnZn, and NiZn) are analyzed in terms of effectiveness when the solid sleeve cores are split. The possibility of split a NC core implies an innovative technique due to the brittleness of this material. Thus, the results obtained from this research make it possible to evaluate this sample's effectiveness compared to the ceramic ones. This characterization is carried out by introducing different gaps between the different split-cores and analyzing their behavior in terms of relative permeability and impedance. The results obtained experimentally are corroborated with the results obtained by a finite element method simulation model with the aim of determining the performance of each material when it is used as an openable core clamp. Likewise, the stability of three solid (not split) and split sleeve cores are characterized in order to determine the influence of DC currents on the impedance response provided.

The results obtained from this study make it possible to compare the different materials to find out which one is the most efficient, depending on the frequency range. Specifically, the findings obtaining by this contribution are the following:

- When the samples are not split, the analysis carried out in terms of impedance provided by each sample reveals that the sample based on MnZn yields the best performance in the low-frequency region, whereas NC core is most effective in the medium-frequency range, and NiZn sample provides the larger impedance values in the high-frequency region.
- When the samples are split and attached without introducing any gap (*g0* situation), the impedance yielded by the NiZn sample is less degraded than the MnZn and NC impedances. In this study case, MnZn provides the best behavior in the low- and medium-frequency range, whereas the NC sample offers lower performance than expected due to its different internal structure.

- When larger gaps are considered, NiZn shows the most effective solution in terms of permeability and impedance. The effectiveness of MnZn has also been reduced but to a lesser extent than the nanocrystalline sample. In this framework, other manufacturing procedures for NC snap-on cores should be investigated to obtain similar performance to what this solution can offer when it is not split.
- There is an excellent agreement between simulated and experimentally obtained results in NiZn and MnZn traces, whereas there is a significant difference in the NC case. This fact correlates with the conclusions obtained from the effective permeability data of NC in the frequency range studied (1–500 MHz). This is caused because NiZn and MnZn core structures can be considered isotropic, whereas this approach cannot be considered in NC core. When NC sample is split, the internal structure is modified, and it is not possible to estimate the performance of the split sample from the original solid core's magnetic properties.
- The NC simulation model magnetic parameters have been modified to obtain a more realistic approximation response. Thereby, the model has been simulated considering three different situations: not split-core for the original sample, split-core without introducing gap (*g0* situation), and split-core with the intended gap (*g1*, *g2*, and *g3* situations). Consequently, the magnetic parameters of *g0* situation correspond to the effective permeability measured with the split-core with both parts attached. The rest of the gapped cases have been simulated by considering the measured effective permeability of the sample when the gap *g1* is introduced. These new simulated results match significantly with the experimental traces.

Consequently, the experimental and simulated results coincide with the conclusions obtained from effective relative permeability data. NiZn is the material with more stable properties since it can provide higher performance and more predictable behavior than those with greater magnetic properties when the core is split. This conclusion is also applied when DC currents are flowing through the cable to be protected since the NiZn solution shows more excellent stability than the other materials.

electronics

MDPI

Article

Performance Study of Split Ferrite Cores Designed for EMI Suppression on Cables

Adrian Suarez [1,*], Jorge Victoria [1,2], Jose Torres [1], Pedro A. Martinez [1], Antonio Alcarria [2], Joaquin Perez [1], Raimundo Garcia-Olcina [1], Jesus Soret [1], Steffen Muetsch [2] and Alexander Gerfer [2]

[1] Department of Electronic Engineering, University of Valencia, 46100 Burjassot, Spain; jorge.victoria@we-online.de (J.V.); jose.torres@uv.es (J.T.); pedro.a.martinez@uv.es (P.A.M.); joaquin.perez-soler@uv.es (J.P.); raimundo.garcia@uv.es (R.G.-O.); jesus.soret@uv.es (J.S.)

[2] Würth Elektronik eiSos GmbH & Co. KG, 74638 Waldenburg, Germany; antonio.alcarria@we-online.de (A.A.); steffen.muetsch@we-online.de (S.M.); alexander.gerfr@we-online.de (A.G.)

* Correspondence: adrian.suarez@uv.es

Received: 14 October 2020; Accepted: 22 November 2020; Published: 24 November 2020

Abstract: The ideal procedure to start designing an electronic device is to consider the electromagnetic compatibility (EMC) from the beginning. Even so, EMC problems can appear afterward, especially when the designed system is interconnected with external devices. Thereby, electromagnetic interferences (EMIs) could be transmitted to our device from power cables that interconnect it with an external power source or are connected to another system to establish wired communication. The application of an EMI suppressor such as a sleeve core that encircles the cables is a widely used technique to attenuate EM disturbances. This contribution is focused on the characterization of a variation of this cable filtering solution based on openable core clamp or snap ferrites. This component is manufactured by two split parts pressed together by a snap-on mechanism which turns this into a quick, easy to install solution for reducing post-cable assembly EMI problems. The performance of three different materials, including two polycrystalline (MnZn and NiZn) materials and nanocrystalline (NC) solution, are analyzed in terms of effectiveness when the solid sleeve cores are split. The possibility of splitting an NC core implies an innovative technique due to the brittleness of this material. Thus, the results obtained from this research make it possible to evaluate this sample's effectiveness compared to the polycrystalline ones. This characterization is carried out by the introduction of different gaps between the different split-cores and analyzing their behavior in terms of relative permeability and impedance. The results obtained experimentally are corroborated with the results obtained by a finite element method (FEM) simulation model with the aim of determining the performance of each material when it is used as an openable core clamp.

Keywords: electromagnetic interference (EMI) suppressors; sleeve ferrite cores; cable filtering; nanocrystalline (NC); split-core; snap ferrite; gap; DC currents; relative permeability; impedance

1. Introduction

The control of EMI in electronic devices is an increasing issue faced by designers in order to ensure that devices comply with EMC requirements to operate simultaneously without inferring with each other. This fact is due to the trends towards higher component integration, printed circuit board (PCB) size and thickness reduction, and the miniaturization of the device housings. Besides, other factors, such as higher switching frequencies in power converters and communication data rates in

digital circuits, could lead to EMI problems [1,2]. Consequently, EMC engineering should be handled with the system approach, considering EMC throughout the design process to prevent possible EMI problems that could degrade device performance. Therefore, adopting specific solutions as early as possible in the design stage to meet the EMC requirements is of primary importance to reduce penalties from the standpoint of costs, time-to-market, and performance [3,4]. The EMC testing process can reveal that the shielding of a certain cable is needed or may even detect an unexpected EMI source when the designed device is connected to external modules, such as a power supply or to another device to communicate with it. When the cables represent the EMI source, that implies failing the conducted or radiated emissions test, and a widely used technique is applying an EMI suppressor such as a cable ferrite [4].

A cable ferrite's effectiveness to reduce EMI in cables is defined by its capability to increase the flux density of a specific field strength created around a conductor. The presence of noise current in a conductor generates an undesired magnetic field around it that can result in EMI problems. When a cable ferrite is applied in the conductor, the magnetic field is concentrated into magnetic flux inside the cable ferrite because it provides a higher magnetic permeability than air. As a result, the flowing noise current in the conductor is reduced and, thus, the EMI is attenuated. Currents that flow in cables (with two or more conductors) can be divided into differential mode (DM) and common mode (CM) depending on the directions of propagation. Although DM currents are usually significantly higher than CM currents, one of the most common radiated EMI problems is originated by CM currents flowing through the cables of the system [5]. CM currents, despite not having a high value, have a much greater interfering potential. This fact is because only a few microamps are required to flow through a cable to fail radiated emission requirements [4]. The use of a cable ferrite is an efficient solution to filter the CM currents in cables because, if a pair of adjacent conductors is considered, when the cable ferrite is placed over both signal and ground wires, the CM noise is reduced. As shown in Figure 1, the CM currents in both wires flow in the same direction, so the two magnetic fluxes in the cable ferrite are added together, and the filtering action occurs. The intended (DM) current is not affected by the presence of the cable ferrite because the DM current travels in opposite directions and it is transmitted through the signal and returns. Thus, the currents of the two conductors are opposing, meaning they cancel out and the cable ferrite has no effect [6]. This ability to attenuate only the undesirable CM disturbances is a very interesting feature of this kind of component [7–9].

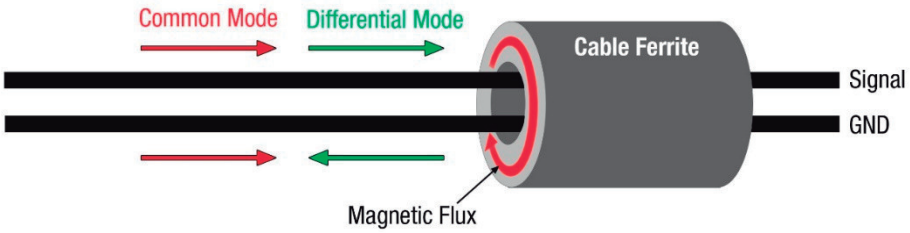

Figure 1. Diagram of common mode (CM) and differential mode (DM) currents passing through a cable ferrite with two adjacent conductors (signal and return paths).

This component represents a solution when the cables turn into an EMI source. It can be applied to peripheral and communication cables such as multiconductor USB or video cables to prevent interferences that could be propagated along the wire, affecting the devices that are interconnected [10,11]. This component is also widely used to reduce high-frequency oscillations caused by the increasingly fast switching in power inverters and converters with cables attached without scarifying the switching speed and increasing the power loss. Therefore, selecting the proper cable ferrite makes it possible to reduce the switching noise by increasing the propagation path impedance in the desired frequency range [5].

The application of cable ferrites is a widely used technique to reduce EMI in cables, despite the drawbacks that the integration of an extra component can involve in terms of cost and production of the system [12]. Nevertheless, these drawbacks are usually compensated by the effectiveness of cable ferrites to filter interferences without having to redesign the electronic circuit [6,7]. Manufacturers provide a wide range of ferrite cores with different shapes, dimensions and compositions, but the most widely used solutions applied to cables are the sleeve (or tube) ferrite cores or their split variation, the openable core clamp (or snap ferrites) [13]. This component is manufactured from two split parts pressed together by a snap-on mechanism, turning this into a quick, easy to install solution for reducing post-cable assembly EMI problems. The main advantage of snap ferrites compared to solid sleeve ferrite cores is the possibility to add them to the final design, without manufacturing a specific cable that includes the sleeve ferrite core before assembling its connectors.

Nevertheless, the halved ferrite's performance will be lower than that of a solid core with the same composition and dimensions in terms of the relative permeability (μr) and hence the impedance introduced in the cable [14]. This performance degradation is caused by the gap introduced between the split parts. Additionally, the presence of a defined air gap between the split parts can turn into an advantage from the standpoint of the core saturation because it allows for higher DC currents before saturation is reached as compared to solid cores. For applications such as power supplies or motor drivers, high DC currents flow through the cable, and the performance of the cable ferrite can be degraded [8]. Therefore, in these situations, it is interesting to halve the cable ferrite with the aim of introducing a controlled gap that reduces the influence of DC currents into it [15,16].

The materials selected to carry out the characterization in terms of cable ferrite performance considering gap and stability to DC currents are two ceramic cores based on MnZn and NiZn and a third core of nanocrystalline (NC) structure. One of the main advantages of MnZn and NiZn materials is the possibility of creating cores with many different shapes and the possibility of halving them without modifying their internal structure [17,18]. Preliminary studies have shown that NC sleeve ferrite cores provide a significant effectiveness when used as an EMI suppressor [17,19,20]. Nevertheless, the internal structure and manufacturing process have traditionally made it complicated to obtain a split-core sample that can be used as a snap ferrite, keeping its effectiveness. Therefore, a prototype of a split-core of an NC sample has been manufactured based on a new cutting and assembling technique that makes it possible to analyze this material's performance when it is halved.

Consequently, one of the main objectives of this contribution is to analyze the dependencies between the gap parameter and the performance in terms of impedance provided by the snap ferrite. This analysis is performed through an experimental measurement setup that is compared with the results obtained through a finite element method (FEM) simulation model. The simulation model helps to determine the study's accuracy, specifically in the high-frequency range where parasitic elements may affect the experimental results [20]. Likewise, the stability of three solid (not split) and split cable ferrites based on different compositions are characterized in order to determine the influence of DC currents on the impedance response provided. The results obtained from this study make it possible to compare the different materials to find out which one is the most efficient, depending on the frequency range.

Thereby, the three different materials and their structures are described in Section 2 through the main magnetic parameters, such as the relative permeability and the reluctance caused by introducing a gap. Section 3 defines the measurement setups employed to perform the experimental results and the designed FEM simulation model description. Subsequently, in Section 4, the three different samples' performance under test is shown in terms of impedance versus frequency. The dependencies on the air gap introduced in the split-cores and the influence on the injection of DC currents are discussed. Finally, the main conclusions are summarized in Section 5 to determine the performance of each material when used as an openable core clamp.

2. Magnetic Properties

The magnetically soft ferrites are widely used for manufacturing EMI suppressors as cable ferrites. Conventionally, the most used ferrite cores for filtering applications are based on ceramic materials (also known as polycrystalline materials) and, although they do not belong to the metals group, they are made from metal oxides such as ferrite, nickel and zinc. MnZn and NiZn represent two extensively used solutions due to their heat resistance, hardness, and high resistance to pressure. An advantage of ceramic materials is the possibility of manufacturing components with many different shapes and dimensions. The remarkable fact about the ceramic ferrites is that they combine extremely high electrical resistivity with reasonably good magnetic properties [21]. The starting material is iron oxide Fe_2O_3 that is mixed with one or more divalent transition metals, such as manganese, zinc, nickel, cobalt or magnesium [14]. The manufacturing procedure can be divided into these steps. First, the base materials are weighed into the desired proportions and wet mixed in ball mills to obtain a uniform distribution and particle size. Next, the water is removed in a filter press, and the ferrite is loosely pressed into blocks and dried. It is then pre-fired (calcined) at about 1000 °C to form the ferrite. The pre-sintered material is then milled to obtain a specific particle size. Subsequently, the dry powder is mixed with an organic binder and lubricants before being shaped by a pressing technique to obtain the final form. Finally, the resultant green core is subjected to a heating and cooling cycle, reaching temperatures higher than 1150 °C, promoting any unreacted oxides to be formed into ferrite. The manufacturing procedure and the material mix are essential to define a ceramic core's magnetic properties. With MnZn materials, it is possible to obtain samples that provide initial permeabilities of the order of 1000–20,000 and provide a low resistivity (0.1–100 Ω·m). Their range of frequency for EMI suppression applications covers from hundreds of kHz to some MHz.

Regarding NiZn materials, these provide initial permeabilities of the order of 100–2000, so they are intended for a higher frequency operation than MnZn, covering from tens of MHz up to several hundreds of MHz. In terms of resistivity, NiZn materials reach high values (about 10^4–10^6 Ω·m) [15,21,22]. Therefore, considering the structure of ceramic cores, they can be considered as isotropic.

The structure and manufacturing technique used for ceramics make it possible to produce split-cores or cut a solid core after its production with water-cooled diamond tools to build snap ferrites [14]. The NC cores' manufacturing procedure is quite different from the one used for ceramic production since they are formed by a continuous laminar structure that is wound to form the final core. The tape-wound structure is based on an amorphous ribbon of only 7–25 micrometers in thickness. It is generated by melting the base material by heating it at 1300 °C and depositing it on a high-speed cooling wheel (100 km/h) that reduces the temperature of the material to 20 °C at a rate of 10^6 K/s. After that, the rolled material is exposed to an annealing process, usually under a transversal and longitudinal magnetic field. This treatment affects the magnetic properties, resulting in ultrafine crystals with a size of the order of 7–20 nm. Finally, an epoxy coating or an additional protective case is needed to protect the sample, due to the brittle nature of the tape. Depending on the parameters selected during the manufacturing procedure, NC samples can provide initial permeability values in the range of 15,000 to 150,000. Electrical resistivity is relatively high even if it is considered a metallic material, generally over 10^{-6} Ω·m [14,15,17,23]. The NC material structure presents the advantage of designing smaller components with more significant magnetic properties for EMI suppression [19,20,24–27]. Figure 2 shows the NC core before adding the protective coating and its manufacturing procedure diagram.

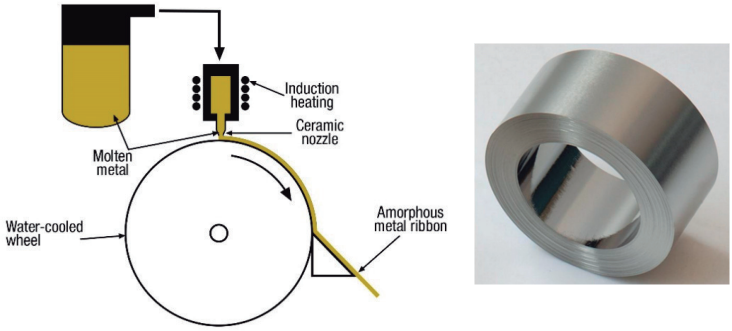

Figure 2. Nanocrystalline manufacturing procedure diagram and nanocrystalline (NC) final core sample without the protective coating.

Ceramic and NC samples can be manufactured as sleeve cores but have a different internal structure. From the point of view of the flux, it travels only in the rolling direction of the amorphous ribbon in the NC core. In ceramics, the flux is distributed uniformly because the material is a single homogeneous unit [21]. This different structure will result in a different behavior when the core is split into two parts for use as a snap ferrite. In ceramic cores, a performance reduction in terms of relative permeability when they are split is expected. However, we could anticipate that in the case of the NC structure, this decrease would be significant. This fact could be considered because when the NC sample is halved, the wound core is cut, limiting the flux path. Thereby, the halved faces have been plated in order to connect both halved parts with the aim of reducing the gap of the resultant snap core. Table 1 and Figure 3 show the dimensions of the samples used to develop characterization. Note that the split samples have the same dimensions as the solid cores.

Table 1. List of cable ferrite samples used in this research.

Magnetic Material	Outer Diameter (OD) (mm)	Inner Diameter (ID) (mm)	Height (H) (mm)	Thickness (mm)
NC	19.2	11.7	25.4	7.5
MnZn	18.6	10.2	25.2	8.4
NiZn	18.6	10.2	25.1	8.4

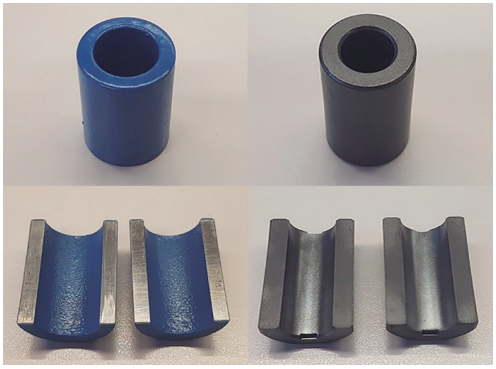

Figure 3. Non-split NC and split-core sample (**left**) and non-split ceramic and split-core sample (**right**).

The solid and split-cores' behavior based on the three different materials is analyzed in this section through the relative permeability. The permeability of magnetic materials generally depends on the magnetic flux density, DC bias currents, temperature, frequency, and intrinsic material properties [15,17]. When an air gap is included in a closed magnetic circuit, the circuit's total permeability is called the effective relative permeability μ_e and this is lower than the permeability of the original solid core without the presence of the air gap. In terms of EMI suppression, reducing the relative permeability in a cable ferrite is generally related to the decrease in its ability to attenuate interferences. However, the presence of an air gap is sometimes desired to increase the DC bias capability of the core or to reduce the permeability to achieve a more predictable and stable response with the aim of shifting the resonance frequency (f_r) to higher values to reduce the effects of dimensional effects [28,29].

When the two parts of the split-core are joined, a certain air gap remains between them that results in a magnetic reluctance (R) increase, since the gap represents an opposition to the magnetic flux (Φ) normal flow [15,30]. As shown in Figure 4, this effect is analogous to adding a series resistor in an electronic circuit to reduce the magnitude of the current. In Figure 4, R_c represents the reluctance of the core, R_g the reluctance of the gap, Φ the magnetic flux that flows through the magnetic path length of the core (l_c), l_g the length of the air gap, i the current that flows through the conductor and N the number of turns.

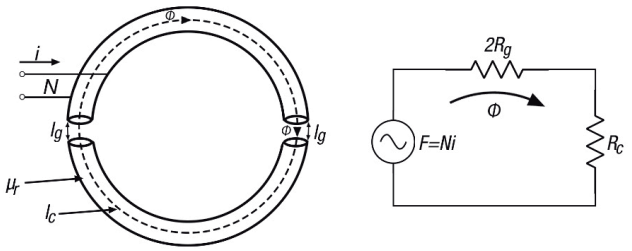

Figure 4. Split-core with air gaps: (**a**) Magnetic flux distribution diagram and (**b**) the magnetic circuit of a split-core with two air gaps.

The general expression to obtain the magnetic reluctance is given by [15]:

$$R = \frac{l}{\mu_r \mu_0 A} \, [H^{-1}] \tag{1}$$

where l corresponds to the magnetic path length and A to the cross-sectional area. The l and A parameters are obtained from the dimensional features of the sample, considering a toroid with a rectangular cross-section:

$$l = \pi \left(\frac{OD}{2} + \frac{ID}{2} \right) [m] \tag{2}$$

$$A = H \left(\frac{OD}{2} - \frac{ID}{2} \right) [m] \tag{3}$$

where H is the core's height and OD and ID are the outer and inner diameter, respectively. The overall reluctance of the split-core considering the air gap can be calculated from (1) as the sum of the reluctance core (R_c) and reluctance air gap (R_g) [13,15]:

$$R = R_c + 2R_g = \frac{l_c - l_g}{\mu_r \mu_0 A} + \frac{2l_g}{\mu_0 A} \, [H^{-1}] \tag{4}$$

thereby, the air gap factor (F_g) is

$$F_g = \frac{R}{R_c} = \frac{R_c + 2R_g}{R_c} = 1 + \frac{2R_g}{R_c} = 1 + \frac{\mu_r 2l_g}{l_c} \quad (5)$$

and the effective relative permeability of a core with an air gap is [14,15,31]:

$$\mu_e = \frac{\mu_r}{1 + \frac{\mu_r 2l_g}{l_c}} = \frac{\mu_r}{F_g}. \quad (6)$$

Equation (6) represents the most common and simplified model to approximate the effective permeability caused by an air gap since it underestimates the value of μ_e because it does not consider the effect of the fringing flux across the air gap [32]. In the case of toroid cores, to estimate the influence of the air gap introduced when the core is split into two parts, l_g is usually considered to be twice the spacer thickness [15,32]. In order to characterize the reduction of the relative permeability caused by an air gap, the three solid (not split) cores of Table 1 are compared with three split-cores of the same material and dimensions but introducing four different gaps. Thereby, five study cases are carried out for each core material:

1. Non-split-core: core without a gap.
2. Split-core *g*0: both parts of the core are joined without fixing a gap value. In order to differentiate this case with the non-split-core, a gap value of 0.01 mm is considered.
3. Split-core *g*1: both parts of the core are joined by fixing a gap value of 0.07 mm.
4. Split-core *g*2: both parts of the core are joined by fixing a gap value of 0.14 mm.
5. Split-core *g*3: both parts of the core are joined by fixing a gap value of 0.21 mm.

Figure 5 shows the experimental relative permeability measured for each of the three cores included in Table 1, considering the five different cases in terms of the gap introduced. The experimental traces (solid traces) are compared with the effective relative permeability calculated (dotted traces) by using Equation (6), considering the four gaps defined above. This parameter has been calculated from the experimental relative permeability of the non-split-core sample. These data are expressed through a vector formed by 801 frequency points with their corresponding permeability values. The effective relative permeability of a core with a specific gap is determined by computing these values point by point. Thereby, the air gap factor value F_g changes throughout the frequency range analyzed. It is possible to observe that both NiZn and MnZn graphs show a similar response between calculated and experimental results. There is a significant match in the low-frequency region, particularly in the NiZn samples, since they provide a lower and more stable permeability than MnZn cores. In the high-frequency region, the calculated effective relative permeability is lower than the experimentally measured one, verifying that Equation (6) provides an underestimation of this. Another difference between NiZn and MnZn traces is observed by comparing the *g*0 traces because the initial permeability decreases mostly in MnZn because the original non-split-core yields a higher initial permeability than the NiZn sample. The estimation of *g*0 traces was obtained by fixing a gap of 0.01 mm between both split parts in order to simulate the real snap ferrite's behavior, and the estimated values match with the experimental data [13]. The NC graph shows a different behavior than the ceramic core since the experimental and calculated permeability only matches in the low-frequency region. Therefore, unlike ceramic cores, it is not possible to estimate with Equation (6) the effective relative permeability of NC in the middle and high-frequency region when used as a snap ferrite due to its different internal structure.

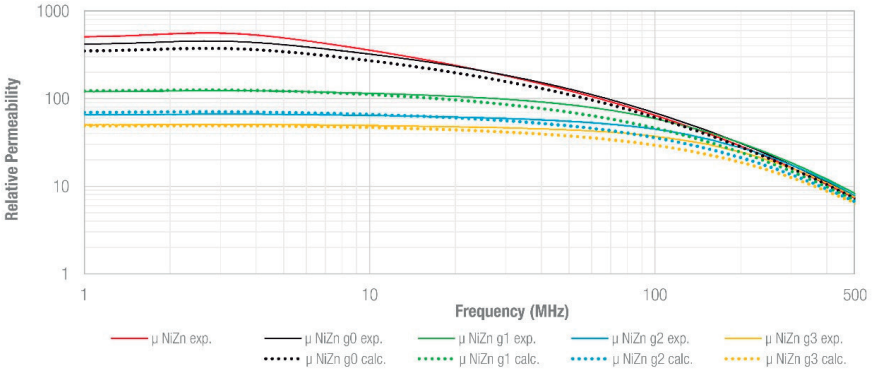

(**a**)

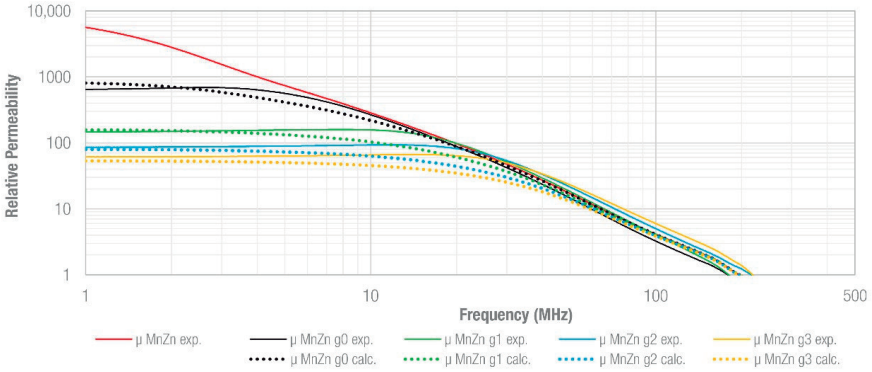

(**b**)

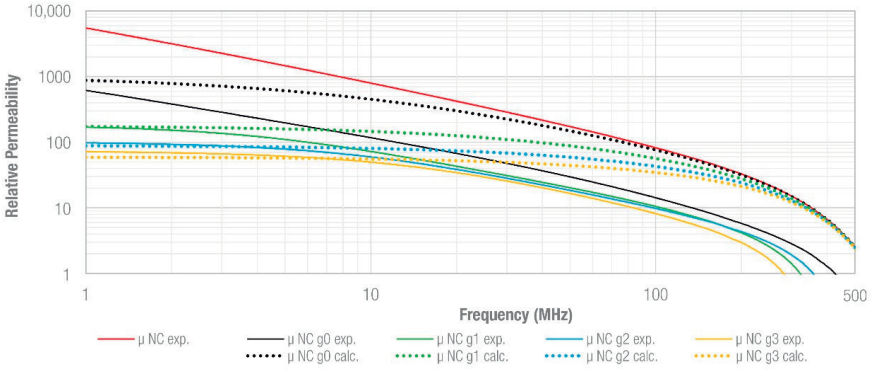

(**c**)

Figure 5. Comparison between experimental (solid traces) and estimated (dotted traces) effective permeability considering different gaps for NiZn, MnZn and NC samples: (**a**) NiZn non-split (red trace) and split cases; (**b**) MnZn non-split (red trace) and split cases and (**c**) NC non-split (red trace) and split cases.

3. Characterization Setups

EMI suppressors, such as cable ferrites, are usually classified by the impedance that they can introduce in a specific frequency range when they embrace a conductor. This parameter represents the magnitude of the impedance that can be represented from a series equivalent circuit mainly based on a resistive and inductive component [13,20]. The resistive component is connected to the imaginary part of the relative permeability representing the core's losses, whereas the real part of the permeability is related to the inductive component [22]. Therefore, there is a direct relationship between the core material's magnetic behavior and its performance in terms of impedance. Other factors that contribute to defining the impedance provided by a cable ferrite are the dimensions and the shape [19].

3.1. *Impedance Measurement Setup*

The experimental magnitude of the impedance of each sample is obtained by using the E4991A RF Impedance/Material Analyzer (Keysight, Santa Rosa, CA, USA) connected to the Terminal Adapter 16201A (Keysight, Santa Rosa, CA, USA). This adapter makes it possible to introduce into the measurement setup the 16200B External DC Bias (Keysight, Santa Rosa, CA, USA) that allows for supplying a bias current through the cable ferrite of up to 5 A using a 7 mm port and an external DC current source. Finally, the cable ferrite is connected by means of the Spring Clip Fixture 16092A (Keysight, Santa Rosa, CA, USA) that is connected to the 16200B test fixture [33]. After it is properly calibrated, this measurement setup is able to characterize cable ferrites from 1 MHz to 500 MHz since the E4991A equipment can operate from 1 MHz and the 16200B test fixture up to 500 MHz. Figure 6 shows the described experimental measurement setup.

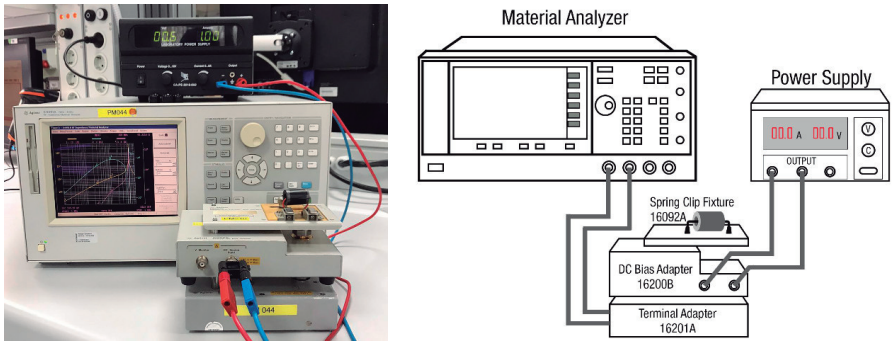

(**a**) (**b**)

Figure 6. Impedance measurement setup with the DC bias test fixture connected: (**a**) Photograph of the measurement setup and (**b**) diagram blocks of the measurement setup.

This setup provides the experimental impedance of the split and non-split-cores, analyzing them when there is no presence of DC currents and increasing this parameter up to 5 A. The results obtained can be compared to analyze the behavior of each of the three materials characterized in this contribution in terms of the gap introduced in the core and the value of bias current injected.

3.2. *Simulation Model*

The different split and non-split cable ferrites' performance and the relationship between the impedance provided and the air gap introduced are specifically examined through an electromagnetic analysis simulator (Ansys Electronics Desktop). The proposed simulation model is shown in Figure 7. It is formed by a copper conductor that crosses a cylindrical core defined by the material properties of each of the materials described in Section 2. The conductor is connected to two

ports (input and output) referenced to a perfect electrical plane located at a certain distance under it. This simulation setup represents a transmission line based on a parallel line (or single wire) considering a single wire over a ground plane that allows for designing a system with a characteristic impedance of $Z_0 = 150\ \Omega$. This parameter is fixed by selecting the distance from the plane to the center of the conductor H = 15 mm, the diameter of the conductor d = 4.9 mm and considering that it is surrounded by air [34–36]. By setting the ports' impedance to 150 Ω, it is possible to extract the cable ferrite's impedance under test without the characterization system influencing the results obtained. This value is a reference value adopted in different EMC standards to characterize and calibrate devices such as common mode absorption devices (CMADs) intended for measuring EMI disturbances in cables [11]. These fixtures are characterized using the through-reflect-line (TRL) calibration method based on measuring the S-parameters of CMADs, as described in CISPR 16-1-4 [11]. Therefore, this simulation model provides a reference system that can extract the impedance introduced in the conductor by the cable ferrite. The procedure performed to emulate the different studied gap cases ($g0$, $g1$, $g2$ and $g3$) is based on a parametric gap sweep. This technique makes it possible to determine the sleeve core's impedance when it is split into two parts and a specific gap is introduced. It is expected that this simulation model is able to provide the performance of the split samples from the original relative permeability (the values obtained for the non-split-core sample) by fixing the gaps described in Section 2. In the $g0$ case, the 0.01 mm distance value was introduced to differentiate it from the original non-split core.

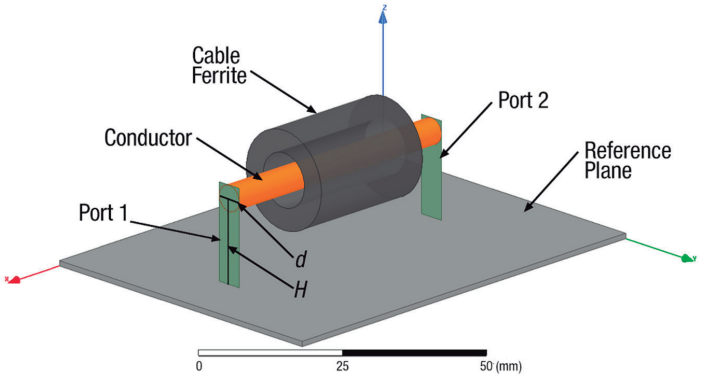

Figure 7. Cable ferrite simulation model.

4. Results and Discussion

This section focuses on analyzing the EMI suppression performance of the three described materials when they are split to be employed as snap ferrites. The results obtained from the experimental measurement setup and those provided by the simulation model are compared through each materials' impedance. This comparison is carried out to verify that the experimental results are not influenced by elements such as stability of the calibration setup in the high-frequency region and undesired high-frequency resonances caused by parasitic elements that could reduce the accuracy of the measurement. As is shown in Figure 8, the results are organized in three graphs, one per material: NiZn (a), MnZn (b) and NC (c)). These graphs represent the experimental (solid traces) and computed (dotted traces) impedance provided by the cable ferrite, considering the non-split situation and the split cases where the core is separated into two parts.

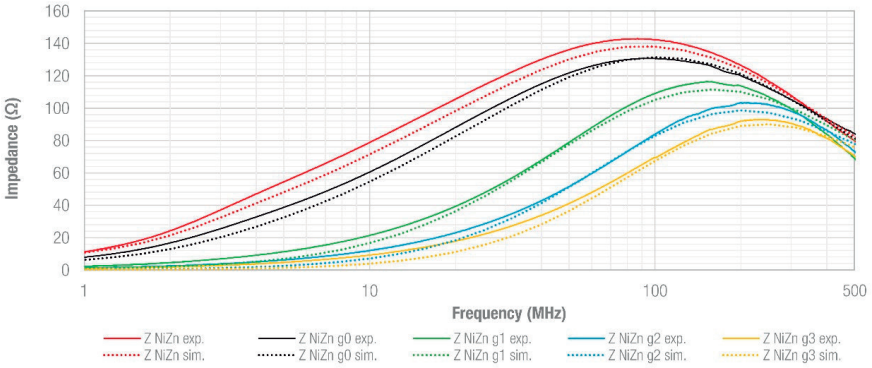

(**a**)

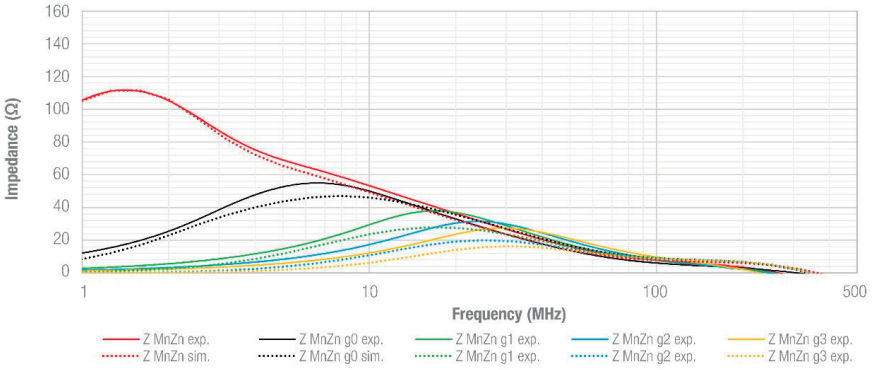

(**b**)

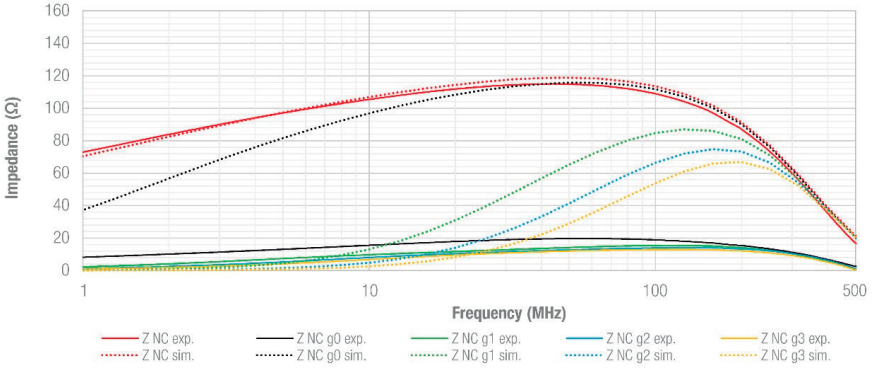

(**c**)

Figure 8. Comparison between experimental (solid traces) and simulated (dotted traces) impedance considering different gaps (non-split and split with gaps *g*0, *g*1, *g*2 and *g*3) for NiZn, MnZn and NC cable ferrites: (**a**) NiZn non-split (red trace) and split cases; (**b**) MnZn non-split (red trace) and split cases and (**c**) NC non-split (red trace) and split cases.

From the results obtained, the red traces of the graphs show the impedance provided by each non-split sample and it is possible to verify that the simulated and experimental results are a good

match and, consequently, the data derived from the experimental setup can be considered in the whole frequency range analyzed. Consequently, a parametric gap sweep was performed in the simulation model by setting the four defined gap situations ($g0$, $g1$, $g2$ and $g3$) and keeping the same magnetic properties introduced to the non-split model. As can be observed, there is an excellent agreement between simulated and experimentally obtained results in NiZn and MnZn traces, whereas there is a significant difference in the NC case. This fact correlates with the conclusions obtained from the effective permeability data of the NC sample, shown in Section 2. Therefore, it is not possible to determine the NC sample's behavior when it is split and gapped by considering the non-split sample's magnetic properties. This is because the cut section's metallization is not able to maintain the high performance of the original NC sample. Then, the NC experimental results are considered to compare its performance with that provided by NiZn and MnZn samples.

Based on the results of three materials, halving the cable ferrite and using it as a snap ferrite ($g0$ situation) results in a shift of the resonance frequency at which the sample is able to provide the maximum attenuation ratio at the same time that the impedance is reduced. From the standpoint of the equivalent inductance and resistance series circuit of the sleeve core, the f_r is produced when the inductive component (X_L) turns into negative values and the resistive part (R) reaches the maximum value. Above this frequency value, the sleeve core's performance is degraded by the parasitic capacitive effect. Therefore, the f_r to higher frequencies shift results in extending the frequency range in which the sleeve core is effective to reduce EMI. This effect is lower for the NiZn cable ferrite since the f_r is increased from 86.7 MHz to 92.3 MHz, providing 142.9 Ω and 130.7 Ω, respectively. It represents a reduction of 8.5% in terms of impedance and an increase in the resonance frequency of f_r = 5.6%. Regarding the results obtained when a gap is introduced, an impedance of Z = 116.3 Ω (34.9% reduction) at f_r = 152.2 MHz for the $g1$ case, Z = 103.3 Ω (27.7% reduction) at f_r = 199.0 MHz for the $g2$ case and Z = 93.0 Ω (27.7% reduction) at f_r = 240.6 MHz for the $g3$ case. In the case of MnZn, it is possible to observe that the impedance traces are significantly modified when the sample is split since the original sample provides a maximum value of Z = 111.7 Ω at f_r = 1.4 MHz. The split-core with one part attached to the other ($g0$ case) provides Z = 55.0 Ω at f_r = 6.6 MHz, so the performance of the cable ferrite is reduced by about 50.8%. It is a relevant performance reduction compared to the attenuation ratio reduction of the NiZn sample. For the rest of the MnZn study cases where a higher gap is introduced ($g1$, $g2$ and $g3$), the impedance is mostly reduced (66.1%, 58.0% and 75.6%, respectively), compared to the NiZn results. Regarding the NC results, as described above, the simulated results obtained for the non-split sample match significantly with the experimental ones. Nevertheless, when the core is split, the simulated results overestimate the experimental data since the maximum impedance provided by the not split sample corresponds to 115.0 Ω, whose f_r = 45.5 MHz, whereas when it is split with both parts attached as closely as possible, the impedance is reduced by about 82.9%. When a specific gap is introduced ($g1$, $g2$ and $g3$ cases), the attenuation ratio produced is 86–89%.

The NC simulation model magnetic parameters were modified with the objective of obtaining a more realistic approximation response. Thereby, the model was simulated considering three different situations: non-split-core for the original sample, split-core without introducing a gap ($g0$) and split-core with the intended gap ($g1$, $g2$ and $g3$). Consequently, the magnetic parameters of the $g0$ situation correspond to the effective permeability measured with the split-core with both parts attached. The rest of gapped cases ($g1$, $g2$ and $g3$) were simulated by considering the measured effective permeability of the sample when the gap $g1$ is introduced. Figure 9 shows that the new simulated results match significantly with the experimental traces.

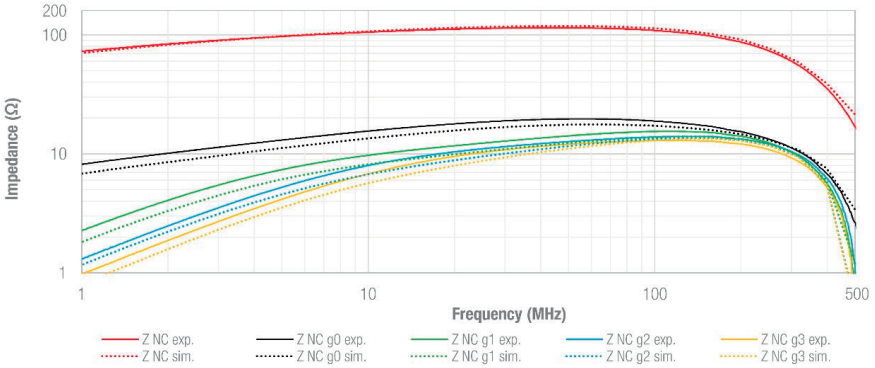

Figure 9. Comparison between experimental (solid traces) and new simulated (dotted traces) impedance, considering different gaps (non-split and split with gaps *g*0, *g*1, *g*2 and *g*3) for NC cable ferrites.

The comparison of the three different cable ferrites by separating them depending on the gap introduced is shown in Figure 10. As can be observed in Figure 10a, when cores are not split, they can be divided into three frequency ranges based on their performance. As expected, MnZn provides the larger impedance value in the low-frequency region, yielding the best performance up to 2.9 MHz. The NiZn cable ferrite offers higher impedance than MnZn and NC samples above 23.4 MHz, representing the most effective solution to reduce EMI disturbances in the high-frequency region. The NC core offers excellent performance in the medium-frequency region, providing a great impedance throughout the frequency band from 2.9 MHz to 23.4 MHz.

Additionally, the non-split NC core is able to yield a more stable response up to its maximum impedance value and it shows a better performance than ceramic cores to reduce EMI disturbances when they are distributed in a wideband frequency range (from the low-frequency region up to about 100 MHz). Figure 10b shows the impedance comparison when the cores are split into two parts and attached as closely as possible, emulating a snap ferrite's function. In this case, NC has significantly reduced its performance and MnZn provides the best performance up to 8.4 MHz. From this frequency value, NiZn yields the highest impedance value. In the rest of the analyzed gaps (*g*1, *g*2 and *g*3), the NiZn sample mainly represents the most interesting solution because MnZn and NC cable ferrites offer a lower impedance response. Thus, when a significant gap is introduced, the material with lower permeability is able to yield the best EMI attenuation.

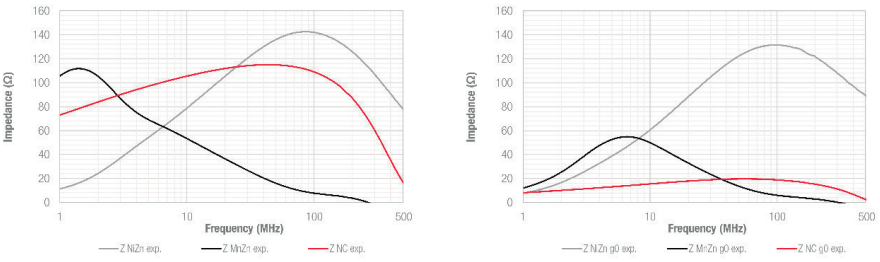

(**a**) (**b**)

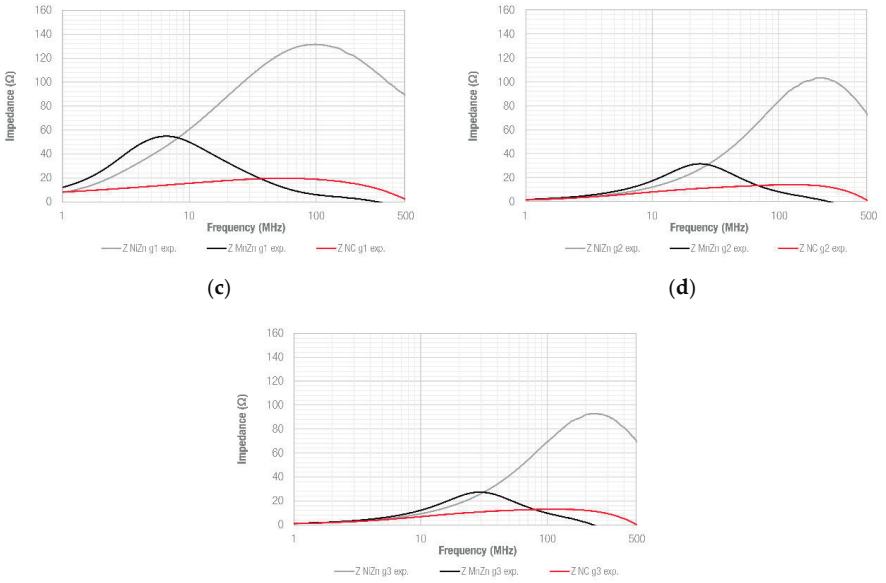

Figure 10. Comparison between the measured impedance of NiZn, MnZn and NC cable ferrites, considering five different gap cases: (**a**) NiZn, MnZn and NC non-split-cores; (**b**) NiZn, MnZn and NC $g0$ split-cores; (**c**) NiZn, MnZn and NC $g1$ split-cores; (**d**) NiZn, MnZn and NC $g2$ split-cores and (**e**) NiZn, MnZn and NC $g3$ split-cores.

How splitting a cable ferrite into two parts, to be employed as a snap ferrite, modifies the impedance behavior was analyzed. Depending on the core's magnetic properties and structure, this involves a certain degradation of the EMI suppression ability. Nevertheless, splitting a cable ferrite could result in an advantage if the component is intended to encircle cables where DC currents are flowing. To further investigate this effect of the DC currents on the impedance, Figure 11 shows the impedance response of each of the three different materials studied when they are under DC bias conditions. Each material is represented in a separate graph and the response of the non-split sample is shown when different values of DC currents are injected (0 A, 0.5 A, 1 A, 2 A and 5 A), as described in Section 3. Figure 11a shows that the five traces have a similar trend, but the higher the DC current value, the lower the sample's impedance. This effect is observed from the lowest DC current value (0.5 A) and does not modify the impedance response significantly when compared to MnZn and NC results (Figure 11b,c, respectively). It is interesting how the resonance frequency is moved to higher frequencies when an increasing DC current is injected into the MnZn sample, specifically in the cases of 2 A and 5 A. As regards NC behavior, it shows a significant impedance decrease in the low-frequency region and its performance is reduced more than that of ceramic cores when a DC bias flows through the cable.

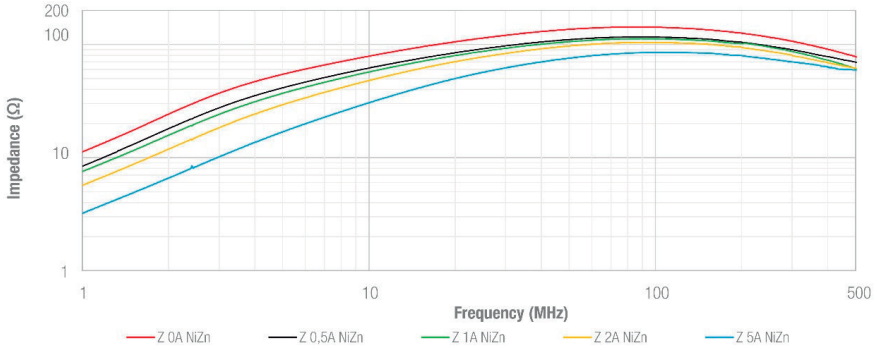

(**a**)

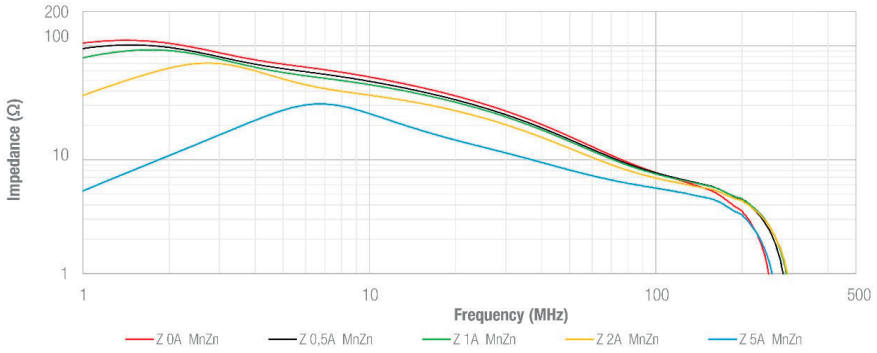

(**b**)

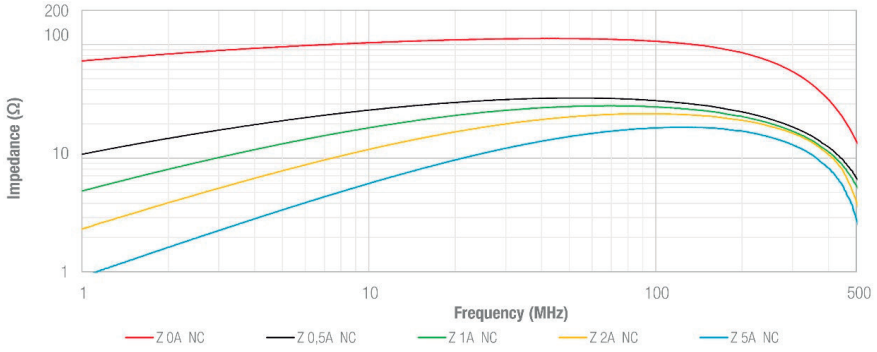

(**c**)

Figure 11. Impedance analysis considering different values of DC currents for the three different non-split samples: (**a**) NiZn; (**b**) MnZn and (**c**) NC.

The same analysis is repeated in Figure 12 for different gap values introduced in each of the samples. Thereby, the first row corresponds to the split NiZn samples, the second to the split MnZn samples and the third to the split NC samples. The left column shows the behavior of each material when the $g0$ gap is considered, and the right column shows the results obtained when $g1$ (dotted traces), $g2$ (short dashed traces) and $g3$ (long dashed traces) gaps are introduced. When the effect on the impedance response of splitting the samples to be attached without an intended gap is observed,

the $g0$ traces show quite similar behavior in the three materials. NC traces have the same behavior over most of the frequency range, whereas NiZn traces show the same match between traces except for the 5 A case. In the case of MnZn, there is a difference between traces in the low-frequency region, producing a shift of the resonance frequency when DC currents higher than 0.5 A are applied. When the rest of the gaps are analyzed, the three materials have the same response when DC currents up to 5 A are injected. Moreover, from a certain frequency value, the materials' traces match independently of the DC current value and gap introduced.

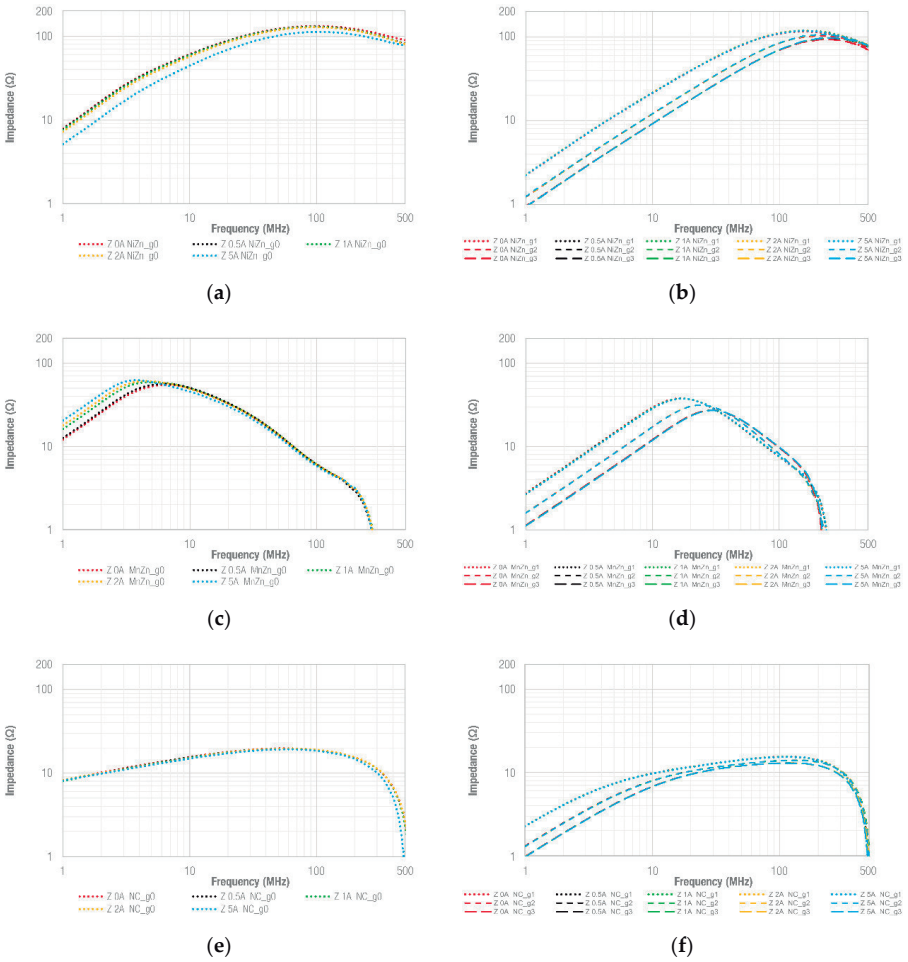

Figure 12. Impedance analysis considering different values of DC currents and gap conditions for the split samples: (**a**) NiZn $g0$ case; (**b**) NiZn $g1$, $g2$ and $g3$ cases; (**c**) MnZn $g0$ case; (**d**) MnZn $g1$, $g2$ and $g3$ cases; (**e**) NC $g0$ case and (**f**) NC $g1$, $g2$ and $g3$ cases.

5. Conclusions

The performance of the three different materials to build up ferrite cores was evaluated when they are split in order to determine their EMI suppression ability to be used as an openable core clamp. When the samples are not split, the analysis carried out in terms of impedance provided by each sample reveals that a ferrite core based on MnZn yields the best performance in the low-

frequency region, whereas an NC core is most effective in the medium-frequency range and the NiZn sample provides larger impedance values in the high-frequency region.

When the samples are split and attached without introducing any gap ($g0$ situation), the impedance yielded by the NiZn sample is less degraded than the MnZn and NC impedances. In this study case, MnZn provides the best behavior in the low- and medium-frequency range, whereas the NC sample offers lower performance than expected due to its different internal structure. When larger gaps are considered, NiZn shows the most effective solution in terms of impedance. In this framework, other manufacturing procedures for NC snap-on cores should be investigated to obtain similar performance to what this solution can offer when it is not split.

The results obtained from the transmission line simulation model verify that the experimental results are in agreement and, thus, the data derived from the experimental measurement setup can be considered as an accurate approach in the frequency range studied (1–500 MHz). Consequently, the experimental and simulated results coincide with the conclusions obtained from effective relative permeability data. The material with more stable properties can provide higher performance and more predictable behavior than those with greater magnetic properties when the core is split. This conclusion is also applied when DC currents are flowing through the cable to be shielded since the NiZn solution shows better stability than the other materials.

Author Contributions: Conceptualization, A.S., J.V. and J.T.; Formal analysis, A.S., P.A.M., R.G.-O. and J.S.; Investigation, A.S., J.V., J.T., P.A.M. and A.A.; Methodology, A.S., P.A.M. and A.A.; Project administration, J.V., J.T., J.S., S.M. and A.G.; Supervision, J.V., J.T., J.S. and S.M.; Writing—original draft, A.S., J.T., P.A.M., J.P. and R.G.-O.; Writing—review and editing, J.V., J.T., P.A.M., A.A., J.P., R.G.-O., J.S., S.M. and A.G. All authors have read and agreed to the published version of the manuscript.

Funding: The APC was funded by the Universitat de València.

Acknowledgments: This work was supported by the Catedra Würth-EMC, a research collaboration agreement between the University of Valencia and Würth Elektronik eiSos GmbH & Co. KG.

Conflicts of Interest: The authors declare no conflict of interest. The founding sponsors had no role in the design of the study; in the collection, analyses, or interpretation of data; in the writing of the manuscript, and in the decision to publish the results.

References

1. González-Vizuete, P.; Domínguez-Palacios, C.; Bernal-Méndez, J.; Martín-Prats, M.A. Simple Setup for Measuring the Response to Differential Mode Noise of Common Mode Chokes. *Electronics* **2020**, *9*, 381, doi:10.3390/electronics9030381.
2. Kim, J.; Rotaru, M.D.; Baek, S.; Park, J.; Iyer, M.K.; Kim, J. Analysis of noise coupling from a power distribution network to signal traces in high-speed multilayer printed circuit boards. *IEEE Trans. Electromagn. Compat.* **2006**, *48*, 319–330, doi:10.1109/TEMC.2006.873865.
3. Crovetti, P.S.; Musolino, F. Interference of Spread-Spectrum EMI and Digital Data Links under Narrowband Resonant Coupling. *Electronics* **2020**, *9*, 60, doi:10.3390/electronics9010060.
4. Ott, H.W. *Electromagnetic Compatibility Engineering*; John Wiley & Sons: Hoboken, NJ, USA, 2009.
5. Yao, J.; Li, Y.; Zhao, H.; Wang, S. Design of CM Inductor Based on Core Loss for Radiated EMI Reduction in Power Converters. In Proceedings of the 2019 IEEE Applied Power Electronics Conference and Exposition (APEC), Anaheim, CA, USA, 17–21 March 2019; pp. 2673–2680, doi:10.1109/APEC.2019.8721972.
6. Kraftmakher, Y. Experiments on ferrimagnetism. *Eur. J. Phys.* **2012**, *34*, 213.
7. Williams, T. *EMC for Product Designers*; Elsevier Science & Technology: Burlington, MA, USA, 2006; pp. 361–364, doi:10.1088/0143-0807/34/2/213.
8. Goldman, A. *Modern Ferrite Technology*, 2nd ed.; Springer: Pittsburgh, PA, USA, 2006.
9. Bondarenko, N.; Shao, P.; Orlando, A.; Koledintseva, M.Y.; Beetner, D.G.; Berger, P. Prediction of common-mode current reduction using ferrites in systems with cable harnesses. In Proceedings of the 2012 IEEE International Symposium on Electromagnetic Compatibility, Pittsburgh, PA, USA, 6–10 August 2012; pp. 80–84, doi:10.1109/ISEMC.2012.6351807.
10. Paul, C.R. *Introduction to Electromagnetic Compatibility*, 2nd ed.; Wiley Interscience: Hoboken, NJ, USA, 2006.

11. Urabe, J.; Fujii, K.; Dowaki, Y.; Jito, Y.; Matsumoto, Y.; Sugiura, A. A Method for Measuring the Characteristics of an EMI Suppression Ferrite Core. *IEEE Trans. Electromagn. Compat.* **2006**, *48*, 774–780, doi:10.1109/TEMC.2006.884507.
12. Tong, X.C. *Advanced Materials for Electromagnetic Interference Shielding*, 1st ed.; CRC Press: Boca Raton, FL, USA, 2009.
13. Orlando, A.; Koledintseva, M.Y.; Beetner, D.G.; Shao, P.; Berger, P. A lumped-element circuit model of ferrite chokes. In Proceedings of the 2010 IEEE International Symposium on Electromagnetic Compatibility, Fort Lauderdale, FL, USA, 25–30 July 2010; pp. 754–759, doi:10.1109/ISEMC.2010.5711373.
14. Van den Bossche, A.; Valchev, V.C. *Inductors and Transformers for Power Electronics*; CRC Press: Boca Raton, FL, USA, 2005.
15. Kazimierczuk, M.K. *High-Frequency Magnetic Components*; John Wiley & Sons: Hoboken, NJ, USA, 2009.
16. Weinschrott, A. New measurement method for high frequency cable mounted ferrites. In Proceedings of the 2005 International Symposium on Electromagnetic Compatibility, Chicago, IL, USA, 8–12 August 2005; pp. 312–314, doi:10.1109/ISEMC.2005.1513530.
17. Suarez, A.; Victoria, J.; Alcarria, A.; Torres, J.; Martinez, P.A.; Martos, J.; Soret, J.; Garcia-Olcina, R.; Muetsch, S. Characterization of Different Cable Ferrite Materials to Reduce the Electromagnetic Noise in the 2–150 kHz Frequency Range. *Materials* **2018**, *11*, 174, doi:10.3390/ma11020174.
18. Damnjanovi, M.; Stojanovi, G.; Živanov, L.; Desnica, V. Comparison of different structures of ferrite EMI suppressors. *Microelectron. Int.* **2006**, *23*, 42–48, doi:10.1108/13565360610680758.
19. Suarez, A.; Victoria, J.; Martinez, P.A.; Alcarria, A.; Torres, J.; Molina, I. Analysis of different Sleeve Ferrite Cores Performance according to their Dimensions. In Proceedings of the 2019 International Symposium on Electromagnetic Compatibility-EMC EUROPE, Barcelona, Spain, 2–6 September 2019; pp. 88–93, doi:10.1109/EMCEurope.2019.8872078.
20. Suarez, A.; Victoria, J.; Torres, J.; Martinez, P.A.; Alcarria, A.; Martos, J.; Garcia-Olcina, R.; Soret, J.; Muetsch, S.; Gerfer, A. Effectiveness Assessment of a Nanocrystalline Sleeve Ferrite Core Compared with Ceramic Cores for Reducing Conducted EMI. *Electronics* **2019**, *8*, 800, doi:10.3390/electronics8070800.
21. Cullity, B.D.; Graham, C.D. *Introduction to Magnetic Materials*; Wiley: Hoboken, NJ, USA, 2009.
22. Kącki, M.; Rylko, M.S.; Hayes, J.G.; Sullivan, C.R. Magnetic material selection for EMI filters. In Proceedings of the 2017 IEEE Energy Conversion Congress and Exposition (ECCE), Cincinnati, OH, USA, 1–5 October 2017; pp. 2350–2356, doi:10.1109/ECCE.2017.8096456.
23. Cuellar, C. HF Characterization and Modeling of Magnetic Materials for the Passive Components Used in EMI Filters. Ph.D. Thesis, University of Lille, Lille, France, 2013.
24. Sixdenier, F.; Morand, J.; Salvado, A.; Bergogne, D. Statistical study of nanocrystalline alloy cut cores from two different manufacturers. *IEEE Trans. Magn.* **2014**, *50*, 1–4, doi:10.1109/TMAG.2013.2285274.
25. Brander, T.; Gerfer, A.; Rall, B.; Zenkner, H. *Trilogy of Magnetics: Design Guide for EMI Filter Design, SMP & RF Circuits*, 4th ed.; Swiridoff Verlag: Künzelsau, Germany, 2010.
26. Roc'h, A.; Leferink, F. Nanocrystalline core material for high-performance common mode inductors. *IEEE Trans. Electromagn. Compat.* **2012**, *54*, 785–791, doi:10.1109/TEMC.2012.2188103.
27. Thierry, W.; Thierry, S.; Benoît, V.; Dominique, G. Strong volume reduction of common mode choke for RFI filters with the help of nanocrystalline cores design and experiments. *J. Magn. Magn. Mater.* **2006**, *304*, 847–849, doi:10.1016/j.jmmm.2006.03.014.
28. Brockman, F.G.; Dowling, P.H.; Steneck, W.G. Dimensional effects resulting from a high dielectric constant found in a ferromagnetic ferrite. *Phys. Rev.* **1950**, *77*, 85–93, doi:10.1103/PhysRev.77.85.
29. Ponomarenko, N. Study of Frequency and Microstructure Dependencies of Magnetic Losses of Ferrite Materials and Components. Ph.D. Thesis, Riga Technical University, Riga, Latvia, 2014.
30. Fiorillo, F. *Measurement and Characterization of Magnetic Materials*; Elsevier: Amsterdam, The Netherlands, 2004.
31. Bhuiyan, R.H.; Dougal, R.A.; Ali, M. A miniature energy harvesting device for wireless sensors in electric power system. *IEEE Sens. J.* **2010**, *10*, 1249–1258, doi:10.1109/JSEN.2010.2040173.
32. McLyman, C.W.T. *Transformer and Inductor Design Handbook*; Dekker: New York, NY, USA, 1988.
33. Keysight 16200B External DC Bias Adapter Operation and Service Manual. Available online: http://literature.cdn.keysight.com/litweb/pdf/16200B.pdf (accessed on 28 September 2020).
34. Chang, K. *Handbook of Microwave and Optical Components, Fiber and Electro-Optical Components*; Wiley: Hoboken, NJ, USA, 1991.

35. International Telephone, & Telegraph Corporation. *Reference Data for Radio Engineers*; Howard W. Sams and Company: Indianapolis, Indiana, 1968.
36. Haase, H.; Nitsch, J.; Steinmetz, T. Transmission-line super theory: A new approach to an effective calculation of electromagnetic interactions. *URSI Radio Sci. Bull.* **2003**, 307, 33–60, doi:10.23919/URSIRSB.2003.7909507.

Chapter 7. Conclusions and future work

This final chapter presents the general and specific conclusions drawn from this doctoral thesis. In addition, this chapter identifies possible lines of future work that could be derived from this Ph.D. study.

7.1 Conclusions

The nanocrystalline material has been studied, analyzed and evaluated in this Ph.D. thesis proving to be an interesting alternative to conventional ceramic materials, traditionally used to manufacture EMI suppression components. Additionally, this Ph.D. study gives a thorough characterization of a sleeve core EMI suppressor through different experimental measurement setups and a simulation model that makes it possible to determine its performance from the standpoint of the magnetic properties, impedance provided, and insertion loss when it is introduced in a certain system.

The first stage of the research has been focused on the characterization of the novel nanocrystalline material to reduce EMI problems (supraharmonics) in the 2–150 kHz frequency range. These electromagnetic disturbances are generated by modern systems based on active switching converters that are generally integrated into power conversion and supply applications. Thereby, new materials that can provide significant EMI suppression had to be studied to ensure electromagnetic compatibility in the 2–150 kHz frequency band. This is a critical frequency spectral due to interferences generated by a wide range of devices and, specifically, communication problems in the new technologies and devices incorporated into the traditional grid to convert it into a Smart Grid.

This research is carried out from the point of view of the manufacturing process, magnetic properties and EMI suppression ability. This last item is carried out through two analysis procedures: a theoretical method by determining the attenuation ratio from the impedance parameter, and proposing a new experimental technique based on directly measuring the insertion loss parameter introduced by each sample under test. Thus, it is possible to determine the nanocrystalline's performance compared to conventional cable ferrite compositions to reduce the interferences in this controversial frequency range. The

results presented in this contribution demonstrate the suitability of the novel sleeve core based on nanocrystalline composition in the 2–150 kHz frequency range compared with MnZn or NiZn materials. The research carried out on nanocrystalline material's performance to reduce supraharmonics showed that this material could offer significant effectiveness at frequencies higher than those studied could. Consequently, it was decided to continue the research line related to the study of the novel NC sleeve core performance to reduce EMI at higher frequencies. Chapter 3 and Chapter 4 focus on the study of characterization methodologies for sleeve core EMI suppressors, extending the frequency region analyzed from 2 kHz up to 200 MHz. The following conclusions can be drawn from these chapters:

- NC sleeve core shows excellent stability of the initial permeability compared to MnZn and NiZn. NC initial permeability remains at values higher than 80%, up to about 150 °C.

- From the hysteresis curve measurement, it is observed that the NC sleeve core provides the higher magnetic saturation of the three analyzed materials.

- The limitations of the measurement impedance setup are described and characterized. It is necessary to consider the wire introduced into the sleeve core in the calibration procedure in order to avoid the influence of its impedance in the total impedance provided by the equipment.

- EMI suppression is determined through two analysis procedures: a theoretical method by determining the attenuation ratio from the impedance parameter and proposing a new experimental technique based on directly measuring the insertion loss parameter introduced by each sample under test.

- Two experimental measurement setups to determine the insertion loss introduce by each sleeve core under test are presented. These techniques generate controlled EMI into a load with a stable impedance through a characterized cable over the frequency range studied (2–150 kHz and 0.1–200 MHz) to determine the insertion loss.

- The insertion loss provided by the sleeve cores under test is significantly low in systems with a total impedance close to 1000 Ω, even when the NC sample is introduced.

- When the EMI disturbances are located specifically in the low-region MnZn represents an effective solution, whereas if these are located from 50 MHz, a NiZn may be used. Nonetheless, if the EMI interferences are distributed outside of these regions or from the low-frequency region up to about 100 MHz, the NC sleeve core shows a better performance than ceramics to reduce EMI emissions in a wideband frequency range.

After the positive results of the novel NC material and the measurement setups developed, the research efforts associated with this Ph.D. work were oriented towards studying the performance of different sleeve cores with respect to their dimensions. As described in Chapter 5, the dimensional parameter that defines a sleeve core was first analyzed. Subsequently, it is determined the *K* parameter that allows a designer to obtain the size of a sleeve core to provide the necessary impedance to attenuate a certain EMI disturbance. Hence, it is possible to optimize the dimensions of the component to select it with the minimum volume, weight, and cost. From the results presented in this chapter, we have reached the following conclusions:

- Five ceramic materials with different initial permeabilities from 380 up to 5000 have been compared with the novel NC (μ_i = 90000) core by representing their impedance traces. The results presented show that, considering samples with the exactly same dimensions, NC provides the higher impedance throughout the frequency range of 1-500 MHz.

- It is observed an impedance difference between sleeve cores with the same volume and composition that demonstrates that only the volume information is not enough to select a core, since a core with low volume can provide a greater performance.

- It is possible to find cores with the same material composition that yield the same impedance response but having different volumes. This approach can lead to select, besides the core material with the best performance to attenuate EMI in a specific frequency, the sleeve core that provides the maximum impedance with the minimum volume.

- It is interesting to select the maximum *OD*/*ID* ratio and height at the same time that the *ID* is as tight as possible to the cable diameter to maximize the impedance of a sleeve core. The impedance is proportional to the natural logarithm of the outer to inner diameter ratio and directly proportional to the height. Even though *h* is directly proportional to the impedance, the natural logarithm provides an attenuation factor when the *ID* is lower than 2.7 times the *OD*, so that it is important not selecting thin cores.

- *K* parameter relates the impedance per unit of core inductance (Z_{SC}/L_0), making it possible to calculate the impedance of a new sample based on the same material and geometry from the new core dimensions. It is carried out by multiplying *K* by the air core inductance (L_0) of the new sleeve core. This principle has been validated by calculating the impedance of new cores with different dimensions from the calculated *K* parameter obtained by a first core. This theoretical impedance of the new cores is compared with the experimentally obtained, and a significant match between both data is obtained.

Finally, in **Chapter 6**, the conclusions obtained from the last contributions were validated through a FEM simulation model. The simulation model makes it possible to determine the insertion loss and the impedance response provided by a sleeve core defined by its magnetic properties and dimensions. In addition, it is studied the dependencies between the gap parameter and the performance in terms of impedance provided by openable core clamps (snap ferrites) based on the three materials evaluated in this Ph.D. study (NC, MnZn, and NiZn). Thereby, the performance of these sleeve core components is analyzed in terms of effectiveness when the solid sleeve cores are split. The possibility of split a NC core implies an innovative technique due to the brittleness of this material. Thus, the results obtained from this research make it possible to evaluate this sample's effectiveness compared to the ceramic ones. Thereby, the main findings of this chapter are summarized in the following conclusions:

- There is an excellent agreement between simulated and experimentally obtained results in NiZn and MnZn traces, whereas there is a significant difference in the NC case. This is caused because NiZn and MnZn core structures can be considered isotropic, whereas this approach cannot be considered in NC core. When NC sample is split, the internal structure is modified and it is not possible to estimate the performance of the split sample from the original solid core's magnetic properties.
- The NC simulation model magnetic parameters have been modified to obtain a more realistic approximation response. Thereby, the model has been simulated considering three different situations: not split-core for the original sample, split-core without introducing gap (*g0* situation), and split-core with the intended gap (*g1*, *g2*, and *g3* situations). These new simulated results match significantly with the experimental traces
- When the samples are split and attached without introducing any gap (*g0* situation), the impedance yielded by the NiZn sample is less degraded than the MnZn and NC impedances. In this study case, MnZn provides the best behavior in

the low- and medium-frequency range, whereas the NC sample offers lower performance than expected due to its different internal structure.

- When larger gaps are considered, NiZn shows the most effective solution in terms of permeability and impedance. The effectiveness of MnZn has also been reduced but to a lesser extent than the nanocrystalline sample
- NiZn is the material with more stable properties that can provide higher performance and more predictable behavior than those with more significant magnetic properties when the core is split. This conclusion is also applied when DC currents are flowing through the cable to be protected.

The conclusions drawn from this Ph.D. study highlight the suitability and significant performance of sleeve core based on nanocrystalline material to reduce EMI problems in cables in a wide frequency region. This is one of the reasons why the company Würth Elektronik started to commercialize a range of nanocrystalline sleeve core EMI suppressors at the end of the last year. This new range of products has been designated as WE-AENA Axial EMI Suppression Nanocrystalline, offering nine toroidal and sleeve cores with different dimensions.

7.2 Future work

This doctoral thesis has presented advances in finding a new material to manufacture more effective and innovative sleeve core EMI suppressors. Thereby, the nanocrystalline material has been studied, analyzed, evaluated, and compared to conventional ceramic materials, traditionally used to manufacture EMI suppression components. Nevertheless, the nanocrystalline material has a margin for improvements, and the limits in terms of the frequency range of the measurement setups described may be increased.

- Improvements on the nanocrystalline snap-on core. In Chapter 6, it has been analyzed the performance of a novel prototype of NC split cores, but the results presented show that its performance compared to the provided in solid cores is significantly reduced. Other manufacturing procedures for obtaining NC snap-on cores should be investigated to obtain similar performance to what this solution can offer when it is not split.
- Measurement of the nanocrystalline magnetic parameters with a coaxial airline method. In order to obtain relative permeability and permittivity data for frequencies higher than 500 MHz, it is necessary to use an alternative method characterization method. One of the most accuracy methods to measure sleeve samples up to several gigahertz is the transmission line system based on a sample holder connected to a network analyzer that is able to extract these magnetic parameters from the S-parameters measured. The sample holder employed to analyze the

material under test limits the dimensions of the sample to *OD* = 7.00 mm and *ID* = 3.04 mm. It is currently complicated to manufacture a NC sample with these dimensions, but it could be interesting to obtain the permeability and permittivity of this material in a higher frequency range to introduce them into the simulation model.

- Improvements on the measurement setups to obtain impedance and insertion loss results up to at least 1 GHz. It could be interesting to adapt the current measurement method to obtain the insertion loss parameter presented in **Chapter 4** with the aim of obtaining results up to 1 GHz. From the insertion loss data, it could be possible to obtain the impedance without measuring it, as demonstrated in this Ph.D. study. If the insertion loss of a sleeve core in this high-frequency region is determined, it might be evaluated its performance to attenuate EMI in the radiated emission frequency range.

REFERENCES

1. González-Vizuete, P.; Domínguez-Palacios, C.; Bernal-Méndez, J.; Martín-Prats, M.A. Simple Setup for Measuring the Response to Differential Mode Noise of Common Mode Chokes. *Electronics* **2020**, *9*, 381. doi:10.3390/electronics9030381.
2. Valenzuela, R. Novel Applications of Ferrites. *Phys. Res. Int.* **2012**, *2012*, pp. 1–9. doi:10.1155/2012/591839.
3. Balcells, J.; Daura, F.; Esparza, R.; Pallás, R. *Interferencias electromagnéticas en sistemas electrónicos*. Marcombo: Barcelona, Spain, 1992.
4. Crovetti, P.S.; Musolino, F. Interference of Spread-Spectrum EMI and Digital Data Links under Narrowband Resonant Coupling. *Electronics* **2020**, *9*, 60. doi:10.3390/electronics9010060.
5. Ott, H.W. *Electromagnetic Compatibility Engineering*; John Wiley & Sons: Hoboken, NJ, USA, 2009.
6. Suarez, A.; Victoria, J.; Alcarria, A.; Torres, J. Characterization of electromagnetic noise suppression sheet for aerospace applications. In Proceedings of the ESA Workshop on Aerospace EMC, Valencia, Spain, 23–25 May 2016; pp. 1–6.
7. Victoria, J.; Suarez, A.; Torres, J.; Martinez, P.A.; Alcarria, A.; Martos, J.; Garcia-Olcina, R.; Soret, J.; Muetsch, S.; Gerfer, A. Transmission Attenuation Power Ratio Analysis of Flexible Electromagnetic Absorber Sheets Combined with a Metal Layer. *Materials* **2018**, *11*, 1612. doi:10.3390/ma11091612.
8. Yao, J.; Li, Y.; Zhao, H.; Wang, S. Design of CM Inductor Based on Core Loss for Radiated EMI Reduction in Power Converters, Proceedings of the 2019 IEEE Applied Power Electronics Conference and Exposition (APEC), Anaheim, CA, USA, 2019; IEEE; pp. 2673–2680. doi:10.1109/APEC.2019.8721972.
9. Bondarenko, N.; Shao, P.; Orlando, A.; Koledintseva, M. Y.; Beetner, D. G.; Berger, P. Prediction of common-mode current reduction using ferrites in systems with cable harnesses, Proceedings of the 2012 IEEE International Symposium on Electromagnetic Compatibility, Pittsburgh, PA, USA, 2012; IEEE; pp. 80–84. doi:10.1109/ISEMC.2012.6351807.
10. Kraftmakher, Y. Experiments on ferrimagnetism. *European Journal of Physics* **2012**, 34, 213.

11. Chiu, H.J.; Pan, T.F.; Yao, C.J.; Lo, Y.K. Automatic EMI measurement and filter design system for telecom power supplies. *IEEE Trans. Instrum. Meas.* **2007**, 56. doi:10.1109/TIM.2007.907948.

12. Williams, T. *EMC for Product Designers*; Elsevier Science & Technology: Burlington, MA, USA, 2006, pp. 361–364. doi:10.1088/0143-0807/34/2/213.

13. Van den Bossche, A.; Valchev, V.C. *Inductors and Transformers for Power Electronics*; CRC Press: Boca Raton, FL, USA, 2005.

14. Cullity, B.D.; Graham, C.D. *Introduction to Magnetic Materials*; Wiley: Hoboken, NJ, USA, 2009.

15. Shaikh, S.F.; Ubaidullah, M; Mane, R.S.; Al-Enizi, A.M. Types, Synthesis methods and applications of ferrites. In *Spinel Ferrite Nanostructures for Energy Storage Devices*; Mane, R.S.; Vijaykumar, V.J. Elsevier Science & Technology: Burlington, VT, USA, 2020.

16. Kazimierczuk, M.K. *High-Frequency Magnetic Components*; John Wiley & Sons: Hoboken, NJ, USA, 2009.

17. Vaid, K.; Chaurasia, A.; Rathore, D.; Singhal, R.; Dwivedi, U.K. Study of dielectric and electromagnetic shielding behaviour of BaTiO3-CoFe2O4 filled LDPE composite. *Polymer Composites*. 2020. doi: 10.1002/pc.25867.

18. Kącki, M.; Rylko, M.S.; Hayes, J.G.; Sullivan, C.R. Magnetic material selection for EMI filters. Proceedings of the 2017 IEEE Energy Conversion Congress and Exposition (ECCE), Cincinnati, OH, USA, 2017; IEEE; pp. 2350–2356. doi:10.1109/ECCE.2017.8096456.

19. Thierry, W.; Thierry, S.; Benoît, V.; Dominique, G. Strong volume reduction of common mode choke for RFI filters with the help of nanocrystalline cores design and experiments. *J. Magn. Magn. Mater.* **2006**, *304*, 847–849. doi:10.1016/j.jmmm.2006.03.014.

20. Herzer, G. Modern soft magnets: Amorphous and nanocrystalline materials. *Acta Mater.* **2013**, *61*, 718–734.

21. Liu, Y.; Han, Y.; Liu, S.; Lin, F. Pulse Magnetic Properties Measurement and Characterization of Fe-Based Nanocrystalline Cores for High-Voltage Pulse Magnetics Applications. *IEEE Trans. Power Electron.* **2015**, *30*, 6883–6896. doi:10.1109/TPEL.2014.2386916.

22. Naishadham, K. Closed-Form Design Formulas for the Equivalent Circuit Characterization of Ferrite Inductors. *IEEE Trans. Electromagn. Compat.* **2011**, *53*, 923–932. doi:10.1109/TEMC.2011.2116795.

23. Sixdenier, F.; Morand, J.; Salvado, A.; Bergogne, D. Statistical study of nanocrystalline alloy cut cores from two different manufacturers. *IEEE Trans. Magn.* **2014**, *50*. doi:10.1109/TMAG.2013.2285274.

24. Roc'h, A.; Leferink, F. Nanocrystalline core material for high-performance common mode inductors. *IEEE Transactions on Electromagnetic Compatibility* **2012**, *54*, 785–791. doi:10.1109/TEMC.2012.2188103.

25. Cuellar, C.; Tan, W.; Margueron, X.; Benabou, A.; Idir, N. Measurement method of the complex magnetic permeability of ferrites in high frequency. In Proceedings of the Instrumentation and Measurement Technology Conference (I2MTC), Graz, Austria, 13–16 May 2012; pp. 63–68.

26. Sharma, A.; Rahman, N.; Obol, M.; Afsar, M. Precise characterization and design of composite absorbers for wideband microwave applications. In Proceedings of European Microwave Conference, Paris, France, 28–30 September 2010; pp. 160–163.

27. Goldman, A. *Modern ferrite technology*, 2nd ed.; Springer Science & Business Media: Pittsburgh, PA, USA, 2006.

28. Hu, P.; Yang, H.B.; Pan, D.A.; Wang, H.; Tian, J.J.; Zhang, S.; Wang, X.; Volinsky, A.A. Heat treatment effects on microstructure and magnetic properties of Mn-Zn ferrite powders. *J. Magn. Magn. Mater.* **2010**, *322*, 173–177. doi:10.1016/j.jmmm.2009.09.002.

29. Beatrice, C.; Bottauscio, O.; Chiampi, M.; Fiorillo, F.; Manzin, A. Magnetic loss analysis in Mn-Zn ferrite cores. *J. Magn. Magn. Mater.* **2006**, *304*, e743–e745. doi:10.1016/j.jmmm.2006.02.209.

30. Sun, G.L.; Li, J.B.; Sun, J.J.; Yang, X.Z. The influences of Zn^{2+} and some rare-earth ions on the magnetic properties of nickel-zinc ferrites. *J. Magn. Magn. Mater.* **2004**, *281*, 173–177,doi:10.1016/j.jmmm.2004.04.099.

31. Costa, A.C.F.M.; Tortella, E.; Morelli, M.R.; Kiminami, R.H.G.A. Synthesis, microstructure and magnetic properties of Ni-Zn ferrites. *J. Magn. Magn. Mater.* **2003**, *256*, 174–182. doi:10.1016/S0304-8853(02)00449-3.

32. Snelling, E.C. *Soft Ferrites, Properties and Applications*, 2nd ed.; Butterworth: Boston, MA, USA, 1988.

33. Reeve, W.D.; Hagen, T. Applying and Measuring Ferrite Beads: Part I Ferrite Bead Properties and Test Fixtures. Available online: http://www.reeve.com/Documents/Articles%20Papers/Ferrite%20Beads/Reeve-Hagen_FerriteBeads_P1.pdf (accessed on 10 January 2021).

34. Herzer, G. Modern soft magnets: Amorphous and nanocrystalline materials. *Acta Mater.* **2013**, *61*, 718-734.

35. Brander, T.; Gerfer, A.; Rall, B.; Zenkner, H. *Trilogy of Magnetics: Design Guide for EMI filter design, SMP & RF circuits*, 4th ed.; Swiridoff Verlag: Künzelsau, Germany, 2010.

36. Weinschrott, A. New measurement method for high frequency cable mounted ferrites. In Proceedings of the 2005 International Symposium on Electromagnetic Compatibility, Chicago, IL, USA, 8–12 August 2005; pp. 312–314.

37. Paul, C.R. *Introduction to Electromagnetic Compatibility*, 2nd ed.; Wiley Interscience: Hoboken, NJ, USA, 2006.

38. Ott, H.W. *Noise Reduction Techniques in Electronic Systems*; John Wiley & Sons: Hoboken, NJ, USA, 1988.

39. Keysight E5061B-3L3/3L4/3L5 LF-RF Network Analyzer with Option 005 Impedance Analysis Function. Available online: http://literature.cdn.keysight.com/litweb/pdf/5990-7033EN.pdf (accessed on 10 January 2021).

40. Schulze, S.; Al-Hamid, M.; Leone, M. Detailed study of different cable ferrite characterization methods using simulation and measurement. In Proceedings of the 2017 International Symposium on Electromagnetic Compatibility-EMC Europe, Angers, France, 4–7 September 2017; pp. 1–5.

41. Keysight 16200B External DC Bias Adapter Operation and Service Manual. Available online: http://literature.cdn.keysight.com/litweb/pdf/16200B.pdf (accessed on 10 January 2021).

42. Chang, K. *Handbook of Microwave and Optical Components, Fiber and Electro-Optical Components;* Wiley: Hoboken, NJ, USA, 1991.

43. International Telephone, & Telegraph Corporation. *Reference data for radio engineers*. Howard W. Sams and Company: Indianapolis, Indiana, USA, 1968.

44. Haase, H.; Nitsch, J.; Steinmetz, T. Transmission-line super theory: A new approach to an effective calculation of electromagnetic interactions. *URSI Radio Science Bulletin* **2003**, 307, 33-60. doi:10.23919/URSIRSB.2003.7909507.

45. Urabe, J.; Fujii, K.; Dowaki, Y.; Jito, Y.; Matsumoto, Y.; Sugiura, A. A Method for Measuring the Characteristics of an EMI Suppression Ferrite Core. *IEEE Trans. Electromagn. Compat.* **2006**, *48*, 774–780. doi:10.1109/TEMC.2006.884507.

46. Brockman, F.G.; Dowling, P.H.; Steneck, W.G. Dimensional effects resulting from a high dielectric constant found in a ferromagnetic ferrite. *Phys. Rev*. **1950**, *77*, 85–93. doi:10.1103/PhysRev.77.85.

47. Ponomarenko, N. Study of Frequency and Microstructure Dependencies of Magnetic Losses of Ferrite Materials and Components. PhD Thesis, Riga Technical University, Riga, Latvia, 2014.

48. Fiorillo, F. *Measurement and Characterization of Magnetic Materials*; Elsevier: Amsterdam, The Netherlands, 2004.

49. Orlando, A.; Koledintseva, M. Y.; Beetner, D. G.; Shao, P.; Berger, P. A lumped-element circuit model of ferrite chokes, Proceedings of the 2010 IEEE International Symposium on

Electromagnetic Compatibility, Fort Lauderdale, FL, USA, 2010; IEEE; pp. 754–759. doi:10.1109/ISEMC.2010.5711373.

50. Bhuiyan, R. H.; Dougal, R. A.; Ali, M. A miniature energy harvesting device for wireless sensors in electric power system. *IEEE Sensors Journal* 2010, *10*, 1249–1258. doi:10.1109/JSEN.2010.2040173.

51. McLyman, C.W.T. *Transformer and inductor design handbook*; Dekker: New York, NY, USA, 1988.

Appendix A. Scientific contributions

This section includes a list of all the scientific publications and conferences derived from this Ph.D. work in chronological order.

A.1 Peer-reviewed scientific articles in journals

Suarez, A.; Victoria, J.; Alcarria, A.; Torres, J.; Martinez, P.A.; Martos, J.; Soret, J.; Garcia-Olcina, R.; Muetsch, S. Characterization of Different Cable Ferrite Materials to Reduce the Electromagnetic Noise in the 2–150 kHz Frequency Range. *Materials* 2018, *11*, 174.
https://doi.org/10.3390/ma11020174

Suarez, A.; Victoria, J.; Torres, J.; Martinez, P.A.; Alcarria, A.; Martos, J.; Garcia-Olcina, R.; Soret, J.; Muetsch, S.; Gerfer, A. Effectiveness Assessment of a Nanocrystalline Sleeve Ferrite Core Compared with Ceramic Cores for Reducing Conducted EMI. *Electronics* 2019, *8*, 800.
https://doi.org/10.3390/electronics8070800

Suarez, A.; Victoria, J.; Torres, J.; Martinez, P.A.; Alcarria, A.; Perez, J.; Garcia-Olcina, R.; Soret, J.; Muetsch, S.; Gerfer, A. Performance Study of Split Ferrite Cores Designed for EMI Suppression on Cables. *Electronics* 2020, *9*, 1992.
https://doi.org/10.3390/electronics9121992

A.2 Peer-reviewed scientific articles in conferences

Suarez, A.; Victoria, J.; Martinez, P. A.; Alcarria, A.; Torres, J.; Molina, I. Analysis of different Sleeve Ferrite Cores Performance according to their Dimensions. Proceedings of the 2019 International Symposium on Electromagnetic Compatibility-EMC EUROPE, Barcelona, Spain, 2019; IEEE; pp. 88–93.
https://doi.org/10.1109/EMCEurope.2019.8872078

Suarez, A.; Victoria, J.; Torres, J.; Martinez, P. A.; Martinez, V.; Molina, I.; Muetsch, S.; Garcia-Olcina, R.; Soret, J.; Martos, J. Determination of Core Size Dependency on the EMI Suppression in Cable Ferrites. Proceedings of the 2020 International Symposium on Electromagnetic Compatibility-EMC EUROPE, Rome, Italy, 2020; IEEE; pp. 1–6.
https://doi.org/10.1109/EMCEUROPE48519.2020.9245745

A.3 Presentations and posters in conferences

2019 IEEE International Symposium on Electromagnetic Compatibility-EMC EUROPE, Barcelona, Spain, September 2019. Poster presentation titled “Analysis of different Sleeve Ferrite Cores Performance according to their Dimensions”.

2020 IEEE International Symposium on Electromagnetic Compatibility-EMC EUROPE, Rome, Italy, September 2020. Oral presentation titled “Determination of Core Size Dependency on the EMI Suppression in Cable Ferrites”.

A.4 Edited book chapter

Suarez, A.; Victoria, J; Torres, J.; Martinez, P.A.; Amaro, A.; Martos, J. Characterization of Nanocrystalline cores for EMI Suppression in cables. In *Nanocrystals*; Mallik, A., Eds.; IntechOpen: London, United Kingdom, 2020; ISBN 978-1-83968-823-2.
https://dx.doi.org/10.5772/intechopen.96694

Appendix B. List of symbols and abbreviations

This section includes a list of all the symbols and abbreviations included in this Ph.D. work in alphabetical order.

μ'	Real component of the complex relative permeability
μ''	Imaginary component of the complex relative permeability
μ_0	Vacuum permeability
μ_e	Effective relative permeability
μ_i	Initial permeability
μ_r	Relative permeability
A	Insertion loss
AC	Alternating current
B	magnetic flux density
B_R	remnant flux density
B_S	magnetic saturation
C	Capacitance
CM	Common-mode current
CMAD	Common Mode Absorption Devices
d	Conductor diameter
dB	Decibels
DC	Direct current
DM	Differential-mode current
EMC	Electromagnetic compatibility
EMI	Electromagnetic interference

FEM	Finite element method
F_g	Air gap factor
f_m	Resonance frequency
H	Magnetic field strength
h	Height of a sleeve core
H_C	Point of coercivity
I	Current
IR	Inner radius
L	Inductance
ℓ	Effective magnetic path length of a toroidal core
L_0	Air core inductance
ℓ_c	Magnetic path length of the core
ℓ_g	Length of the air gap
L_m	Inductance of the core considering its magnetic properties
MnZn	Manganese zinc composition
N	Number of turns
NC	Nanocrystalline composition
NiZn	Nickel zinc composition
OR	Outer radius
PCB	Printed circuit board
R	Resistance
r	Side rectangular cross-section
R_c	Reluctance of the core
R_g	Reluctance of the gap
R_m	Total magnetic reluctance
S	Cross-sectional area
SEM	Scanning electron microscopy
SRF	Self-resonance frequency
TRL	Through-reflect-line
X_L	Inductive reactance

Z_0	Characteristic impedance
Z_A	Impedance of a system A
Z_B	Impedance of a system B
Z_{SC}	Impedance of a sleeve core
λ	Wavelength
ω	Angular frequency
Φ	Magnetic flux